Observer-based boundary control of distributed parameter systems : a port- Hamiltonian approach

Jesús Pablo Toledo Zucco

Thèse de doctorat de l'établissement
Université Bourgogne Franche-Comté
preparée à l'Université de Franche-Comté

École doctorale n° 37
Sciences Pour l'Ingénieur et Microtechniques

Doctorat de Automatique

Par

Jesús Pablo Toledo Zucco

Synthèse de lois de commande à base d'observateurs pour les systèmes à paramètres distribués: une approache Hamiltonienne à ports

Thèse présentée et soutenue à Besançon, le 01 Juillet 2021

Composition du Jury :

Laurent Lefèvre	Professeur des Universités, Grenoble INP-Esisar	Rapporteur
Alessandro Macchelli	Maître de conférences, HDR, Université de Bologna	Rapporteur
Thomas Meurer	Professeur, Université de Kiel	Examinateur
Bernhard Maschke	Professeur des Universités, Université Claude Bernard Lyon1	Examinateur
Paul Kotyczka	Maître de conférences, HDR, Université technique de Munich	Examinateur
Yongxin Wu	Maître de conférences, ENSMM Besançon	Co-directeur
Hector Ramirez	Maître de conférences, HDR, Université Federico Santa María	Co-directeur
Yann Le Gorrec	Professeur des Universités, ENSMM Besançon	Directeur de thèse

UBFC
UNIVERSITÉ
BOURGOGNE FRANCHE-COMTÉ

femto-st
SCIENCES &
TECHNOLOGIES

PH.D. THESIS OF THE UNIVERSITY BOURGOGNE FRANCHE-COMTÉ PREPARED AT THE UNIVERSITY OF FRANCHE-COMTÉ

DOCTORAL SCHOOL N° 37
ENGINEERING SCIENCES AND MICROTECHNOLOGIES

Ph.D in Automatic

BY

Jesús Pablo TOLEDO ZUCCO

Observer-based boundary control of distributed parameter systems: a port-Hamiltonian approach

Thesis defended publicly on July 01, 2021, in Besançon

Composition of jury :

Laurent Lefèvre	Professor of University, Grenoble INP-Esisar	Reviewer
Alessandro Macchelli	Associate Professor, University of Bologna	Reviewer
Thomas Meurer	Professor, Kiel University	Member
Bernhard Maschke	Professor of University, Claude Bernard University Lyon 1	Member
Paul Kotyczka	Associate Professor, Technical University of Munich	Member
Yongxin Wu	Associate Professor, ENSMM Besançon	Co-supervisor
Hector Ramirez	Associate Professor, Federico Santa María Technical University	Co-supervisor
Yann Le Gorrec	Professor of University, ENSMM Besançon	Supervisor

To my mother, father and brothers.

Acknowledgements

I want to start by thanking the most important people of my life, my family. I am who I am because of all of you: Paola, Enrique, Enrique, Nicolás and José. I also want to thank my grandfathers, uncles and cousins for all the support you have given me throughout my life. I want to thank, as well, my nephews and their mother for the immense joy that they have brought to our family.

I want to continue with the people who have made this thesis possible: Yann, Héctor and Yongxin. Thank you for including me in your group, introducing me to the port-Hamiltonian (pH) community and the world of Partial Differential Equations. Thanks, as well, for discussing with me, explaining complex stuff in simple words, working on our papers, reading my manuscript and correcting it. More important, thank you for worrying not only about the scientific aspects but also the social ones. It is not an easy task to leave your country, but you have made it too much simpler for me. I want to thank, as well, Daniel from the University of Concepción. He has motivated me to follow the scientific career in the domain of automatic control.

I want to thank the reviewers of my thesis: Laurant and Alessandro. Thank you for taking your time to read my manuscript and give me your feedback that has contributed to a better quality of the final version of this manuscript. I want to thank, as well, the jury members of my defense. Bernhard, Thomas and Paul. Thank you for all the scientific discussions we have had before, during, and after my defense. Your remarks have improved the quality of the final version of this manuscript, as well. I want to thank Bernhard for assisting in person to my defense during a complex period. Your assistance made the thesis defense more pleasant.

This thesis has been supported by the French-German ANR-DFG INFIDHEM project ANR-16-CE92-0028. In this project, I met very nice and interesting people whom I want to thank for all the moments lived together in meetings, conferences, summer schools, etc. In particular, I want to thank Denis, Andrea and Annas from Toulouse, Bernhard from Lyon, Birgit and Julia from Wuppertal, Thomas and Bastian from Kiel, Paul and Tobias from Munich, and Marc from Paris.

Most of my work has been within the pH team at the AS2M department of Femto-ST. I want to thank, again, Yann, Yongxin and Héctor for their patience discussing with me. I want to thank Vincent, even if we couldn't have too many discussions, his discretization method was useful for my thesis. I want to thank Luis for all the discussion that we have had and for recently helping me with the final format of this thesis. I want to thank Ning for helping me, from the first day that I met her, with the french, the new theory, the administrative paperwork, and many other things. Finally, I want to thank a very good friend, Andrea. Thank you for supporting me from the beginning of my thesis, spending a lot of time discussing with me complex math concepts, receiving me in your home, introducing me to your lovely family, sharing your culture, playing football, hiking, etc.

I want to thank Alika, from the doctoral school, for her patience and all the help she gave me during the doctoral period. Similarly, I want to thank Isabelle and Estelle from the AS2M department for their cooperation concerning all the administrative stuff. At the AS2M department, I met a lot of people to whom I want to thank everyone. Thanks for all discussions during the coffee break. From the permanent staff, I would like to thank Phillipe, Jean-Marc, Kanty, Christophe,

Nicolas, Aude, Cedric, Zeina, Guillaume, Patrick R., Patrick N., and Jean-Yves. From the non-permanent staff, I would like to thank Abbas, Romain, Benjamin, Maxime, Omar, Hugo, Amine, Belal, Alexis, Aicha, Anh, Aurélie, Chibundo, Daniel, Maribel, and Yucely. I would like to especially thank Chifaa, for being a very good friend, being a very nice and happy person, helping me with the french and sharing very nice moments. Also, I want to thank all my office colleagues for theirs cultural exchanges, general discussion, and nice moments lived together in our great office. Thank Joël, Marwa, Ning, Bhawnath, Yuning, Olivier, and Luc.

Many non-academic activities kept me active and allowed me to recharge my energy and rest my mind. I want to thank the football team of USport which I have spent almost every Tuesday at noon. In general, I am very grateful to the USport. They have provided nice activities like hiking, skiing, and volley nights that helped me distract myself and rest my mind. Also, I want to thank the football team of BBF, especially Daniel, Adrien and Billy. I want to thank as well a more recently hiking group that keeps me active on Sundays. In all these activities, I met wonderful people that I will never forget. I want to thank some good friends that I met during my stay in Besançon: Diego, Veronica, and Wilmar, and some friends from Chile with whom I kept in touch all this time: Felipe, Andrés, Eric, Enrique, Natalia, Héctor, Alejandro, and Rodrigo.

Finally, I want to thank the person who was next to me, supporting me, encouraging me, and making me happy. Thank Irina for being with me during this period. I will always be grateful to you and your family for including me in your activities and celebrations. I also want to thank you for bringing Olympe to our home. She has always been a source of energy and happiness.

Jesús Toledo Zucco, September 15, 2021, in Besançon, France.

"Gracias a la vida que me ha dado tanto,
me ha dado la marcha de mis pies cansados,
con ellos anduve ciudades y charcos,
playas y desiertos, montañas y llanos,
y la casa tuya, tu calle y tu patio."

Violeta Parra

Notation

Symbols

t	Time variable.
ζ	Spatial variable.
$\mathbb{R}$	Set of all scalar with real values.
$\mathbb{R}^n$	Set of all column vectors with real values.
$\mathbb{R}^{n\times n}$	Set of all matrices with real values.
$M_n(\mathbb{R})$	Space of all real $n \times n$ matrices.
$H^1([a,b],\mathbb{R}^n)$	Vector space of all function from $[a,b]$ to $\mathbb{R}^n$, which are square integrable, absolutely continuous and the derivative is again square integrable.
$\mathcal{L}(X)$	Vector space of bounded linear operators from X to X.
$\mathcal{L}(U,X)$	Vector space of bounded linear operators from U to X.
$L^2([a,b],\mathbb{R}^n)$	Space of all square-integrable functions ion $\mathbb{R}^n$ evaluated at $[a,b]$.
$\Diamond$	Ending a Theorem, Proposition, Lemma, or Corollary.
■	Ending a Proof.
♣	Ending an Example, Remark, Definition, or Assumption.

Acronyms

BCSs	Boundary control systems.
BC-PHSs	Boundary controlled port-Hamiltonian systems.
PR	Positive real.
SPR	Strictly positive real.
ODEs	Ordinary differential equations.
PDEs	Partial differential equations.
ZSD	Zero state detectable.
OSP	Output strictly passive.
LTI	Linear time invariant.
NTI	Nonlinear time invariant.
LPSs	Lumped parameter systems.
DPSs	Distributed parameter systems.
LQR	Linear quadratic regulator.
OBSF	Observer-based state feedback.
i.e.	abbreviation for *id est* (that is).

Contents

Chapter I
Context

I.1 Main introduction

In control theory, state feedback control is the most efficient way to assign desired behaviour to dynamical systems and to guarantee closed-loop stability [Kalman 69]. The main drawback of this control strategy is that it requires knowledge of the complete or partial state. Since the state is not always available from sensors, this control law is, in general, applied using observers [Luenberger 64]. An observer is a dynamical system that uses the model and the available data from sensors and actuators to estimate, in real-time, the state variables of the system. Then, the desired state feedback is applied using the observed values instead of the real ones. This is known as *observer-based state feedback* (OBSF) control. In this thesis, we study the synthesis of this type of control laws for port-Hamiltonian systems described by *partial differential equations* (PDEs) defined on a one-dimensional domain with actuators and sensors collocated at the spatial boundaries.

The port-Hamiltonian formulation of systems described by *ordinary differential equations* (ODEs) has been introduced in [Maschke 92], and it has shown to be well suited for modelling, analysis and control of multiphysical systems [Dalsmo 98, van der Schaft 00, Stramigioli 01, Duindam 09]. A port-Hamiltonian system is characterized by its energy and the power that is exchanged with the environment (controllers, perturbations, or other systems). For this type of systems, the most popular control technique is the control by *energy shaping and damping injection*. This control technique consists in assigning the closed-loop energy function and guaranteeing closed-loop stability by adding damping [Maschke 98, Ortega 02, Ortega 04]. For *linear time-invariant* (LTI) systems, control by *energy shaping and damping injection* can be compared with classical control techniques as *pole placement*, *linear quadratic regulation* (LQR), or H_∞*-control* [Prajna 02]. The control law obtained using this technique usually ends in a state feedback control law. To implement it, the use of observers is necessary. Using the port-Hamiltonian approach, the synthesis of observers has been quite intensively studied for *lumped parameter systems* (LPSs) [Venkatraman 10a, Kotyczka 15, Vincent 16, Yaghmaei 18, Biedermann 18], but only a few studies have been addressed for *distributed parameter systems* (DPSs) [Toledo 20, Malzer 20a].

The port-Hamiltonian formulation has been extended to DPSs or systems described by PDEs in [van der Schaft 02], showing in a period of twenty years to be a successful approach for the modelling, analysis, and control design of DPSs [Rashad 20]. The general formulation of *boundary control systems* (BCSs) [Fattorini 68, Curtain 12] using the port-Hamiltonian approach is addressed in [Le Gorrec 05], where a new class of BCSs is defined as *boundary controlled port-Hamiltonian systems* (BC-PHSs). BC-PHSs are DPSs with actuators and sensors located at the spatial boundaries and with the state variables chosen as the energy variables. This class of systems can model beams and waves [Macchelli 04b, Voß 14], open channels [Hamroun 06], piezoelectric structures [Schöberl 08], ionic polymer-metal composite [Nishida 11, Liu 21], chemical reactors [Le Gorrec 06, Zhou 17], fluid motion in containers [Cardoso-Ribeiro 17], rotating flexible spacecrafts [Aoues 17], among others.

The existence and uniqueness of solutions for BC-PHSs have been studied using functional analysis for the linear case in [Le Gorrec 05, Le Gorrec 06, Zwart 10, Jacob 12, Jacob 15, Jacob 18, Augner 20] and for the nonlinear case in [Augner 19, Hastir 19]. In [Jacob 19], the authors have shown that every well-posed linear BC-PHS is *exact controllable* and *exact observable*. The stabilization and the synthesis of control laws for BC-PHSs have been addressed in [Villegas 07] using static output feedback [Villegas 09] and dynamic output feedback [Villegas 05, Ramirez 14, Macchelli 18, Macchelli 20]. The *energy shaping and damping injection* techniques have been extended from the

finite-dimensional formulation to the infinite-dimensional one in [Macchelli 04a, Pasumarthy 07, Hamroun 10, Schöberl 12, Macchelli 17]. Some others approaches have been studied using backstepping boundary control [Vu 17, Ramirez 17b] and nonlinear dynamic boundary control for linear BC-PHSs [Ramirez 17a, Califano 18]. In this thesis, we are interested in the observer-based state feedback design for the class of impedance energy preserving BC-PHSs. To this end, we employ both *early-lumping* and *late-lumping* approaches [Meurer 12].

In the early-lumping approach, the infinite-dimensional system is first discretized into a finite-dimensional system by using suitable approximation methods as finite element [Golo 04, Bassi 07, Pasumarthy 12], geometric approaches [Seslija 12, Kotyczka 18], partitioned finite element [Brugnoli 19a, Brugnoli 19b, Serhani 19], and finite difference [Trenchant 18]. Then, the synthesis of the OBSF controller is based on a discretized model (finite-dimensional system). Finally, the OBSF controller is applied to the infinite-dimensional system, *i.e.* to the BC-PHS. The main advantage of using this approach is the high number of tools available in the literature for the synthesis of the OBSF gains. These are, for instance, the *linear quadratic regulator* (LQR) [Anderson 07], the pole-placement [Brasch 70], and the *interconnection and damping assignment passivity based control* (IDA-PBC) [Prajna 02]. The main drawback when using the *early-lumping* approach is that since the OBSF controller is designed on an approximated model and not on the BC-PHS, the closed-loop stability is not guaranteed when applying the OBSF controller to the BC-PHS. The closed-loop instability generated when applying an OBSF controller (finite-dimensional system) to a BC-PHS (infinite-dimensional system) is known as *spillover effect* [Balas 78]. This closed-loop instability is mainly due to the fact that some high-frequency modes, that are not considered during the design, are destabilized by the OBSF controller. In this thesis, we design the OBSF controller such that it is equivalent to the control by interconnection with a passive controller. In this way, the closed-loop stability is guaranteed when the OBSF controller is applied to the BC-PHS. To satisfy this structure, we propose two methodologies for the design of the OBSF gains.

In the *late-lumping* approach, the infinite-dimensional model is used for the design of the OBSF controller. In this case, the observer is an infinite-dimensional system as in [Smyshlyaev 05], [Hidayat 11, Meurer 13, Schaum 18], and for the implementation, the infinite-dimensional observer has to be discretized by using suitable approximation methods like the ones mentioned before. The main advantage of using this approach is that the infinite-dimensional structure is completely used for analysis and control. This approach is increasingly used in applications such as the wave equation [Guo 07, Krstic 08, Guo 09, Smyshlyaev 09, Meurer 11, Feng 16, Auriol 19] or the diffusion-convection-reaction processes [Smyshlyaev 05, Meurer 09, Schaum 18], among others. The main difficulty when using this approach is the generalization of the OBSF design for the class of infinite-dimensional systems of interest. In this thesis, we propose a general setting for the design of infinite-dimensional observers for impedance energy preserving BC-PHSs [Toledo 20, Malzer 20a]. We analyze different cases depending on the measured output. We cover the cases when the co-energy variables are measured and when the integral over time of them are. For mechanical systems, these are the cases when velocities and displacements are measured, for instance. Finally, some first steps towards the OBSF control design for BC-PHSs are presented using the vibrating string as an example. In this case, we combine the *energy shaping and damping injection* techniques with infinite-dimensional observers to stabilize the undamped vibrating string.

I.2 Organization of the thesis

This thesis is composed of three main chapters. In Chapter II, a background on BC-PHSs is provided. In Chapter III, we consider the *early-lumping* approach for the synthesis of OBSF controllers. Finally, in Chapter IV, we consider the *late-lumping* approach for the design. We summarize the content of each chapter as follows:

In Chapter II, we provide a background on BC-PHSs. We first introduce the class of systems that we are interested in. This class is exemplified with some classic examples modelled as BC-PHSs. Then, we recall the concepts of *well-posedness*, *exact controllability* and *exact observability*. We give some results on the stabilization of BC-PHSs using static and dynamic output feedback. Finally, we provide a motivation example, where we use observers for the practical implementation of the control law that has been designed using *energy shaping* and *damping injection*.

In Chapter III, we use the *early-lumping* approach for the synthesis of OBSF controllers. Using this approach, the BC-PHS is first discretized into a finite-dimensional model. Then, the observer and controller gains are designed based on the finite-dimensional model. Since the discretized model is a finite-dimensional system, one can use classical control tools for the design (LQR or *pole placement*, for example). However, using a counterexample, we show that the closed-loop stability is not always guaranteed when the OBSF controller is applied to the infinite-dimensional system. To overcome this issue, we impose a passive structure on the OBSF controller. This structure can guarantee closed-loop stability when applying the OBSF controller to the BC-PHS. We propose two methods for the synthesis of the OBSF gains. In the first one, the state feedback gain is designed freely using classical tools and the observer gain is designed such that the passive structure is guaranteed. In the second one, the observer gain is designed freely and the state feedback gain is designed to achieve the desired structure. Both methods are exemplified using the vibrating string and the Timoshenko beam models. Finally, we extend this idea to a class of nonlinear finite-dimensional systems. In this case, the nonlinear system is first linearized into an LTI system. Then, the same methods can be used for the synthesis of the OBSF gains. In the same way as before, the passive structure guarantees closed-loop stability when applying the OBSF controller to the nonlinear system.

In Chapter IV, we use the *late-lumping* approach for the synthesis of OBSF controllers. Using this approach, the observer is an infinite-dimensional system and has to be discretized for implementation. First, we propose infinite-dimensional observers that can estimate the state of the BC-PHS. We analyze different cases depending on the available sensors, and we give the conditions to achieve asymptotic or exponential convergence of the observer. The port-Hamiltonian formalism is used to show the stability of the error system. Once again, the results are exemplified with the vibrating string and the Timoshenko beam models. Then, we apply two OBSF control laws to the vibrating string. First, we apply *observer-based damping injection* at both sides of the string in the case when a force sensor is available at one side only and in the case when a displacement sensor is available at one side only. Then, we use *observer-based energy shaping and damping injection* at one side of the string in the case when a velocity sensor and a force actuator are available at the same side.

The thesis ends with some conclusions and perspectives.

I.3 Publications

The publications related to this thesis are the followings:

Toledo, J., Wu, Y., Ramirez, H., & Le Gorrec, Y. (2020). Observer-based boundary control of distributed port-Hamiltonian systems. Automatica, 120, 109130.
doi.org/10.1016/j.automatica.2020.109130 (Draft)

Toledo, J., Ramirez, H., Wu, Y., & Le Gorrec, Y. (2020). Linear Matrix Inequality Design of Observer-Based Controllers for port-Hamiltonian Systems. Submitted to IEEE Transactions on Automatic Control.
arxiv.org/abs/2010.06314 (Draft)

Malzer, T., Toledo, J., Gorrec, Y. L., & Schöberl, M. (2020). Energy-based in-domain control and observer design for infinite-dimensional port-Hamiltonian systems. In Proceedings of the 24th International Symposium on Mathematical Theory of Networks and Systems, 24-28 August 2020, Cambridge, UK.
arxiv.org/abs/2002.01717

Toledo, J., Wu, Y., Ramirez, H., & Le Gorrec, Y. (2019). Observer-Based State Feedback Controller for a class of Distributed Parameter Systems. Paper presented at the 3rd IFAC Workshop on Control of Systems Governed by Partial Differential Equations CPDE 2019, 20–24 May 2019, Oaxaca, Mexico.
doi.org/10.1016/j.ifacol.2019.08.020

Toledo, J., Ramirez, H., Wu, Y., & Le Gorrec, Y. (2019). Passive observers for distributed port-Hamiltonian systems. In Proceedings of the 21st IFAC World Congress, Berlin, Germany, July 12-17, 2020.
doi.org/10.1016/j.ifacol.2020.12.1356 (Draft)

Mattioni, A., Toledo, J., & Le Gorrec, Y. (2019). Observer Based Nonlinear Control of a Rotating Flexible Beam. In Proceedings of the 21st IFAC World Congress, Berlin, Germany, July 12-17, 2020.
doi.org/10.1016/j.ifacol.2020.12.1306

I.4 Main contributions

The main contribution of Chapter II is the background on BC-PHSs. Besides, in this chapter, we present an example that shows the importance of using observers to implement state feedback control laws like the ones derived using *energy shaping and damping injection*.

The main contribution of Chapter III is a design procedure of finite-dimensional OBSF controllers (Proposition III.6.1 and Proposition III.7.1) for BC-PHSs. This procedure guarantees closed-loop stability when applying the finite-dimensional OBSF controller to the BC-PHS (Theorem III.5.1). The achieved closed-loop performances are close to the desired ones as soon as the discretized model is close to the BC-PHS. Another contribution of this chapter is that the same design procedure can be used to design OBSF controllers for a class of finite-dimensional nonlinear systems. We can guarantee closed-loop stability when applying the linear OBSF controller to this class of systems (Proposition III.8.3).

The main contribution of Chapter IV is the generalization of infinite-dimensional observer for BC-PHSs. We cover a large number of cases depending on the type of available measurements. One can use Proposition IV.3.1 when the full conjugated output is measured, Proposition IV.3.2 when the conjugated output is partially measured, Proposition IV.3.3 when the conjugated output is not measured but the integral over time of it is, or Proposition IV.3.4 when the conjugated output and the integral over time of it are both measured. These are, for instance, the cases of measuring forces, velocities and displacements in mechanical systems. Then, some first steps towards observer-based *damping injection and energy shaping* are studied for the stabilization of the vibrating string. In Proposition IV.4.1, the closed-loop system is shown to be exponentially stable when applying the observer-based *damping injection* at both sides using a force sensor at one side only. In Proposition IV.4.2, the closed-loop system is shown to be asymptotically stable when applying the observer-based *damping injection* at both sides using a displacement sensor at one side only. Finally, in Section IV.5, the closed-loop system is shown to be asymptotically stable when applying observer-based *energy shaping and damping injection* to the vibrating string. In this case, we consider the vibrating string attached at one side and with a force actuator and velocity sensor at the other side.

Chapter II

Background on boundary controlled port-Hamiltonian systems

II.1 Introduction

Boundary control systems (BCSs) [Fattorini 68, Curtain 12] is a class of control systems described by *partial differential equations* (PDEs) with actuation and measurement situated at the boundaries of the spatial domain. This class of systems is more and more encountered in engineering applications and system control theory due to the recent progress in modelling and analysis of complex systems. In many cases, the system of interest can be represented as a BCS. These are, for instance, the cases of beams and waves in mechanical systems, heat bars and bed reactors in chemical systems, or telegraph equations in electric systems.

Recently, the BCS formulation has been addressed by the port-Hamiltonian approach using *Stokes-Dirac* structures [van der Schaft 02, Le Gorrec 05, Jacob 12] and *jet bundles* [Ennsbrunner 05, Schöberl 14]. Port-Hamiltonian systems are an extension of the Hamiltonian formulation for mechanical systems to open multi-physical systems [Duindam 09]. This formalism has shown to be suitable for modelling and control of complex physical systems, such as systems described by nonlinear equations or PDEs. For the latter, the formulation of *boundary controlled port-Hamiltonian systems* (BC-PHSs) has shown to be very useful for the modelling, discretization, control and analysis [Rashad 20]. In this chapter, we present a background on BC-PHSs. We recall the concepts of *existence and uniqueness of solutions*, *exact controllability* and stability for this class of systems.

First, we recall the parametrization of the boundary conditions proposed in [Le Gorrec 05], leading to a *well-posed* system, *i.e.* the BC-PHS has a solution, and it is unique. Then, we present some classic examples of BC-PHSs. We recall the *exact controllability* property that every BC-PHS satisfies when it is *well-posed* [Jacob 19]. Some stability results from [Villegas 07] are provided in the case when static output feedback is applied to the BC-PHS [Villegas 09] and in the case when dynamic output feedback is [Villegas 05, Ramirez 14, Macchelli 18]. Finally, we use the example of the vibrating string to motivate the use of *observer-based state feedback* (OBSF) control laws. We consider the vibrating string attached at one side and with a force actuator at the other side. The objective is to apply a state feedback control law derived through *energy shaping* [Macchelli 05, Pasumarthy 07, Hamroun 10, Schöberl 12, Macchelli 17] and *damping injection* [Macchelli 04b, Villegas 07]. Since the knowledge of the state is required, we use observers to estimate the state from a collocated velocity sensor only.

We organize the rest of this chapter as follows. In Section II.2, we recall the structure of the considered BC-PHS. In Section II.3, we present three classical examples, the transmission line, the vibrating string and the Timoshenko beam. In Section II.4 and Section II.5, we recall the controllability and stabilizability results for BC-PHSs. Finally, in Section II.6, we give an example to motivate the necessity of using observers.

II.2 Boundary controlled port-Hamiltonian systems

Boundary controlled port-Hamiltonian systems (BC-PHSs) are dynamical system described by the following hyperbolic partial differential equation (PDE):

$$\frac{\partial x}{\partial t}(\zeta,t) = P_1 \frac{\partial}{\partial \zeta}(\mathcal{H}(\zeta)x(\zeta,t)) + P_0\mathcal{H}(\zeta)x(\zeta,t), \quad x(\zeta,0) = x_0(\zeta), \tag{II.1}$$

where $\zeta \in [a,b]$ is the space variable and $t \geq 0$ is the time variable. $x(\zeta,t) \in \mathbb{R}^n$ is the state variable and $x_0(\zeta)$ is the initial condition. $P_1 = P_1^T \in M_n(\mathbb{R})$ is a non-singular matrix, $P_0 = -P_0^T \in M_n(\mathbb{R})$, and $\mathcal{H}(\cdot) = \mathcal{H}(\zeta)^T \in M_n(L_2([a,b];\mathbb{R}))$ is a bounded and continuously differentiable matrix-valued function satisfying for all $\zeta \in [a,b]$ $mI < \mathcal{H}(\zeta) < MI$ with $0 < m < M$ both scalars independent on ζ. $x(\zeta,t)$ is called energy variable and $\mathcal{H}(\zeta)x(\zeta,t)$ is called co-energy variable. The Hamiltonian related to the PDE (II.1) is given by

$$H(t) = \frac{1}{2}\int_a^b x(\zeta,t)^T \mathcal{H}(\zeta)x(\zeta,t)d\zeta. \tag{II.2}$$

Example II.2.1. *[Jacob 12, Chapter 11] The transport equation is given by the following PDE:*

$$\frac{\partial w}{\partial t}(\zeta,t) = \frac{\partial w}{\partial \zeta}(\zeta,t), \qquad w(\zeta,0) = w_0(\zeta), \tag{II.3}$$

and is written as in (II.1) with

$$x(\zeta,t) = w(\zeta,t), \quad P_1 = 1, \quad \mathcal{H} = 1, \quad P_0 = 0, \quad x_0(\zeta) = w_0(\zeta),$$

and Hamiltonian

$$H(t) = \frac{1}{2}\int_a^b x(\zeta,t)^2 d\zeta.$$

♣

The PDE (II.1) by itself does not describe a dynamical system and requires boundary conditions to guarantee the existence and uniqueness of solutions. The *boundary port variables* are instrumental for this and are defined as follows

Definition II.2.1. *[Le Gorrec 05, Definition 3.5] Let $\mathcal{H}(\zeta)x(\zeta,t) \in H^1((a,b),\mathbb{R}^n)$. The boundary port variables associated with (II.1) are the vectors $f_\partial(t)$ and $e_\partial(t) \in \mathbb{R}^n$, defined by*

$$\begin{pmatrix} f_\partial(t) \\ e_\partial(t) \end{pmatrix} = \frac{1}{\sqrt{2}} \begin{pmatrix} P_1 & -P_1 \\ I & I \end{pmatrix} \begin{pmatrix} \mathcal{H}(b)x(b,t) \\ \mathcal{H}(a)x(a,t) \end{pmatrix}. \tag{II.4}$$

♣

The time derivative of the Hamiltonian is equivalent to the multiplication between the *boundary port variables*. This is shown in the following theorem.

Theorem II.2.1. *The balance equation of the Hamiltonian energy (II.2) related to the PDE (II.1) is given by*

$$\dot{H}(t) = f_\partial(t)^T e_\partial(t). \tag{II.5}$$

♢

Proof. *In [Le Gorrec 05], the skew symmetry of the operator defined in (II.1) is used to express the time derivative of the Hamiltonian with respect to the boundary conditions (using integration by parts). These boundary conditions can be splitted using the formulation (II.4).* ■

In [Le Gorrec 05], the authors proposed a parametrization of the *boundary port variables* for defining inputs and outputs of BC-PHSs. In the following theorem, we recall the parametrization of all possible boundary conditions such that the dynamic system defined by the PDE (II.1) is well-posed (Definition II.4.1).

Theorem II.2.2. *[Le Gorrec 05, Theorem 4.1] Let $W_{\mathcal{B}} \in \mathbb{R}^{n\times 2n}$ be a full rank matrix. Define the operator $\mathcal{A}$ with domain $D(\mathcal{A})$ as*

$$\mathcal{A}x = P_1 \frac{d}{d\zeta}(\mathcal{H}x) + P_0(\mathcal{H}x) \tag{II.6}$$

$$D(\mathcal{A}) = \left\{ x \in X \mid \mathcal{H}x \in H^1([a,b];\mathbb{R}^n),\ W_{\mathcal{B}} \begin{pmatrix} f_\partial(t) \\ e_\partial(t) \end{pmatrix} = 0 \right\}. \tag{II.7}$$

Then, $\mathcal{A}$ generates a contraction semigroup on $X = L_2([a,b],\mathbb{R}^n)$ if and only if $W_{\mathcal{B}}$ satisfies $W_{\mathcal{B}}\Sigma W_{\mathcal{B}}^T \geq 0$ with $\Sigma = \left(\begin{smallmatrix} 0_n & I_n \\ I_n & 0_n \end{smallmatrix}\right)$. ◊ Now, we define the inputs and outputs of the considered BC-PHS. Among all possible choices, we consider the input $u(t)$ and the output $y(t)$ such that the system is an *impedance energy preserving* system [Staffans 05]. This class of system are such that the energy balance is given by $\dot{H}(t) = u(t)^T y(t)$. Then, inputs and outputs have a physical interpretation. They can be, for instance, forces and velocities for mechanical systems and voltages and currents for electrical ones.

Theorem II.2.3. *[Le Gorrec 05, Theorem 4.2 and Theorem 4.4] Let $W_{\mathcal{B}} \in \mathbb{R}^{n\times 2n}$ be a full rank matrix such that $W_{\mathcal{B}}\Sigma W_{\mathcal{B}}^T \geq 0$ with $\Sigma = \left(\begin{smallmatrix} 0_n & I_n \\ I_n & 0_n \end{smallmatrix}\right)$. Define the input $u(t) \in L^2_{loc}((0,\infty),\mathbb{R}^n)$. The PDE (II.1) with boundary conditions*

$$W_{\mathcal{B}} \begin{pmatrix} f_\partial(t) \\ e_\partial(t) \end{pmatrix} = u(t) \tag{II.8}$$

is a boundary control system. Furthermore, define the output as

$$y(t) = W_{\mathcal{C}} \begin{pmatrix} f_\partial(t) \\ e_\partial(t) \end{pmatrix}, \tag{II.9}$$

with $W_{\mathcal{C}} \in \mathbb{R}^{n\times 2n}$ a full rank matrix such that $\left(\begin{smallmatrix} W_{\mathcal{B}} \\ W_{\mathcal{C}} \end{smallmatrix}\right)$ is invertible. In addition, if $W_{\mathcal{B}}\Sigma W_{\mathcal{B}}^T = W_{\mathcal{C}}\Sigma W_{\mathcal{C}}^T = 0_n$ and $W_{\mathcal{C}}\Sigma W_{\mathcal{B}}^T = I_n$, for all $u(t) \in C^2((0,\infty),\mathbb{R}^n)$, $\mathcal{H}(\zeta)x(\zeta,0) \in H^1((a,b);\mathbb{R}^n)$, and $u(0) = W_{\mathcal{B}} \left(\begin{smallmatrix} f_\partial(0) \\ e_\partial(0) \end{smallmatrix}\right)$, then the following balance equation of the Hamiltonian is satisfied

$$\dot{H}(t) = u(t)^T y(t). \tag{II.10}$$

◊

Remark II.2.1. *Roughly speaking, Theorem II.2.3 says that if $W_{\mathcal{B}}$ is a full rank and $W_{\mathcal{B}}\Sigma W_{\mathcal{B}}^T \geq 0$ is satisfied, we can impose some function $u(t)$ at the spatial boundaries of the PDE (II.1), i.e. we can do control.* ♣

Finally, we define the class of *boundary controlled port-Hamiltonian systems* (BC-PHSs) of interest in this thesis. We consider these type of systems in Chapter III and Chapter IV for the OBSF control design.

Definition II.2.2. *A BC-PHS is defined as a system composed by the PDE (II.1), the input (II.8), and the output (II.9) according to Theorem II.2.3. We also refer to a BC-PHS as in the following compact form:*

$$\mathcal{P} \begin{cases} \dfrac{\partial x}{\partial t}(\zeta,t) = P_1 \dfrac{\partial}{\partial \zeta}(\mathcal{H}(\zeta)x(\zeta,t)) + P_0\mathcal{H}(\zeta)x(\zeta,t), \quad x(\zeta,0) = x_0(\zeta), \\ W_{\mathcal{B}} \left(\begin{smallmatrix} f_\partial(t) \\ e_\partial(t) \end{smallmatrix}\right) = u(t), \\ y(t) = W_{\mathcal{C}} \left(\begin{smallmatrix} f_\partial(t) \\ e_\partial(t) \end{smallmatrix}\right). \end{cases} \tag{II.11}$$

♣

Remark II.2.2. *If the BC-PHS* (II.11) *satisfies the balance equation* (II.10)*, then it is called an impedance energy preserving BC-PHS [Staffans 05].* ♣

Remark II.2.3. *The BC-PHS* (II.11) *is the lossless form of a more general representation in where the internal dissipation can be included replacing* P_0 *by* $P_0 - G_0$*, where* G_0 *is a semi-positive definite matrix.* ♣

In the following, we present some classic examples of BC-PHSs.

II.3 Examples of BC-PHSs

We present three examples of dynamical systems that we can represent as BC-PHSs (II.11). First, the *transmission line* used for modelling electric power transmissions [Duindam 09]. Then, the *string equation* used for modelling water, sound and seismic waves [Villegas 07, Jacob 12]. And finally, the *Timoshenko beam* used for modelling thick beams [Macchelli 04b].

II.3.1 The transmission line

In Figure II.1, we show a transmission line used for electrical power distribution. Due to the extensions of the lines, we cannot neglect the spatial distribution. We can model, a *lossless transmission line* with the following PDEs:

Figure II.1 – Electrical power distribution

$$\frac{\partial Q}{\partial t}(\zeta,t) = -\frac{\partial}{\partial \zeta}\left(\frac{\phi(\zeta,t)}{L(\zeta)}(\zeta,t)\right), \quad Q(\zeta,0) = Q_0(\zeta), \tag{II.12}$$

$$\frac{\partial \phi}{\partial t}(\zeta,t) = -\frac{\partial}{\partial \zeta}\left(\frac{Q(\zeta,t)}{C(\zeta)}(\zeta,t)\right), \quad \phi(\zeta,0) = \phi_0(\zeta), \tag{II.13}$$

where $\zeta \in [a,b]$ and $t \geq 0$ are the space and time variables, respectively. $Q(\zeta,t)$ is the electric charge with initial condition $Q_0(\zeta)$, $\phi(\zeta,t)$ is the magnetic flux with initial condition $\phi_0(\zeta)$, $C(\zeta)$ is the distributed capacity and $L(\zeta)$ is the distributed inductance. We can write the *lossless transmission line* equations as in (II.11) with

$$x(\zeta,t) = \begin{pmatrix} Q(\zeta,t) \\ \phi(\zeta,t) \end{pmatrix}, \quad x_0(\zeta) = \begin{pmatrix} Q_0(\zeta) \\ \phi_0(\zeta) \end{pmatrix},$$

$$P_1 = \begin{pmatrix} 0 & -1 \\ -1 & 0 \end{pmatrix}, \quad P_0 = \begin{pmatrix} 0 & 0 \\ 0 & 0 \end{pmatrix}, \quad \mathcal{H} = \begin{pmatrix} \frac{1}{C(\zeta)} & 0 \\ 0 & \frac{1}{L(\zeta)} \end{pmatrix}.$$

The total energy is given by the sum of the electrical and magnetic one as follows:

$$H(t) = \frac{1}{2}\int_a^b \left[\frac{Q(\zeta,t)^2}{C(\zeta)} + \frac{\phi(\zeta,t)^2}{L(\zeta)}\right] d\zeta.$$

We obtain the boundary port variables from (II.4) as:

$$f_\partial(t) = \frac{1}{\sqrt{2}} \begin{pmatrix} \frac{\phi(a,t)}{L(a)} - \frac{\phi(b,t)}{L(b)} \\ \frac{Q(a,t)}{C(a)} - \frac{Q(b,t)}{C(b)} \end{pmatrix}, \quad e_\partial(t) = \frac{1}{\sqrt{2}} \begin{pmatrix} \frac{Q(a,t)}{C(a)} + \frac{Q(b,t)}{C(b)} \\ \frac{\phi(a,t)}{L(a)} + \frac{\phi(b,t)}{L(b)} \end{pmatrix}.$$

Then, we can choose the following inputs and outputs:

$$\begin{pmatrix} \frac{Q(a,t)}{C(a)} \\ \frac{Q(b,t)}{C(b)} \end{pmatrix} = u(t), \quad y(t) = \begin{pmatrix} \frac{\phi(a,t)}{L(a)} \\ \frac{-\phi(b,t)}{L(b)} \end{pmatrix},$$

from the *boundary port variables*, satisfying the conditions of Theorem II.2.3 with

$$W_{\mathcal{B}} = \frac{1}{\sqrt{2}} \begin{pmatrix} 0 & 1 & 1 & 0 \\ 0 & -1 & 1 & 0 \end{pmatrix}, \quad W_{\mathcal{C}} = \frac{1}{\sqrt{2}} \begin{pmatrix} 1 & 0 & 0 & 1 \\ 1 & 0 & 0 & -1 \end{pmatrix}, \quad \Sigma = \begin{pmatrix} 0_2 & I_2 \\ I_2 & 0_2 \end{pmatrix}.$$

Note that, the variables $\frac{Q(\cdot,t)}{C(\cdot)}$ and $\frac{\phi(\cdot,t)}{L(\cdot)}$ are respectively the voltage and the current. In this example, we impose the voltage in both boundaries of the transmission line and we measure the currents at both sides.

II.3.2 The vibrating string

In Figure II.2, we show the deformations of the strings of a guitar. We can model these deformations using the one-dimensional wave equation. We can model a single string with the following PDE:

$$\frac{\partial^2 w}{\partial t^2}(\zeta,t) = \frac{1}{\rho(\zeta)}\frac{\partial}{\partial \zeta}\left(T(\zeta)\frac{\partial w}{\partial \zeta}(\zeta,t)\right), \quad \begin{pmatrix} w(\zeta,0) \\ \frac{\partial w}{\partial t}(\zeta,0) \end{pmatrix} = \begin{pmatrix} w_0(\zeta) \\ v_0(\zeta) \end{pmatrix}, \tag{II.14}$$

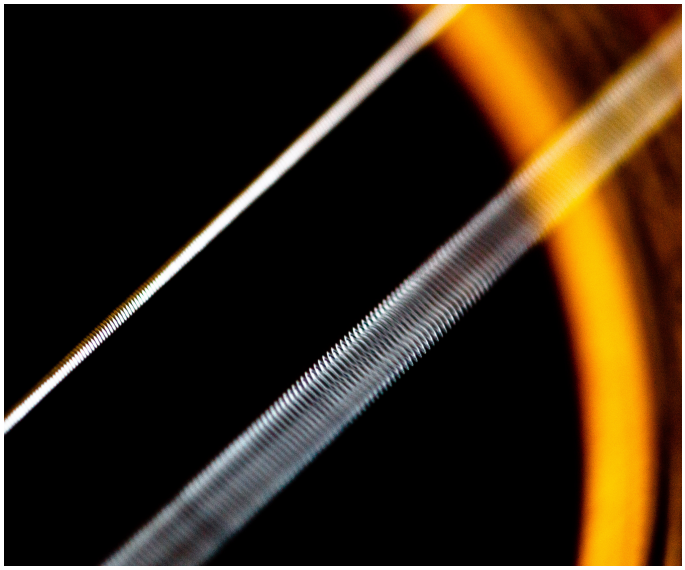

Figure II.2 – Vibrating strings in a guitar

where $\zeta \in [a, b]$ and $t \geq 0$ are the space and time variable, respectively. $w(\zeta, t)$ is the vertical position of the string with initial position and velocity given by $w_0(\zeta)$ and $v_0(\zeta)$, respectively. $T(\zeta)$ is the Young's modulus and $\rho(\zeta)$ is the mass density of the string. Note that, if the mass density and Young's modulus are constant, the PDE becomes

$$\frac{\partial^2 w}{\partial t^2}(\zeta, t) = c^2 \frac{\partial^2 w}{\partial \zeta^2}(\zeta, t), \quad c^2 = \frac{T}{\rho}. \tag{II.15}$$

We define as state variables the strain $q(\zeta, t) = \frac{\partial w}{\partial \zeta}(\zeta, t)$ and the momentum distribution $p(\zeta, t) = \rho(\zeta)\frac{\partial w}{\partial t}(\zeta, t)$, with initial conditions $q_0(\zeta) = \frac{dw_0}{d\zeta}(\zeta)$ and $p_0(\zeta) = \rho(\zeta)v_0(\zeta)$, respectively. Then, we can represent the vibrating string as in (II.11) with

$$x(\zeta, t) = \begin{pmatrix} q(\zeta, t) \\ p(\zeta, t) \end{pmatrix}, \quad x_0(\zeta) = \begin{pmatrix} q_0(\zeta) \\ p_0(\zeta) \end{pmatrix},$$

$$P_1 = \begin{pmatrix} 0 & 1 \\ 1 & 0 \end{pmatrix}, \quad P_0 = \begin{pmatrix} 0 & 0 \\ 0 & 0 \end{pmatrix}, \quad \mathcal{H} = \begin{pmatrix} T(\zeta) & 0 \\ 0 & \frac{1}{\rho(\zeta)} \end{pmatrix}.$$

The total energy is given by the sum of the kinetic and potential ones as follows:

$$H(t) = \frac{1}{2} \int_a^b \left[T(\zeta) q(\zeta, t)^2 + \frac{1}{\rho(\zeta)} p(\zeta, t)^2 \right] d\zeta.$$

The boundary port variables are obtained from (II.4) as follows

$$f_\partial(t) = \frac{1}{\sqrt{2}} \begin{pmatrix} \frac{p(b,t)}{\rho(b)} - \frac{p(a,t)}{\rho(a)} \\ T(b)q(b,t) - T(a)q(a,t) \end{pmatrix}, \quad e_\partial(t) = \frac{1}{\sqrt{2}} \begin{pmatrix} T(b)q(b,t) + T(a)q(a,t) \\ \frac{p(b,t)}{\rho(b)} + \frac{p(a,t)}{\rho(a)} \end{pmatrix}.$$

Then, the following input and output can be chosen as

$$\begin{pmatrix} \frac{p(a,t)}{\rho(a)} \\ T(b)q(b,t) \end{pmatrix} = u(t), \quad y(t) = \begin{pmatrix} -T(a)q(a,t) \\ \frac{p(b,t)}{\rho(b)} \end{pmatrix}$$

satisfying the conditions of Theorem II.2.3 with

$$W_{\mathcal{B}} = \frac{1}{\sqrt{2}} \begin{pmatrix} -1 & 0 & 0 & 1 \\ 0 & 1 & 1 & 0 \end{pmatrix}, \quad W_{\mathcal{C}} = \frac{1}{\sqrt{2}} \begin{pmatrix} 0 & 1 & -1 & 0 \\ 1 & 0 & 0 & 1 \end{pmatrix}, \quad \Sigma = \begin{pmatrix} 0_2 & I_2 \\ I_2 & 0_2 \end{pmatrix}.$$

Note that, the variables $T(\cdot)q(\cdot,t)$ and $\frac{p(\cdot,t)}{\rho(\cdot)}$ are respectively the force and the velocity. Here, we can for example act with a force actuator at the right side and clamp the string on the left side. The conjugated outputs are the force at the left side and the velocity at the right side.

II.3.3 The Timoshenko beam

We can use the Timoshenko beam to model the deformation of thick beams. We can use this, for instance, to model the solar panel deformation of a satellite, as shown in Figure II.3. We can

Figure II.3 – Satellite

represent the Timoshenko beam model with the following PDEs:

$$\rho(\zeta)\frac{\partial^2 w}{\partial t^2}(\zeta,t) = \frac{\partial}{\partial \zeta}\left(K(\zeta)\left(\frac{\partial w}{\partial \zeta}(\zeta,t) - \phi(\zeta,t)\right)\right) \tag{II.16}$$

$$I_\rho(\zeta)\frac{\partial^2 \phi}{\partial t^2}(\zeta,t) = \frac{\partial}{\partial \zeta}\left(EI(\zeta)\frac{\partial \phi}{\partial \zeta}(\zeta,t)\right) + K(\zeta)\left(\frac{\partial w}{\partial \zeta}(\zeta,t) - \phi(\zeta,t)\right) \tag{II.17}$$

$$\begin{pmatrix} w(\zeta,0) \\ \frac{\partial w}{\partial t}(\zeta,0) \end{pmatrix} = \begin{pmatrix} w_0(\zeta) \\ v_0(\zeta) \end{pmatrix}, \quad \begin{pmatrix} \phi(\zeta,0) \\ \frac{\partial \phi}{\partial t}(\zeta,0) \end{pmatrix} = \begin{pmatrix} \phi_0(\zeta) \\ \omega_0(\zeta) \end{pmatrix}, \tag{II.18}$$

where $\zeta \in [a, b]$ and $t \geq 0$ are the space and time, respectively. $w(\zeta, t)$ is the transverse displacement of the beam with initial displacement and velocity given by $w_0(\zeta)$ and $v_0(\zeta)$, respectively. $\phi(\zeta, t)$ is the rotation angle of a filament of the beam with initial rotation angle and angular velocity given by $\phi_0(\zeta)$ and $\omega_0(\zeta)$, respectively. $K(\zeta)$, $\rho(\zeta)$, $EI(\zeta)$ and $I_\rho(\zeta)$ are respectively the shear modulus, the mass density, the Young's modulus of elasticity multiplied by the moment of inertia of a cross section and the rotary moment of inertia of a cross section. We define as state variables the shear displacement $x_1(\zeta, t)$, the momentum $x_2(\zeta, t)$, the angular displacement $x_3(\zeta, t)$ and the angular momentum $x_4(\zeta, t)$ as follows:

$$\begin{aligned}
x_1(\zeta,t) &= \frac{\partial w}{\partial \zeta}(\zeta,t) - \phi(\zeta,t), & x_1(\zeta,0) &= x_{10}(\zeta),\\
x_2(\zeta,t) &= \rho(\zeta)\frac{\partial w}{\partial t}(\zeta,t), & x_2(\zeta,0) &= x_{20}(\zeta),\\
x_3(\zeta,t) &= \frac{\partial \phi}{\partial \zeta}(\zeta,t), & x_3(\zeta,0) &= x_{30}(\zeta),\\
x_4(\zeta,t) &= I_\rho(\zeta)\frac{\partial \phi}{\partial t}(\zeta,t), & x_4(\zeta,0) &= x_{40}(\zeta),
\end{aligned}$$

with $x_{10}(\zeta) = \frac{dw_0}{d\zeta}(\zeta) - \phi_0(\zeta)$, $x_{20}(\zeta) = \rho(\zeta)v_0(\zeta)$, $x_{30}(\zeta) = \frac{d\phi_0}{d\zeta}(\zeta)$ and $x_{40}(\zeta) = I_\rho(\zeta)\omega_0(\zeta)$. Then, we can represent the Timoshenko beam as in (II.11) with

$$x(\zeta,t) = \begin{pmatrix} x_1(\zeta,t)\\ x_2(\zeta,t)\\ x_3(\zeta,t)\\ x_4(\zeta,t)\end{pmatrix}, \quad x_0(\zeta) = \begin{pmatrix} x_{10}(\zeta)\\ x_{20}(\zeta)\\ x_{30}(\zeta)\\ x_{40}(\zeta)\end{pmatrix},$$

$$P_1 = \begin{pmatrix} 0 & 1 & 0 & 0\\ 1 & 0 & 0 & 0\\ 0 & 0 & 0 & 1\\ 0 & 0 & 1 & 0\end{pmatrix}, \quad P_0 = \begin{pmatrix} 0 & 0 & 0 & -1\\ 0 & 0 & 0 & 0\\ 0 & 0 & 0 & 0\\ 1 & 0 & 0 & 0\end{pmatrix}, \quad \mathcal{H} = \begin{pmatrix} K(\zeta) & 0 & 0 & 0\\ 0 & \frac{1}{\rho(\zeta)} & 0 & 0\\ 0 & 0 & EI(\zeta) & 0\\ 0 & 0 & 0 & \frac{1}{I_\rho(\zeta)}\end{pmatrix}.$$

The total energy is given by the sum of the kinetic and the potential ones as follows:

$$H(t) = \frac{1}{2}\int_a^b \left[K(\zeta)x_1(\zeta,t)^2 + \frac{1}{\rho(\zeta)}x_2(\zeta,t)^2 + EI(\zeta)x_3(\zeta,t)^2 + \frac{1}{I_\rho(\zeta)}x_4^2(\zeta,t)\right]d\zeta.$$

We obtain the boundary port variables from (II.4) as follows:

$$f_\partial(t) = \frac{1}{\sqrt{2}}\begin{pmatrix} \frac{x_2(b,t)}{\rho(b)} - \frac{x_2(a,t)}{\rho(a)}\\ K(b)x_1(b,t) - K(a)x_1(a,t)\\ \frac{x_4(b,t)}{I_\rho(b)} - \frac{x_4(a,t)}{I_\rho(a)}\\ EI(b)x_3(b,t) - EI(a)x_3(a,t)\end{pmatrix}, \; e_\partial(t) = \frac{1}{\sqrt{2}}\begin{pmatrix} K(b)x_1(b,t) + K(a)x_1(a,t)\\ \frac{x_2(b,t)}{\rho(b)} + \frac{x_2(a,t)}{\rho(a)}\\ EI(b)x_3(b,t) + EI(a)x_3(a,t)\\ \frac{x_4(b,t)}{I_\rho(b)} + \frac{x_4(a,t)}{I_\rho(a)}\end{pmatrix}.$$

Then, we can choose the following inputs and outputs:

$$\begin{pmatrix} \frac{x_2(a,t)}{\rho(a)} \\ \frac{x_4(a,t)}{I_\rho(a)} \\ K(b)x_1(b,t) \\ EI(b)x_3(b,t) \end{pmatrix} = u(t), \quad y(t) = \begin{pmatrix} -K(a)x_1(a,t) \\ -EI(a)x_3(a,t) \\ \frac{x_2(b,t)}{\rho(b)} \\ \frac{x_4(b,t)}{I_\rho(b)} \end{pmatrix},$$

satisfying the conditions of Theorem II.2.3 with

$$W_{\mathcal{B}} = \frac{1}{\sqrt{2}} \begin{pmatrix} -1 & 0 & 0 & 0 & 0 & 1 & 0 & 0 \\ 0 & 0 & -1 & 0 & 0 & 0 & 0 & 1 \\ 0 & 1 & 0 & 0 & 1 & 0 & 0 & 0 \\ 0 & 0 & 0 & 1 & 0 & 0 & 1 & 0 \end{pmatrix}, \quad W_{\mathcal{C}} = \frac{1}{\sqrt{2}} \begin{pmatrix} 0 & 1 & 0 & 0 & -1 & 0 & 0 & 0 \\ 0 & 0 & 0 & 1 & 0 & 0 & -1 & 0 \\ 1 & 0 & 0 & 0 & 0 & 1 & 0 & 0 \\ 0 & 0 & 1 & 0 & 0 & 0 & 0 & 1 \end{pmatrix},$$

$$\Sigma = \begin{pmatrix} 0_4 & I_4 \\ I_4 & 0_4 \end{pmatrix}.$$

Note that, the variables $K(\cdot)x_1(\cdot,t)$, $\frac{x_2(\cdot,t)}{\rho(\cdot)}$, $EI(\cdot)x_3(\cdot,t)$, $\frac{x_4(\cdot,t)}{I_\rho(\cdot)}$ are respectively the force, the velocity, the torque and the angular velocity. Here, we can for example act with a force and torque actuator at the right side and clamp the beam on the left side. The outputs are the force and torque at the left side and the transverse and angular velocity at the right side.

II.4 Controllability and observability of BC-PHSs

In control systems theory, the following two questions arise concerning the choice of the inputs and outputs:

(i) Is the input sufficient to move the state of the system to a desired one?

(ii) Is the output enough to describe the whole state of the system?

Controllability and *observability* are the properties of a control system that answer these questions. For linear *lumped parameter systems* (LPSs), these properties are guaranteed by checking a matrix condition [Kalman 69]. However, for linear *distributed parameter systems* (DPSs), it is not the case, and in general, it has to be analyzed on a case by case basis. See for example [Gugat 05, Zuazua 93] dealing with the one-dimensional wave equation. Concerning the BC-PHS (II.11), the questions become

(i) Is the input $u(t)$ sufficient to move the state $x(\zeta,t)$ to a desired state in the space $X = L_2([a,b],\mathbb{R}^n)$?

(ii) Is the knowledge of $y(t)$ enough to describe all the state $x(\zeta,t)$?

Recently, it has been shown that BC-PHSs are *exactly controllable* when they are *well-posed* [Jacob 19]. Similarly, BC-PHSs are *exactly observable* when they are *well-posed*. The *well-posedness* of a system is related to the existence and uniqueness of solutions of a system for some initial conditions. In the following, we define the *well-posedness*. Then, we show that the BC-PHS (II.11) is *well-posed*. Then, we define *exact controllability*. Finally, we recall the main theorem from [Jacob 19] which states that the BC-PHS (II.11) is *exactly controllable*.

Definition II.4.1. *[Jacob 19, Definition 2] The BC-PHS (II.11) is well-posed if there exist a $\tau > 0$ and $m_\tau \geq 0$ such that for all $x_0 \in D(\mathcal{A})$ and $u \in C^2([0,\tau];\mathbb{R}^n)$ with $u(0) = \mathcal{B}x_0$, the classical solution x (Definition A.4.2) and the output y satisfiy*

$$\|x(\tau)\|_X^2 + \int_0^\tau \|y(t)\|^2 \, dt \leq m_\tau \left(\|x_0\|_X^2 + \int_0^\tau \|u(t)\|^2 \, dt \right). \tag{II.19}$$

♣

As it has been mentioned in [Jacob 19], *the well-posedness* of a system is in general difficult to show for BCSs. See for example [Staffans 05] and [Tucsnak 14]. However, for BC-PHSs of the form (II.11), we can show it by a matrix condition as we show in the following theorem and remark.

Theorem II.4.1. *[Jacob 12, Theorem 13.2.2] The port-Hamiltonian system (II.11) is well-posed if and only if the operator*

$$Ax = \left(P_1 \frac{d}{d\zeta} + P_0 \right) (\mathcal{H}x), \quad x \in D(A) \tag{II.20}$$

with domain

$$D(A) = \left\{ x \in X, \;\; \mathcal{H}x \in H^1([a,b];\mathbb{R}^n) \mid W_{\mathcal{B}} \begin{pmatrix} f_\partial(t) \\ e_\partial(t) \end{pmatrix} = 0 \right\} \tag{II.21}$$

generates a strongly continuous semigroup on X (Definition A.4.4). ◊

Remark II.4.1. *Note that, from Theorem II.2.2, if $W_{\mathcal{B}} \Sigma W_{\mathcal{B}}^T \geq 0$, then the operator (II.20) with domain (II.21) generates a contraction semigroup on X. Thus, (II.11) is well-posed* ♣

Since the BC-PHS of interest is *well-posed*, we can show that it is *exactly controllable* also. To this end, we define the *exact controllability* and we recall the main result of [Jacob 19].

Definition II.4.2. *[Jacob 19, Definition 6] The well-posed port-Hamiltonian system (II.11) is exactly controllable, if there exists a time $\tau > 0$ such that for all $x_1 \in X$ there exists a control function $u(t) \in L^2([0,\tau],\mathbb{R}^n)$ such that the corresponding mild solution (Definition A.4.3) satisfies $x(0) = 0$ and $x(\tau) = x_1$.* ♣

Theorem II.4.2. *[Jacob 19] Every well-posed port-Hamiltonian system (II.11) is exactly controllable.* ◊

Similarly, as it is mentioned in [Jacob 19], by duality the BC-PHS (II.11) is also *exactly observable.*

Remark II.4.2. *Basically, in the fully actuated and fully sensed case, Theorem II.4.2 and its dual allow us to design controllers for achieving all possibles states on the space X and also, to design observers to reconstruct the state variables from the measurement of the output.* ♣

II.5 Stabilization of BC-PHSs

In [Villegas 07], the stabilization of BC-PHSs is studied. It is shown that by static or dynamic output feedback, the BC-PHS can be stabilized asymptotically or exponentially. When static output feedback is applied to the BC-PHS, exponential stability is achieved in closed-loop even when partial output feedback is applied [Villegas 09]. When dynamic output feedback is applied to the BC-PHS, asymptotic stability is achieved if the dynamical controller is *strictly positive real* (SPR) [Villegas 05].

This result is extended in [Ramirez 14], where the authors have shown that if the controller is a strictly inputs passive system, the closed-loop system is exponentially stable. In [Augner 14], the closed-loop stability is studied for a more general class of BC-PHSs that includes the Euler-Bernoulli beam, for example. Finally, in [Macchelli 13, Macchelli 17, Macchelli 20], the authors have studied the *energy shaping and damping injection* techniques. The resulting control laws using these strategies correspond, in general, to a state feedback control law. To implement these control laws, we require observers for the state variable estimation.

In the following, we recall the main stability results for BC-PHSs in closed-loop. We start with an important property, which states that the Hamiltonian of a BC-PHS is always bounded by the time integral of the co-energy variable evaluated at the spatial boundaries. Then, this result is used for showing the closed-loop stability when a controller is applied to the system.

Theorem II.5.1. *[Villegas 07, Theorem 5.17] Consider the BC-PHS (II.11) with $W_{\mathcal{B}}$ such that $W_{\mathcal{B}}\Sigma W_{\mathcal{B}}^T \geq 0$. If $u(t) = 0$, for all $t \geq 0$, then the Hamiltonian energy $H(t) = \frac{1}{2}\|x(t)\|_{\mathcal{H}}^2$ satisfies for τ large enough*

$$\begin{aligned} H(\tau) &\leq c(\tau) \int_0^\tau \|\mathcal{H}(b)x(b,t)\|_{\mathbb{R}}^2 dt, \quad \text{and} \\ H(\tau) &\leq c(\tau) \int_0^\tau \|\mathcal{H}(a)x(a,t)\|_{\mathbb{R}}^2 dt \end{aligned} \tag{II.22}$$

where $c(\tau)$ is a constant that only depends on τ. ◊

II.5.1 Static output feedback

The static output feedback for the BC-PHS (II.11) is represented as shown in Figure II.4 and is defined as follows:

$$u(t) = r(t) - \alpha y(t), \tag{II.23}$$

with $\alpha \in \mathbb{R}^{n\times n}$ such that $\alpha > 0$ and $r(t)$ an external input. Since we consider the BC-PHS (II.11)

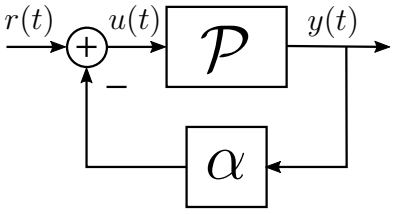

Figure II.4 – Static output feedback

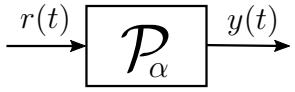

Figure II.5 – Equivalent representation of the static output feedback

as an impedance energy preserving system ($W_{\mathcal{B}}\Sigma W_{\mathcal{B}}^T = W_{\mathcal{C}}\Sigma W_{\mathcal{C}}^T = 0_n$ and $W_{\mathcal{C}}\Sigma W_{\mathcal{B}}^T = I_n$), the time derivative of the Hamiltonian is given by

$$\begin{aligned} \dot{H}(t) &= u(t)^T y(t) \\ &= r(t)^T y(t) - y(t)^T \alpha y(t). \end{aligned} \tag{II.24}$$

Then, the closed-loop system can be represented as a BC-PHS as well, but not anymore as an impedance energy preserving system. The closed-loop system is equivalently represented, as shown in Figure II.5 with the new input $r(t)$. The closed-loop system is written as the following BC-PHS:

$$\mathcal{P}_\alpha \begin{cases} \dfrac{\partial x}{\partial t}(\zeta,t) = P_1 \dfrac{\partial}{\partial \zeta}(\mathcal{H}(\zeta)x(\zeta,t)) + P_0\mathcal{H}(\zeta)x(\zeta,t), \quad x(\zeta,0) = x_0(\zeta), \\ W_\alpha \begin{pmatrix} f_\partial(t) \\ e_\partial(t) \end{pmatrix} = r(t), \qquad W_\alpha = W_\mathcal{B} + \alpha W_\mathcal{C}, \\ y(t) = W_\mathcal{C} \begin{pmatrix} f_\partial(t) \\ e_\partial(t) \end{pmatrix}. \end{cases} \tag{II.25}$$

Theorem II.5.2. *[Villegas 07, Theorem 5.17] The closed-loop system between the impedance energy preserving BC-PHS (II.11) and the static output feedback (II.23) is exponentially stable if $\alpha > 0$ and $r(t) = 0$.* ◊

Proof. *The reader is refer to [Villegas 07, Theorem 5.17] for the proof. However, since it is important for the following sections, we develop it in here.The proof is equivalent to show that the system (II.25) is exponentially stable. Note that the closed-loop system (II.25) is a BC-PHS as well. In fact, one can verify $W_\alpha \Sigma W_\alpha^T = \alpha^T + \alpha > 0$. Then, the system (II.25) satisfies the conditions of Theorem II.5.1 with respect to the new input $r(t)$ and the new input matrix W_α. Then, the Hamiltonian satisfies the estimations (II.22). Using one of these estimations, one can show the exponential stability by showing that the Hamiltonian is such that*

$$H(\tau) \leq \frac{c(\tau)}{c(\tau) + \alpha_1 m_1} H(0) \tag{II.26}$$

for some positive constants $c(\tau)$, α_1, m_1, and τ large enough. To find the estimation (II.26), we write the new input $r(t)$ and the output $y(t)$ as follows

$$\begin{pmatrix} r(t) \\ y(t) \end{pmatrix} = \frac{1}{\sqrt{2}} \begin{pmatrix} W_\alpha \\ W_\mathcal{C} \end{pmatrix} \begin{pmatrix} P_1 & -P_1 \\ I_n & I_n \end{pmatrix} \begin{pmatrix} \mathcal{H}(b)x(b,t) \\ \mathcal{H}(a)x(a,t) \end{pmatrix}. \tag{II.27}$$

We define the matrix

$$M = \frac{1}{\sqrt{2}} \begin{pmatrix} W_\alpha \\ W_\mathcal{C} \end{pmatrix} \begin{pmatrix} P_1 & -P_1 \\ I_n & I_n \end{pmatrix}. \tag{II.28}$$

The matrix $R_{ext} = \frac{1}{\sqrt{2}} \begin{pmatrix} P_1 & -P_1 \\ I_n & I_n \end{pmatrix}$ is invertible (See [Le Gorrec 05, Lemma 3.4]). The matrix $\begin{pmatrix} W_\alpha \\ W_\mathcal{C} \end{pmatrix}$ is also invertible. Indeed $\begin{pmatrix} W_\alpha \\ W_\mathcal{C} \end{pmatrix}$ is invertible if and only if $\begin{pmatrix} W_\alpha \Sigma W_\alpha^T & W_\alpha \Sigma W_\mathcal{C}^T \\ W_\mathcal{C} \Sigma W_\alpha^T & W_\mathcal{C} \Sigma W_\mathcal{C}^T \end{pmatrix}$ is invertible with $\Sigma = \begin{pmatrix} 0_n & I_n \\ I_n & 0_n \end{pmatrix}$ (See [Le Gorrec 05, Theorem 4.2]). Then, one can compute

$$\begin{pmatrix} W_\alpha \Sigma W_\alpha^T & W_\alpha \Sigma W_\mathcal{C}^T \\ W_\mathcal{C} \Sigma W_\alpha^T & W_\mathcal{C} \Sigma W_\mathcal{C}^T \end{pmatrix} = \begin{pmatrix} \alpha^T + \alpha & I_n \\ I_n & 0_n \end{pmatrix}, \tag{II.29}$$

which has an inverse and it is $\begin{pmatrix} 0_n & I_n \\ I_n & -(\alpha^T + \alpha) \end{pmatrix}$. Then, the matrix M in (II.28) is invertible as well. This implies that $\|Mw\|_\mathbb{R}^2 \geq m_1 \|w\|_\mathbb{R}^2$, for some vector w of appropriated dimension and a constant m_1 that can be the smallest eigenvalue of M, for instance. If we compute the norm at both sides of (II.27) with $r(t) = 0$ (by definition), we obtain the following

$$\|y(t)\|_\mathbb{R}^2 = \left\| M \begin{pmatrix} \mathcal{H}(b)x(b,t) \\ \mathcal{H}(a)x(a,t) \end{pmatrix} \right\|_\mathbb{R}^2 \geq m_1 \left\| \begin{pmatrix} \mathcal{H}(b)x(b,t) \\ \mathcal{H}(a)x(a,t) \end{pmatrix} \right\|_\mathbb{R}^2 \geq m_1 \|\mathcal{H}(b)x(b,t)\|_\mathbb{R}^2,$$

implying that the norm of the co-energy variables evaluated at the spatial boundaries are bounded by the norm of the output as follows

$$\|\mathcal{H}(b)x(b,t)\|_{\mathbb{R}}^2 \leq \frac{1}{m_1}\|y(t)\|_{\mathbb{R}}^2 \tag{II.30}$$

(similar for $\|\mathcal{H}(b)x(a,t)\|_{\mathbb{R}}^2$). Moreover, since α is positive definite, the norm of the output can be also bounded as follows

$$\|y(t)\|_{\mathbb{R}}^2 \leq \frac{1}{\alpha_1} y(t)^T \alpha y(t), \tag{II.31}$$

with α_1 a positive scalar that can be for instance the smallest eigenvalue of α. Then, from (II.30) and (II.31), one can conclude

$$\|\mathcal{H}(b)x(b,t)\|_{\mathbb{R}}^2 \leq \frac{1}{m_1\alpha_1} y(t)^T \alpha y(t). \tag{II.32}$$

Since the closed-loop system (II.25) is a BC-PHS and satisfies the conditions of Theorem II.5.1 with respect to the new input $r(t)$ and new input matrix W_α, we can use the estimations (II.22). Then, using (II.22) and (II.32) we obtain the following estimation for the Hamiltonian

$$H(\tau) \leq \frac{c(\tau)}{m_1\alpha_1} \int_0^\tau y(t)^T \alpha y(t) dt. \tag{II.33}$$

Finally, from (II.24) we obtain

$$H(\tau) - H(0) = -\int_0^\tau y(t)^T \alpha y(t) dt, \tag{II.34}$$

with $r(t) = 0$ (by definition). Replacing (II.34) into the estimation (II.33), we obtain the estimation (II.26), concluding the exponential stability of the closed-loop system. ■

Note that the last theorem corresponds to the case of a fully actuated and fully sensed scenario, *i.e.* when n actuators and n sensors are available. This is not always possible, either due to the lack of actuators or the lack of sensors. However, one can also achieve closed-loop exponential stability by partially output feedback if an additional condition is satisfied, as we state in the following corollary. In this case, the static output feedback for the BC-PHS (II.11) is defined as follows:

$$u(t) = r(t) - \beta y(t), \tag{II.35}$$

with $\beta \in \mathbb{R}^{n\times n}$ such that $\beta \geq 0$ and $r(t)$ an external input. Similarly as before, the closed-loop system is written as follows

$$\mathcal{P}_\beta \begin{cases} \dfrac{\partial x}{\partial t}(\zeta,t) = P_1 \dfrac{\partial}{\partial \zeta}(\mathcal{H}(\zeta)x(\zeta,t)) + P_0\mathcal{H}(\zeta)x(\zeta,t), \quad x(\zeta,0) = x_0(\zeta), \\ W_\beta \begin{pmatrix} f_\partial(t) \\ e_\partial(t) \end{pmatrix} = r(t), \qquad W_\beta = W_{\mathcal{B}} + \alpha W_{\mathcal{C}}, \\ y(t) = W_{\mathcal{C}} \begin{pmatrix} f_\partial(t) \\ e_\partial(t) \end{pmatrix}. \end{cases} \tag{II.36}$$

Corollary II.5.1. *[Villegas 07, Corollary 5.19]. The closed-loop system between the impedance energy preserving BC-PHS (II.11) and the static output feedback (II.35) is exponentially stable if $\beta \geq 0$, $r(t) = 0$, and one of the following conditions is satisfied*

$$\begin{aligned} \|\mathcal{H}x(b,t)\|^2_{\mathbb{R}} &\leq k_1 y(t)^T \beta y(t) \quad or \\ \|\mathcal{H}x(a,t)\|^2_{\mathbb{R}} &\leq k_1 y(t)^T \beta y(t) \end{aligned} \tag{II.37}$$

for some positive constant k_1. ◊

Proof. *The proof is equivalent to show that the system (II.36) is exponentially stable. One can show that the closed-loop system (II.36) is again a BC-PHS and satisfies the conditions in Theorem II.5.1 with respect to the new input $r(t)$ and the new input matrix W_β. Indeed, one can verify $W_\beta \Sigma W_\beta^T = \beta^T + \beta \geq 0$. Then, the closed-loop system (II.36) satisfies the estimations (II.5.1). Then, using (II.5.1) and (II.37), the following estimation is satisfied*

$$H(\tau) \leq c(\tau) k_1 \int_0^\tau y(t)^T \beta y(t) dt \tag{II.38}$$

Finally, from (II.24) we obtain

$$H(\tau) - H(0) = -\int_0^\tau y(t)^T \beta y(t) dt, \tag{II.39}$$

with $r(t) = 0$ (by definition). Replacing (II.39) into the estimation (II.38), we obtain the estimation

$$H(\tau) \leq \frac{c(\tau)}{c(\tau) + k_1^{-1}} H(0). \tag{II.40}$$

This concludes the proof. ■

When applying *damping injection* (static output feedback), the achievable closed-loop performances are limited to the change of the damping ratio, only. If other performances are required in closed-loop (modifying the settling time, for instance), dynamic output feedback has to be considered. In the following section, we present the case when the controller is a dynamic system, and the control law depends on the state variables of the controller. With this type of controller, one can use the *energy shaping* control strategy, for instance.

II.5.2 Dynamic output feedback

The dynamic output feedback is represented in Figure II.6, where $\mathcal{P}$ is the BC-PHS (II.11), and C is the finite-dimensional controller in a port-Hamiltonian form. $u(t)$ and $y(t)$ are respectively the input and output of the BC-PHS, and $u_c(t)$ and $y_c(t)$ are respectively the input and output of the controller. $r(t)$ is an external input, and the passive interconnection is given by

$$\begin{pmatrix} u(t) \\ u_c(t) \end{pmatrix} = \begin{pmatrix} 0 & -1 \\ 1 & 0 \end{pmatrix} \begin{pmatrix} y(t) \\ y_c(t) \end{pmatrix} + \begin{pmatrix} 1 \\ 0 \end{pmatrix} r(t). \tag{II.41}$$

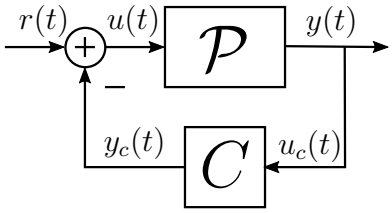

Figure II.6 – Dynamic output feedback

The finite-dimensional controller C is defined as follows:

$$C\begin{cases}\dot{x}_c(t) = A_c x_c(t) + B_c u_c(t)\\ y_c(t) = C_c x_c(t) + D_c u_c(t),\end{cases} \tag{II.42}$$

where $x_c \in \mathbb{R}^{n_c}$, $u_c \in \mathbb{R}^{m_c}$, $y_c \in \mathbb{R}^{m_c}$ are the state, input, and output, respectively. $A_c \in \mathbb{R}^{n_c \times n_c}$, $B_c \in \mathbb{R}^{n_c \times m_c}$, $C_c \in \mathbb{R}^{m_c \times n_c}$ and $D_c \in \mathbb{R}^{m_c \times m_c}$ are all matrices to be designed, such that $A_c = (J_c - R_c)Q_c$, $B_c = G_c - P_c$, $C_c = (G_c + P_c)^\top Q_c$ and $D_c = M_c + S_c$, where $J_c = -J_c^\top$, $R_c = R_c^\top$, $M_c = -M_c^\top$ and $S_c = S_c^\top$, satisfying

$$\begin{pmatrix} R_c & P_c \\ P_c^\top & S_c \end{pmatrix} \geq 0 \quad \textit{and} \quad Q_c = Q_c^\top > 0.$$

Furthermore, we assume for the system (II.42) that (A_c, B_c) is controllable and (A_c, C_c) is observable. The Hamiltonian of the controller is given by

$$H_c(t) = \frac{1}{2} x_c(t)^T Q_c x_c(t), \tag{II.43}$$

and the closed-loop Hamiltonian related to the closed-loop system represented in Figure II.6 is given by

$$V(t) = \frac{1}{2}\int_a^b x(\zeta,t)^T \mathcal{H}(\zeta) x(\zeta,t) d\zeta + \frac{1}{2} x_c(t)^T Q_c x_c(t). \tag{II.44}$$

If we impose some conditions on the dynamic controller, we can guarantee the closed-loop stability between the BC-PHS (II.11) and the dynamic controller (II.42) (represented in Figure II.6). In [Morgül 94, Morgul 98, Morgül 02, Yang 05] the authors use *positive real* (PR) and *strictly positive real* (SPR) controllers to stabilize the one-dimensional wave equation. This idea is extended and generalized for BC-PHSs in [Villegas 07, Ramirez 14]. In the following, we recall these results. To this end, the definitions of *positive real*, and *strictly positive real* systems are presented (Definition (II.5.1) and Definition (II.5.2)). The equivalent state-space representation of SPR systems is presented in Lemma II.5.1. Finally, a particular case of finite-dimensional port-Hamiltonian systems is presented as an SPR system (Corollary II.5.2).

Definition II.5.1. *A $n \times n$ matrix $G(s)$ of real rational functions is positive real (PR) if:*

1. *All elements of $G(s)$ are analytic in the open right-half plane $Re(s) > 0$.*
2. *Poles of any element of $G(s)$ on the jw-axis are distinct, and the associated residue matrix of $G(s)$ is ≥ 0.*

3. $G(jw) + G^T(-jw) \geq 0$ *for all* w *which are not a pole of any element of* $G(jw)$*.*

♣

Definition II.5.2. *A* $n \times n$ *matrix* $G(s)$ *of real rational functions is strictly positive real (SPR) if there exists a scalar* $\varepsilon > 0$ *such that* $G(s-\varepsilon)$ *is PR.* ♣

Example II.5.1. *The following scalar transfer function* $G(s) = \frac{1}{s}$*.* $G(s)$ *has all its coefficients positives, it has a single pole at* $s = 0$ *with residue* 1*, and* $G(jw) + G^T(-jw) = 0$ *for all* $w \neq 0$*. However,* $G(s)$ *is not SPR, since* $G(s-\varepsilon)$ *is not PR due to the first and third condition of Definition II.5.1.* ♣

Lemma II.5.1. *(Kalman-Yakubovich-Popov KYP-Lemma) Assume for the system (II.42) that* (A_c, B_c) *is controllable and* (A_c, C_c) *is observable. Then, the transfer matrix* $G(s) = C_c(sI - A_c)^{-1}B_c + D_c$ *is SPR if and only if there exist real matrices* $P = P^T > 0$*,* Γ*,* W *and a scalar* $\varepsilon > 0$ *such that*

$$PA_c + A_c^T P = -\Gamma^T\Gamma - \varepsilon P \tag{II.45a}$$

$$C_c - B_c^T P = W^T\Gamma \tag{II.45b}$$

$$D_c + D_c^T = W^T W \tag{II.45c}$$

◊

Corollary II.5.2. *The system (II.42) with* $A_c = (J_c - R_c)Q_c$*,* $C_c = B_c^T Q_c$ *and* $D_c = 0$ *is strictly positive real if* $J_c = -J_c^T$*,* $R_c = R_c^T > 0$ *and* $Q_c = Q_c^T > 0$*.* ◊

Proof. *From Lemma II.5.1 choose* $P = Q_c$ *and* $W = 0$*, then (II.45c) is trivial, (II.45b) is* $C_c = B_c^T Q_c$ *and (II.45a) becomes*

$$\Gamma^T\Gamma = 2Q_c R_c Q_c - \varepsilon Q_c \tag{II.46}$$

then, for $R_c > 0$ *there exists a constant* $\varepsilon > 0$ *such that the right hand side is positive definite, giving a solution for* Γ*, using for instance Cholesky factorization. See for example [Horn 12, Corollary 7.2.9].* ■

From Corollary II.5.2, one can show that the finite-dimensional port-Hamiltonian system (II.42) is SPR if $D_c = 0$ and $R_c > 0$. In the following theorem, the asymptotic stability is guaranteed when an SPR finite-dimensional controller is applied to the BC-PHS in a power preserving way.

Theorem II.5.3. *[Villegas 07, Chapter 5.1.2] Consider the impedance energy preserving BC-PHS (II.11) with* $W_\mathcal{B}$ *and* $W_\mathcal{C}$ *defined according to Theorem II.2.3. Consider the finite-dimensional controller (II.42) such its transfer matrix is SPR (Lemma II.5.1). Then, the closed-loop system between (II.11) and (II.42) using the interconnection (II.41) is well-posed and converges asymptotically to zero for* $r(t) = 0$*.* ◊

Proof. *The reader is refer to [Villegas 07, Theorem 5.8] for the well-posedness of the closed-loop system, to [Villegas 07, Theorem 5.9] for the precompactness of the solution trajectories of the closed-loop system, and to [Villegas 07, Theorem 5.10] for the asymptotic stability of the closed-loop.* ■

A particular case of Theorem II.5.3 is when the dynamic controller (II.42) is defines as in Corollary II.5.2. Then, we can write the following Corollary from Theorem II.5.3.

Corollary II.5.3. *Consider the impedance energy preserving BC-PHS (II.11) with $W_{\mathcal{B}}$ and $W_{\mathcal{C}}$ defined according to Theorem II.2.3. Consider the finite-dimensional controller (II.42) with $A_c = (J_c - R_c)Q_c$, $C_c = B_c^T Q_c$, $D_c = 0$, $J_c = -J_c^T$, $R_c = R_c^T > 0$ and $Q_c = Q_c^T > 0$. Assume that (A_c, B_c) is controllable and (A_c, C_c) is observable. The closed-loop system between (II.11) and (II.42) using the interconnection (II.41) is well-posed and converges asymptotically to zero for $r(t) = 0$.* ◊

Proof. *In this case, the controller is an SPR system as well as in Theorem II.5.3 (see Corollary II.5.2 to verify the conditions). Then, for the well-posedness of the closed-loop system, this is an application case of [Villegas 07, Theorem 5.8]. For the precompactness of the solution trajectories of the closed-loop system, this is an application case of [Villegas 07, Theorem 5.9]. Then, for the asymptotic stability, we use LaSalle's invariance principle provided that the closed-loop is well-posed and the solution trajectories are precompact (See [Luo 12, Theorem 3.64]). It follows that all solutions of the closed-loop system tend to the maximal invariant set of*

$$\vartheta_c = \{x \in L_2([a,b], \mathbb{R}^n),\ x_c \in \mathbb{R}^{n_c} \mid \dot{V}(t) = 0\}. \tag{II.47}$$

We define the maximal invariant subset of ϑ_c as $\mathcal{I}$, and we show that $\mathcal{I}$ only contains the zero state, i.e. $\mathcal{I} = \{x(\zeta, t) = 0,\ x_c(t) = 0\}$. From (II.44), (II.11), and (II.42), we obtain the following balance equation

$$\dot{V}(t) = -x_c(t)^T Q_c R_c Q_c x_c(t). \tag{II.48}$$

Since $R_c > 0$, $\dot{V}(t) = 0$ implies $x_c(t) = 0$, which implies $\dot{x}_c(t) = 0$. Then, from (II.42) $B_c u_c(t) = 0$. Since the controller is controllable, $u_c(t) = 0$. Since $D_c = 0$ and $x_c(t) = 0$, from (II.42) $y_c(t) = 0$. Since $u_c(t) = y_c(t) = 0$, from the interconnection we can conclude (II.41) $y(t) = u(t) = 0$. Then, since the invariant solution of the closed-loop system, subject to $\dot{V}(t) = 0$, corresponds to the solution of the PDE with all the boundary variables set to zero, hence from Holmgren's Theorem (See [John 49]) the only solution is $x(\zeta, t) = 0$. Thus, the asymptotic stability of the closed-loop system is guaranteed. ■

Achieving exponential stability when interconnecting the BC-PHS (II.11) with the finite-dimensional controller (II.42) as Figure II.6 shows, requires and additional conditions on the controller. The controller has to be strictly input passive [Ramirez 14], *i.e.* $D_c > 0$.

Theorem II.5.4. *[Ramirez 14, Theorem IV.2] Consider the BC-PHS (II.11), the controller (II.42), and the interconnection (II.41) with $r(t) = 0$, for all $t \geq 0$. The closed-loop is exponentially stable if A_c is Hurwitz, D_c is positive definite and one of the following conditions is satisfied*

$$\begin{aligned} &\|u(t)\|^2 + \|y(t)\|^2 \geq \epsilon \|\mathcal{H}(b)x(b,t)\|^2, \quad \text{or} \\ &\|u(t)\|^2 + \|y(t)\|^2 \geq \epsilon \|\mathcal{H}(a)x(a,t)\|^2. \end{aligned} \tag{II.49}$$

◊

Assigning performances to the closed-loop system is in general achieved using *damping injection* and *energy shaping* [Macchelli 04a, Pasumarthy 07, Macchelli 11, Schöberl 12, Macchelli 13, Macchelli 17, Malzer 19]. *Damping injection* (static output feedback) allows ensuring the closed-loop stability, while *energy shaping* allows assigning performances in terms of the closed-loop energy. The *energy shaping* control strategy is achieved by relating the state of the controller to the state of the system. Then, the closed-loop energy (II.44) can be shaped by choosing Q_c. This is usually achieved by using structural invariants or *Casimir functions* [Schöberl 12, Macchelli 17, Macchelli 20]. Since

the state of the controller is related to the state of the plant, the control law can be applied either by state feedback $u(t) = \beta(x(\cdot, t))$ or by *control by interconnection* ($u(t) = -y_c(t)$) between the BC-PHS (II.11) and the dynamic controller (II.42) through (II.41). For the state feedback, knowledge of the state of the system is required. For the *control by interconnection* technique, proper initialization of the dynamic controller is required.

In this thesis, we use observers for applying the state feedback control law without requiring the knowledge of the complete state of the plant, neither a proper initialization of the controller. In the following section, a motivational example is presented using the vibrating string example, where some desired control law (derived by *energy shaping* and *damping injection*) is implemented using observers. We illustrate the effect of improper initialization when applying the desired control law using a dynamic controller. Then, an alternative observer-based control strategy is proposed using both *early* and *late-lumping* approaches.

II.6 Motivation example: observer-based control

In this section, we consider the vibrating string of Example II.3.2 with $\rho(\zeta) = T(\zeta) = 1$, and $\zeta \in [a, b] = [0, 1]$. The string is attached at the left side and is controlled with a force actuator at the right side. The desired control law is obtained using for instance the *energy shaping* method proposed in [Macchelli 17]. The obtained control law is a state feedback control law and we compare it with the closed-loop when *control by interconnection* is used instead of the state feedback, and when the observer-based approach is used. Using *control by interconnection* we show that the controller has to be initialized properly, and using the observer-based approach, we show that a proper initialization is not required.

The PDE and boundary conditions describing the system are given by

$$\mathcal{P}\begin{cases} \dfrac{\partial}{\partial t}\begin{pmatrix} q(\zeta,t) \\ p(\zeta,t) \end{pmatrix} = \begin{pmatrix} 0 & 1 \\ 1 & 0 \end{pmatrix} \dfrac{\partial}{\partial \zeta}\begin{pmatrix} q(\zeta,t) \\ p(\zeta,t) \end{pmatrix}, \quad \begin{pmatrix} q(\zeta,0) \\ p(\zeta,0) \end{pmatrix} = \begin{pmatrix} q_0(\zeta) \\ p_0(\zeta) \end{pmatrix}, \\ p(0,t) = 0, \\ q(1,t) = u(t), \\ y(t) = p(1,t), \end{cases} \tag{II.50}$$

Note that, with unitary parameters, the strain is equivalent to the force and the momentum is equivalent to the velocity. We consider the following control law

$$u(t) = -w(1,t) - p(1,t), \tag{II.51}$$

where $w(1,t)$ and $p(1,t)$ are respectively, the displacement and the velocity at $\zeta = 1$. Due to the fact that $q(\zeta,t) = w_\zeta(\zeta,t)$ and that the string is attached at the left side ($w(0,t) = 0$), the control law (II.51) can be written equivalently as

$$u(t) = -\int_0^1 q(\zeta,t)d\zeta - p(1,t), \tag{II.52}$$

and it can be seen as a state feedback control law. Then, for the real implementation it is required the velocity at $\zeta = 1$, and either the string deformation at $\zeta = 1$, or the force $q(\zeta,t)$. In the following, three different control laws are applied to (II.50) in order to approach the desired control law (II.51) or (II.52), using as measurement the velocity at $\zeta = 1$ only.

In each case, we simulate the BC-PHS (II.50) using the discretization methods proposed in [Trenchant 18]. The reader is refered to Appendix A for further details. For the spatial discretization we use finite differences on staggered grid with 200 state variables, and for the time discretization we use the midpoint rule with time step $\delta t = 0.1ms$. We consider the following initial conditions for the BC-PHS (II.50)

$$q_0(\zeta) = 0.1, \quad p_0(\zeta) = 0, \quad w(\zeta,0) = 0.1\zeta.$$

Using the desired control law ((II.51) or (II.52)), the string deformation $w(\zeta,t)$ along time and space is shown in Figure II.7. In this figure, and in all subsequent figures the bold black lines represent the initial and final string deformation ($w(\zeta,0)$, $w(\zeta,10)$), and the green line represents the desired end-tip string deformation $w(1,t)$. We consider that the response shown in Figure II.7 is the desired one. In the following sections, we aim to apply the control law (II.51) by measuring $p(1,t)$ only.

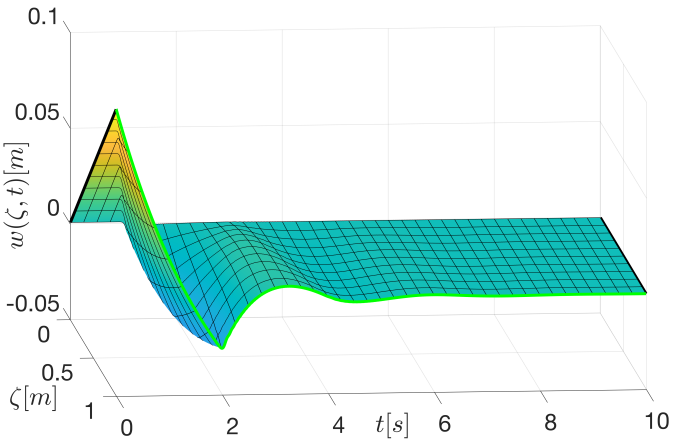

Figure II.7 – String deformation (Desired behavior)

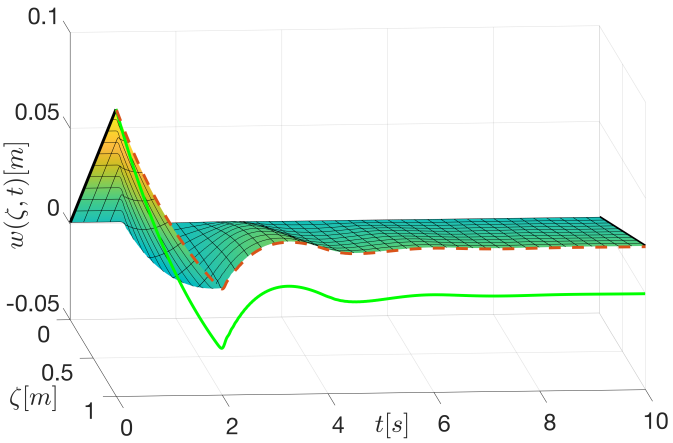

Figure II.8 – String deformation (*control by interconnection*)

Remark II.6.1. *Note that, the control law* (II.52) *is a particular case of a more general control law given by* $u(t) = -q_c \int_0^1 q(\zeta,t)d\zeta - d_c \frac{1}{\rho(1)} p(1,t)$. *In this more general representation, by properly tuning the parameters* q_c *and* d_c, *one can speed up or speed down the end-tip position of the string, allowing to modify its settling time. The reader is referred to [Macchelli 17] for further details of this control law.* ♣

II.6.1 Control by interconnection

One way to achieve the desired behavior (Figure II.7) by only measuring $p(1,t)$ is using the *control by interconnection* method between (II.50) and the dynamic controller

$$\dot{x}_c(t) = u_c(t), \qquad x_c(0) = x_{c0} \tag{II.53a}$$
$$y_c(t) = x_c(t) + u_c(t), \tag{II.53b}$$

with the passive interconnection (II.41). In this case, the structural invariant is $x_c(t) = w(1,t)$ if $x_c(0) = w(1,0)$. With this initialization, the interconnection with the dynamic controller is equivalent to the state feedback (II.52). In what follows, we consider the initialization is not ideal.

We simulate the BC-PHS (II.50) with the control law obtained using the controller (II.53) and the interconnection (II.41) with $r(t) = 0$ and initial condition $x_c(0) = x_{c0} = 0.05$. Figure II.8 shows the deformation response, where a similar behaviour to the desired one (Figure II.7) is obtained. However, the end-tip response $w(1,t)$ (orange dashed line) does not approach the desired end-tip response (green line). And indeed, both closed-loop systems converge to a different equilibrium position for the string deformation. We see then, that *control by interconnection* is not robust with respect to the error in the initialization. In the following, we use observers for achieving the same equilibrium independently of the initial conditions.

II.6.2 Observer-based control: *early-lumping approach*

Using the *early-lumping approach*, the infinite-dimensional model (II.50) is first discretized into a finite-dimensional one. Then, a state feedback and a Luenberger observer are designed on the finite-dimensional model. We define the following Luenberger observer-based control law

$$u(t) = -K\hat{x}(t) \tag{II.54}$$

$$\dot{\hat{x}}(t) = A_d\hat{x}(t) + B_d u(t) + L(y(t) - C_d\hat{x}(t)), \quad \hat{x}(0) = \hat{x}_0, \tag{II.55}$$

where $\hat{x}(t) \in \mathbb{R}^{n_d}$ is the estimation of the finite-dimensional state (from the discretized model), $\hat{x}_0 \in \mathbb{R}^{n_d}$ is the initial condition of the observer, $u(t) \in \mathbb{R}$ is the control law, and $y(t) \in \mathbb{R}$ is the measured velocity at $\zeta = 1$. For simplicity, the matrices $A_d \in \mathbb{R}^{n_d \times n_d}$, $B_d \in \mathbb{R}^{n_d \times 1}$, and $C_d \in \mathbb{R}^{1 \times n_d}$ are obtained using finite-differences on staggered grids [Trenchant 18]. Note that, it is the same discretization method for the BC-PHS (II.50), but the observer (II.54) uses less state variables than the BC-PHS. For simplicity, we show in Figure II.9 a grid example that takes $n_d = 8$, *i.e.* 4 elements for the force $q(\zeta, t)$ and 4 elements for the velocity $p(\zeta, t)$.

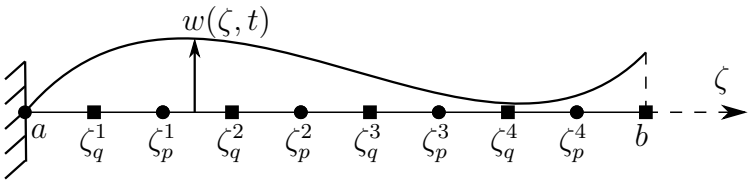

Figure II.9 – Discretization scheme using staggered grids.

In this case, the observer state is given by

$$\hat{x}(t) = \begin{pmatrix} \hat{q}(t) \\ \hat{p}(t) \end{pmatrix}, \quad \hat{q}(t) = \begin{pmatrix} \hat{q}_1(t) \\ \vdots \\ \hat{q}_{n_q}(t) \end{pmatrix}, \quad \hat{p}(t) = \begin{pmatrix} \hat{p}_1(t) \\ \vdots \\ \hat{p}_{n_p}(t) \end{pmatrix},$$

where $\hat{q}_i(t)$ is the observed strain at $\zeta = \zeta_q^i$ for $i = \{1, \cdots, n_q\}$, and $\hat{p}_i(t)$ is the observed momentum at $\zeta = \zeta_p^i$ for $i = \{1, \cdots, n_p\}$, and $n_q = n_p = \frac{n_d}{2}$. The following control law

$$u(t) = -h \sum_{i=1}^{n_q} \hat{q}_i(t) - \hat{p}_{n_p}(t) \tag{II.56}$$

approximates the state feedback (II.52) with $h = \frac{2}{n_d+1}$ being the length of the grid.

Remark II.6.2. *Since we aim to apply a complete observer-based state feedback, we use* $\hat{p}_{np}(t)$ *instead of* $y(t) = p(1,t)$ *in the control law* (II.56). ♣

The state feedback gain K is obtained directly from (II.56) as

$$K = \begin{pmatrix} K_q & K_p \end{pmatrix}_{n_d \times 1}, \quad K_q = \begin{pmatrix} h & \cdots & h \end{pmatrix}_{n_q \times 1}, \quad K_p = \begin{pmatrix} 0 & \cdots & 0 & 1 \end{pmatrix}_{n_p \times 1}.$$

The matrix L is obtained such that the Luenberger observer in (II.54) estimates the state variables of the finite-dimensional model and such that (II.54) stabilizes asymptotically the BC-PHS (II.50). In Chapter III, the synthesis of the observer gain is developed such that this is satisfied.

Using the observer-based state feedback controller (II.54) with initial conditions $\hat{x}(0) = 0$ and $n_d = 80$, the string deformation behaves as shown in Figure II.10, and the observed deformation behaves as in Figure II.11. We see that using the observer-based controller, similar performances than the ones obtained in Figure II.7 are achieved. Figure II.12 and Figure II.13 show closed-loop simulations with different initial conditions. Once again the observer-based controller allows to achieve the desired closed-loop performances.

Remark II.6.3. *The observer-based controller* (II.54) *is a dynamic system with* $n_d = 80$ *state variables and the vibrating string* (II.50) *is simulated as a finite-dimensional system using* 200 *state variables.* ♣

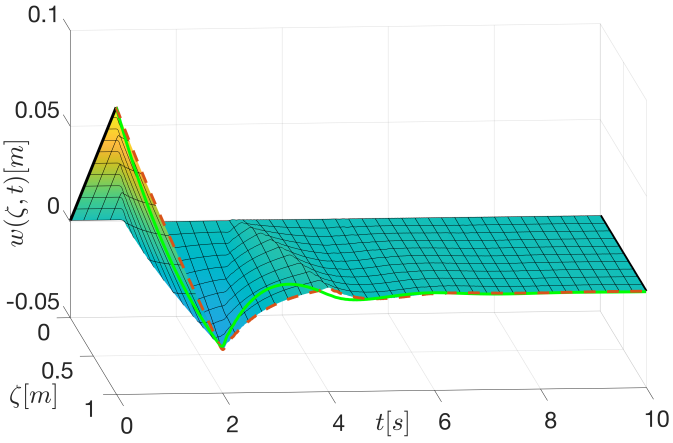

Figure II.10 – String deformation

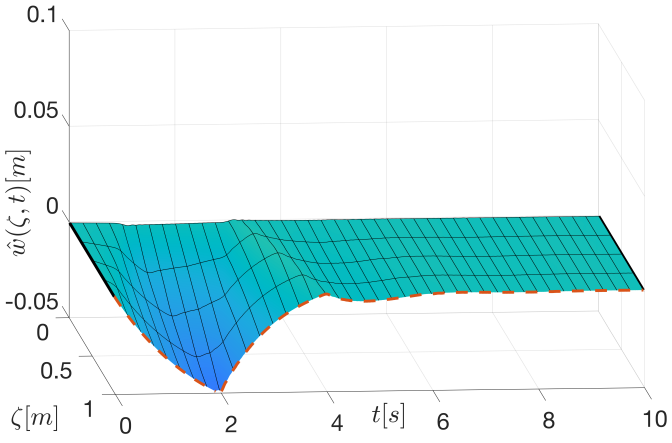

Figure II.11 – Observed deformation

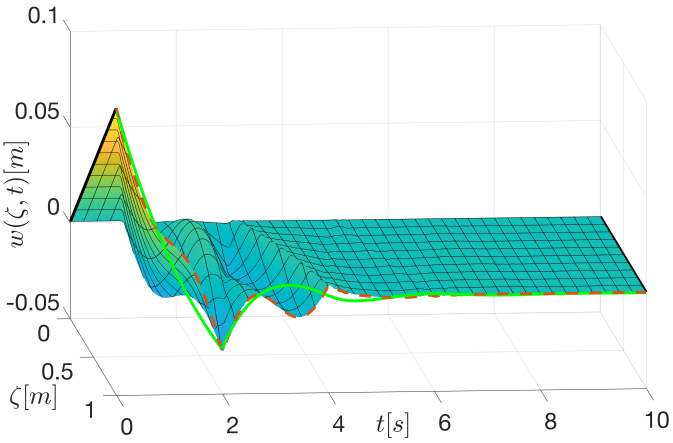

Figure II.12 – String deformation

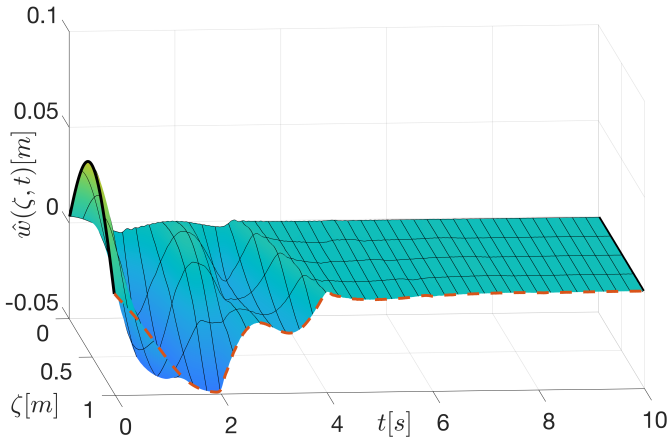

Figure II.13 – Observed deformation

II.6.3 Observer-based control: *late-lumping approach*

Using the *late-lumping approach*, the infinite-dimensional model (II.50) is used for the observer design. We define the following infinite-dimensional observer

$$\begin{aligned}\frac{\partial}{\partial t}\begin{pmatrix}\hat{q}(\zeta,t)\\ \hat{p}(\zeta,t)\end{pmatrix} &= \begin{pmatrix}0 & 1\\ 1 & 0\end{pmatrix}\frac{\partial}{\partial \zeta}\begin{pmatrix}\hat{q}(\zeta,t)\\ \hat{p}(\zeta,t)\end{pmatrix}, \quad \begin{pmatrix}\hat{q}(\zeta,0)\\ \hat{p}(\zeta,0)\end{pmatrix} = \begin{pmatrix}\hat{q}_0(\zeta)\\ \hat{p}_0(\zeta)\end{pmatrix},\\ \hat{p}(0,t) &= 0,\\ \hat{q}(1,t) &= u(t) + y(t) - \hat{p}(1,t),\end{aligned} \tag{II.57}$$

where $\hat{q}(\zeta,t)$ is the estimation of the strain $q(\zeta,t)$, and $\hat{p}(\zeta,t)$ is the estimation of the momentum $p(\zeta,t)$. $\hat{q}_0(\zeta)$ and $\hat{p}_0(\zeta)$ are the observer initial condition for the strain and momentum, respectively. $u(t)$ is the control law and $y(t)$ is the velocity of the string at $\zeta = 1$. In Chapter IV, we will show that the observer (II.57) converges exponentially to the state of the BC-PHS (II.50). Then, the following control law

$$u(t) = -\int_0^1 \hat{q}(\zeta,t)d\zeta - \hat{p}(1,t) \tag{II.58}$$

approximates the desired one (II.52) as soon as the observer converge to the real state. In Chapter IV, we show that this control law makes the closed-loop system (composed by (II.50),(II.57), and (II.58)) asymptotically stable.

Using the infinite-dimensional observer (II.57) with the control law (II.58) in the BC-PHS (II.50) the string deformation behaves as shown in Figure II.14, and the observed deformation behaves as in Figure II.15. Both variables achieve the zero equilibrium, and independently of the observer initial conditions, the same equilibrium is achieved as shown in Figure II.16 and Figure II.17 where different initial conditions are considered.

Remark II.6.4. *Different to the early-lumping approach, in this case the observer is an infinite-dimensional system and it has to be discretized for practical implementations. However, since the discretization is not the aim of this thesis, both systems (the vibrating string* (II.50) *and the observer* (II.57)*) are simulated as finite-dimensional systems with* 200 *state variables each one.* ♣

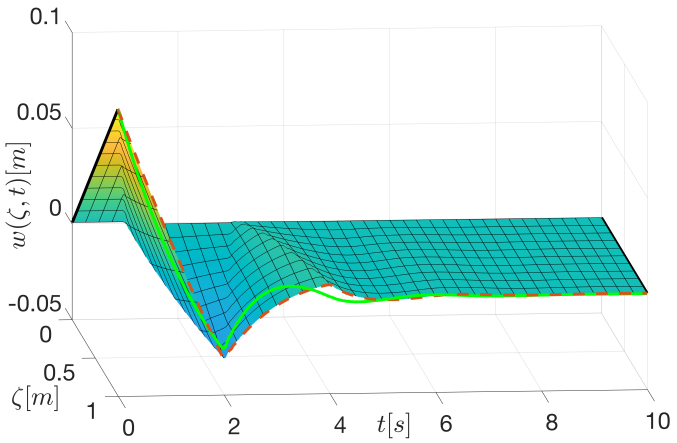

Figure II.14 – String deformation

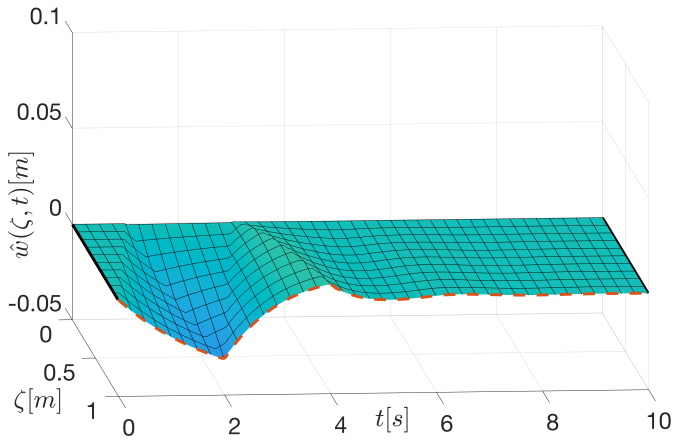

Figure II.15 – Observed deformation

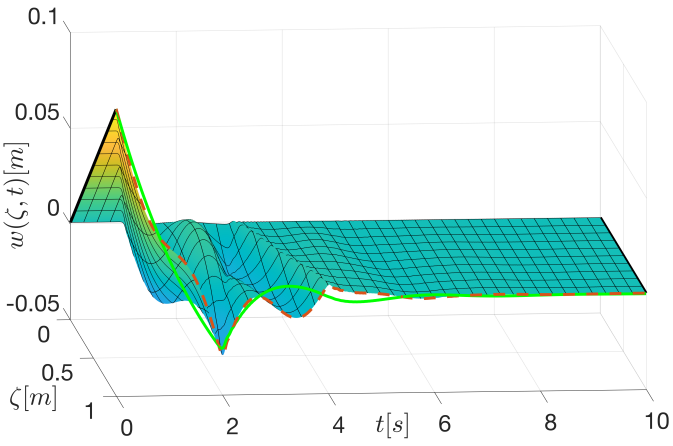

Figure II.16 – String deformation

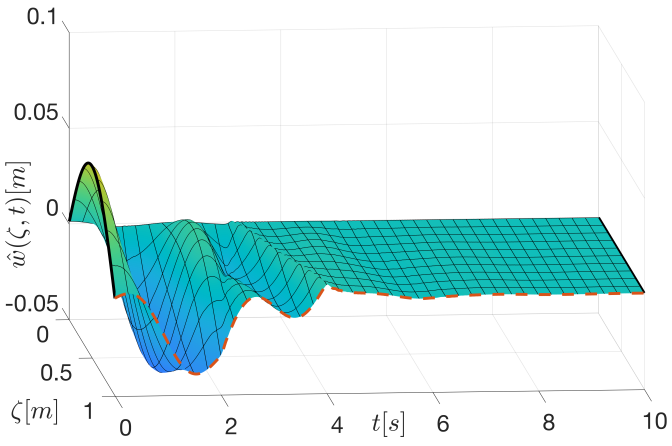

Figure II.17 – Observed deformation

II.7 Conclusion

In this chapter, a background on boundary controlled port-Hamiltonian systems (BC-PHSs) has been presented. First, we have introduced the class of *impedance energy preserving* BC-PHSs of interest in this thesis. Then, we have given some classic examples of them. The parametrization of the boundary conditions leading to a *well-posed* system has been given as well. Then, the *exact controllability* and the *exact observability* properties have been discussed for BC-PHSs. Finally, the closed-loop stability has been studied when static output feedback and dynamic output feedback is applied to the BC-PHS of interest. In both cases, the conditions for guaranteeing closed-loop stability has been presented.

This chapter has ended with a motivation example showing the necessity of developing observers for the implementation of a state feedback controller derived using *energy shaping* or *damping injection*, for example.

Chapter III

Finite-dimensional observer-based boundary controllers: early-lumping approach

III.1 Introduction

In the previous chapter, we have introduced the class of *boundary controlled port-Hamiltonian systems* (BC-PHSs) [Le Gorrec 05] of interest in this thesis. We have seen that this class of systems can be stabilized by applying static output feedback or dynamic output feedback [Villegas 07]. In this chapter, we stabilize the BC-PHS by using *observer-based state feedback* (OBSF) controllers. To this end, we employ an *early-lumping approach*. Using this approach, the BC-PHS is first discretized into a *linear time-invariant* (LTI) system (or discretized model). This is, the set of *partial differential equations* (PDEs) is approximated by a set of *ordinary differential equations* (ODEs) by using suitable structure-preserving discretization methods as, for instance, *mixed finite-element* [Golo 04] or *finite-difference on staggered grids* [Trenchant 18] techniques. Then, the synthesis of the OBSF gains is based on the LTI system. Finally, the OBSF controller has to guarantee the closed-loop stability when it is applied to the BC-PHS.

One of the main advantages of using an *early-lumping approach* is the number of tools available in the literature for designing the OBSF gains of LTI systems [Kalman 69, Luenberger 64]. These techniques are, for instance, the *linear quadratic regulator* (LQR) [Anderson 07], the pole-placement [Brasch 70], and more recently, the *control by interconnection* using *Casimirs* [Ortega 08], and the *interconnection and damping assignment passivity based control* (IDA-PBC) [Ortega 02, Prajna 02]. However, since the design is based on the discretized model (LTI system) and not on the BC-PHS, the closed-loop stability is not guaranteed when applying the OBSF controller to the BC-PHS. We use an example to show this issue. We design some OBSF gains using classical control techniques for LTI systems. Then, we show that when applying the OBSF controller to the BC-PHS, the closed-loop system becomes unstable. This phenomenon is known as spillover effect [Balas 78] and it occurs when some high-frequency modes that are not considered for the design destabilize the closed-loop system. To overcome this effect and to guarantee closed-loop stability (when applying the OBSF controller to the BC-PHS), the classical control techniques have to be adapted.

In this chapter, we impose a passive structure on the OBSF controller. This structure guarantees the closed-loop stability when the OBSF controller is applied to the BC-PHS. We convert the classical OBSF representation into an equivalent dynamic output feedback representation [Villegas 05, Villegas 07, Wu 18]. As we have seen in the previous chapter, if the dynamic output feedback controller (or equivalently the OBSF controller) is *strictly positive real* (SPR), the closed-loop between the infinite-dimensional system (BC-PHS) and the OBSF controller is asymptotically stable [Morgül 94, Morgul 98, Yang 05, Villegas 07]. To achieve this structure, we propose two methodologies for the synthesis of the OBSF gains. In the first method, the state feedback gain is freely designed by using classical control techniques. Then, the observer gain is designed (through the resolution of an algebraic Riccati equation) such that the OBSF controller is SPR. In the second method, the observer gain is freely designed and the state feedback gain is designed (through the resolution of a set of linear matrix inequalities) such that the OBSF is SPR. In both cases, it is not completely free the design of one of the two gains. The benefit of using these constraints is that we can guarantee closed-loop stability when applying the OBSF controller to the BC-PHS. We use the vibrating string and the Timoshenko beam as application examples.

In the last section of this chapter, we extend these design methods to a class of *nonlinear time-invariant* (NTI) systems. We show that the proposed OBSF controller is *output strictly passive* (OSP) and *zero state detectable* (ZSD). Then, the OBSF controller can stabilize nonlinear systems that are

OSP and ZSD too [van der Schaft 00, Brogliato 20]. Similarly to the *early-lumping approach*, the NTI system is first linearized into an LTI system. Then, the OBSF gains are designed on the LTI system by using the aforementioned methodologies. Finally, we show that the closed-loop stability is guaranteed when applying the OBSF controller to the NTI system. We use a microelectromechanical system to exemplify the synthesis method.

This chapter is organized as follows. In Section III.2, we introduce the structure of the BC-PHS of interest and the discretized model used for design. In Section III.3, we present the classic OBSF controller for LTI systems. In the same section, by using a counterexample, we show that if we use classical control tools for the design, the closed-loop stability is not guaranteed when applying the OBSF controller to the BC-PHS. In Section III.4, we impose a passive structure to the OBSF controller such that when applying it to the BC-PHS, the closed-loop stability is guaranteed. In Section III.5, we show the asymptotic stability when applying the OBSF controller to the BC-PHS. In Section III.6 and Section III.7, we propose two methodologies for designing the controller and observer gains. We exemplify these methodologies using the vibrating string and the Timoshenko beam models. Finally, in Section III.8, we extend these methodologies to a class of finite-dimensional nonlinear systems. In this case, the synthesis of the OBSF controller is based on a linearized model and the closed-loop stability is guaranteed when the OBSF controller is applied to the nonlinear system. We use a microelectromechanical system to exemplify this extension. Some conclusions are presented in Section III.9.

III.2 Preliminaries

We consider the following BC-PHS:

$$\mathcal{P}\begin{cases}\dfrac{\partial x}{\partial t}(\zeta,t)=P_1\dfrac{\partial}{\partial\zeta}(\mathcal{H}(\zeta)x(\zeta,t))+P_0\mathcal{H}(\zeta)x(\zeta,t), \quad x(\zeta,0)=x_0(\zeta),\\ W_{\mathcal{B}}\begin{pmatrix}f_\partial(t)\\ e_\partial(t)\end{pmatrix}=u(t),\\ y(t)=W_{\mathcal{C}}\begin{pmatrix}f_\partial(t)\\ e_\partial(t)\end{pmatrix},\end{cases} \tag{III.1}$$

where $\zeta\in[a,b]$ is the spatial variable and $t\geq 0$ is the time variable. $x(\zeta,t)\in\mathbb{R}^n$ is the state variable with initial condition $x_0(\zeta)$. $P_1=P_1^T\in M_n(\mathbb{R})$ is a non-singular matrix, $P_0=-P_0^T\in M_n(\mathbb{R})$, $\mathcal{H}(\cdot)\in M_n(L_2([a,b];\mathbb{R}))$ is a bounded and continuously differentiable matrix-valued function satisfying for all ζ, $\mathcal{H}(\zeta)=\mathcal{H}^T(\zeta)$ and $mI<\mathcal{H}(\zeta)<MI$ with $0<m<M$ both constant scalars. $W_{\mathcal{B}}$ and $W_{\mathcal{C}}$ are two $n\times 2n$ full rank real matrices such that $W_{\mathcal{B}}\Sigma W_{\mathcal{B}}^T=W_{\mathcal{C}}\Sigma W_{\mathcal{C}}^T=0_n$ and $W_{\mathcal{C}}\Sigma W_{\mathcal{B}}^T=I_n$, with $\Sigma=\left(\begin{smallmatrix}0_n & I_n\\ I_n & 0_n\end{smallmatrix}\right)$. The *boundary port variables* are defined as in [Le Gorrec 05] as follows:

$$\begin{pmatrix}f_\partial(t)\\ e_\partial(t)\end{pmatrix}=\frac{1}{\sqrt{2}}\begin{pmatrix}P_1 & -P_1\\ I & I\end{pmatrix}\begin{pmatrix}\mathcal{H}(b)x(b,t)\\ \mathcal{H}(a)x(a,t)\end{pmatrix}, \tag{III.2}$$

and the Hamiltonian energy is given by

$$H(t)=\frac{1}{2}\int_a^b x(\zeta,t)^T\mathcal{H}(\zeta)x(\zeta,t)d\zeta. \tag{III.3}$$

Since the input $u(t)$ and the output $y(t)$ of the BC-PHS (III.1) are defined in terms of the *boundary port variables* and the matrices $W_{\mathcal{B}}$ and $W_{\mathcal{C}}$ satisfy $W_{\mathcal{B}}\Sigma W_{\mathcal{B}}^T=W_{\mathcal{C}}\Sigma W_{\mathcal{C}}^T=0_n$ and $W_{\mathcal{C}}\Sigma W_{\mathcal{B}}^T=I_n$, the Hamiltonian (III.3) satisfies

$$\dot{H}(t)=u(t)^Ty(t). \tag{III.4}$$

In this chapter, the synthesis of an OBSF controller for the BC-PHS (III.1) is proposed using an *early-lumping approach*. Using this approach, the BC-PHS is first discretized into a system described by ODEs (discretized model). Then, the synthesis of the OBSF gains is based on the discretized model such that the closed-loop system between the BC-PHS (III.1) and the OBSF controller is stable. To achieve this stability requirement, the OBSF controller is restricted to be passive. Even with this restriction, one can assign a desired behavior (settling time, rise time, overshoot, etc) to the closed-loop system between the discretized model and the OBSF controller, but more important one can guarantee the closed-loop stability when applying the OBSF controller to the BC-PHS (III.1) (infinite-dimensional system).

The first step in an *early-lumping approach* is to discretize the BC-PHS into a finite-dimensional model. In the literature we can found different techniques that preserve the port-Hamiltonian structure. These techniques are, for instance, the *mixed finite element* [Golo 04, Hamroun 06], *finite differences on staggered grids* [Trenchant 18], *discrete exterior geometry* [Seslija 12], and *partitioned finite element* [Brugnoli 19a, Serhani 19, Cardoso-Ribeiro 21]. For simplicity, in this thesis, we use the *finite differences on staggered grids* method proposed in [Trenchant 18]. The reader is referred to the Appendix A for further details of this method. The following assumption is considered concerning the structure of the discretized model used for the design of the OBSF controller proposed in this chapter.

Assumption III.2.1. *There exists a discretized model for the system (III.1) with input $u(t)$ and output $y(t)$ of the following form*

$$P\begin{cases}\dot{x}_d(t) &= (J_d - R_d)Q_d x_d(t) + B_d u(t)\\ y(t) &= B_d^T Q_d x_d(t)\end{cases} \tag{III.5}$$

where $x_d \in \mathbb{R}^{n_d}$ with n_d given by the size of the discretization, $J_d = -J_d^T$, $R_d = R_d^T \geq 0_{n_d}$, $Q_d = Q_d^T > 0_{n_d}$ all of them in $M_{n_d}(\mathbb{R})$ and $B_d \in \mathbb{R}^{n_d \times n}$. Furthermore we assume (III.5) to be controllable and observable. For simplicity, we shall define $A_d = (J_d - R_d)Q_d$ and $C_d = B_d^T Q_d$ and we refer to the system (A_d, B_d, C_d) as the approximated model of (III.1). ♣

Remark III.2.1. *As soon as n_d increases, the discretized model (III.5) approaches the infinite-dimensional system (III.1).* ♣

III.3 State feedback and Luenberger observer

State feedback allows to assign the overall closed-loop eigenvalues and may also be used to assign a part of the closed-loop eigenstructure [Kalman 69, Andry 83, Jiang 94]. For example, state feedback may be used to assign settling time, rise time, damping ratio or overshoot. The main drawback of this control strategy is that it requires the measurement of the overall state. To overcome this, the state is reconstructed using observers. An observer is a dynamical system that uses the dynamical model of the system and the measurement of the input and output to reconstruct the state variables [Luenberger 64].

Definition III.3.1. *A full observer-based state feedback controller for the system (III.5) is defined as follows:*

$$u(t) = -K\hat{x}(t) + r(t) \tag{III.6a}$$

$$\dot{\hat{x}}(t) = A_d\hat{x}(t) + B_d u(t) + L(y(t) - C_d\hat{x}(t)), \quad \hat{x}(0) = \hat{x}_0, \tag{III.6b}$$

where (III.6a) is the observed state feedback and (III.6b) is a Luenberger observer. $K \in \mathbb{R}^{n \times n_d}$ and $L \in \mathbb{R}^{n_d \times n}$ are the controller and the observer gains, respectively. These gains are designed such that $A_d - B_d K$ and $A_d - LC_d$ are Hurwitz matrices. $\hat{x}(t) \in \mathbb{R}^{n_d}$ is the observed state with initial condition $\hat{x}_0$, and $r(t) \in \mathbb{R}^n$ is an external input. ♣

The system (III.5) is assumed to be observable and controllable. Then, the synthesis of the state feedback and observer gains can be designed using classical control tools. However, several issues can occur when applying the OBSF controller to the BC-PHS (III.1). The most critical one is the instability in closed-loop caused by the spillover effect. In this case, the high frequency modes that have not been taken into account during the design are destabilized when the OBSF controller is applied to the BC-PHS. This effect is shown in the following example.

Example III.3.1. *Consider the one-dimensional wave equation with unitary parameters and Neumann boundary control at both sides, i.e. with force actuators at both sides. The system can be written as a BC-PHS (III.1) with*

$$P_1 = \begin{bmatrix} 0 & 1 \\ 1 & 0 \end{bmatrix}, \quad P_0 = 0, \quad \mathcal{H} = I_2.$$

This model is discretized by using finite differences on staggered grids in order to preserve the structure of the system [Trenchant 18]. Consider $n_d = 59$ elements for the discretization. All the eigenvalues of A_d are on the imaginary axis as shown in Figure III.1 (a). (A_d, B_d) is controllable and (A_d, C_d) is observable, hence K and L can be designed such that $A_K = A_d - B_d K$ and $A_L = A_d - LC_d$ are Hurwitz matrices. Using for instance the LQR method, the closed-loop eigenvalues can be assigned as shown in Figure III.1 (a).

The question that naturally arises is if the same OBSF controller, i.e. the same choice of matrices K and L, preserves the stability when applying it to the infinite-dimensional system. The answer is in general no. In this particular case for instance, when applying the designed OBSF controller (with $n_d = 59$ states) to a more precise discretized model that uses for example $n_d = 67$ states, the closed-loop system turns unstable as shown in Figure III.1 (b).

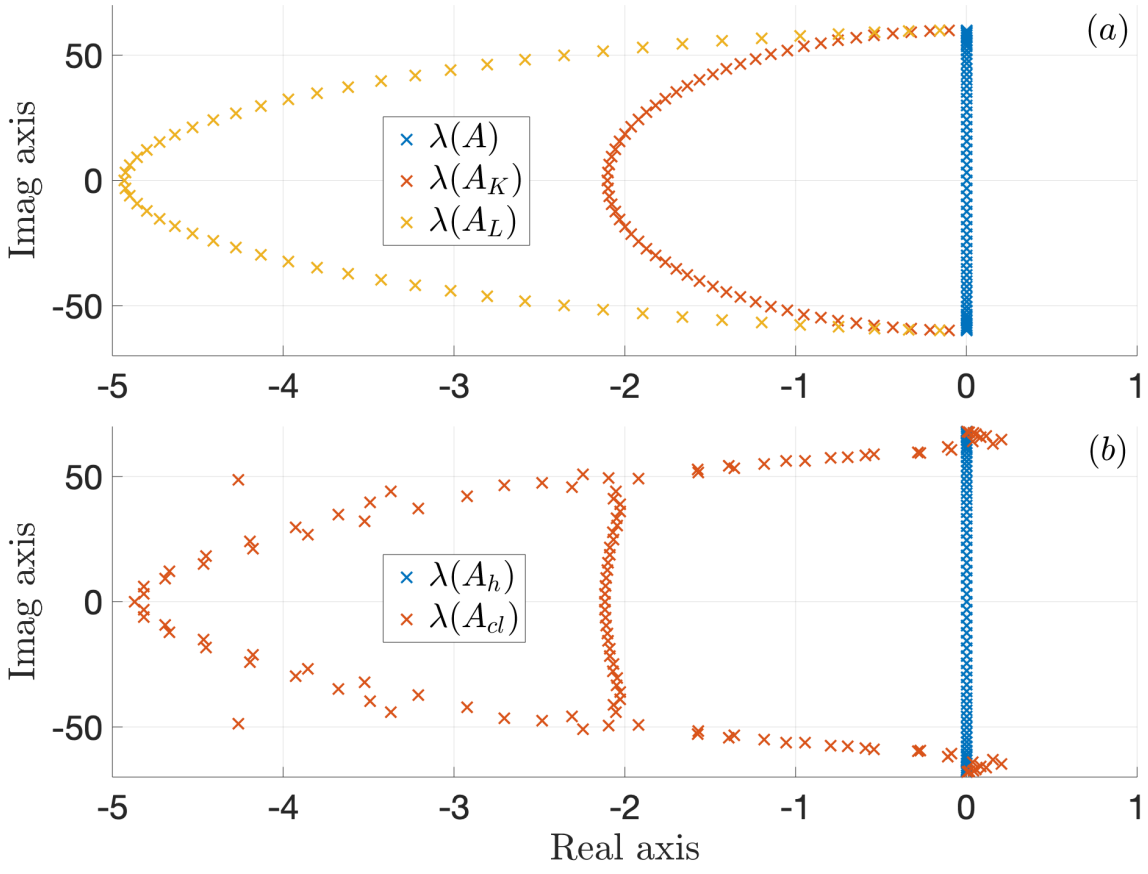

Figure III.1 – (a): $\lambda(A)$: Eigenvalues of A_d with $n_d = 59$, $\lambda(A_K)$: $A_d - B_d K$ eigenvalues and $\lambda(A_L)$: $A_d - LC_d$ eigenvalues. (b): $\lambda(A_h)$: discretized model eigenvalues with $n_d = 67$, $\lambda(A_{cl})$: closed-loop eigenvalues.

♣

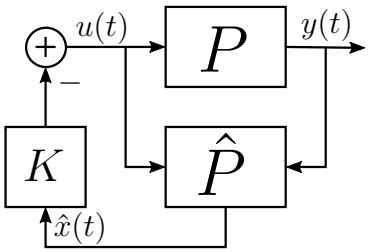

Figure III.2 – Observer-based state feedback diagram block

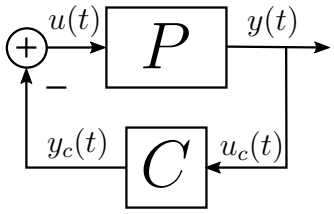

Figure III.3 – Passive observer-based state feedback diagram block.

In Example III.3.1, we have shown that the classical control tools have to be adapted to guarantee closed-loop stability when applying the OBSF controller to the BC-PHS. In the following section, we convert the classical closed-loop structure between (III.5) and (III.6), represented in Figure III.2 with $r(t) = 0$, into an equivalent closed-loop structure represented in Figure III.3, where C represents the OBSF controller. By imposing a passive structure to the dynamic controller C (or the OBSF controller), we can guarantee closed-loop stability when applying the OBSF controller to the BC-PHS. Then, the matrices K and L are restricted to obtain a passive OBSF controller. In the following section, we present the conditions to have a passive OBSF controller and in Sections III.6 and III.7, we propose two methods for the synthesis of the OBSF gains.

III.4 Passive observer-based state feedback structure

In this section, we adapt the OBSF scheme of Figure III.2 into an equivalent closed-loop scheme as shown in Figure III.3, where C is a passive dynamic controller with input $u_c(t)$ and output $y_c(t)$. To this end, we replace (III.6a) in (III.6b)

$$\dot{\hat{x}}(t) = (A_d - B_dK - LC_d)\hat{x}(t) + Ly(t) + B_dr(t). \tag{III.7}$$

Then, the synthesis of the matrices K and L are chosen such that the dynamical system (III.7) is a finite-dimensional port-Hamiltonian system with inputs $y(t)$ and $r(t)$. To do that, the matrices K and L have to be chosen such that

$$A_d - LC_d - B_dK = (J_c - R_c)Q_c \tag{III.8}$$

is satisfied for some $n_c \times n_c$ matrices $J_c = -J_c^T$, $R_c = R_c^T \geq 0$, $Q_c = Q_c^\top > 0$, (A_d, B_d, C_d) defined in (III.5), and n_c the size of the controller given by the discretized model used for design. If (III.8) is satisfied we can write (III.7) as a finite-dimensional port-Hamiltonian system as follows:

$$C\begin{cases} \dot{\hat{x}}(t) = (J_c - R_c)Q_c\hat{x}(t) + B_cu_c(t) + B_dr(t), \quad \hat{x}(0) = \hat{x}_0, \\ y_c(t) = B_c^\top Q_c\hat{x}(t), \\ y_r(t) = B_d^\top Q_c\hat{x}(t). \end{cases} \tag{III.9}$$

with $B_c = L$ and $u_c(t) = y(t)$. The inputs of this system are $u_c(t)$ and $r(t)$ with conjugated outputs $y_c(t)$ and $y_r(t)$, respectively. Then, the closed-loop dynamics when using *control by interconnection* with the passive interconnection

$$\begin{pmatrix} u(t) \\ u_c(t) \end{pmatrix} = \begin{pmatrix} 0 & -1 \\ 1 & 0 \end{pmatrix} \begin{pmatrix} y(t) \\ y_c(t) \end{pmatrix} + \begin{pmatrix} 1 \\ 0 \end{pmatrix} r(t) \tag{III.10}$$

between (III.5) and (III.9) is equivalent to the closed-loop dynamics between (III.6) and (III.5). In the following proposition, the matching conditions (III.8) guaranteeing the equivalence between the scheme of Figure III.2 and the scheme of Figure III.3 are made explicit.

Proposition III.4.1. *The original OBSF controller* (III.6) *applied to* (III.5) *using the scheme of Figure III.2 is equivalent to the control by interconnection between* (III.5) *and* (III.9) *through* (III.10) *as shown in Figure III.3 if the following matching conditions are satisfied*

$$\begin{aligned} (J_c - R_c)Q_c &= A_d - B_dK - LC_d, \\ B_c^TQ_c &= K, \\ B_c &= L. \end{aligned} \tag{III.11}$$

◊

Proof. *The matching equations* (III.11) *are directly obtained replacing* (III.6a) *in* (III.6b) *and identifying with* (III.9) *in order to get a passive and collocated dynamic controller. The first matching condition in* (III.11) *is obtained from* (III.8)*, the second matching condition in* (III.11) *is such that* $y_c(t)$ *is a conjugated output of* $u_c(t)$*. The last condition in* (III.11) *is obtained such that* $y(t)$ *is an input of the controller* (III.9)*.* ■

Then, solving the algebraic equation (III.11) of Proposition III.4.1 and imposing $R_c > 0$ to the controller, we can show the asymptotic stability of the closed-loop system between the discretized model (III.5) and the OBSF controller (III.9) through the passive interconnection (III.10) (Figure III.3).

Theorem III.4.1. *The interconnection* (III.10) *between* (III.5) *and* (III.9) *is asymptotically stable and converges to zero if* $R_c = R_c^T > 0$ *and* $r(t) = 0$. ◊

Proof. *Consider the total energy as Lyapunov function*

$$V(x_d, \hat{x}) = \frac{1}{2} x_d^T Q_d x_d + \frac{1}{2} \hat{x}^T Q_c \hat{x}$$

Then from (III.5) *and* (III.9) *we have*

$$\dot{V}(x_d, \hat{x}) = -{x_d}^T Q_d R_d Q_d x_d - \hat{x}^T Q_c R_c Q_c \hat{x},$$

with $R_d \geq 0$ *and* $R_c > 0$. *From Lasalle's invariance principle the system converges to the invariant set corresponding to* $\dot{V}(x_d, \hat{x}) = 0$, *i.e.* $\hat{x} = 0$ *(since* $R_c > 0$*). In this case,* $\hat{x} = 0$ *implies* $\dot{\hat{x}} = 0$, *which implies* $B_c u_c = 0$ *(from* (III.9) *and* $r = 0$*). The controller being controllable implies* $u_c = 0$ *and* $\hat{x} = 0$ *implies* $y_c = 0$ *(from* (III.9)*). From the interconnection* (III.10) $y = u_c = 0$ *and* $u = -y_c = 0$ *(since* $r = 0$*). The system* (III.5) *being observable implies that the only equilibrium point is* $x_d = 0$. ■

In Theorem III.4.1 we show that the OBSF controller (III.9) stabilizes asymptotically the discretized model (III.5). In the following section we show that the same OBSF controller stabilizes asymptotically the BC-PHS (III.1).

III.5 Asymptotic stability analysis

Now, we apply the OBSF controller (III.9) to the BC-PHS (III.1) in a power preserving way as it is shown in Figure III.4, where $\mathcal{P}$ refers to the BC-PHS (III.1) and C refers to the OBSF controller (III.9). In the following theorem, we show that the controller (III.9), being *strictly positive real*, stabilizes asymptotically the BC-PHS (III.1).

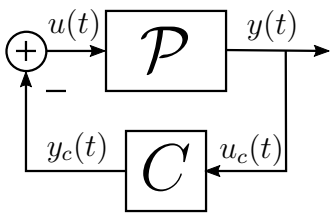

Figure III.4 – Closed-loop system between a BC-PHS and a finite-dimensional controller

Theorem III.5.1. *Consider the closed-loop system obtained from the passive interconnection* (III.10) *between the BC-PHS* (III.1) *and the OBSF controller* (III.9) *with* $r(t) = 0$ *as shown in Figure III.4. If the matrix* R_c *from the OBSF controller* (III.9) *is strictly positive definite, then the followings results hold*

(i) The closed-loop system is well-posed.

(ii) The closed-loop system is asymptotically stable.

◊

Proof. *This is a direct application of Corollary II.5.3.* ■

Theorem III.5.1 uses the passive interconnection (III.10) considering that the full inputs and outputs are available for the interconnection between the BC-PHS and the OBSF controller. However, this is not always possible and some times only some parts of the inputs and outputs are used for the interconnection as shown in Figure III.5. This is for instance, the case of the string attached at one side and actuated at the other side. In these cases, we have to assume that the BC-PHS is *approximately observable* with respect to the interconnected output (as for example the output $y_1(t)$ from Figure III.5). *Approximate observability* [Curtain 12, Corollary 4.1.14] states that if the output of a system with homogenous input is zero for a period of time, then the state of the system is zero as well. Using this property, similarly to Theorem III.5.1, we can use LaSalle's invariance principle to show that the closed-loop system is asymptotically stable.

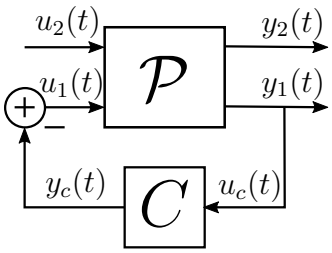

Figure III.5 – Closed-loop system between a BC-PHS and a finite-dimensional controller by partial interconnection

Corollary III.5.1. *Consider the closed-loop scheme of Figure III.5, where* $\mathcal{P}$ *is the impedance energy preserving BC-PHS* (III.1) *with*

$$u(t) = \begin{pmatrix} u_1(t) \\ u_2(t) \end{pmatrix} \quad \text{and} \quad y(t) = \begin{pmatrix} y_1(t) \\ y_2(t) \end{pmatrix},$$

and C *is the OBSF controller* (III.9) *with* $r(t) = 0$. *Provided that the closed-loop system is well-posed and that the solution trajectories are precompact, If the matrix* $R_c > 0$, $u_2(t) = 0$, *and* (III.1) *is approximately observable with respect to the output* $y_1(t)$, *then the closed-loop system is asymptotically stable.* ◊

Proof. *We consider the following as a Lyapunov function:*

$$V(t) = \frac{1}{2}\int_a^b x(\zeta,t)^T \mathcal{H}(\zeta) x(\zeta,t) d\zeta + \frac{1}{2}\hat{x}(t)^T Q_c \hat{x}(t).$$

It follows from LaSalle's invariance principle (See [Luo 12, Theorem 3.64]) that all solutions of the closed-loop system tend to the maximal invariant set of

$$\vartheta_c = \{x \in L_2([a,b],\mathbb{R}^n),\ \hat{x} \in \mathbb{R}^{n_c} \mid \dot{V}(t) = 0\}. \tag{III.12}$$

We define the maximal invariant subset of ϑ_c as $\mathcal{I}$, and we show that $\mathcal{I}$ only contains the zero state, i.e. $\mathcal{I} = \{x(\zeta,t) = 0,\ \hat{x}(t) = 0\}$. From (III.1), (III.9), and $r(t) = 0$, we obtain the following balance for the Lyapunov function:

$$\dot{V}(t) = -\hat{x}(t)^T Q_c R_c Q_c \hat{x}(t). \tag{III.13}$$

Since $R_c > 0$, $\dot{V}(t) = 0$ implies $\hat{x}(t) = 0$, which implies $\dot{\hat{x}}(t) = 0$. Then, from (III.9) $B_c u_c(t) = 0$. Since the controller is controllable, $u_c(t) = 0$. Since $\hat{x}(t) = 0$, from (III.9) $y_c(t) = 0$. Since $u_c(t) = y_c(t) = 0$, from the interconnection (Figure III.5)

$$\begin{pmatrix} u_1(t) \\ u_c(t) \end{pmatrix} = \begin{pmatrix} 0 & -1 \\ 1 & 0 \end{pmatrix} \begin{pmatrix} y_1(t) \\ y_c(t) \end{pmatrix},$$

we can conclude $y_1(t) = u_1(t) = 0$. Then, the maximal invariant set $\mathcal{I}$ contains $\hat{x} = 0$ and the solution of the following BC-PHS:

$$\begin{cases} \dfrac{\partial x}{\partial t}(\zeta,t) = P_1 \dfrac{\partial}{\partial \zeta}(\mathcal{H}(\zeta)x(\zeta,t)) + P_0 \mathcal{H}(\zeta)x(\zeta,t), \quad x(\zeta,0) = x_0(\zeta), \\ W_{\mathcal{B}} \begin{pmatrix} f_\partial(t) \\ e_\partial(t) \end{pmatrix} = \begin{pmatrix} u_1(t) \\ u_2(t) \end{pmatrix} = \begin{pmatrix} 0 \\ 0 \end{pmatrix}, \\ y(t) = W_{\mathcal{C}} \begin{pmatrix} f_\partial(t) \\ e_\partial(t) \end{pmatrix} = \begin{pmatrix} y_1(t) \\ y_2(t) \end{pmatrix} = \begin{pmatrix} 0 \\ y_2(t) \end{pmatrix}. \end{cases}$$

By definition, the latter is approximately observable with respect to $y_1(t)$. This implies that if $y_1(t) = 0$ for an interval of t, then the state is such that $x(\zeta,t) = 0$ (See [Curtain 12, Corollary 4.1.14]). Then, the maximal invariant set $\mathcal{I}$ only contains the states $x(\zeta,t) =$ and $\hat{x}(t) = 0$. Thus, by LaSalle's invariance principle, the asymptotic stability of the closed-loop system is guaranteed. ■

In the following two sections, two methods are provided for the synthesis of the matrices K and L such that the OBSF controller is on the form (III.9) with $R_c > 0$. Then, the asymptotic stability is preserved when applying it to the BC-PHS (III.1) (Figure III.4 or Figure III.5). In the first method, the gain K is freely designed using classical control tools and the gain L is designed such that the OBSF controller is passive. In the second method, the gain L is freely designed using classical control tools and the gain K is designed such that the OBSF controller is passive.

III.6 Observer design for a specific state feedback

In this section, the state feedback gain K is first designed using an approach like *LQR* [Anderson 07], pole-placement [Brasch 70], *control by interconnection* using *Casimirs* [Ortega 08], or IDA-PBC [Ortega 02, Prajna 02]. Then, by solving an *algebraic Riccati equation* (ARE), the observer gain L is designed in order to satisfy the matching conditions of Proposition III.4.1. This section is organized as follows. First, the methodology is proposed, and then, the vibrating string and the Timoshenko beam are used as examples.

III.6.1 Design method

The gains K and L are designed on the discretized model (A_d, B_d, C_d) from (III.5). The discretized model is an approximation of the BC-PHS (III.1). Then, we have to choose n_d (from (III.5)) large enough to have similar performances when applying the OBSF controller to the discretized model than when applying it to the BC-PHS. Since the pair (A_d, B_d) is controllable, the matrix K is chosen with classical control tools such that the following assumption is satisfied.

Assumption III.6.1. *The gain K is designed such that $A_d - B_dK$ is Hurwitz.* ♣

Remark III.6.1. *In this case, the design of the state feedback is free and it can be achieved by using traditional methods such as LQR, pole-placement or the LMI passivity based control proposed in [Prajna 02].* ♣

After designing the gain K such that $A_d - B_dK$ is Hurwitz, we have to design the gain L such that the OBSF controller is passive. To this end, we fix the matrix R_c and we obtain the matrices J_c, Q_c and L such that the matching conditions of Proposition III.4.1 are satisfied. To this end, we have to chose $R_c > 0$ in such a way that there exists a solution for the matching conditions (III.11).

Assumption III.6.2. *The matrix R_c is chosen positive definite such that the following matrix*

$$H_M = \begin{pmatrix} A_K & 2R_c \\ -C_K & -A_K^T \end{pmatrix} \tag{III.14}$$

with

$$A_K = A_d - B_dK, \quad C_K = -(K^TC_d + C_d^TK), \tag{III.15}$$

has no pure imaginary eigenvalues. ♣

The matrix H_M in (III.14) is known as the Hamiltonian matrix related to the *algebraic Riccati equation* (ARE) (III.16). If the H_M has no pure imaginary eigenvalues, then there exists a solution $Q_c = Q_c^T > 0$ for the ARE (III.16). A simple choice to have solution is the choice of $R_c = \alpha I_{n_c}$ for some $\alpha > 0$ small enough such that the matrix (III.14) has no pure imaginary eigenvalues. Finally, using the following proposition, we can complete the design and obtain the gain L such that the matching conditions (III.11) are satisfied.

Proposition III.6.1. *Let Assumptions III.6.1 and III.6.2 be satisfied. There exists a matrix $Q_c = Q_c^T > 0$, solution of the algebraic Riccati equation (ARE)*

$$A_K^TQ_c + Q_cA_K + 2Q_cR_cQ_c + C_K = 0, \tag{III.16}$$

such that the matching equations (III.11) are satisfied with

$$\begin{aligned} J_c &= \frac{1}{2}\left[A_K Q_c^{-1} - Q_c^{-1}A_K^T - Q_c^{-1}(K^T C_d - C_d^T K)Q_c^{-1}\right], \\ B_c &= Q_c^{-1}K^T, \\ L &= B_c. \end{aligned} \tag{III.17}$$

Furthermore, the matrix $A_d - LC_d$ is Hurwitz. ◊

Proof. *From [Kosmidou 07] it is known that if the Hamiltonian matrix (III.14) has no pure imaginary eigenvalues then there exists a solution $Q_c = Q_c^T > 0$ for (III.16). Hence we only need to prove that (III.16) is compatible with the matching equation (III.11) for J_c and L as in (III.17). Since Q_c is invertible and solution of (III.16) we have*

$$\begin{aligned} R_c &= -\frac{1}{2}\left[Q_c^{-1}A_K^T + A_K Q_c^{-1} + Q_c^{-1}C_K Q_c^{-1}\right] \\ &= -\frac{1}{2}\left[Q_c^{-1}A_K^T + A_K Q_c^{-1} - Q_c^{-1}(K^T C_d + C_d^T K)Q_c^{-1}\right]. \end{aligned} \tag{III.18}$$

Then, using (III.17) and (III.18) we have

$$\begin{aligned} (J_c - R_c)Q_c &= \frac{1}{2}(2A_K Q_c^{-1} - 2Q_c^{-1}K^T C Q_c^{-1})Q_c \\ &= A_K - Q_c^{-1}K^T C \\ &= A_K - LC \\ &= A_d - B_d K - LC_d \end{aligned} \tag{III.19}$$

which corresponds to (III.11). From Theorem III.4.1 the closed-loop system

$$\frac{d}{dt}\begin{pmatrix} x_d \\ \hat{x} \end{pmatrix} = \begin{pmatrix} A_d & -B_d K \\ B_c C_d & (J_c - R_c)Q_c \end{pmatrix}\begin{pmatrix} x_d \\ \hat{x} \end{pmatrix} + \begin{pmatrix} B_d \\ B_d \end{pmatrix} r \tag{III.20}$$

is asymptotically stable. Applying the following transformation

$$\begin{pmatrix} x_d \\ \tilde{x} \end{pmatrix} = \begin{pmatrix} I & 0 \\ I & -I \end{pmatrix}\begin{pmatrix} x_d \\ \hat{x} \end{pmatrix},$$

the closed-loop system (III.20) can be written

$$\frac{d}{dt}\begin{pmatrix} x_d \\ \tilde{x} \end{pmatrix} = \begin{pmatrix} A_K & B_d K \\ A_K - B_c C_d - A_c & A_c + B_d K \end{pmatrix}\begin{pmatrix} x_d \\ \tilde{x} \end{pmatrix} + \begin{pmatrix} B_d \\ B_d \end{pmatrix} r \tag{III.21}$$

with $A_K = A_d - B_d K$, $B_c = L$ and $A_c = (J_c - R_c)Q_c = A_d - B_d K - LC_d$ or equivalently

$$\frac{d}{dt}\begin{pmatrix} x_d \\ \tilde{x} \end{pmatrix} = \begin{pmatrix} A_d - B_d K & B_d K \\ 0 & A_d - LC_d \end{pmatrix}\begin{pmatrix} x_d \\ \tilde{x} \end{pmatrix} + \begin{pmatrix} B_d \\ 0 \end{pmatrix} r \tag{III.22}$$

Since A_K is Hurwitz, and the closed-loop system asymptotically stable, $A_d - LC_d$ is also Hurwitz. ■

Note that, using Proposition III.6.1 the design of the matrix L depends on the matrix K, and then, the separation principle is not satisfied using this methodology. However, an important benefit of using this approach is that the controller (III.6) can stabilize not only the discretized model (III.5) but also the BC-PHS (III.1).

Theorem III.6.1. *Consider the BC-PHS* (III.1) *controlled by* (III.6) *with K and L designed using Proposition III.6.1. The closed-loop system converges asymptotically to zero for $r(t) = 0$.* ♢

Proof. *The proof is a direct application of Theorem III.5.1. By Proposition III.6.1, since R_c is positive definite, the controller is SPR and then, from Theorem III.5.1, the closed-loop is asymptotically stable.* ■

In the following, we present a summary of the design procedure of the OBSF controller proposed in this section. Then, the procedure is exemplified in the following sections using the vibrating string and the Timoshenko beam as examples.

Procedure III.6.1. *The design procedure is summarized as follows:*

Step 1: *Represent the BC-PHS as in* (III.1).

Step 2: *Derive a structure-preserving finite-dimensional approximation P as in* (III.5).

Step 3: *Design K such that $A_d - B_d K$ is Hurwitz.*

Step 4: *Choose a matrix $R_c > 0$ such that H_M in* (III.14) *has no pure imaginary eigenvalues. For example $R_c = \alpha I_{n_c}$ with $\alpha > 0$.*

Step 5: *Solve the ARE* (III.16) *to find Q_c.*

Step 6: *Implement the OBSF controller with $L = Q_c^{-1} K^T$.*

♣

III.6.2 Application examples

In this section, we use the vibrating string and the Timoshenko beam examples to show the design procedure proposed in Procedure III.6.1.

Example III.6.1. *We consider the vibrating string of Example II.3.2 with* $\rho(\zeta) = T(\zeta) = 1$*, and* $\zeta \in [a, b] = [0, 1]$*. The string is attached at* $\zeta = 0$ *and it is controlled with a force actuator at* $\zeta = 1$*. By only measuring the velocity at* $\zeta = 1$*, we aim to apply a state feedback control law obtained using energy shaping and damping injection. The control law was introduced in the motivational example in Section II.6, where it was also shown the necessity of using observers to achieve the desired behavior. Now, we follow the Procedure III.6.1 to design the OBSF controller.*

Step 1. The dynamical system is represented as a BC-PHS

$$\frac{\partial}{\partial t}\begin{pmatrix} q(\zeta,t) \\ p(\zeta,t) \end{pmatrix} = \begin{pmatrix} 0 & 1 \\ 1 & 0 \end{pmatrix} \frac{\partial}{\partial \zeta}\begin{pmatrix} q(\zeta,t) \\ p(\zeta,t) \end{pmatrix}, \quad \begin{pmatrix} q(\zeta,0) \\ p(\zeta,0) \end{pmatrix} = \begin{pmatrix} q_0(\zeta) \\ p_0(\zeta) \end{pmatrix},$$
$$p(0,t) = 0,$$
$$q(1,t) = u(t),$$
$$y(t) = p(1,t),$$

where $u(t)$ *and* $y(t)$ *are respectively, the force and the velocity at the right side of the string. In this case, the vibrating string has no internal dissipation. This makes more difficult the stabilization than the case in which internal dissipation is included.*

Step 2. The finite-dimensional approximation of the BC-PHS is obtained using finite differences on staggered grids [Trenchant 18]. The reader is refer to Appendix A for further details. Using this discretization method, the grid is chosen such that the boundary conditions $p(0,t)$ *and* $q(1,t)$ *are exactly located at the respective borders. The discretized model contains as inputs both boundary conditions that, in this case, can be settled equal to* 0 *and* $u(t)$*, respectively. For simplicity, we chose*

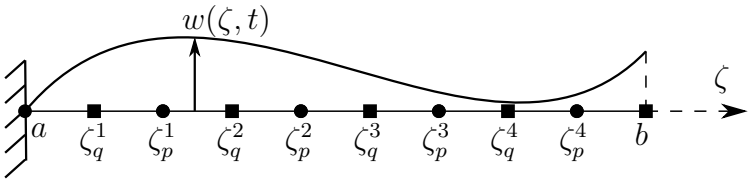

Figure III.6 – Discretization scheme using staggered grids.

$n_d = 8$*, that corresponds to* 4 *elements for the force and* 4 *elements for the velocity. Figure III.6 shows the spatial distribution of the finite-dimensional variables for the force (subscript* q*) and for the velocity (subscript* p*) on staggered grids. The discretized model is represented as (III.5) with*

$$x_d(t) = \begin{bmatrix} q_d(t) \\ p_d(t) \end{bmatrix}, \quad u(t) = q(1,t), \quad y(t) = p_4(t).$$

$$q_d(t) = \begin{bmatrix} q_1(t) \\ \vdots \\ q_4(t) \end{bmatrix}, \qquad p_d(t) = \begin{bmatrix} p_1(t) \\ \vdots \\ p_4(t) \end{bmatrix},$$

where $q_i(t)$ and $p_i(t)$ with $i = \{1, 2, 3, 4\}$ are respectively, the approximation of the strain (force) and the momentum (velocity) along ζ as shown in Figure III.6. The matrices of the discretized model (III.5) are

$$J_d = \begin{bmatrix} 0_4 & D \\ -D^T & 0_4 \end{bmatrix}, \quad R_d = \begin{bmatrix} 0_4 & 0_4 \\ 0_4 & 0_4 \end{bmatrix}, \quad Q_d = h \begin{bmatrix} I_4 & 0_4 \\ 0_4 & I_4 \end{bmatrix}, \quad B_d = \begin{bmatrix} 0_{4\times 1} \\ b_b \end{bmatrix}$$

$$D = \frac{1}{h^2} \begin{bmatrix} 1 & 0 & 0 & 0 \\ -1 & 1 & 0 & 0 \\ 0 & -1 & 1 & 0 \\ 0 & 0 & -1 & 1 \end{bmatrix}, \quad b_b = \frac{1}{h} \begin{bmatrix} 0 \\ 0 \\ 0 \\ 1 \end{bmatrix}$$

where $h = \frac{2}{9}$ is the spatial distance between two consecutive variables as for example $h = \zeta_q^2 - \zeta_q^1 = \zeta_p^2 - \zeta_1^1$.

Step 3. The control law is introduced in Section II.6. It is obtained by using energy shaping and damping injection. The control law ends in the following state feedback:

$$u(t) = -\int_0^1 q(\zeta, t) d\zeta - p(1, t),$$

that it is approximated in terms of the discretized model as follows

$$u(t) = -h \sum_{i=1}^{4} q_i(t) - p_4(t),$$

or equivalently as

$$u(t) = -K x_d(t)$$

with

$$K = \begin{bmatrix} h & h & h & h & 0 & 0 & 0 & 1 \end{bmatrix}.$$

The closed-loop matrix $A_K = A_d - B_d K$ is Hurwitz, since all its eigenvalues have negative real part as shown in Figure III.7.

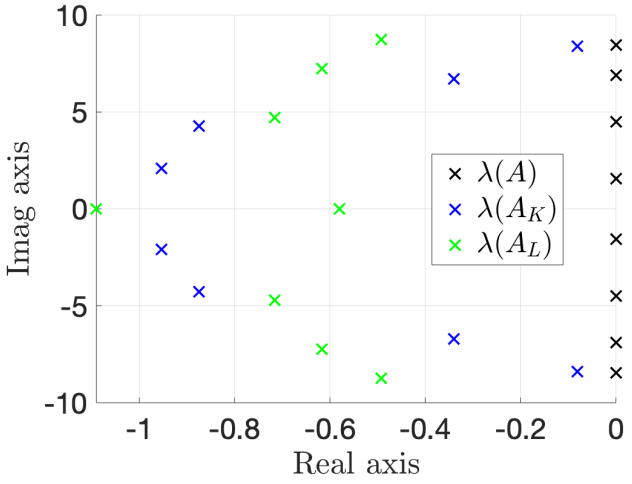

Figure III.7 – Plant eigenvalues $\lambda(A)$, controller eigenvalues $\lambda(A_K)$, and observer eigenvalues $\lambda(A_L)$.

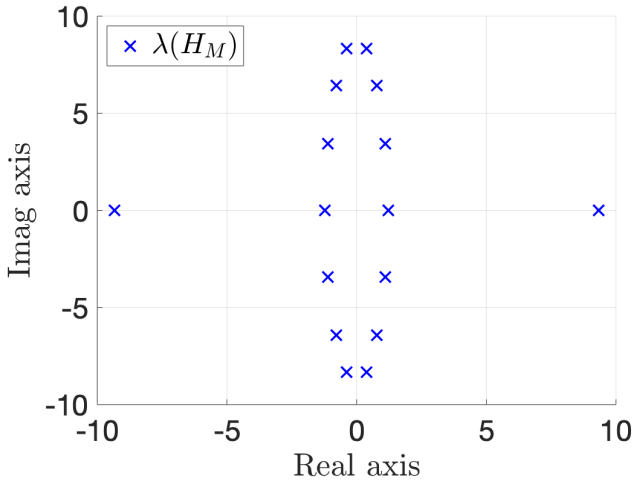

Figure III.8 – Hamiltonian matrix eigenvalues $\lambda(H_M)$.

Step 4. For simplicity, we chose a matrix R_c as a diagonal matrix such that

$$R_c = \begin{pmatrix} 10 & \cdots & 0 & 0 \\ \vdots & \ddots & \vdots & \vdots \\ 0 & \cdots & 10 & 0 \\ 0 & \cdots & 0 & 20 \end{pmatrix}.$$

The matrix H_M has no eigenvalues on the imaginary axis as shown in Figure III.8. Note that, the last element of the diagonal of R_c is chosen bigger than the other ones since the last state variable of the observer is the one related to the available sensor $y(t) = p(1,t)$.

Step 5. We solve the algebraic Riccati equation (III.16) using the numerical method proposed in [Lanzon 08]. The eigenvalues of the matrix Q_c are all pure real and positive define as we show in Figure III.9.

Step 6. We compute $L = Q_c^{-1}K$. The eigenvalues of $A_L = A_d - LC_d$ are shown in Figure III.7.

Finally, we simulate the closed-loop system between the designed OBSF controller and a new discretized model (III.5) that uses $n_d = 200$, i.e. a more precise model of the BC-PHS (III.1). In this case, the closed-loop system is composed by 208 states and all the closed-loop eigenvalues are in the left hand side of the imaginary axis as Figure III.10 shows. Note that, the stability is preserved when applying the OBSF controller to a new model that it has not been used for the design. This is due to the structure imposed to the OBSF controller and not in the model used for design.

We simulate the closed-loop system with initial conditions $w_0(\zeta) = 0.1\zeta$, $q_0(\zeta) = 0.1$, $p_0(\zeta) = 0$, and $\hat{x}_0 = 0$. Figure III.11 shows the string deformation in closed-loop, and Figure III.12 shows the estimated one. Note that, since the size of the model used for the design is $n_d = 8$, some high frequency modes are not considered for the OBSF design. Then, the oscillations due to these frequency modes are not controlled as we can see in Figures III.11 and III.12. To reduce these oscillations, a more precise model has to be used for the design. In the following, we repeat the design from Step 2 using a more precise discretized model for the design.

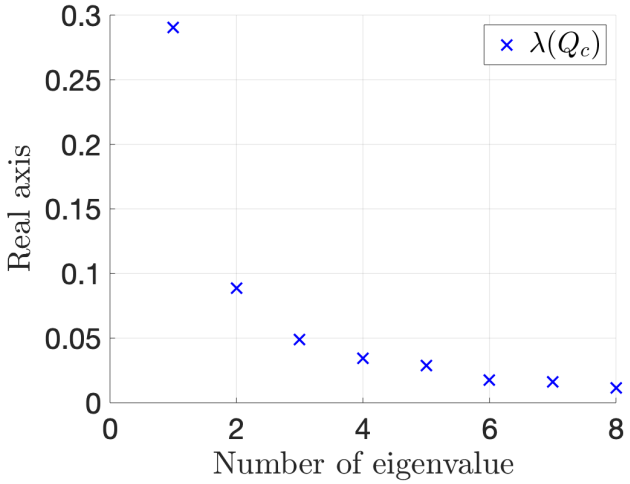

Figure III.9 – Eigenvalues of Q_c $\lambda(Q_c)$

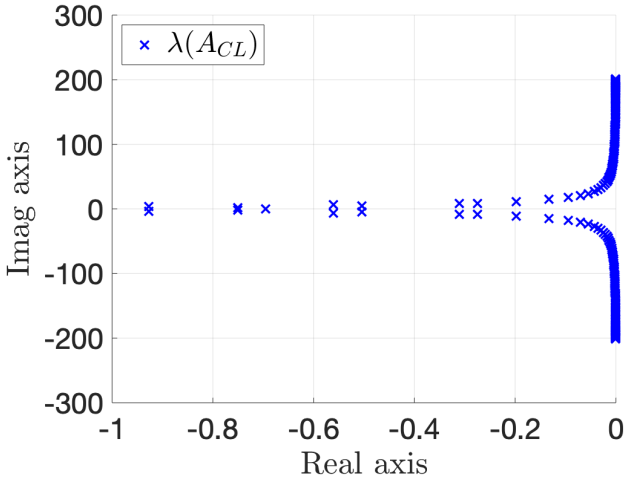

Figure III.10 – Closed-loop eigenvalues $\lambda(A_{CL})$

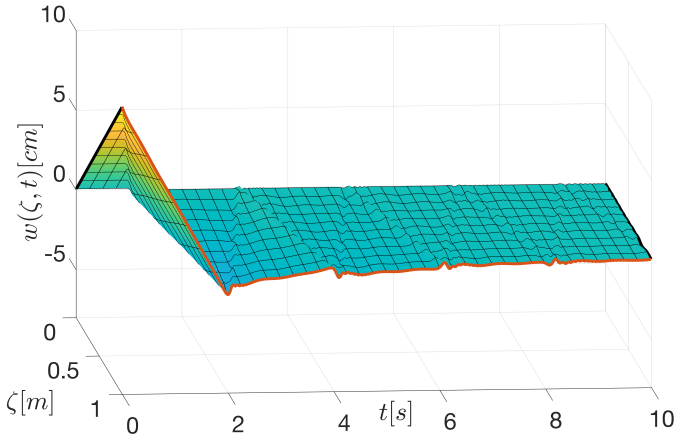

Figure III.11 – Deformation.

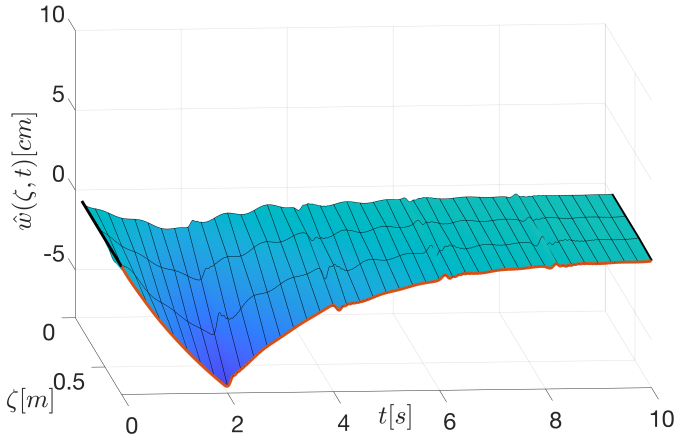

Figure III.12 – Observed deformation.

Step 2. If we chose $n_d = 80$, the discretized model is represented as (III.5) with the same structure as before.

Step 3. Similarly as before, the state feedback matrix is obtained as follows:

$$K = \begin{bmatrix} h & \cdots & h & 0 & \cdots & 0 & 1 \end{bmatrix}_{40\times 1}.$$

The closed-loop matrix $A_K = A_d - B_d K$ is Hurwitz and its eigenvalues are shown in Figure III.13.

Step 4. In this case, we chose a matrix R_c as a diagonal matrix such that

$$R_c = \begin{pmatrix} 1 & \cdots & 0 & 0 & 0 & 0 \\ \vdots & \ddots & \vdots & \vdots & \vdots & \vdots \\ 0 & \cdots & 1 & 0 & 0 & 0 \\ 0 & \cdots & 0 & 500 & 0 & 0 \\ 0 & \cdots & 0 & 0 & 500 & 0 \\ 0 & \cdots & 0 & 0 & 0 & 2500 \end{pmatrix}.$$

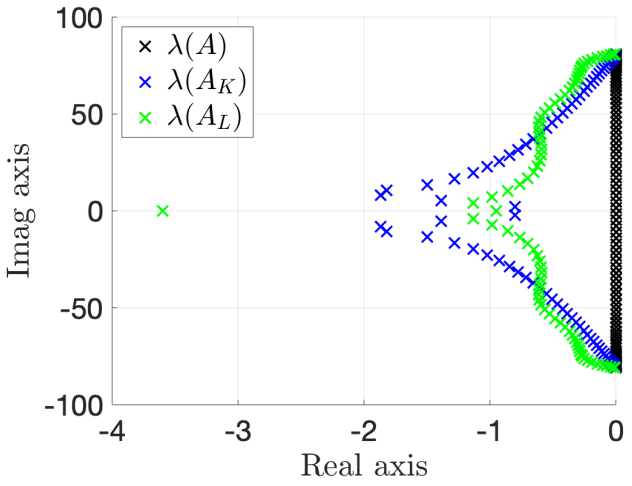

Figure III.13 – Plant eigenvalues $\lambda(A)$, controller eigenvalues $\lambda(A_K)$, and observer eigenvalues $\lambda(A_L)$.

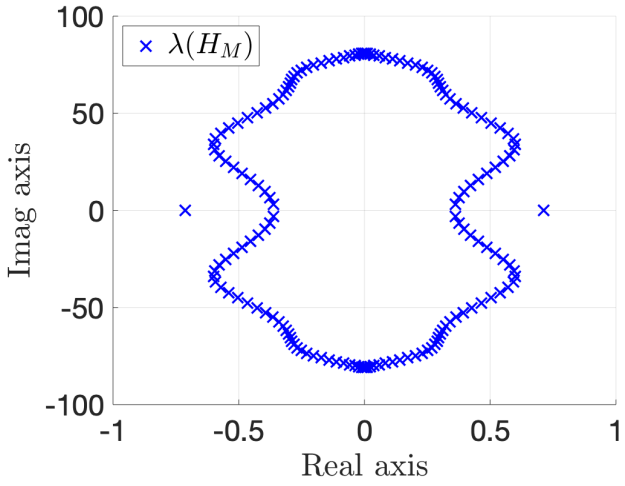

Figure III.14 – Hamiltonian matrix eigenvalues $\lambda(H_M)$.

The matrix H_M has no eigenvalues on the imaginary axis as Figure III.14.

Step 5. We solve the algebraic Riccati (III.16) with the numerical method proposed in [Lanzon 08]. The eigenvalues of the matrix Q_c are all pure real and they are shown in Figure III.15.

Step 6. We compute $L = Q_c^{-1}K$. The eigenvalues of $A_L = A_d - LC_d$ are shown in Figure III.13.

Finally, we simulate the closed-loop system between the obtained observer-based state feedback controller and a new discretized model (III.5) that uses $n_d = 200$, i.e. a more precise model of the BC-PHS (III.1). In this case, the closed-loop system is composed by 280 states and all the closed-loop eigenvalues are in the left hand side of the imaginary axis as Figure III.16 shows. Hence, the stability is preserved when applied the observer-based controller to a more precise discretized model of the BC-PHS.

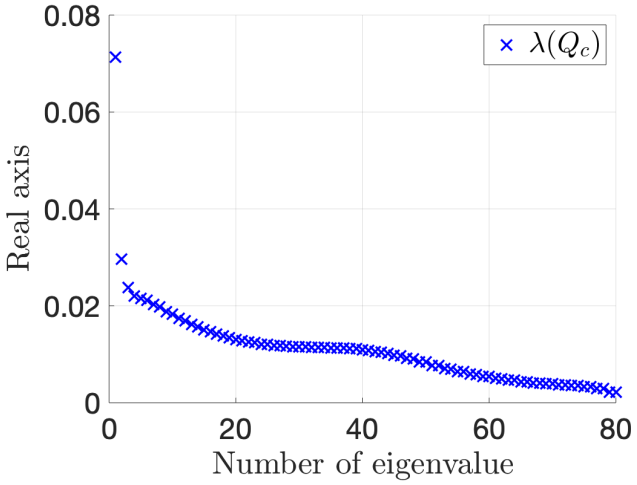

Figure III.15 – Eigenvalues of Q_c $\lambda(Q_c)$.

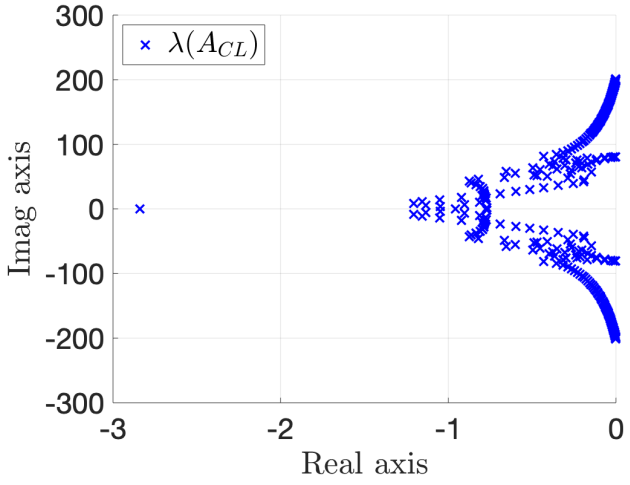

Figure III.16 – Closed-loop eigenvalues $\lambda(A_{CL})$

The initial conditions are $w_0(\zeta) = 0.1\zeta$, $q_0(\zeta) = 0.1$, $p_0(\zeta) = 0$, *and* $\hat{x}_0 = 0$. *Figure III.17 shows the string deformation in closed-loop, and Figure III.18 shows the estimated one. Different to the previous simulation (Figure III.11 and Figure III.12), now the oscillations are reduced. This is mainly due to the fact that more frequency modes are taken into account for the observer-based state feedback controller.*

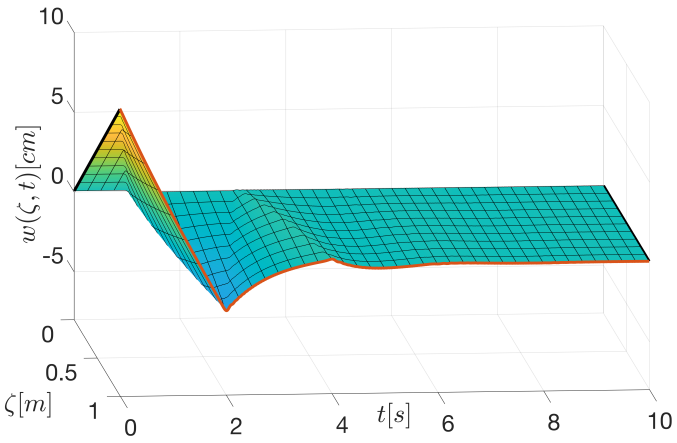

Figure III.17 – Deformation.

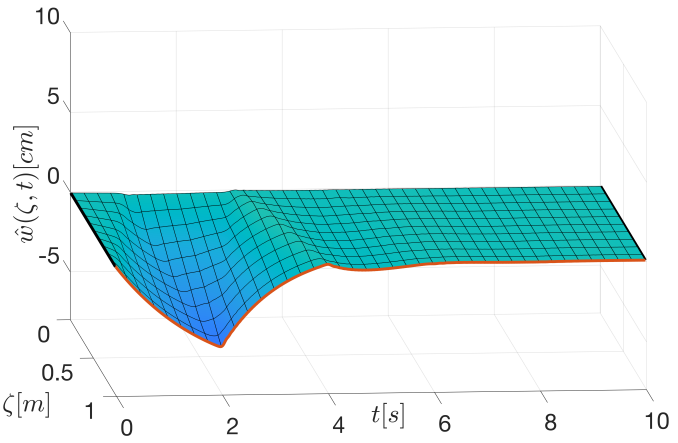

Figure III.18 – Observed deformation.

♣

In the following example, we use the Timoshenko beam to exemplify the Procedure III.6.1. In this case, we use *linear quadratic regulator* for the design of the state feedback matrix K and Proposition III.6.1 for the design of the observer gain L.

Example III.6.2. *We consider the Timoshenko beam of Example II.3.3. The beam is clamped at the left side and actuated at the right side with a force actuator and a torque actuator. We consider that the transverse velocity and angular velocity are measured. The model is presented in Example II.3.3 and the parameters are shown in Table III.1.*

Table III.1 – Plant parameters.

Parameters	Values	Unit
T	3.4531×10^5	Pa
ρ	0.0643	$kg.m^{-1}$
EI	37.0116	$Pa.m^4$
I_ρ	2.1485×10^{-6}	$Kg.m^2$
$[a, b]$	$[0, 0.3]$	m

Step 1. The Timoshenko beam is represented as a BC-PHS

$$\frac{\partial}{\partial t}\begin{pmatrix} x_1 \\ x_2 \\ x_3 \\ x_4 \end{pmatrix} = \begin{pmatrix} 0 & 1 & 0 & 0 \\ 1 & 0 & 0 & 0 \\ 0 & 0 & 0 & 1 \\ 0 & 0 & 1 & 0 \end{pmatrix} \frac{\partial}{\partial \zeta}\begin{pmatrix} Tx_1 \\ \frac{1}{\rho}x_2 \\ EIx_3 \\ \frac{1}{I_\rho}x_4 \end{pmatrix} + \begin{pmatrix} 0 & 0 & 0 & -1 \\ 0 & 0 & 0 & 0 \\ 0 & 0 & 0 & 0 \\ 1 & 0 & 0 & 0 \end{pmatrix}\begin{pmatrix} Tx_1 \\ \frac{1}{\rho}x_2 \\ EIx_3 \\ \frac{1}{I_\rho}x_4 \end{pmatrix}, \quad x(\zeta, 0) = x_0(\zeta),$$

$$\frac{1}{\rho}x_2(a,t) = \frac{1}{I_\rho}x_4(a,t) = 0$$
$$\begin{pmatrix} Tx_1(b,t) \\ EIx_3(b,t) \end{pmatrix} = u(t), \quad y(t) = \begin{pmatrix} \frac{1}{\rho}x_2(b,t) \\ \frac{1}{I_\rho}x_4(b,t) \end{pmatrix}$$

where $u(t)$ contains the force and torque at the right side and $y(t)$ contains the transverse velocity and the angular velocity at the right side.

Step 2. The finite-dimensional approximation of the BC-PHS is obtained using the method proposed in [Trenchant 18] as in Example III.6.1 (See Appendix A). Using this discretization method, the grid is chosen such that the boundary conditions $\frac{1}{\rho}x_2(a,t)$, $\frac{1}{I_\rho}x_4(a,t)$, $Tx_1(b,t)$, and $EIx_3(b,t)$ are exactly located at the respective borders. The discretized model contains as inputs the four boundary conditions that, in this case, can be settled equal to 0, 0, $u_1(t)$, and $u_2(t)$, respectively (with $u(t) = \left(\begin{smallmatrix} u_1(t) \\ u_2(t) \end{smallmatrix}\right)$). We chose for instance, a discretized model with $n_d = 16$ state variables. The force and torque are approximated at $\zeta = \zeta_1^i$, while the transverse and angular velocities are approximated at $\zeta = \zeta_2^i$ for $i = \{1,2,3,4\}$. as shown in Figure III.19.

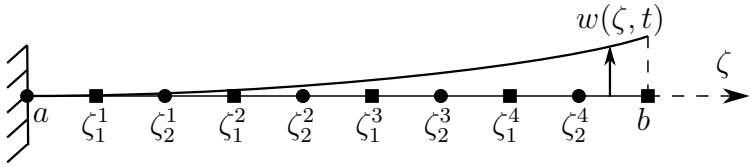

Figure III.19 – Discretization scheme using staggered grids for the Timoshenko beam.

The discretized model used for the design is on the form (III.5) with the following variables:

$$x_d(t) = \begin{bmatrix} x_1^d(t) \\ x_2^d(t) \\ x_3^d(t) \\ x_4^d(t) \end{bmatrix}, u(t) = \begin{bmatrix} Tx_1(b,t) \\ EIx_3(b,t) \end{bmatrix}, y(t) = \begin{bmatrix} \frac{1}{\rho_4}x_2^4(t) + \frac{1}{9}\frac{1}{I_{\rho 4}}x_4^4(t) \\ \frac{1}{I_{\rho 4}}x_4^4(t) \end{bmatrix},$$

$$x_1^d(t) = \begin{bmatrix} x_1^1(t) \\ \vdots \\ x_1^4(t) \end{bmatrix}, \quad x_2^d(t) = \begin{bmatrix} x_2^1(t) \\ \vdots \\ x_2^4(t) \end{bmatrix}, \quad x_3^d(t) = \begin{bmatrix} x_3^1(t) \\ \vdots \\ x_3^4(t) \end{bmatrix}, \quad x_4^d(t) = \begin{bmatrix} x_4^1(t) \\ \vdots \\ x_4^4(t) \end{bmatrix}.$$

The matrices of the discretized model (III.5) are given by

$$J_d = \begin{bmatrix} 0_4 & D & 0_4 & -F \\ -D^T & 0_4 & 0_4 & 0_4 \\ 0_4 & 0_4 & 0_4 & D \\ F^T & 0_4 & -D^T & 0_4 \end{bmatrix}, \qquad R_d = \begin{bmatrix} 0_4 & 0_4 & 0_4 & 0_4 \\ 0_4 & 0_4 & 0_4 & 0_4 \\ 0_4 & 0_4 & 0_4 & 0_4 \\ 0_4 & 0_4 & 0_4 & 0_4 \end{bmatrix},$$
$$Q_d = h \begin{bmatrix} TI_4 & 0_4 & 0_4 & 0_4 \\ 0_4 & \frac{1}{\rho}I_4 & 0_4 & 0_4 \\ 0_4 & 0_4 & EII_4 & 0_4 \\ 0_4 & 0_4 & 0_4 & \frac{1}{I_{\rho 4}} \end{bmatrix}, \quad B_d = \begin{bmatrix} 0_{4\times 1} & 0_{4\times 1} \\ b_{44} & 0_{4\times 1} \\ 0_{4\times 1} & 0_{4\times 1} \\ b_{43} & b_{44} \end{bmatrix}, \tag{III.23}$$

with

$$D = \frac{1}{h^2}\begin{bmatrix} 1 & 0 & \cdots & 0 \\ -1 & 1 & \ddots & 0 \\ \vdots & \ddots & \ddots & \ddots \\ 0 & 0 & \cdots & 1 \end{bmatrix}_{4\times 4}, \; F = \frac{1}{2h}\begin{bmatrix} 1 & 0 & \cdots & 0 \\ 1 & 1 & \ddots & 0 \\ \vdots & \ddots & \ddots & \ddots \\ 0 & 0 & \cdots & 1 \end{bmatrix}_{4\times 4},$$

$$b_{44} = \frac{1}{h}\begin{bmatrix} 0_{3\times 1} \\ 1 \end{bmatrix}, \quad b_{43} = \frac{1}{2}\begin{bmatrix} 0_{3\times 1} \\ 1 \end{bmatrix},$$

and $h = \frac{2}{9}$. *Note that,* n_d *is a design parameter and it has to be chosen multiple of* 4 *in this case. In order to show the structure of the discretized model, we have considered* $n_d = 16$. *However, for the design we chose different values of* n_d. *We show that increasing the precision of the model used for design, the performances are improved. Note that, when changing* n_d, *the model* (III.5) *preserves the same matrices* (III.23) *with appropriated dimensions and* $h = \frac{2(b-a)}{0.5n_d+1}$.

Step 3. The state feedback matrix K *is designed with the linear quadratic regulator (LQR) method using Matlab@ Control System Toolbox (lqr.m). Using this method, the desired control law minimizes the cost function*

$$J_{LQR} = \int_0^\infty \{x^T Q_{LQR} x + u^T R_{LQR} u + 2x^T N_{LQR} u\} dt.$$

We develop three different OBSF controllers. In Table III.2, we show the design parameters. We have changed the size of the OBSF controller (n_d) *and the gain* Q_{LQR}. *The closed-loop matrices*

Table III.2 – Design parameters.

	Design 1	Design 2	Design 3
n_d	8	40	40
Q_{LQR}	$1I_8$	$1I_{40}$	$10I_{40}$
R_{LQR}	$1I_2$	$1I_2$	$1I_2$
N_{LQR}	0	0	0
R_c	$1I_8$	$1I_{40}$	$5I_{40}$

$A_K = A_d - B_d K$ *are all Hurwitz.*

Step 4. For simplicity, the matrix R_c *is chosen as the identity multiply by a scalar as in Table III.2. Note that, for the design 3, the value of* R_c *has been increased in order to achieve a faster convergence of the observer than of the controller. For the three designs, the Hamiltonian matrix* H_M *has no eigenvalues on the imaginary axis.*

Step 5. We solve the algebraic Riccati (III.16) *with the method proposed in [Lanzon 08].*

Step 6. We compute $L = Q_c^{-1} K$. *The matrices* $A_L = A_d - LC_d$ *are all Hurwtiz. For the design 3, in Figure III.20, we show the obtained eigenvalues for the matrices* A_K *and* A_L.

Finally, we simulate the closed-loop system between the OBSF controllers and a new discretized model (III.5) *that uses* $n_d = 200$, *i.e. a more precise model of the BC-PHS* (III.1). *For the design 1, the closed-loop system is composed by* 208 *states, while for the designs 2 and 3 the closed-loop system is composed by 240 states. For the design 3, the closed-loop eigenvalues are shown in Figure*

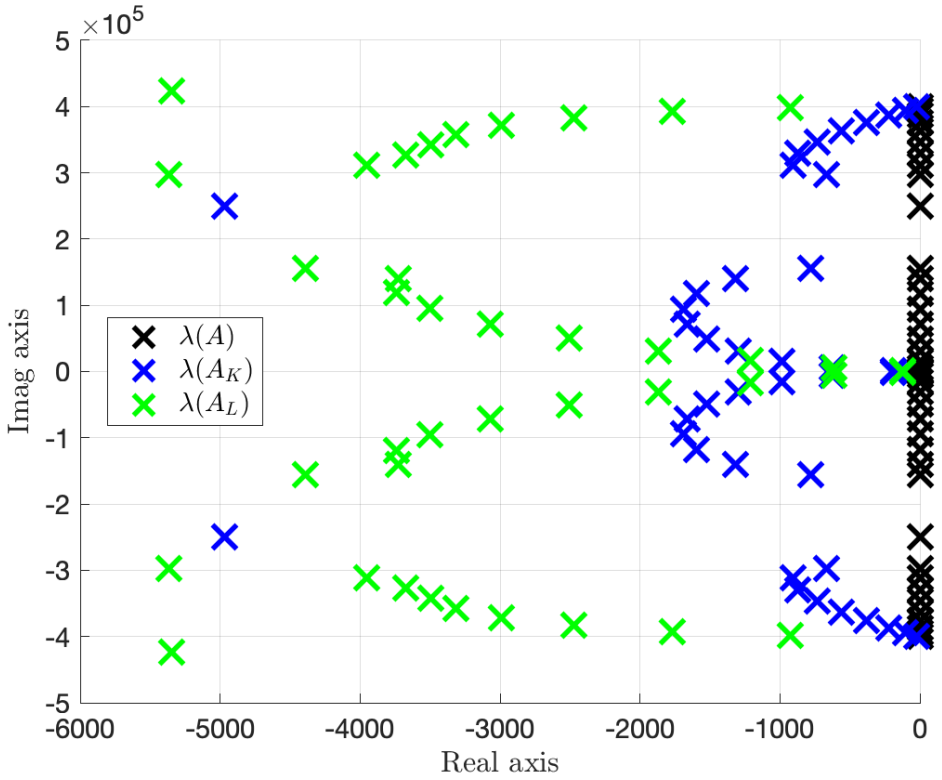

Figure III.20 – Plant $\lambda(A)$, controller $\lambda(A_K)$, and observer eigenvalues $\lambda(A_L)$ for the design 3

III.21. The simulation starts from the initial condition

$$
\begin{aligned}
x_1(\zeta, 0) &= 0.2896 \times 10^{-4}, \\
x_2(\zeta, 0) &= 0, \\
x_3(\zeta, 0) &= -0.2702\zeta + 0.0811, \\
x_4(\zeta, 0) &= 0,
\end{aligned}
$$

corresponding to the equilibrium position associated to a force of $10N$ *applied at the end tip of the beam. The initial condition for the observer is* $\hat{x}(0) = 0$*. Note that, the beam deformation and its estimation are reconstructed from the state variables, considering that the beam and the observed one are clamped at the left side.*

In Figure III.22, we show the end-tip displacement of the beam for the three different designs. We can notice that for design 1, some high-frequency modes are not attenuated. This is because they are not considered in the design. However, these high-frequency mode do not destabilize the system (due to the structure of the OBSF controller). The oscillations due to the high-frequency modes are attenuated using the design 2. The only difference between design 1 and design 2 is the size of the model used for design. With this new design, some high-frequency oscillations are attenuated. Finally, using the design 3, most of the oscillations are reduced. This is mainly due to the increase in the design parameter Q_{LQR} *(See Table III.2).*

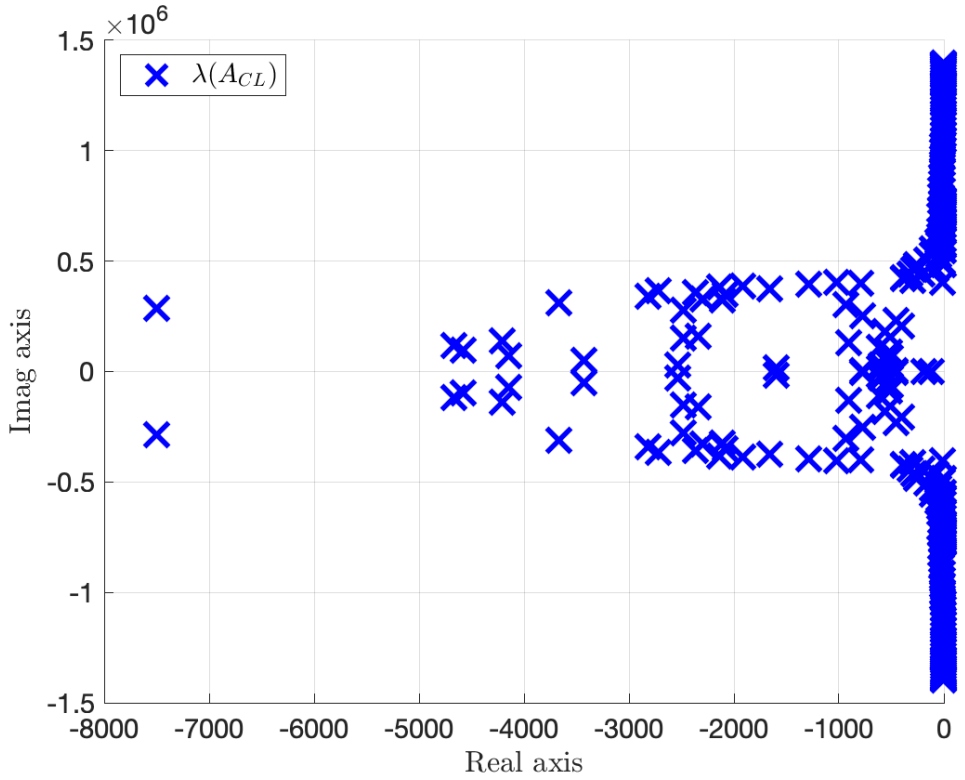

Figure III.21 – Closed-loop eigenvalues $\lambda(A_{CL})$ for the design 3

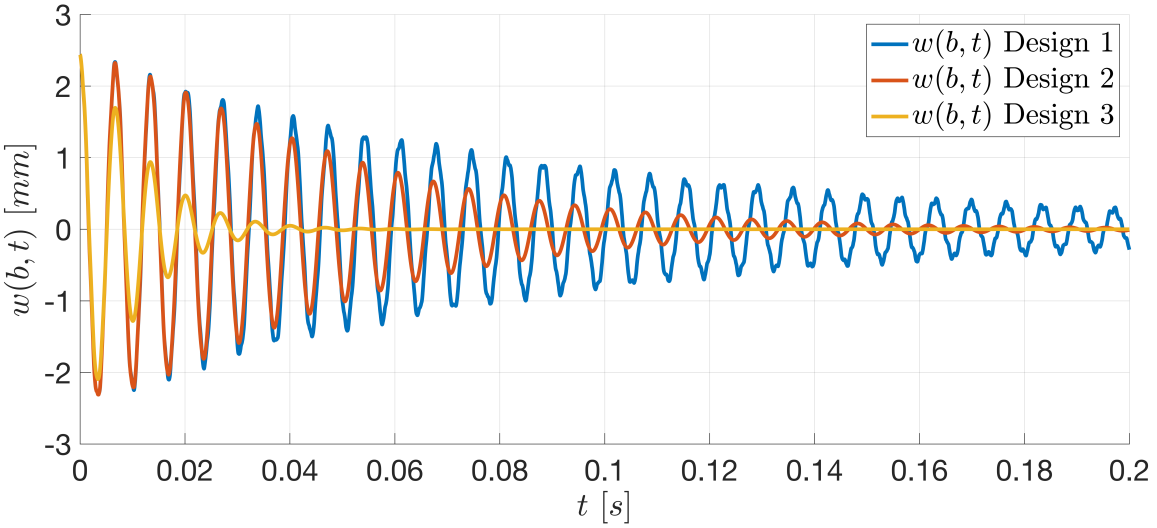

Figure III.22 – End tip deformation

Figure III.23 and Figure III.24 show the spatial and temporal responses for the design 1, Figure III.25 and Figure III.26 show the spatial and temporal responses for the design 2, and Figure III.27 and Figure III.28 show the spatial and temporal responses for the design 3. The only difference

between design 1 and 2 is the precision of the model used for design (see Table III.2). For this initial conditions, the oscillations are reduced when using a more precise model for the OBSF controller. Moreover, when increasing the gains Q_{LQR} and R_c (see design 3 of Table III.2), the oscillations are reduced even more (see Figure III.27 and Figure III.28 for the design 3 and Figure III.25 and Figure III.26 for the design 2).

In Figure III.23, we show the beam deformation along the time and the space for design 1. In Figure III.24, we show the observed one. In these figures, it is more evident that the high-frequency modes can not be attenuated, since the observer (Figure III.24) does not contain enough information of the beam over the space.

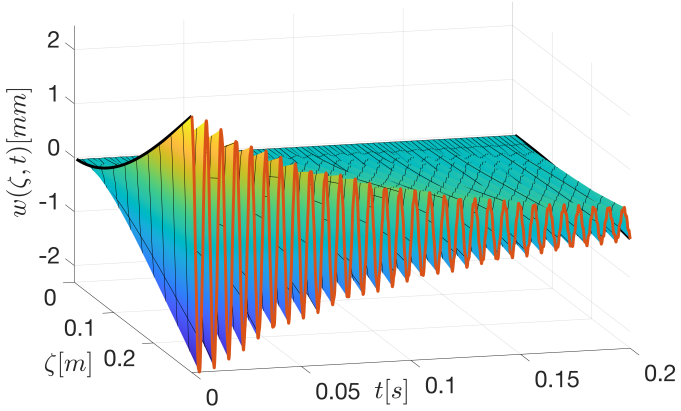

Figure III.23 – Beam deformation (design 1)

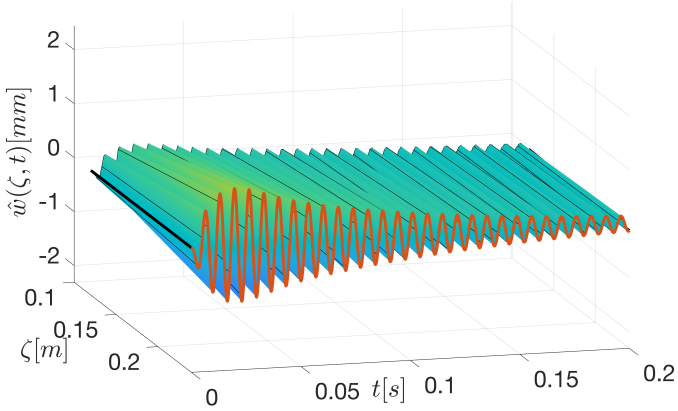

Figure III.24 – Observed deformation (design 1)

In Figure III.25, we show the beam deformation along the time and the space for design 2. In Figure III.26, we show the observed one. Now, since the OBSF controller uses more frequency modes for describing the infinite-dimensional system than the one of design 1, these high-frequency modes can be attenuated (see the end-tip response in Figure III.22 as well). Note that, the only difference between design 1 and design 2 is the size of the discretized model used for the design (See Table III.2). Then, both closed-loop systems have similar settling times. In order to reduce the settling time, one can modify the design parameter Q_{LQR} as we show in the following for design 3.

In Figure III.27, we show the beam deformation along the time and the space for design 3. In Figure III.28, we show the observed one. Now, since we have increased the design parameter Q_{LQR}, the convergence to zero is faster than for designs 1 and 2 (see the end-tip response in Figure III.22 as well).

♣

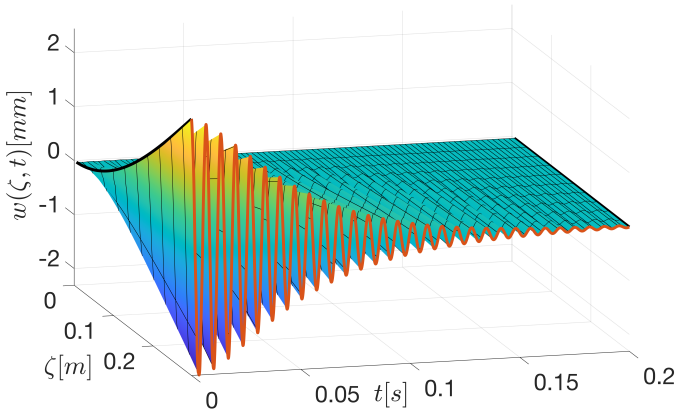

Figure III.25 – Beam deformation (design 2)

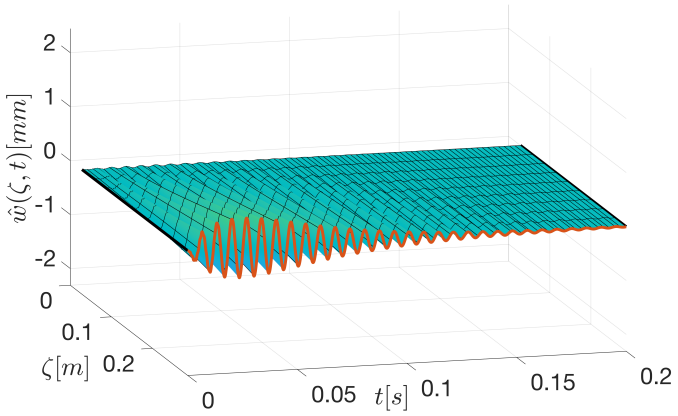

Figure III.26 – Observed deformation (design 2)

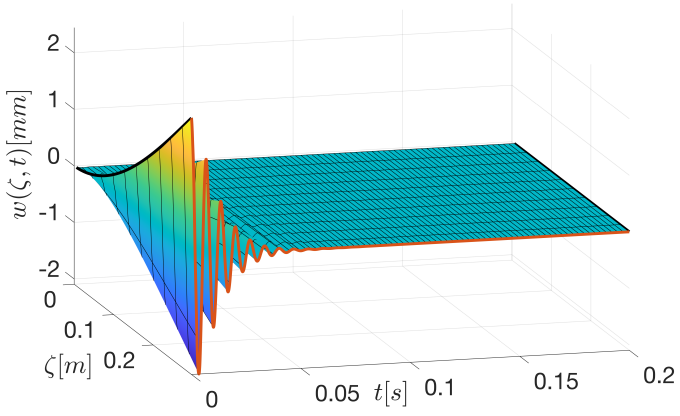

Figure III.27 – Beam deformation (design 3)

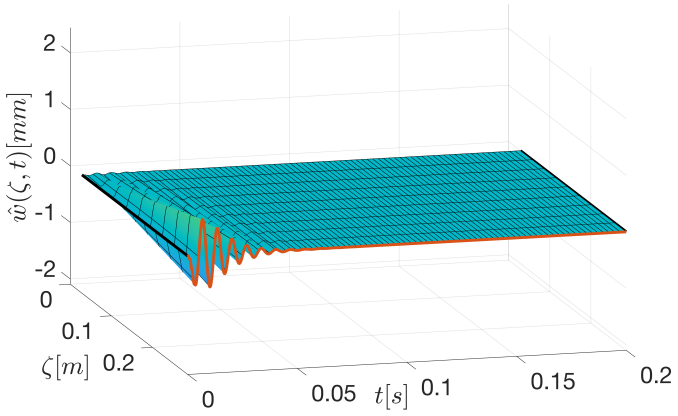

Figure III.28 – Observed deformation (design 3)

III.7 State feedback design for a specific observer

Different to the previous section, the methodology proposed in this section allows to design the observer gain L (as a dual problem of designing K) with different approaches like LQR [Anderson 07], pole-placement [Brasch 70], *control by interconnection* using *Casimirs* [Ortega 08], or IDA-PBC [Ortega 02, Prajna 02]. Then, by solving a set of *linear matrix inequalities* (LMIs), we perform the state feedback gain K in order to satisfy the matching conditions of Proposition III.4.1. This section is organized as follows. First, the methodology is proposed, and then, the Timoshenko beam is used as example.

III.7.1 Design method

Since the pair (A_d, C_d) is observable, the gain L of the observer is chosen with classical control tools such that the following assumption is satisfied.

Assumption III.7.1. *The gain L is designed such that $A_d - LC_d$ is Hurwitz.* ♣

Remark III.7.1. *In this case, the design of the observer gain is free and it can be achieved by using traditional methods such as LQR design, pole-placement or the LMI proposed in [Prajna 02]. For the last one, the details can be found in Appendix A.3.* ♣

After the gain L is designed such that Assumption III.7.1 is satisfied, we design the feedback gain K such that the matching conditions (III.11) are satisfied. The degrees of freedom of this methodology are related to the lower and upper bounds of the matrices R_c and Q_c from the OBSF controller (III.9). In the following proposition, the design of the state feedback gain K is achieved by tuning the lower and upper bounds of the matrices R_c and Q_c.

Proposition III.7.1. *Consider the finite-dimensional port-Hamiltonian system (III.5) and the matrix L such that $A_L := A_d - LC_d$ is Hurwitz, if the following LMIs:*

$$\begin{aligned} 2\Gamma_1 - B_dL^\top - LB_d^\top + A_L\mathbf{X} + \mathbf{X}A_L^\top \leq 0,\\ -2\Gamma_2 + B_dL^\top + LB_d^\top - A_L\mathbf{X} - \mathbf{X}A_L^\top \leq 0,\\ -\Delta_1^{-1} + \mathbf{X} \leq 0,\\ \Delta_2^{-1} - \mathbf{X} \leq 0, \end{aligned} \tag{III.24}$$

have a solution in the unknown matrix $\mathbf{X} = \mathbf{X}^\top$, for some $n_d \times n_d$ symmetric matrices Γ_1, Γ_2, Δ_1 and Δ_2 such that $0 \leq \Gamma_1 < \Gamma_2$ and $0 < \Delta_1 < \Delta_2$, then with the interconnection (III.10) between (III.5) and (III.9) and matrices

$$\begin{aligned} S_c &= A_L\mathbf{X} - B_dL^\top, & J_c &= \tfrac{1}{2}(S_c - S_c^\top),\\ R_c &= -\tfrac{1}{2}(S_c + S_c^\top), & Q_c &= \mathbf{X}^{-1},\\ B_c &= L, & K &= B_c^\top Q_c, \end{aligned} \tag{III.25}$$

the following results hold:

(i) $\lim_{t\to\infty}(x_d(t) - \hat{x}(t)) = 0$ *with the performances given by the matrix A_L;*

(ii) Matrices R_c and Q_c satisfy

  (a) $\Gamma_1 \leq R_c \leq \Gamma_2$;

  (b) $\Delta_1 \leq Q_c \leq \Delta_2$;

(iii) The controller (III.9) is a finite-dimensional port-Hamiltonian system. Moreover, if $\Gamma_1 > 0$, it is SPR.

◊

Proof. *Since the error is given by $\tilde{x}(t) = x(t) - \hat{x}(t)$, the result (i) in Proposition III.7.1 is equivalent to prove that the error $\tilde{x}(t)$ converges asymptotically to zero. The error dynamic $\dot{\tilde{x}}(t)$ is obtained from (III.5) and (III.9). Then, replacing the interconnection (III.10) and matrices (III.25) the error dynamic becomes $\dot{\tilde{x}}(t) = (A_d - LC_d)\tilde{x}(t)$. Since $A_L = A_d - LC_d$ is Hurwitz, the error converge asymptotically to zero. For the result (ii), we check from the LMI (III.24) that*

$$\begin{aligned} 2\Gamma_1 \leq B_dL^\top + LB_d^\top - A_L\mathbf{X} - \mathbf{X}A_L^\top \leq 2\Gamma_2\\ {\Delta_2}^{-1} \leq \mathbf{X} \leq {\Delta_1}^{-1} \end{aligned}$$

Replacing $\mathbf{X}$, S_c and $S_c^\top$ from (III.25) and inverting the second inequality we obtain

$$\begin{aligned} 2\Gamma_1 \leq -(S_c + S_c^\top) \leq 2\Gamma_2\\ \Delta_1 \leq Q_c \leq \Delta_2 \end{aligned}$$

then, replacing R_c from (III.25) we can conclude the result (ii). The controller (III.9) is a port-Hamiltonian system since $J_c = -J_c^\top$, $R_c = R_c^\top \geq 0$ and $Q_c = Q_c^\top > 0$ are satisfied from (III.25) and (ii). Finally, by Lemma II.5.1 and Corollary II.5.2, the controller (III.9) is SPR if $R_c > 0$. The matrix R_c is strictly positive definite if the matrix Γ_1 so is.

■

Remark III.7.2. *The simplest choice for Γ_1, Γ_2, Δ_1 and Δ_2 is to consider an identity matrix multiplied by a scalar.* ♣

Remark III.7.3. *Although, the design parameters related to the matrix R_c are Γ_1 and Γ_2, when they are modified, the obtained matrix Q_c is also. Similar for the design paramenters Δ_1 and Δ_2 that are related to the matrix Q_c.* ♣

The design is completed by using Proposition III.7.1. Then, we apply the OBSF controller (III.6) to the BC-PHS (III.1). The closed-loop stability between the BC-PHS and the OBSF controller is guaranteed due to the structure imposed to the OBSF controller. Since, it is SPR the closed-loop system between the BC-PHS and the OBSF controller is asymptotically stable.

Theorem III.7.1. *Consider the BC-PHS (III.1) and the control law (III.6) with K and L designed using Proposition III.7.1. If $\Gamma_1 > 0$, the closed-loop system converges asymptotically to zero for $r(t) = 0$.* ♢

Proof. *The proof is a direct application of Theorem III.5.1. By Proposition III.7.1, $\Gamma_1 > 0$ implies $R_c > 0$. Since R_c is positive definite, the controller is SPR (See Corollary II.5.2).* ■

In the following, we present a procedure for the design of the observer-based state feedback controller proposed in this section.

Procedure III.7.1. *The design procedure is summarized as follows:*

Step 1: *Represent the BC-PHS as in (III.1).*

Step 2: *Derive a finite-dimensional approximation P as in (III.5).*

Step 3: *Design L such that $A_d - LC_d$ is Hurwitz.*

Step 4: *Choose matrices Γ_1, Γ_2, Δ_1 and Δ_2. For example, the identity by a positive constant.*

Step 5: *Solve the LMI (III.24) to find Q_c.*

Step 6: *Implement the OBSF controller with $K = L^T Q_c$.*

♣

III.7.2 Application example

In this subsection, the Timoshenko beam of Example II.3.3 is considered to apply the Procedure III.7.1.

Example III.7.1. *We consider the Timoshenko beam clamped at the left side and actuated at the right side with force and torque actuators. We consider that the transverse velocity and angular velocity are measured (see Example II.3.3). For simplicity, we use unitary parameters as in Table III.3.*

Table III.3 – Plant Parameters.

	Value	Measurement unit
T	1	Pa
ρ	1	$kg.m^{-1}$
EI	1	$Pa.m^4$
I_ρ	1	$Kg.m^2$
$[a, b]$	$[0, 1]$	m

In this case, Step 1 and Step 2 are the same as the ones given in the subsection III.6.2, with the only difference on the plant parameters that in this case are given in Table III.3. Then, we continue with Step 3 described in the previous section.

Step 3. The observer gain L is designed using IDA-PBC method proposed in [Prajna 02]. This method uses linear matrix inequalities (LMIs) for solving the IDA-PBC problem for LTI systems. It is worth stressing that the gain L can be designed using classical approaches like LQR or pole placement. In this example, we use this approach to have a complete design based on LMIs. In Appendix A.3, we recall the main Propositions of this method. For the design of L, we follow Proposition A.3.2 from Appendix A.3. Note that, from Remark A.3.2 we have to replace A_d by A_d^T, B_d by C_d^T and F by $-L^T$ in order to obtain the matrix L.

Three different OBSF controllers are developed. The observer gains are designed using Proposition A.3.2 with the design parameters of Table III.4. Note that, for the observer, designs 1 and 2 are equivalent and the design 3 uses a more precise model for the synthesis. The matrices $A_L = A_d - LC_d$ are all Hurwitz (in Figure III.29, we show the eigenvalues of the matrix A_L for design 3).

Table III.4 – Observer design parameters.

	Design1	Design 2	Design 3
Λ_1	$0.1I_{20}$	$0.1I_{20}$	$0.1I_{40}$
Λ_2	$5000I_{20}$	$5000I_{20}$	$5000I_{40}$
Ξ_1	$1I_{18}$	$1I_{18}$	$1I_{38}$
Ξ_2	$1000I_{18}$	$1000I_{18}$	$1000I_{38}$
γ	10	10	10
n_d	5	5	10

Step 4. For simplicity, we chose the matrices Γ_1, Γ_2, Δ_1, and Δ_2 as shown in Table III.5 for the state feedback design. Note that, $\Gamma_1 > 0$ in every case, and we only change the design parameters related to the energy matrix Q_c.

Step 5. The LMI from Proposition III.7.1 is solved using the Matlab@ Robust Control Toolbox. Note that, in every case $\Delta_1 < Q_c < \Delta_2$ and $\Gamma_1 < R_c < \Gamma_2$.

Step 6. We compute $K = L^T Q_c$. The matrix $A_K = A_d - B_d K$ is Hurwitz. For the design 3, in Figure III.29, we show the obtained eigenvalues for the matrices A_K and A_L.

Finally, we simulate the closed-loop system obtained using the OBSF state feedback controllers and a new discretized model (III.5) that uses $n_d = 200$, (a more precise model of the BC-PHS (III.1)). For the designs 1 and 2, the closed-loop system is composed by 220 states, while for the design 3

Table III.5 – Controller design parameters

Matrix	Design 1	Design 2	Design 3
Γ_1	I_{20}	I_{20}	I_{40}
Γ_2	$1000I_{20}$	$1000I_{20}$	$1000I_{40}$
Δ_1	$0.005I_{20}$	$0.015I_{20}$	$0.015I_{40}$
Δ_2	$1I_{20}$	$1I_{20}$	$0.1I_{40}$
n_d	5	5	10

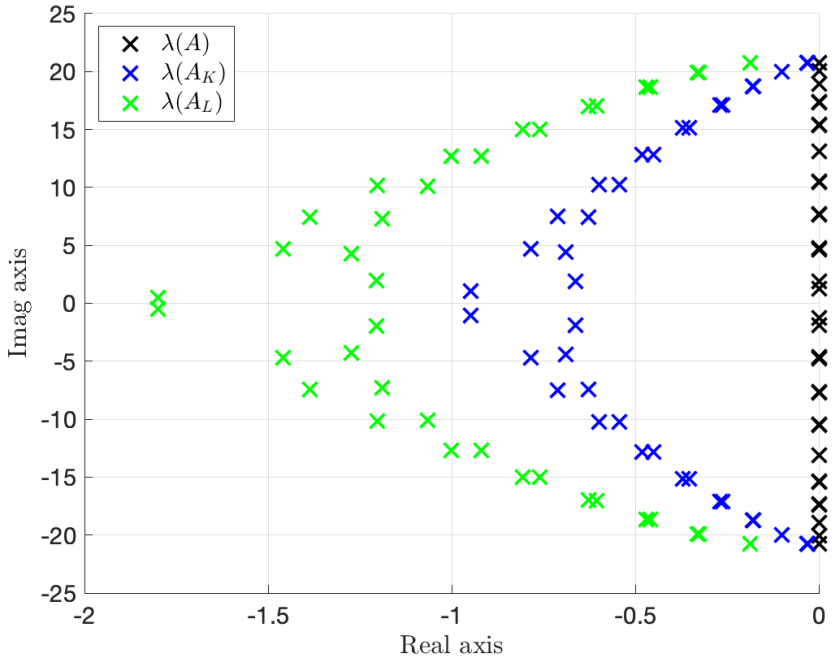

Figure III.29 – Plant $\lambda(A)$, controller $\lambda(A_K)$, and observer eigenvalues $\lambda(A_L)$ (design 3)

the closed-loop system is composed by 240 states. For the design 3, the closed-loop eigenvalues are shown in Figure III.30. The simulation starts from the initial condition

$$
\begin{aligned}
x_1(\zeta, 0) &= 0.01, \\
x_2(\zeta, 0) &= 0, \\
x_3(\zeta, 0) &= -0.01(\zeta - 1), \\
x_4(\zeta, 0) &= 0,
\end{aligned}
$$

corresponding to the equilibrium position associated to a force of $0.01N$ *applied at the end tip of the beam. The initial condition for the observer is* $\hat{x}(0) = 0$.

In Figure III.31, we show the end-tip displacement of the beam for the three different designs. We can notice that the settling time of design 2 is faster than the one of design 1. This is because the design parameter Δ_1 *is bigger in design 2 than in design 1. This implies a matrix* Q_c *with bigger*

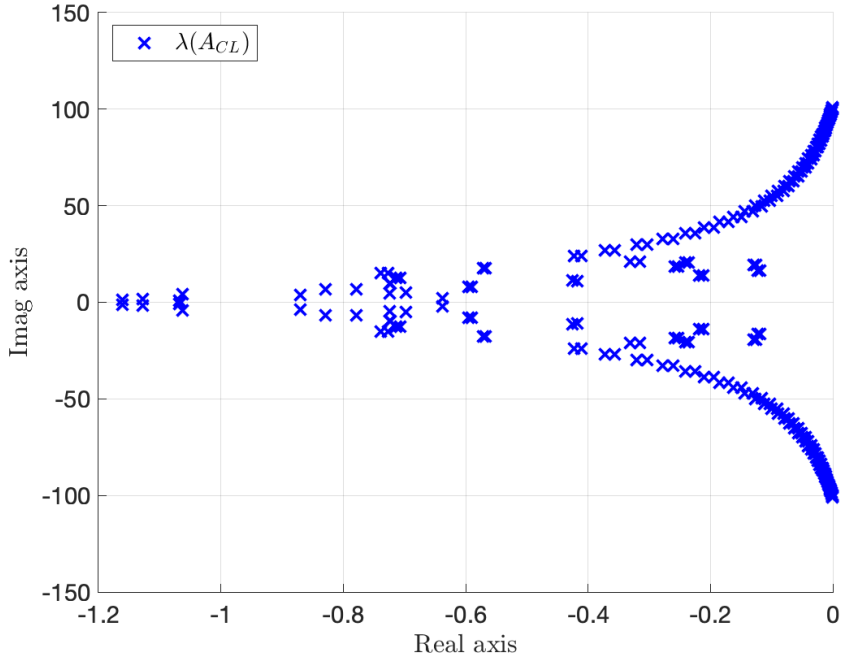

Figure III.30 – Closed-loop eigenvalues $\lambda(A_{CL})$ (design 3)

eigenvalues for design 2 than design 1. Finally, using design 3, we can notice that high-frequency oscillations are attenuated. This is because the model used in design 3 is more precise than the one used for design 2.

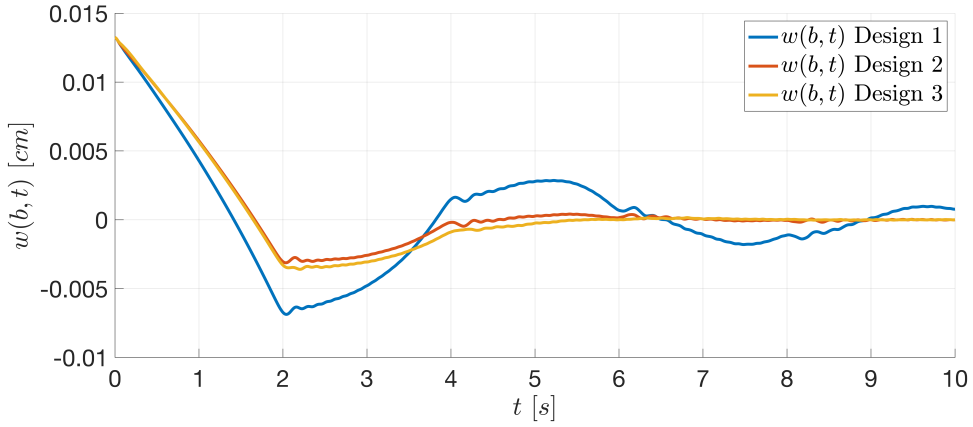

Figure III.31 – End tip deformation

In Figure III.32 and Figure III.33, we show the beam deformation along the space and the time for design 1. The settling time is improved using design 2 as shown in Figure III.34 and Figure III.35. We can notice that the beam reaches the equilibrium approximately at $t = 6\,s$. For $t > 6\,s$, some high-frequency oscillations remain unattenuated. However, due to the structure imposed on the OBSF controller, these oscillations do not destabilize the closed-loop system.

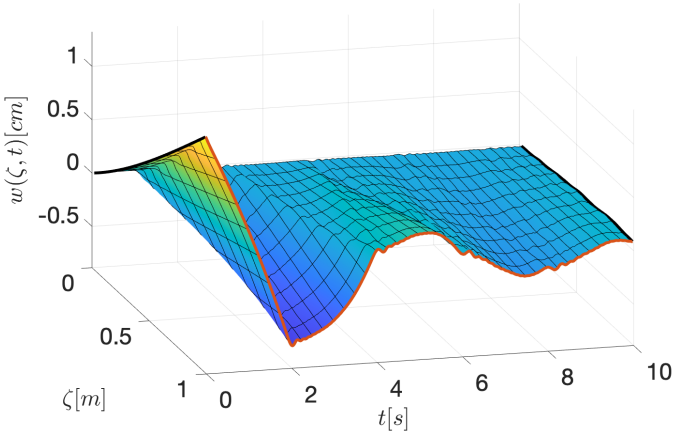

Figure III.32 – Beam deformation

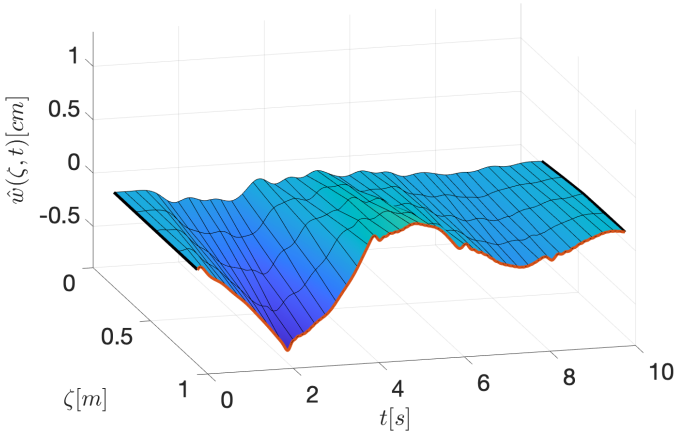

Figure III.33 – Observed deformation

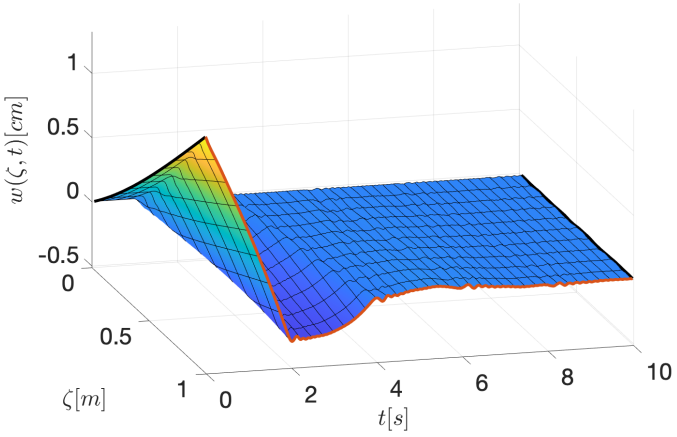

Figure III.34 – Beam deformation

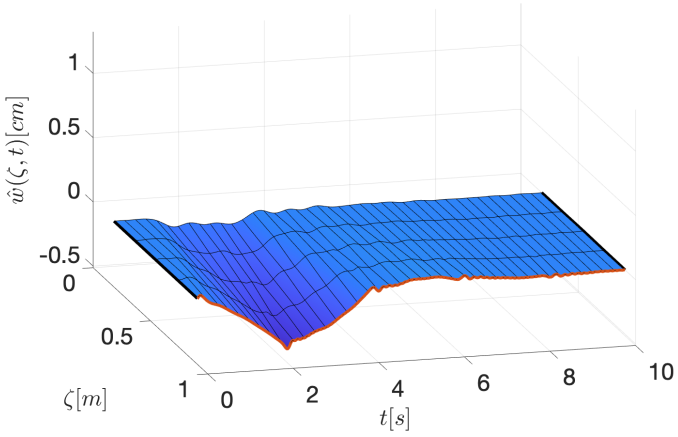

Figure III.35 – Observed deformation

Finally, in Figure III.36 and Figure III.37, we show the beam deformation along the space and time for design 3. The main difference with design 2 is that in design 3, the OBSF controller contains a more accurate model of the infinite-dimensional system. By increasing n_d (see Table III.4 and Table III.5), some higher frequency oscillations can also be attenuated.

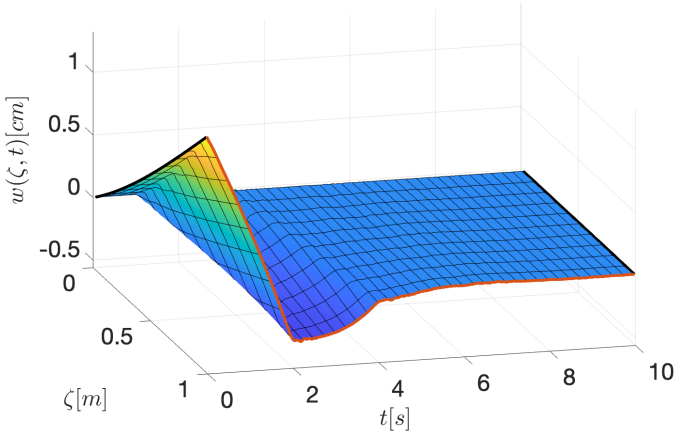

Figure III.36 – Beam deformation

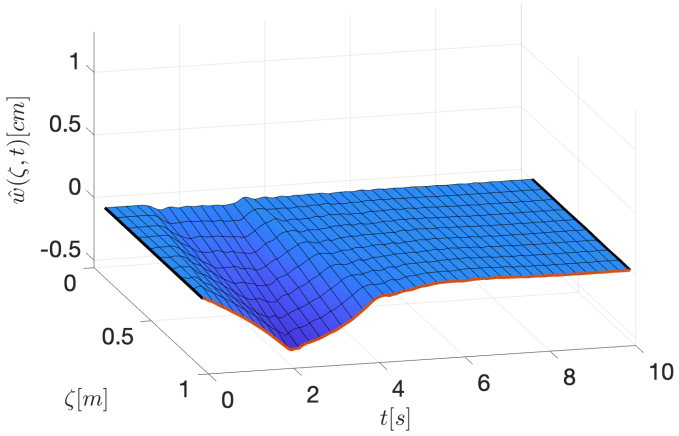

Figure III.37 – Observed deformation

♣

III.8 Extension to a class of nonlinear systems

The *strictly positive real* (SPR) structure imposed to the OBSF controller in Section III.4 can be advantageously used to stabilize a wide class of systems. In Section III.5, we have shown that, due to that structure, the OBSF controller can stabilize a *boundary controlled port-Hamiltonian system* (BC-PHS). In this section, we show that the same structure can stabilize a class of *nonlinear time invariant* (NTI) systems. This class is restricted to the NTI systems that are *output strictly passive* (OSP) and *zero state detectable* (ZSD). Then, we sow that the OBSF controller can be designed on a linear approximation of the NTI system using the same design methodologies proposed in Section III.6 and Section III.7. Finally, we show that when applying the OBSF controller to the NTI system, the stability is preserved.

III.8.1 Design method

In this section, we consider the following finite-dimensional nonlinear system:

$$\mathcal{P}\begin{cases}\dot{x}(t) = f(x(t),u(t)), & x(0) = x_0\\ y(t) = h(x(t),u(t)),\end{cases} \tag{III.26}$$

with $x(t) \in \mathbb{R}^n$, $x_0 \in \mathbb{R}^n$, $u(t) \in \mathbb{R}^m$, $y(t) \in \mathbb{R}^m$ and $f(\cdot)$ and $h(\cdot)$ sufficiently smooth differentiable mappings. The NTI system (III.26) is restricted to the class of nonlinear systems that are OSP and ZSD. In the following, we define these two characteristics.

Definition III.8.1. *[van der Schaft 00, Definition 3.1.4] The nonlinear system (III.26) is output strictly passive (OSP) if there exists $\epsilon > 0$ such that it is dissipative with respect to the supply rate $s(u,y) = u^\top y - \epsilon\|y\|^2$.* ♣

Definition III.8.2. *[van der Schaft 00, Definition 3.2.15] The nonlinear system (III.26) is zero state detectable (ZSD) if $u(t) = 0$, $y(t) = 0$, $\forall t \geq 0$, implies $\lim_{t\to\infty} x(t) = 0$.* ♣

We consider that the nonlinear system (III.26) is first linearized around an operational point. Then, the OBSF controller is designed on the linear approximation. Finally, the closed-loop stability is shown to be asymptotic when applying the OBSF controller to the nonlinear system. The following assumption is considered concerning the linearization.

Assumption III.8.1. *There exists a linear approximation of the NTI system (III.26) around the steady state $x = x^*$, $u = u^*$ and $y = y^*$ with the following structure*

$$P\begin{cases}\dot{x_\delta}(t) &= Ax_\delta(t) + Bu_\delta(t)\\ y_\delta(t) &= Cx_\delta(t)\end{cases} \tag{III.27}$$

where $x_\delta(t) = x(t) - x^*$, $u_\delta(t) = u(t) - u^*$ and $y_\delta(t) = y(t) - y^*$. $A \in \mathbb{R}^{n\times n}$, $B \in \mathbb{R}^{n\times m}$, and $C \in \mathbb{R}^{m\times n}$. Furthermore, we assume (III.27) to be controllable and observable. For simplicity, we refer to the system (A, B, C) as the approximated model of (III.26). ♣

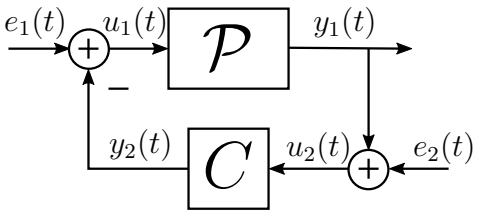

Figure III.38 – Passive interconnection.

Now, we show that, using the same approaches than the ones of the previous sections, we can design an OBSF controller on the linearized model (III.27). Then, we show that when applying the OBSF to the NTI system (III.26), the closed-loop stability is preserved. To this end, we recall a Proposition from [van der Schaft 00], wherein the asymptotic stability of a closed-loop system resulting from the power preserving interconnection between two OSP and ZSD systems is guaranteed. Figure III.38 shows the power preserving interconnection, where $\mathcal{P}$ represents the NTI system (III.26) and C represents the linear controller.

Proposition III.8.1. *[van der Schaft 00, Proposition 4.3.1] Assume that for every pair of allowed external input functions $e_1(\cdot)$, $e_2(\cdot)$ there exist allowed input functions $u_1(\cdot)$, $u_2(\cdot)$ of the closed-loop system of Figure III.38. Suppose that $\mathcal{P}$ and C are OSP and ZSD, and that S_1, S_2 satisfying*

$$\begin{aligned} S_1(x_1(t_1)) &\leq S_1(x_1(t_0)) + \int_{t_0}^{t_1} \left[u_1(t)^T y_1(t) - \varepsilon_1 \|y_1(t)\|^2\right] dt\\ S_2(x_2(t_1)) &\leq S_2(x_2(t_0)) + \int_{t_0}^{t_1} \left[u_2(t)^T y_2(t) - \varepsilon_2 \|y_2(t)\|^2\right] dt \end{aligned} \tag{III.28}$$

with $\varepsilon_1 > 0$ and $\varepsilon_2 > 0$, S_1 and S_2 are C^1 and have strict local minima at $x_1^* = 0$, respectively $x_2^* = 0$. Then, $x_1 = 0$ and $x_2 = 0$ is an asymptotically stable equilibrium when $e_1 = e_2 = 0$. ♢

Using Proposition III.8.1, we can show that the OBSF controller of the previous sections can stabilize a class of NTI systems. Indeed, if the the finite-dimensional controller (III.9) is designed using either Proposition III.6.1 or Proposition III.7.1, then we can show that the controller is OSP and ZSD. Finally, if the nonlinear system (III.26) is OSP and ZSD also, then the closed-loop system is asymptotically stable.

Proposition III.8.2. *Consider the dynamic controller (III.9). If $R_c > 0$, then (III.9) is strictly positive real (SPR), output strictly passive (OSP) and zero state detectable (ZSD) with respect to the input u_c and output y_c.* ◊

Proof. *The SPR property is a direct application of Corollary II.5.2. The OSP property follows noting that $R_c > 0$ and the Hamiltonian of the controller $H_c = \frac{1}{2}x_c^\top Q_c x_c$ satisfies*

$$\begin{aligned}\dot{H}_c &= -x_c^\top Q_c^\top R_c Q_c x_c + y_c^\top u_c \\ &= -x_c^\top Q_c (R_c - \epsilon B_c B_c^\top) Q_c x_c + y_c^\top u_c - \epsilon \|y_c\|^2\end{aligned} \tag{III.29}$$

where we have added $\pm\epsilon y_c^\top y_c$, with $\epsilon > 0$, to the first line of (III.29) and used $y_c = B_c^\top Q_c x_c$ and $Q_c = Q_c^\top$ in the second line of (III.29). Hence it is always possible to find a small enough ϵ such that (III.9) is dissipative with respect to the supply rate $y_c^\top u_c - \epsilon\|y_c\|^2$, implying that (III.9) is OSP. The ZSD property is inferred from (III.29) setting $u_c = y_c = B_c^\top Q_c x_c = 0$ and noting that since $R_c > 0$, the states of (III.9) converge exponentially to zero. ■

Finally, we add the following proposition, where the two design methods provided in the previous sections (Proposition III.6.1 and Proposition III.7.1) are suitable for the design of a linear OBSF controller for the NTI system (III.26).

Proposition III.8.3. *Consider the nonlinear system (III.26) and assume that is OSP and ZSD. Consider also, the control law given by*

$$u_\delta(t) = -K\hat{x}_\delta(t) + r_\delta(t) \tag{III.30a}$$

$$\dot{\hat{x}}_\delta(t) = A\hat{x}_\delta(t) + Bu_\delta(t) + L(y_\delta(t) - C\hat{x}_\delta(t)), \quad \hat{x}_\delta(0) = \hat{x}_{\delta 0}, \tag{III.30b}$$

with (A, B, C) from Assumption III.8.1. If K and L are designed either by Proposition III.6.1 or by Proposition III.7.1 (with $A_d = A$, $B_d = B$, and $C_d = C$), and the Hamiltonian has a minimum in $x = x^* = 0$, then $x = 0$ is an asymptotically stable equilibrium of the closed-loop system when $r_\delta(t) = 0$. ◊

Proof. *This proposition is a direct application of Proposition III.8.1. Indeed, from Proposition III.8.1, one can take $e_1 = e_2 = 0$, $x_1 = x$, $x_2 = \hat{x}_\delta$, $S_1(x_1) = H(x)$, $S_2(x_2) = H_c(\hat{x}_\delta) = \frac{1}{2}\hat{x}_\delta^T Q_c \hat{x}_\delta$, $u_1 = u$, $y_1 = y$, $u_2 = u_c = y_\delta$ and $y_2 = y_c = -u_\delta$. We assume that the nonlinear system (III.26) is OSP and ZSD. From Proposition III.8.2 we know that the observer-based controller (III.30) is OSP and ZSD if the matrix R_c is positive define. Using both Propositions III.6.1 and III.7.1, the matrix R_c is always positive define. Then, we have the passive interconnection between two OSP and ZSD systems, which implies that the closed-loop system is asymptotically stable.* ■

III.8.2 Application example

In the following example, we use a Microelectromechanical systems (MEMSs) to exemplify the finite-dimensional nonlinear case. We follow Procedure III.7.1 for the design of an OBSF controller for the MEMS.

Example III.8.1. *We consider the MEMS of Figure III.39, where $q(t)$ is the deformation of the non linear spring with spring coefficients k_1 and k_2, $p(t)$ is the momentum of the moving mass m, and $Q(t)$ is the charge in the capacitor $C(q(t))$ that depends on the spring deformation. b is the damping coefficient of the damper, r is resistance of the circuit, and $u(t)$ is the voltage input considered as an actuator.*

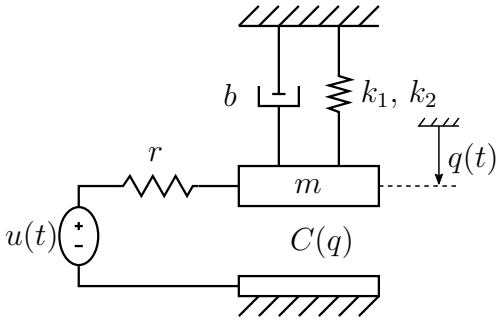

Figure III.39 – Microelectromechanical systems (MEMS)

The nonlinearities are due to the capacitance $C(q(t))$ and the spring force $F_k(q(t))$ given by:

$$C(q(t)) = \frac{\varepsilon A_s}{q_{max} - q(t)},$$
$$F_k(q(t)) = k_1 q(t) + k_2 q(t)^3,$$

where ε is the dielectric constant, A_s is the surface of the MEMS and q_{max} is such that $q(t) < q_{max}$. The parameters of the system are shown in Table III.6.

Table III.6 – Plant Parameters.

	Value	Unit
k_1	0.46	Nm^{-1}
k_2	1×10^{11}	Nm^{-3}
m	2.4×10^{-8}	kg
ε	8.854×10^{-12}	Fm^{-1}
A_s	4×10^{-4}	m^2
q_{max}	10^{-5}	m
b	10^{-7}	Ns
r	0.5×10^{6}	Ω

Step 1. We consider the port-Hamiltonian representation [Venkatraman 10b], where the Hamiltonian is given by

$$H(t) = \frac{p(t)^2}{2m} + \frac{1}{2}k_1 q(t)^2 + \frac{1}{4}k_2 q(t)^4 + \frac{Q(t)^2}{2C(q(t))}.$$

The dynamical model of the MEMS is

$$\begin{pmatrix} \dot{q} \\ \dot{p} \\ \dot{Q} \end{pmatrix} = \begin{pmatrix} 0 & 1 & 0 \\ -1 & -b & 0 \\ 0 & 0 & \frac{-1}{r} \end{pmatrix} \begin{pmatrix} \frac{\partial H}{\partial q} \\ \frac{\partial H}{\partial p} \\ \frac{\partial H}{\partial Q} \end{pmatrix} + \begin{pmatrix} 0 \\ 0 \\ \frac{1}{r} \end{pmatrix} u, \quad \begin{pmatrix} q(0) \\ p(0) \\ Q(0) \end{pmatrix} = \begin{pmatrix} q_0 \\ p_0 \\ Q_0 \end{pmatrix}, \tag{III.31}$$
$$y = \frac{1}{r}\frac{\partial H}{\partial Q}$$

where the input of the system is the voltage $u(t)$ and the output is the supplied current $y(t)$. q_0, p_0, Q_0 are the initial conditions of the system. The balance equation of the Hamiltonian is given by

$$\dot{H}(t) = -b\left(\frac{p(t)}{m}\right)^2 - ry(t)^2 + y(t)u(t)$$

which implies that the system is OSP. Assuming $Q(t) > 0$ for all $t > 0$, the system is ZSD.

Step 2. The linearization of (III.31) is done around the equilibrium point defined in Table III.7. The linearized model is on the form of (III.27) with the following matrices

Table III.7 – Linearization point.

	Value	Unit
q^*	0.5×10^{-6}	m
p^*	0	kg m s^{-1}
Q^*	4.1445×10^{-11}	C
u^*	0.1112	V
y^*	2.2234×10^{-8}	A

$$A = \begin{pmatrix} 0 & \frac{1}{m} & 0 \\ -3k_2(q^*)^2 - k_1 & -\frac{b}{m} & \frac{Q^*}{A_s\varepsilon} \\ \frac{Q^*}{A_s\varepsilon r} & 0 & \frac{q^* - q_{max}}{A_s\varepsilon r} \end{pmatrix} \tag{III.32}$$
$$B = \begin{pmatrix} 0 \\ 0 \\ \frac{1}{r} \end{pmatrix}, \qquad C = \begin{pmatrix} \frac{-Q^*}{A_s\varepsilon r} & 0 & \frac{-q^* - q_{max}}{A_s\varepsilon r} \end{pmatrix}$$

The linearized model approaches the nonlinear one near the equilibrium point. To show the influence of the nonlinearities, we simulate the nonlinear model and the linearized one in open loop with a step input, which moves away the system from the linearization point. Figure III.40 shows the step input $u(t)$, the output response of the nonlinear system $y(t)$ and the linearized one $y_\delta(t)$, and the

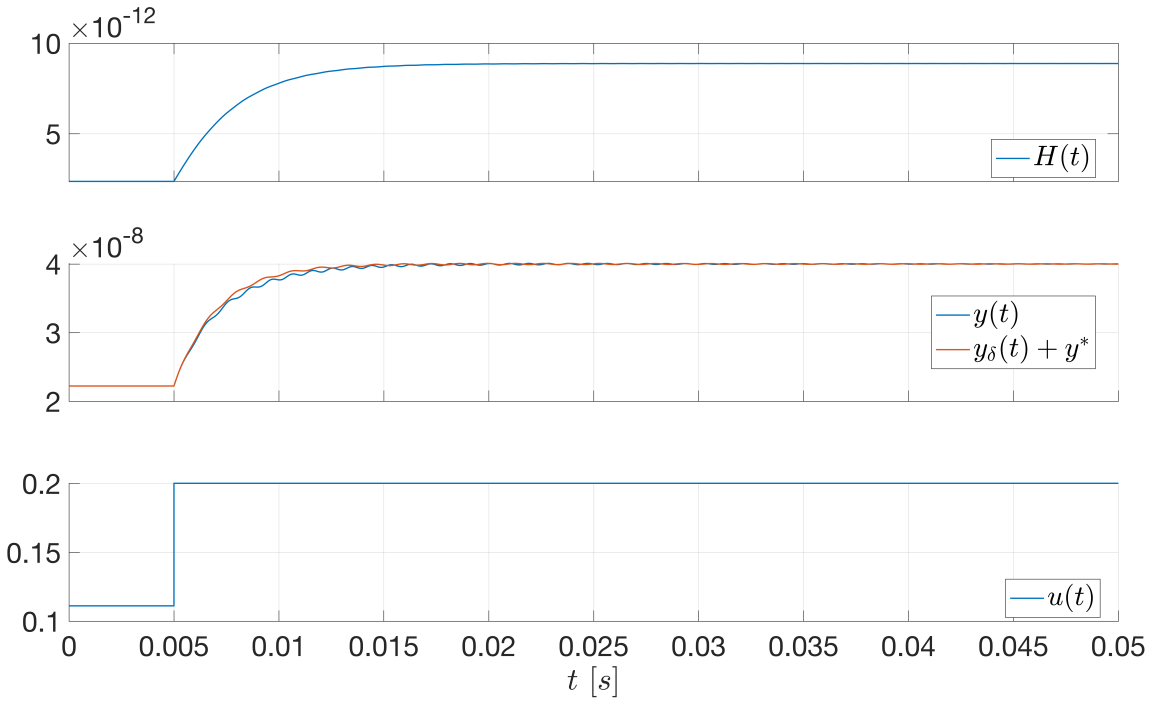

Figure III.40 – Top: Energy response in open loop. Middle: Output response of the nonlinear model (blue) and the linearized one (red). Bottom: Applied input.

Hamiltonian $H(t)$. We can see that the output of the linearized system reaches the same equilibrium as the output of the nonlinear one. However, during the transition the linearized system differs from the nonlinear one.

Figure III.41 shows the state response of the nonlinear system and the linearized one to a step input in open loop. The top figure shows the deformation of the string $q(t)$ and the linearized one $q_\delta(t)$. The middle figure shows the momentum of the mass $p(t)$ and the linearized one $p_\delta(t)$. And the bottom figure shows the charge in the capacitor $Q(t)$ and the linearized one $Q_\delta(t)$. Since, we take away the system from the linearization point, the reached equilibrium of the linearized model is not the same as the one of the nonlinear one (Top and bottom figures of Figure III.41). Also, in the middle figure (Figure III.41), we can see changes in frequency that are characteristic of nonlinear systems. In this particular example, this change of frequency is due to the high value of the spring coefficient k_2 in Table III.6.

The linearized model (III.27), with matrices (III.32) is used for the synthesis of the OBSF controller. Similar as the previous example, the gain L is designed using the IDA-PBC approach of [Prajna 02]. Then, we use Proposition III.7.1 for design of the state feedback gain K. In this way, the complete design is based on LMIs.

Step 3. The Luenberger gain L is designed using the LMI method proposed in [Prajna 02]. We follow Propositions A.3.2 from Appendix A.3 with the observer design parameters of Table III.8. Note that, from Remark A.3.2 we have to replace A by A^T, B by C^T and F by $-L^T$ in order to

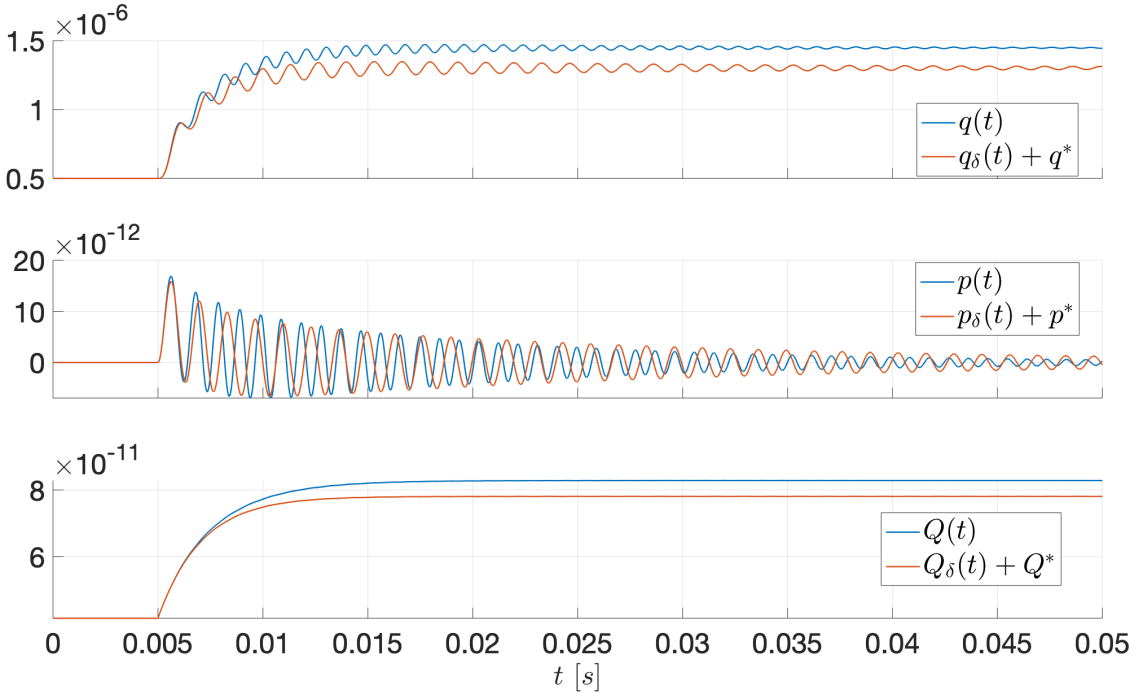

Figure III.41 – State response in open loop of the nonlinear model (blue) and the linearized one (red)

obtain the matrix L. The eigenvalues of the matrix A are shown in Figure III.42 as well as the eigenvalues of the obtained matrix $A_L = A - LC$. Note that, we can move the eigenvalues of A_L along the real axis by changing the design parameter γ (Table III.8).

Table III.8 – Observer design parameters

Matrix	Value
Λ_1	$1 \times 10^{-2} \times diag([1, 200, 1])$
Λ_2	$1 \times 10^{10} I_3$
Ξ_1	$1 \times 10^{-1} I_2$
Ξ_2	$1 \times 10^{4} I_2$
γ	30×10^{4}

As well as before, we simulate the open loop system composed by the nonlinear system and the observer. We use the same step input as before (Figure III.40). In Figure III.43, we show the state response of the nonlinear system in open loop (blue line), the linearized one (red line), and observed one (yellow line). In this case, the observer is initialized such that it is not at the linearization point ($\hat{x}_\delta(0) \neq 0$), and it considers as measurement the nonlinear output. Then, due to the nonlinearities, the error between the nonlinear system and the observer ($\tilde{x}(t) = x(t) - \hat{x}(t)$) is different to zero during the transitional period as shown in Figure III.44.

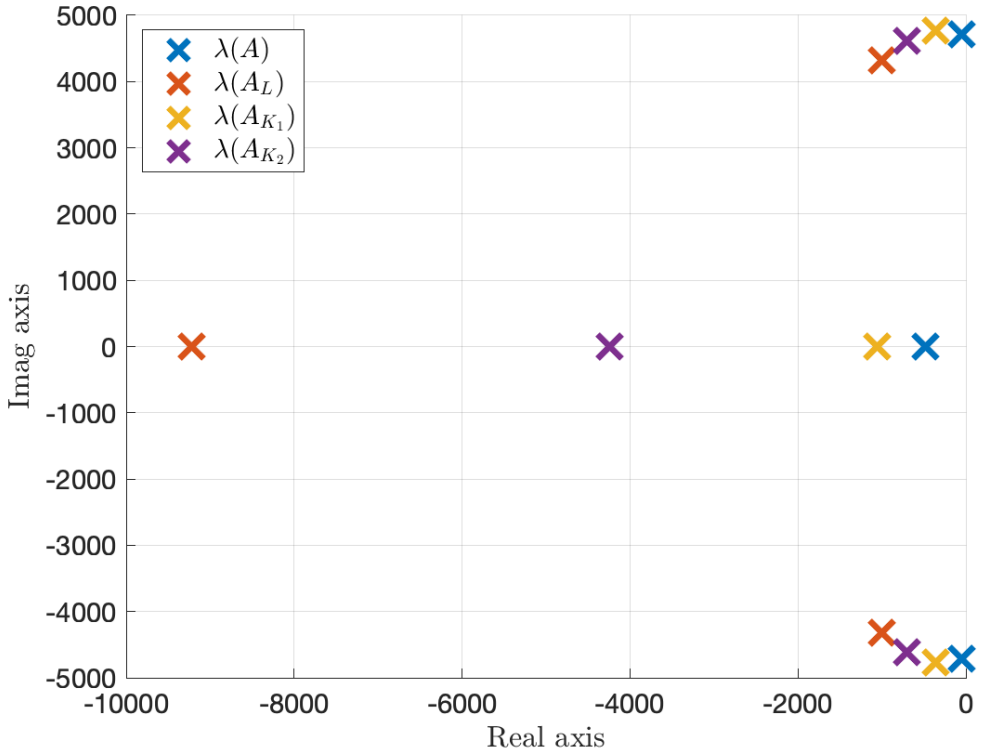

Figure III.42 – Plant $\lambda(A)$, observer $\lambda(A_L)$, controller 1 $\lambda(A_{K_1})$, and controller 2 $\lambda(A_{K_2})$ eigenvalues.

In the following, we design the state feedback gain using Proposition III.7.1. The benefit of using this proposition is that even if the state of the observer does not converge to the state of the nonlinear system (when the state is far from the linearization point), the closed-loop stability is guaranteed when applying the OBSF controller to the NTI system. Moreover, since the observer is more precise when it is closer to the linearization point, the performances can be assigned near this point.

Step 4. In order to show the different performances that can be achieved, we design two state feedback matrices K_1 and K_2 using the same observer gain obtained in Step 3. We use Proposition III.7.1 and for simplicity, we choose the matrices Γ_1, Γ_2, Δ_1, and Δ_2 as in Table III.9. Note that, the only difference on the design is given by Δ_1, implying bigger eigenvalues for the matrix Q_c in design 2 than design 1.

Table III.9 – Controller design parameters

Matrix	Design 1	Design 2
Γ_1	$1 \times 10^{-10} I_3$	$1 \times 10^{-10} I_3$
Γ_2	$1 \times 10^{10} I_3$	$1 \times 10^{10} I_3$
Δ_1	$0.1 I_3$	$0.3 I_3$
Δ_2	$1 \times 10^{10} I_3$	$1 \times 10^{10} I_3$

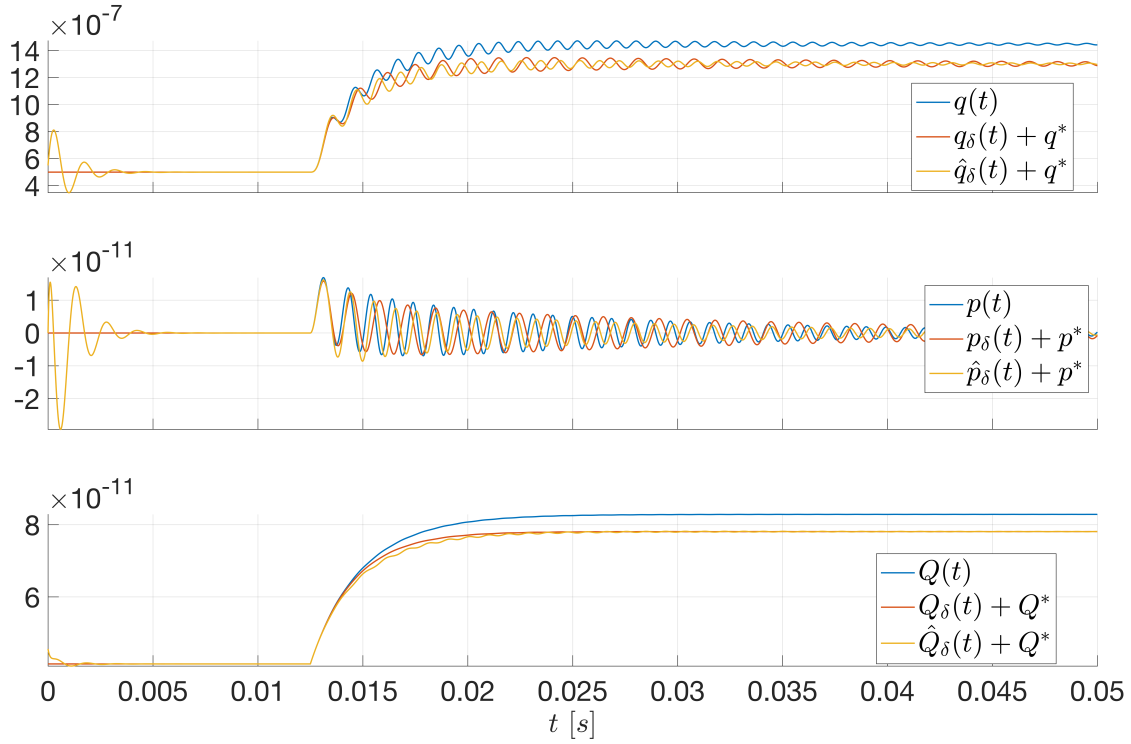

Figure III.43 – State response in open loop of the nonlinear model (blue), the linearized one (red), and the observed one (red).

Step 5. The LMI from Proposition III.7.1 is solved with $A_d = A$, $B_d = B$, $C_d = C$ *using the Matlab@ Robust Control Toolbox. For design 1, we obtain the following eigenvalues for the matrices* J_c, R_c *and* Q_c

$$\lambda(J_c) = \begin{pmatrix} +30.3578i \\ -30.3578i \\ 0 \end{pmatrix}, \quad \lambda(R_c) = \begin{pmatrix} 3.6621 \times 10^4 \\ 0.0359 \\ 4.8491 \times 10^{-7} \end{pmatrix}, \quad \lambda(Q_c) = \begin{pmatrix} 2.2934 \times 10^9 \\ 4.0314 \times 10^4 \\ 0.1217 \end{pmatrix},$$

and for design 2, the following eigenvalues are obtained

$$\lambda(J_c) = \begin{pmatrix} +13.5810i \\ -13.5810i \\ 0 \end{pmatrix}, \quad \lambda(R_c) = \begin{pmatrix} 4.9313 \times 10^3 \\ 0.0287 \\ 2.3287 \times 10^{-8} \end{pmatrix}, \quad \lambda(Q_c) = \begin{pmatrix} 8.1510 \times 10^9 \\ 1.0215 \times 10^5 \\ 0.3055 \end{pmatrix}.$$

Since (III.31) is OSP and ZSD and for booth controllers $\Gamma_1 > 0$ *(*$R_c > 0$*), the closed-loop system between the nonlinear system and the OBSF controller is asymptotically stable by Proposition III.8.3.*

Step 6. We compute $K = L^T Q_c$*. The eigenvalues of* $A_K = A - BK$ *are shown in Figure III.42 for the two cases, where* K_1 *and* K_2 *are the gain obtained for design 1 and 2, respectively.*

In Figures III.45, we show the state response using design 1. We show three different behaviors along the time. First, since the state of the nonlinear system is initialized at the linearization point and the observer is not, the initial behavior is due to both, the observer and controller. Then, at

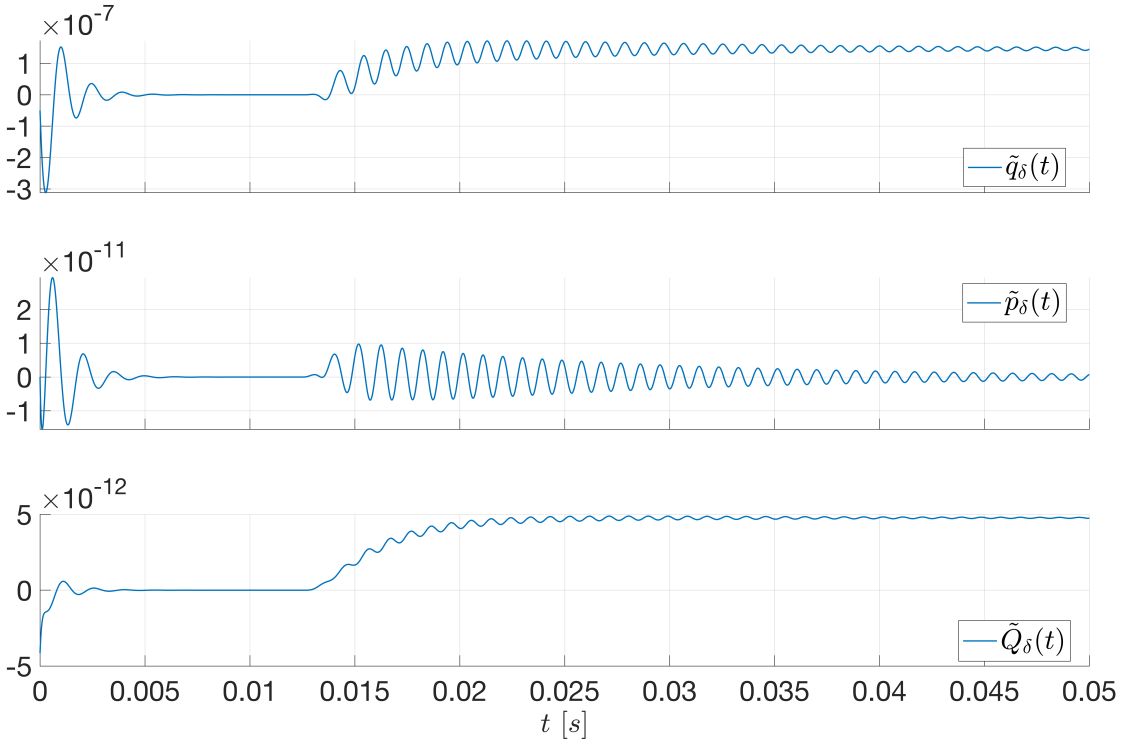

Figure III.44 – Error between the states of the nonlinear system and the states of the observer in open loop.

$t = 0.0125\,s$ *an external output is applied to change the equilibrium position. In this case, the behavior is mainly due to the controller. Since, the new equilibrium position is different to the linearization point, the nonlinear state achieves a different equilibrium position than the observed one. Even so, closed-loop stability is preserved. Finally, when the state goes closer to the equilibrium position, the observer state approaches the states of the nonlinear system, and the performances are closer to the desired ones. In Figure III.46, we show the input and output responses for design 1. We can see that the output of the nonlinear system achieves the same value of the output of the observer, even far from the linearization point.*

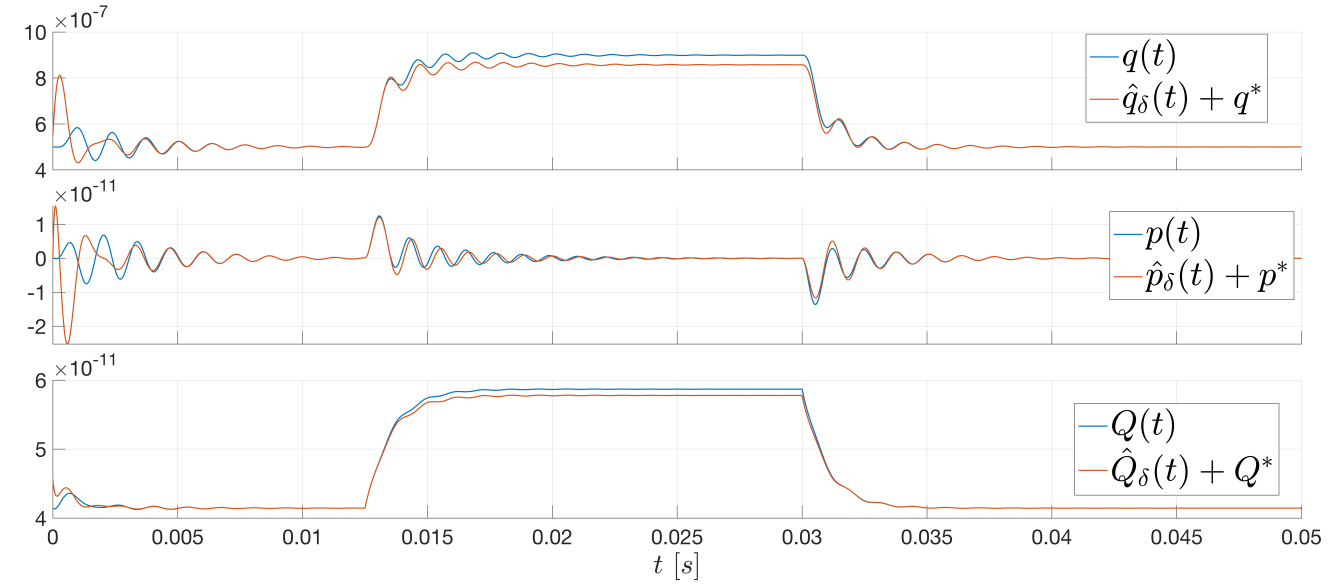

Figure III.45 – Design 1. State variable of the nonlinear system (blue) and state variable of the observer (red).

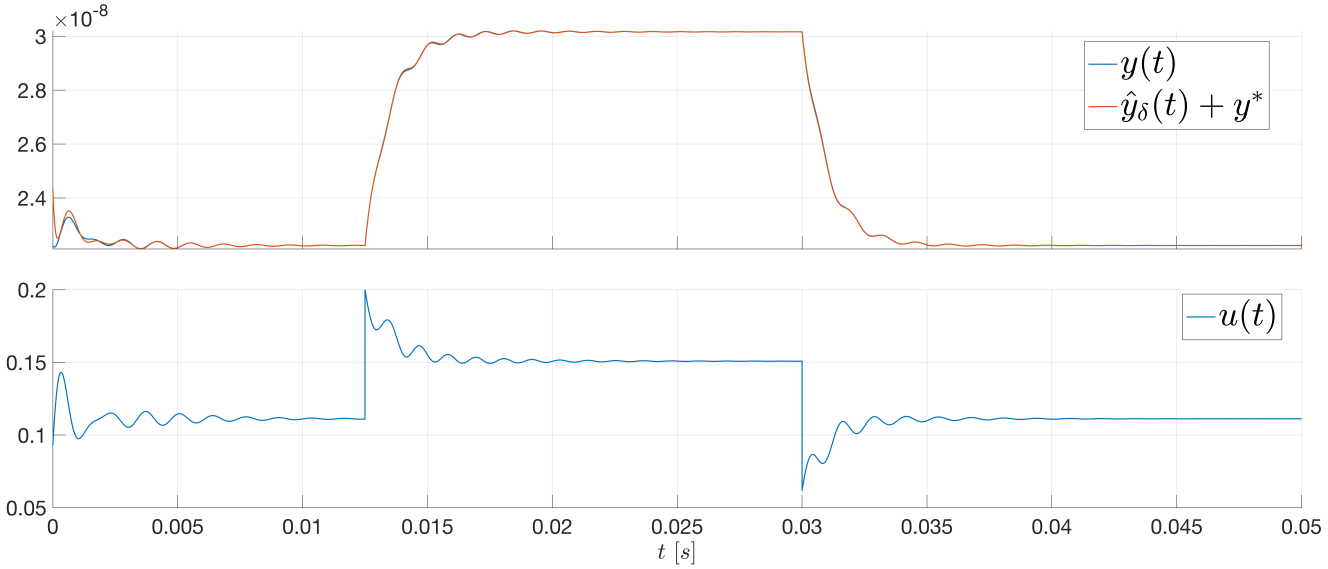

Figure III.46 – Design 1. Output of the nonlinear system (blue), output of the observer (red), and control law (bottom figure).

Similarly, in Figure III.47 and Figure III.48, we show the results for design 2. The main difference between design 1 and design 2 is the design parameter Δ_1 (See Table III.9). This implies bigger eigenvalues of the matrix Q_c for design 2 than design 1. In this case, when increasing the eigenvalues of Q_c we obtain a faster response but with overshoot.

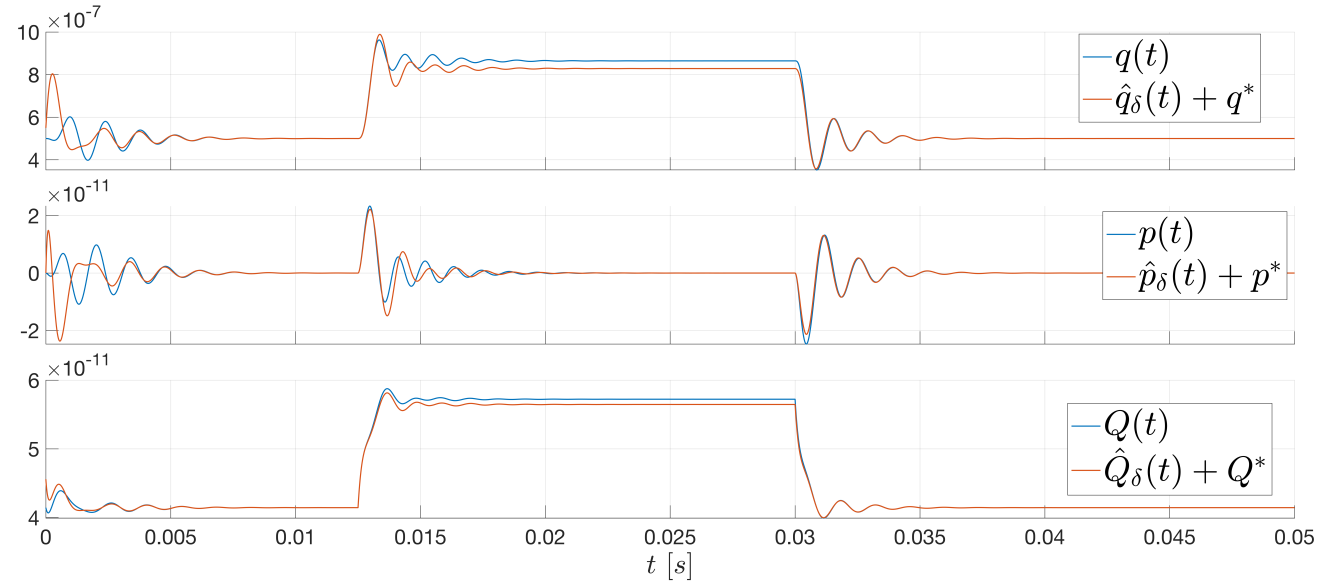

Figure III.47 – Design 2. State variable of the nonlinear system (blue) and state variable of the observer (red).

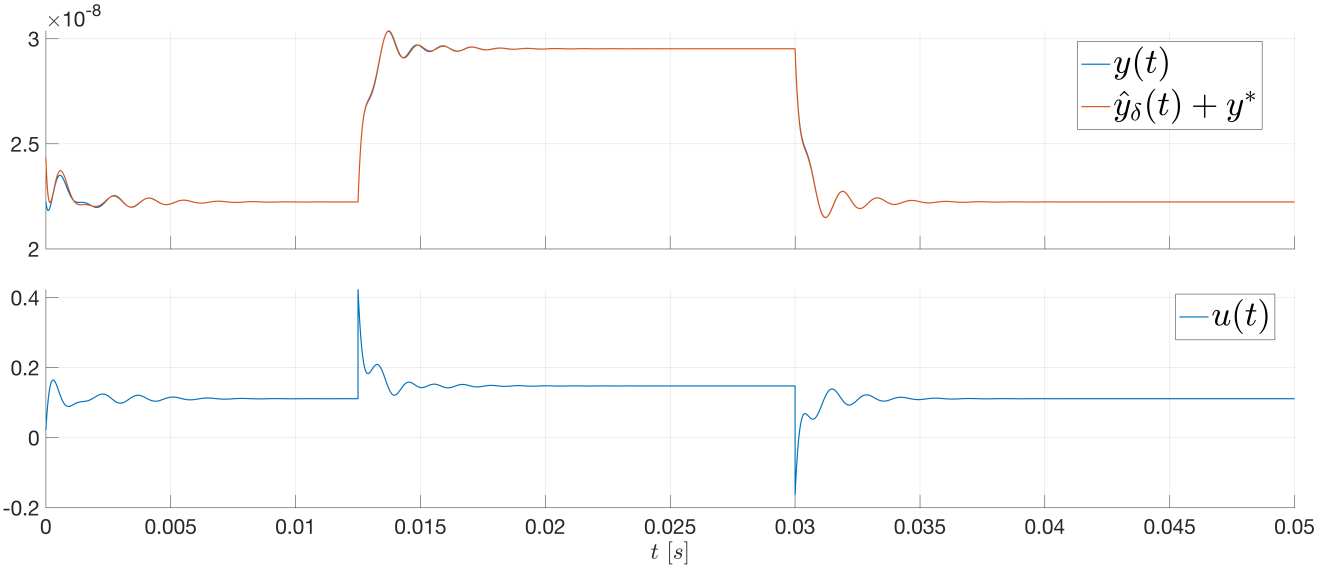

Figure III.48 – Design 2. Output of the nonlinear system (blue), output of the observer (red), and control law (bottom figure)

♣

III.9 Conclusions

In this chapter, we have used the *early-lumping approach* to design OBSF controllers for the stabilization of BC-PHSs. Using this approach, the BC-PHS is first discretized and the synthesis of the OBSF gains is based on the discretized model. Using an example, we have shown that if the OBSF gains are designed using classical control tools (like LQR or pole placement), then the closed-loop stability is not guaranteed when the OBSF controller is applied to the BC-PHS. Indeed, some high-frequency modes are destabilized by the OBSF controller, since they are not considered during the design.

To guarantee the closed-loop stability, we have imposed a passive structure on the OBSF controller. We have shown that using this structure, the OBSF controller stabilizes the BC-PHS. Then, we have proposed two methodologies for the synthesis of the OBSF gains. In the first method, the state feedback gain is freely designed by using classical control techniques, for instance, *linear quadratic regulator* or *pole placement*. Then, the observer gain is designed such that either the OBSF controller achieves a passive structure and some performances are assigned to the observer. In the second method, the observer gain is freely designed and the state feedback gain is designed such that either the OBSF controller achieves the desired structure and some performances are assigned to the state feedback gain. In both cases, the design of one of the two gains (K or L) is not completely free. This is the price to pay to achieve closed-loop stability when applying the OBSF controller to the BC-PHS. To exemplify these methodologies, we have used the vibrating string and the Timoshenko beam models.

We have extended this result to a class of *nonlinear time-invariant* (NTI) systems. We have shown that the proposed OBSF controller is *output strictly passive* (OSP) and *zero state detectable* (ZSD). Then, the OBSF controller can stabilize nonlinear systems that are OSP and ZSD too. In this way, the synthesis of the OBSF gains can be developed using the aforementioned methodologies. In this case, the synthesis is based on a linearized model. We have shown that when applying the OBSF controller to the NTI system, the closed-loop stability is guaranteed. We have used a microelectromechanical system to exemplify the synthesis method.

Chapter IV

Infinite-dimensional observer-based boundary controllers: late-lumping approach

IV.1 Introduction

Some first steps towards the design of observer-based control laws for impedance energy preserving boundary controlled port-Hamiltonian systems (BC-PHSs) [Le Gorrec 05] are presented in this chapter using the late-lumping approach. Using this approach, the observer is an infinite-dimensional system, and it has to be discretized for the real-time implementation.

First, we propose a general setting for the design of infinite-dimensional observers [Demetriou 04, Smyshlyaev 05, Hidayat 11, Meurer 13] for the class of impedance energy preserving BC-PHSs [Toledo 20, Malzer 20a]. The infinite-dimensional observer is designed in the case when the conjugated output is measured and in the case when the conjugated output is not measured but the integral over time of it is. Note that, we define the conjugated output with respect to the input such that the power of the system is given by the multiplication between the input and the conjugated output. In this chapter, we cover the cases in which either velocities, forces or displacements are measured in mechanical systems. To exemplify, we use the vibrating string with different kinds of sensors (force, velocity and displacement sensors) and the Timoshenko beam in the case where the transverse displacement and the rotation angle are measured at the end tip of the beam.

Then, we use these infinite-dimensional observers to apply control by *damping injection* and *energy shaping* [Schöberl 12, Macchelli 17] using the observed values [Malzer 20b]. For simplicity, we use the vibrating string example to illustrate these observer-based control techniques. First, we apply *observer-based damping injection* at both sides of the vibrating string with the measurement available only at one side of the spatial domain. This control strategy allows adding additional damping at the unmeasured side of the string. In this case, the settling time is smaller than when only one side damping is applied. We study the case when a force sensor is available and the case when a displacement sensor is available. Finally, we apply *energy shaping* and *damping injection* to the vibrating string using the observed values of the infinite-dimensional observer. In this case, we consider the vibrating string attached at one side and with a force actuator and velocity sensor at the other side. This control law allows to shape the closed-loop energy and does not require a proper initialization of the observer-based controller.

This chapter is organized as follows: in Section IV.2, we present the BC-PHS of interest, the observer structure and the resulting error system. In Section IV.3, we propose infinite-dimensional observers to estimate the state variables of the BC-PHS when different measurements are available. In Section IV.4, we consider the vibrating string, and we apply *damping injection* using the observed values when the force is measured on the left side and when the displacement is measured on the right side. In Section IV.5, we present some first steps towards observer-based *energy shaping* and *damping injection* for the vibrating string example. Some conclusion and future work are proposed in Section IV.6.

Scope of this chapter

Concerning the design of the infinite-dimensional observers presented in this chapter, in Table IV.1 and Table IV.2, we present an overview of the achievable examples related to the vibrating string and the Timoshenko beam, respectively. For the vibrating string, $F(a,t)$ is the force at $\zeta = a$, $v(b,t)$ is the velocity at $\zeta = b$ and $w(b,t)$ is the displacement at $\zeta = b$. For the Timoshenko beam,

$F(a,t)$ is the force at $\zeta = a$, $T(a,t)$ is the torque at $\zeta = a$, $v(b,t)$ is the velocity at $\zeta = b$ and, $\omega(b,t)$ is the angular velocity at $\zeta = b$, $w(b,t)$ is the displacement at $\zeta = b$, and $\phi(b,t)$ is the angular displacement at $\zeta = b$.

Table IV.1 – Scope of the observers for the vibrating string of this chapter

Measurements	Convergence	Example	Proposition
$F(a,t)$, $v(b,t)$	Exponential	Example IV.3.1	Proposition IV.3.1
$F(a,t)$	Exponential	Example IV.3.1	Proposition IV.3.2
$w(b,t)$	Asymptotic	Example IV.3.2	Proposition IV.3.3
$w(b,t)$, $v(b,t)$	Exponential	Section IV.3.4	Proposition IV.3.4

Table IV.2 – Scope of the observers for the Timoshenko beam of this chapter

Measurements	Convergence	Example	Proposition
$F(a,t)$, $T(a,t)$	Exponential		Proposition IV.3.2
$v(b,t)$, $\omega(b,t)$	Exponential		Proposition IV.3.2
$w(b,t)$, $\phi(b,t)$	Asymptotic	Section IV.3.3	Proposition IV.3.3

Similarly, in Table IV.3, we present an overview of the results concerning *observer-based damping injection and energy shaping* for the vibrating string. In this table, we show the type of sensors, the type of actuators, the closed-loop stability and the control strategy. In this case, $F(a,t)$ is the force at $\zeta = a$, $F(b,t)$ is the force at $\zeta = b$, $w(b,t)$ is the displacement at $\zeta = b$, $v(a,t)$ is the velocity at $\zeta = a$, and $v(b,t)$ is the velocity at $\zeta = b$.

Table IV.3 – Control scope for the vibrating string

Sensors	Actuators	Stability	Control law	Section
$F(a,t)$	$v(a,t)$, $F(b,t)$	Exponential	Damping injection (DI)	Section IV.4.1
$w(b,t)$	$v(a,t)$, $F(b,t)$	Asymptotic	Damping injection (DI)	Section IV.4.2
$v(b,t)$	$F(b,t)$	Asymptotic	Energy shaping + DI	Section IV.5

IV.2 Preliminaries

We consider the following BC-PHS:

$$\mathcal{P}\begin{cases}\dfrac{\partial x}{\partial t}(\zeta,t) = P_1\dfrac{\partial}{\partial\zeta}(\mathcal{H}(\zeta)x(\zeta,t)) + P_0\mathcal{H}(\zeta)x(\zeta,t), \quad x(\zeta,0) = x_0(\zeta),\\ W_{\mathcal{B}}\begin{pmatrix} f_\partial(t)\\ e_\partial(t)\end{pmatrix} = u(t),\\ y(t) = W_{\mathcal{C}}\begin{pmatrix} f_\partial(t)\\ e_\partial(t)\end{pmatrix},\\ y_m(t) = \mathcal{C}_m x(\zeta,t),\end{cases} \tag{IV.1}$$

where $\zeta \in [a,b]$ is the spatial variable and $t \geq 0$ is the time variable. $x(\zeta,t) \in \mathbb{R}^n$ is the state variable with initial condition $x_0(\zeta)$. $P_1 = P_1^T \in M_n(\mathbb{R})$ is a non-singular matrix, $P_0 = -P_0^T \in M_n(\mathbb{R})$, $\mathcal{H}(\cdot) \in M_n(L_2([a,b];\mathbb{R}))$ is a bounded and continuously differentiable matrix-valued function satisfying for all $\zeta \in [a,b]$, $\mathcal{H}(\zeta) = \mathcal{H}^T(\zeta)$ and $mI < \mathcal{H}(\zeta) < MI$ with $0 < m < M$ both scalars independent of ζ. The Hamiltonian of the BC-PHS (IV.1) is given by

$$H(t) = \frac{1}{2}\int_a^b x(\zeta,t)^T\mathcal{H}(\zeta)x(\zeta,t)d\zeta. \tag{IV.2}$$

The *boundary port variables* [Le Gorrec 05] associated to the BC-PHS (IV.1) are obtained such that $\dot{H} = f_\partial(t)^T e_\partial(t)$ as follows:

$$\begin{pmatrix} f_\partial(t)\\ e_\partial(t)\end{pmatrix} = \frac{1}{\sqrt{2}}\begin{pmatrix} P_1 & -P_1\\ I & I\end{pmatrix}\begin{pmatrix}\mathcal{H}(b)x(b,t)\\ \mathcal{H}(a)x(a,t)\end{pmatrix}. \tag{IV.3}$$

$W_{\mathcal{B}}$ is defined such that it has full rank and satisfies $W_{\mathcal{B}}\Sigma W_{\mathcal{B}}^T = 0$, with $\Sigma = \begin{pmatrix} 0_n & I_n\\ I_n & 0_n\end{pmatrix}$. $W_{\mathcal{C}}$ is defined such that (IV.1) is an impedance energy preserving system, *i.e.* $W_{\mathcal{C}}\Sigma W_{\mathcal{C}}^T = 0$ and $W_{\mathcal{C}}\Sigma W_{\mathcal{B}}^T = I$. Finally, $u(t) \in \mathbb{R}^n$ is the input, $y(t) \in \mathbb{R}^n$ is the conjugated output, and $y_m(t) \in \mathbb{R}^p$ is the measured output, with $\mathcal{C}_m$ a boundary operator which maps the state into the measured variables located at the spatial boundaries of the domain of ζ.

Definition IV.2.1. *The following infinite-dimensional system:*

$$\hat{\mathcal{P}}\begin{cases}\dfrac{\partial\hat{x}}{\partial t}(\zeta,t) = P_1\dfrac{\partial}{\partial\zeta}(\mathcal{H}\hat{x}(\zeta,t)) + P_0(\mathcal{H}\hat{x}(\zeta,t)), \quad \hat{x}(\zeta,0) = \hat{x}_0(\zeta)\\ W_{\mathcal{B}}\begin{pmatrix}\hat{f}_\partial(t)\\ \hat{e}_\partial(t)\end{pmatrix} = \hat{u}(t),\\ \hat{y}(t) = W_{\mathcal{C}}\begin{pmatrix}\hat{f}_\partial(t)\\ \hat{e}_\partial(t)\end{pmatrix},\\ \hat{y}_m(t) = \mathcal{C}_m\hat{x}(\zeta,t),\end{cases} \tag{IV.4}$$

is an observer of the BC-PHS (IV.1) if $\hat{x}(\zeta,t)$ converge to $x(\zeta,t)$ for some initial condition $\hat{x}_0(\zeta) \neq x_0(\zeta)$. P_1, P_0, $\mathcal{H}$, $W_{\mathcal{B}}$, $W_{\mathcal{C}}$, and $\mathcal{C}_m$ are defined in (IV.1), and the observer boundary port variables $\begin{pmatrix}\hat{f}_\partial(t)\\ \hat{e}_\partial(t)\end{pmatrix}$ are defined in the same way as in (IV.3). ♣

Since the system $\hat{\mathcal{P}}$ in (IV.4) is virtual, the input $\hat{u}(t)$ is designed with all the available information, i.e. $\hat{u}(t) = f(u(t), y_m(t), \hat{x}(\zeta,t))$, where $u(t)$ and $y_m(t)$ are considered known from (IV.1) and $f(\cdot)$ is a function to be designed. In the following section, we design this function for different types

of measurements $y_m(t)$. To analyze the convergence of the observer, it is convenient to analyze the error between the state of (IV.1) and the state of (IV.4). To this end, we define the error between the BC-PHS (IV.1) and the observer (IV.4) as:

$$\tilde{x}(\zeta,t) := x(\zeta,t) - \hat{x}(\zeta,t). \tag{IV.5}$$

Then, from (IV.1) and (IV.4), we obtain the error dynamics equations as follows:

$$\tilde{\mathcal{P}}\begin{cases} \dfrac{\partial \tilde{x}}{\partial t}(\zeta,t) = P_1 \dfrac{\partial}{\partial \zeta}(\mathcal{H}\tilde{x}(\zeta,t)) + P_0(\mathcal{H}\tilde{x}(\zeta,t)), \quad \tilde{x}(\zeta,0) = \tilde{x}_0(\zeta) \\ W_{\mathcal{B}}\begin{pmatrix} \tilde{f}_\partial(t) \\ \tilde{e}_\partial(t) \end{pmatrix} = \tilde{u}(t), \\ \tilde{y}(t) = W_{\mathcal{C}}\begin{pmatrix} \tilde{f}_\partial(t) \\ \tilde{e}_\partial(t) \end{pmatrix}. \end{cases} \tag{IV.6}$$

We define the Hamiltonian of the error system as:

$$\tilde{H}(t) = \frac{1}{2}\|\tilde{x}(t)\|^2_{\mathcal{H}} = \frac{1}{2}\int_a^b \tilde{x}(\zeta,t)^T \mathcal{H}(\zeta)\tilde{x}(\zeta,t)d\zeta. \tag{IV.7}$$

Since $W_{\mathcal{B}}$ and $W_{\mathcal{C}}$ are such that $W_{\mathcal{C}}\Sigma W_{\mathcal{B}}^T = I$, the time derivative of $\tilde{H}(t)$ satisfies

$$\dot{\tilde{H}}(t) = \tilde{u}(t)^T \tilde{y}(t). \tag{IV.8}$$

An important property of BC-PHS is shown in the following theorem. This property is in general used for showing the exponential stability of BC-PHSs. In this chapter, we use it for showing that the error system is exponentially stable for different kinds of observers. This theorem states that the Hamiltonian of the error system $\tilde{H}(t)$ is bounded by the integral over time of the co-energy variables evaluated at the spatial boundaries.

Theorem IV.2.1. *Consider the error system (IV.6) with $W_{\mathcal{B}}$ such that $W_{\mathcal{B}}\Sigma W_{\mathcal{B}}^T \geq 0$ and $\Sigma = \begin{pmatrix} 0_n & I_n \\ I_n & 0_n \end{pmatrix}$. If $W_{\mathcal{B}}\begin{pmatrix} \tilde{f}_\partial(t) \\ \tilde{e}_\partial(t) \end{pmatrix} = 0$, for all $t \geq 0$, then the Hamiltonian of the error system $\tilde{H}(t) = \frac{1}{2}\|\tilde{x}(t)\|^2_{\mathcal{H}}$ satisfies for τ large enough*

$$\begin{aligned} \tilde{H}(\tau) &\leq c(\tau)\int_0^\tau \|\mathcal{H}(b)\tilde{x}(b,t)\|^2_{\mathbb{R}}dt, \quad \textit{and} \\ \tilde{H}(\tau) &\leq c(\tau)\int_0^\tau \|\mathcal{H}(a)\tilde{x}(a,t)\|^2_{\mathbb{R}}dt \end{aligned} \tag{IV.9}$$

where $c(\tau)$ is a constant that only depends on τ. ♢

Proof. *This result is a direct application of [Villegas 07, Theorem 5.17] to the error system (IV.6).* ■

Remark IV.2.1. *Note that, we consider BC-PHSs (IV.1) that are impedance energy preserving systems, i.e. $W_{\mathcal{B}}\Sigma W_{\mathcal{B}}^T = W_{\mathcal{C}}\Sigma W_{\mathcal{C}}^T = 0$ and $W_{\mathcal{C}}\Sigma W_{\mathcal{B}}^T = I$. Then, the condition of Theorem IV.2.1 are satisfied. Moreover, even if $W_{\mathcal{B}}\Sigma W_{\mathcal{B}}^T \geq 0$, we can use Theorem IV.2.1. We use this property in the following section to show the exponential convergence of the proposed observers.* ♣

IV.3 Infinite-dimensional observers

In this section, the synthesis of infinite-dimensional observers for BC-PHSs is studied. The aim of these observers is to reconstruct the overall state from partial measurement. We consider three different cases depending on the nature of the measurements. First, we consider the case where we can measure the conjugated output or a part of it. This is the case for instance, when the velocity can be measured in a vibrating string. Then, we consider the case where the conjugated output is not available but its integral over time is. This is the case for instance, when the deformation is measured instead of the velocity in a vibrating string. Finally, we consider the case where both are measured together.

IV.3.1 The co-energy variables are measured

When the full conjugated output $y(t)$ (co-energy variables) from (IV.1) is measured, it is straightforward to design an exponential convergent observer for the BC-PHS (IV.1). Indeed, the observer design problem is equivalent to the *damping injection* approach for BC-PHS. In the following proposition, the convergence of the observer (IV.4) is guaranteed to be exponentially when the full conjugated output is measured.

Proposition IV.3.1. *Consider the BC-PHS (IV.1). Assume that the full conjugated output is measurable, i.e. $y_m(t) = y(t)$. The state of the observer (IV.4) with*

$$\hat{u}(t) = u(t) + L(y_m(t) - \hat{y}_m(t)), \tag{IV.10}$$

converge exponentially to the state of the BC-PHS (IV.1) if $0 < L + L^T \in \mathbb{R}^{n\times n}$.

◊

Proof. *This is an application case of [Villegas 07, Theorem 5.17]. We show the exponential convergence of the observer by showing that the error (IV.5) converges to zero exponentially. Using (IV.10) in the observer (IV.4), the input of the error system (IV.6) reads*

$$\tilde{u}(t) = -L\tilde{y}(t), \tag{IV.11}$$

and the balance equation (IV.8) becomes

$$\dot{\tilde{H}}(t) = -\tilde{y}(t)^T L\tilde{y}(t). \tag{IV.12}$$

Finally, the error system can be written as

$$\begin{cases} \dfrac{\partial\tilde{x}}{\partial t}(\zeta,t) = P_1\dfrac{\partial}{\partial\zeta}(\mathcal{H}\tilde{x}(\zeta,t)) + P_0(\mathcal{H}\tilde{x}(\zeta,t)), \quad \tilde{x}(\zeta,0) = \tilde{x}_0(\zeta) \\ W_L\begin{pmatrix}\tilde{f}_\partial(t)\\ \tilde{e}_\partial(t)\end{pmatrix} = 0, \quad W_L = W_\mathcal{B} + LW_\mathcal{C}, \\ \tilde{y}(t) = W_\mathcal{C}\begin{pmatrix}\tilde{f}_\partial(t)\\ \tilde{e}_\partial(t)\end{pmatrix}. \end{cases} \tag{IV.13}$$

According to [Le Gorrec 05, Theorem 4.1], the error system (IV.13) is well-posed if $W_L\Sigma W_L^T \geq 0$. Since $W_L = W_\mathcal{B} + LW_\mathcal{C}$, $W_\mathcal{B}\Sigma W_\mathcal{B}^T = W_\mathcal{C}\Sigma W_\mathcal{C}^T = 0$, $W_\mathcal{B}\Sigma W_\mathcal{C}^T = I_n$, and $L = L^T > 0$, the inequality $W_L\Sigma W_L^T \geq 0$ is satisfied. Since $W_L\Sigma W_L^T \geq 0$ and $W_L\begin{pmatrix}\tilde{f}_\partial(t)\\ \tilde{e}_\partial(t)\end{pmatrix} = 0$, the estimations (IV.9) of the Hamiltonian error are satisfied (see Theorem IV.2.1). Then, the proof follows the same line of the proof of Theorem II.5.2 (see [Villegas 07, Theorem 5.17] for further details).

Indeed, we use the estimations (IV.9) *to show that the error system converges to zero exponentially. To this end, we show that, for some* τ *large enough and some positive constants* c_τ, l_1 *and* m_1, *the Hamiltonian of the error system is such that*

$$\tilde{H}(\tau) \leq \frac{c_\tau}{c_\tau + l_1 m_1} \tilde{H}(0). \tag{IV.14}$$

To find the estimation (IV.14), *we write the boundary condition and the output* $\tilde{y}(t)$ *of* (IV.13) *as follows:*

$$\begin{pmatrix} 0 \\ \tilde{y}(t) \end{pmatrix} = \frac{1}{\sqrt{2}} \begin{pmatrix} W_L \\ W_{\mathcal{C}} \end{pmatrix} \begin{pmatrix} P_1 & -P_1 \\ I_n & I_n \end{pmatrix} \begin{pmatrix} \mathcal{H}(b)\tilde{x}(b,t) \\ \mathcal{H}(a)\tilde{x}(a,t) \end{pmatrix}. \tag{IV.15}$$

We define the matrix

$$M = \frac{1}{\sqrt{2}} \begin{pmatrix} W_L \\ W_{\mathcal{C}} \end{pmatrix} \begin{pmatrix} P_1 & -P_1 \\ I_n & I_n \end{pmatrix}. \tag{IV.16}$$

The matrix $R_{ext} = \frac{1}{\sqrt{2}} \left(\begin{smallmatrix} P_1 & -P_1 \\ I_n & I_n \end{smallmatrix}\right)$ *is invertible (See [Le Gorrec 05, Lemma 3.4]). The matrix* $\left(\begin{smallmatrix} W_L \\ W_{\mathcal{C}} \end{smallmatrix}\right)$ *is also invertible. Indeed* $\left(\begin{smallmatrix} W_L \\ W_{\mathcal{C}} \end{smallmatrix}\right)$ *is invertible if and only if* $\left(\begin{smallmatrix} W_L \Sigma W_L^T & W_L \Sigma W_{\mathcal{C}}^T \\ W_{\mathcal{C}} \Sigma W_L^T & W_{\mathcal{C}} \Sigma W_{\mathcal{C}}^T \end{smallmatrix}\right)$ *is invertible with* $\Sigma = \left(\begin{smallmatrix} 0_n & I_n \\ I_n & 0_n \end{smallmatrix}\right)$ *(See [Le Gorrec 05, Theorem 4.2]). Then, one can compute*

$$\begin{pmatrix} W_L \Sigma W_L^T & W_L \Sigma W_{\mathcal{C}}^T \\ W_{\mathcal{C}} \Sigma W_L^T & W_{\mathcal{C}} \Sigma W_{\mathcal{C}}^T \end{pmatrix} = \begin{pmatrix} L^T + L & I_n \\ I_n & 0_n \end{pmatrix}, \tag{IV.17}$$

which has an inverse and it is $\left(\begin{smallmatrix} 0_n & I_n \\ I_n & -(L^T+L) \end{smallmatrix}\right)$. *Then, the matrix* M *in* (IV.16) *is invertible as well. This implies that* $\|Mw\|_{\mathbb{R}}^2 \geq m_1 \|w\|_{\mathbb{R}}^2$, *for some vector* w *of appropriated dimension and a constant* m_1 *that can be the smallest eigenvalue of* M, *for instance. If we compute the norm at both sides of* (IV.15), *we obtain the following:*

$$\|\tilde{y}(t)\|_{\mathbb{R}}^2 = \left\| M \begin{pmatrix} \mathcal{H}(b)\tilde{x}(b,t) \\ \mathcal{H}(a)\tilde{x}(a,t) \end{pmatrix} \right\|_{\mathbb{R}}^2 \geq m_1 \left\| \begin{pmatrix} \mathcal{H}(b)\tilde{x}(b,t) \\ \mathcal{H}(a)\tilde{x}(a,t) \end{pmatrix} \right\|_{\mathbb{R}}^2 \geq m_1 \|\mathcal{H}(b)\tilde{x}(b,t)\|_{\mathbb{R}}^2.$$

This implies that the norm of the error co-energy variables evaluated at the spatial boundaries are bounded by the norm of the output as follows:

$$\|\mathcal{H}(b)\tilde{x}(b,t)\|_{\mathbb{R}}^2 \leq \frac{1}{m_1} \|\tilde{y}(t)\|_{\mathbb{R}}^2 \tag{IV.18}$$

(similar with $\|\mathcal{H}(b)\tilde{x}(a,t)\|_{\mathbb{R}}^2$*). Moreover, since* L *is positive definite, the norm of the output can be also bounded as follows*

$$\|\tilde{y}(t)\|_{\mathbb{R}}^2 \leq \frac{1}{l_1} \tilde{y}(t)^T L \tilde{y}(t), \tag{IV.19}$$

with l_1 *a positive scalar that can be for instance the smallest eigenvalue of* L. *Then, from* (IV.18) *and* (IV.19), *one can conclude*

$$\|\mathcal{H}(b)\tilde{x}(b,t)\|_{\mathbb{R}}^2 \leq \frac{1}{m_1 l_1} \tilde{y}(t)^T L \tilde{y}(t). \tag{IV.20}$$

Since the error system (IV.13) *is a BC-PHS and satisfies the conditions of Theorem IV.2.1* ($W_L\Sigma W_L^T \geq 0$ *and* $W_L\begin{pmatrix}\tilde{f}_\partial(t)\\ \tilde{e}_\partial(t)\end{pmatrix} = 0$*), we can use the estimations* (IV.9). *Then, using* (IV.9) *and* (IV.20) *we obtain the following estimation for the Hamiltonian of the error system:*

$$\tilde{H}(\tau) \leq \frac{c_\tau}{m_1 l_1}\int_0^\tau \tilde{y}(t)^T L\tilde{y}(t)dt. \tag{IV.21}$$

Finally, from (IV.12) *we obtain*

$$\tilde{H}(\tau) - \tilde{H}(0) = -\int_0^\tau \tilde{y}(t)^T L\tilde{y}(t)dt. \tag{IV.22}$$

Replacing (IV.22) *into the estimation* (IV.21)*, we obtain the estimation* (IV.14)*, concluding that the error state* $\tilde{x}(\zeta,t)$ *converges to zero exponentially.*

■

The previous proposition is valid in the case where the full conjugated output is measured. However, the full conjugated output $y(t)$ is not always fully measurable. This is the case, for example, when the sensors are restricted to be at one side of the spatial domain. In these cases, by showing an extra condition, we also can design exponentially convergent observers for the BC-PHS (IV.1). In the following proposition, we give a necessary condition to guarantee the exponential convergence of the observer (IV.4) when the conjugated output is partially measured.

Proposition IV.3.2. *Consider the BC-PHS* (IV.1)*. Assume that the conjugated output is partially measurable, i.e.* $y_m(t) = C_m y(t)$*, with* $C_m = \begin{pmatrix} I_p & 0_{p\times n-p}\end{pmatrix} \in \mathbb{R}^{p\times n}$ *and* $0 < p < n$*. The states of the observer* (IV.4) *with*

$$\hat{u}(t) = u(t) + C_m^T L(y_m(t) - \hat{y}_m(t)) \quad \text{and} \quad L \in \mathbb{R}^{p\times p} \tag{IV.23}$$

converges exponentially to the state of the BC-PHS (IV.1) *if* L *is such that* $C_m^T L^T C_m + C_m^T L C_m \geq 0$*, and one of the following conditions is satisfied*

$$\begin{aligned}\|\mathcal{H}(b)\tilde{x}(b,t)\|_{\mathbb{R}}^2 &\leq \gamma\tilde{y}(t)^T C_m^T L C_m\tilde{y}(t) \quad \text{or}\\ \|\mathcal{H}(a)\tilde{x}(a,t)\|_{\mathbb{R}}^2 &\leq \gamma\tilde{y}(t)^T C_m^T L C_m\tilde{y}(t),\end{aligned} \tag{IV.24}$$

for some scalar $\gamma > 0$. ◊

Proof. *Showing the exponential convergence of the observer is equivalent to show that the error* (IV.5) *converges to zero exponentially. Using* (IV.23) *in the observer* (IV.4)*, the input of the error system* (IV.6) *becomes*

$$\tilde{u}(t) = -C_m^T L C_m\tilde{y}(t), \tag{IV.25}$$

and the balance equation (IV.8) *becomes*

$$\dot{\tilde{H}}(t) = -\tilde{y}(t)^T C_m^T L C_m\tilde{y}(t) = -\tilde{y}_m(t)^T L\tilde{y}_m(t). \tag{IV.26}$$

Finally, the error system can be written as

$$\begin{cases}\dfrac{\partial\tilde{x}}{\partial t}(\zeta,t) = P_1\dfrac{\partial}{\partial\zeta}(\mathcal{H}\tilde{x}(\zeta,t)) + P_0(\mathcal{H}\tilde{x}(\zeta,t)), \quad \tilde{x}(\zeta,0) = \tilde{x}_0(\zeta)\\ W_L\begin{pmatrix}\tilde{f}_\partial(t)\\ \tilde{e}_\partial(t)\end{pmatrix} = 0, \quad W_L = W_{\mathcal{B}} + C_m^T L C_m W_{\mathcal{C}},\\ \tilde{y}(t) = W_{\mathcal{C}}\begin{pmatrix}\tilde{f}_\partial(t)\\ \tilde{e}_\partial(t)\end{pmatrix}.\end{cases} \tag{IV.27}$$

According to [Le Gorrec 05, Theorem 4.1], the error system (IV.27) is well-posed if $W_L \Sigma W_L^T \geq 0$. *Since* $W_L = W_{\mathcal{B}} + C_m^T L C_m W_{\mathcal{C}}$, $W_{\mathcal{B}} \Sigma W_{\mathcal{B}}^T = W_{\mathcal{C}} \Sigma W_{\mathcal{C}}^T = 0$, $W_{\mathcal{B}} \Sigma W_{\mathcal{C}}^T = I_n$, *and* $C_m^T L^T C_m + C_m^T L C_m \geq 0$, *the inequality* $W_L \Sigma W_L^T \geq 0$ *is satisfied.*

The exponential convergence of the error system (IV.27) is a direct application of [Villegas 07, Corollary 5.19]. In fact, we use (IV.9), (IV.26), and (IV.24) to show that the Hamiltonian of the error system decreases exponentially. First, we use (IV.24) to bound the Hamiltonian estimation from (IV.9) as follows

$$\tilde{H}(\tau) \leq c(\tau) \int_0^\tau \|\mathcal{H}(b)\tilde{x}(b,t)\|_{\mathbb{R}}^2 dt \leq c(\tau) \int_0^\tau \gamma \tilde{y}(t)^T C_m^T L C_m \tilde{y}(t) dt,$$

$$\Rightarrow \tilde{H}(\tau) \leq c(\tau)\gamma \int_0^\tau \tilde{y}(t)^T C_m^T L C_m \tilde{y}(t) dt. \tag{IV.28}$$

Then, we integrate along time both sides of equation (IV.26)

$$\tilde{H}(0) - \tilde{H}(\tau) = \int_0^\tau \tilde{y}(t)^T C_m^T L C_m \tilde{y}(t) dt,$$

and finally, we replace the last equation in (IV.28)

$$\tilde{H}(\tau) \leq c(\tau)\gamma \left(\tilde{H}(0) - \tilde{H}(\tau)\right),$$

$$\Leftrightarrow \tilde{H}(\tau) \leq \frac{c(\tau)\gamma}{c(\tau)\gamma + 1} \tilde{H}(0).$$

This concludes the proof. ■

Note that, the conditions (IV.24) are related to the observability of the BC-PHS (IV.1) with measured output $y_m(t) = C_m y(t)$. Indeed, if we are able to show that there exists $\gamma > 0$ such that one of the two conditions in (IV.24) is satisfied, then we can design an exponentially convergent observer. This is the case, for instance, of the vibrating string (Example II.3.2) where one of the two conjugated outputs is measured (the force at $\zeta = a$ or the velocity at $\zeta = b$) and the Timoshenko beam (Example II.3.3) where one only needs to measure two conjugated outputs (either the force and the torque at $\zeta = a$, or the transverse velocity and the angular velocity at $\zeta = b$). In the following, we exemplify the Proposition IV.3.1 and the Proposition IV.3.2 by using the vibrating string of Example II.3.2 in two different scenarios. Firstly, we consider that $y(t)$ is fully measured. Secondly, we consider that $y(t)$ is partially measured.

Example IV.3.1. *We consider the vibrating string of Example II.3.2 with unitary parameters* ($T(\zeta) = \rho(\zeta) = 1$), *unitary length* ($a = 0$, $b = 1$), *and we consider as inputs the velocity at* $\zeta = a$, *and the force at* $\zeta = b$. *The system is written as an impedance energy preserving BC-PHS (IV.1) as follows:*

$$\mathcal{P}\begin{cases} \dfrac{\partial}{\partial t}\begin{pmatrix} q(\zeta,t) \\ p(\zeta,t) \end{pmatrix} = \begin{pmatrix} 0 & 1 \\ 1 & 0 \end{pmatrix} \dfrac{\partial}{\partial \zeta}\begin{pmatrix} q(\zeta,t) \\ p(\zeta,t) \end{pmatrix}, \quad \begin{pmatrix} q(\zeta,0) \\ p(\zeta,0) \end{pmatrix} = \begin{pmatrix} q_0(\zeta) \\ p_0(\zeta) \end{pmatrix}, \\ \begin{pmatrix} p(a,t) \\ q(b,t) \end{pmatrix} = u(t), \\ y(t) = \begin{pmatrix} -q(a,t) \\ p(b,t) \end{pmatrix}, \quad y_m(t) = C_m y(t), \end{cases} \tag{IV.29}$$

where $y_m(t)$ represents the measurements. In all the following examples, the plant and the observer are simulated using the discretization method proposed in [Trenchant 18]. We use finite-differences for the spatial discretization and midpoint rule for the time discretization. The reader is refer to Appendix A for further details about the discretization methods. We use 200 state variables for the plant and 200 state variables for the observer. The time step is $\delta t = 0.1ms$, and the initial conditions are

$$q_0(\zeta) = \frac{dw_0}{d\zeta}(\zeta), \quad p_0(\zeta) = 0, \quad \hat{q}_0(\zeta) = 0, \quad \hat{p}_0(\zeta) = 0, \quad w_0(\zeta) = e^{-16(\zeta-0.5)^2}.$$

Since $q(\zeta,t) = \frac{\partial w}{\partial \zeta}(\zeta,t)$, the string deformation $w(\zeta,t)$ and the observed one $\hat{w}(\zeta,t)$ are numerically obtained by

$$w(\zeta,t) = w(0,t) + \int_0^\zeta q(z,t)dz, \qquad \hat{w}(\zeta,t) = \hat{w}(0,t) + \int_0^\zeta \hat{q}(z,t)dz$$

considering $w(0,t) = \hat{w}(0,t) = 0$.

In the following, we consider two scenarios. Firstly, we consider that the full conjugated output is measured, and secondly, we consider that the conjugated output is partially measured.

(i) We consider firstly the case where the conjugated output is fully measured, i.e.

$$C_m = I_n \quad \Rightarrow \quad y_m(t) = y(t) = \begin{pmatrix} -q(a,t) \\ p(b,t) \end{pmatrix}.$$

Using Proposition IV.3.1 with $u(t) = 0$ (the string is attached at $\zeta = a$ and free at $\zeta = b$), the state of the following observer

$$\frac{\partial}{\partial t}\begin{pmatrix} \hat{q}(\zeta,t) \\ \hat{p}(\zeta,t) \end{pmatrix} = \begin{pmatrix} 0 & 1 \\ 1 & 0 \end{pmatrix} \frac{\partial}{\partial \zeta}\begin{pmatrix} \hat{q}(\zeta,t) \\ \hat{p}(\zeta,t) \end{pmatrix}, \quad \begin{pmatrix} \hat{q}(\zeta,0) \\ \hat{p}(\zeta,0) \end{pmatrix} = \begin{pmatrix} \hat{q}_0(\zeta) \\ \hat{p}_0(\zeta) \end{pmatrix},$$
$$\begin{pmatrix} \hat{p}(a,t) \\ \hat{q}(b,t) \end{pmatrix} = \begin{pmatrix} l_1 & 0 \\ 0 & l_2 \end{pmatrix} \begin{pmatrix} -\left[q(a,t) - \hat{q}(a,t)\right] \\ p(b,t) - \hat{p}(b,t) \end{pmatrix}$$

converges exponentially to the state of the system if l_1, $l_2 > 0$. In this case, $L = \left(\begin{smallmatrix} l_1 & 0 \\ 0 & l_2 \end{smallmatrix}\right) > 0$, and for simplicity, we use $l_1 = l_2 = 1$.

Figure IV.1 shows the string deformation along time and space. Figure IV.2 shows the estimated one (using different initial conditions). Figure IV.3 shows the deformation error. In each figure, the two bold black lines show the initial and the final values of $w(\zeta,t)$, $\hat{w}(\zeta,t)$, and $\tilde{w}(\zeta,t)$, and the orange line shows the end-tip deformations $w(1,t)$, $\hat{w}(1,t)$, and $\tilde{w}(1,t)$. Since there is no internal dissipation and due to the attached/free boundary conditions, the string (Figure IV.1) continues moving along time due to the initial condition that is chosen to show the wave propagation. The observer (Figure IV.2) starts from a zero initial condition and reaches the state of the BC-PHS approximately at $t = 1$. The error deformation (Figure IV.3), starts from a non zero initial condition and reaches zero approximately at $t = 1$.

Finally, in Figure IV.4, we show the Hamiltonians of the plant, the observer and the error system. We can see that due to the boundary conditions the Hamiltonian of the string ($H(t)$) is constant. The Hamiltonian of the error system converges to zero exponentially ($\tilde{H}(t)$) and the Hamiltonian of the observer ($\hat{H}(t)$) reaches the Hamiltonian of the string.

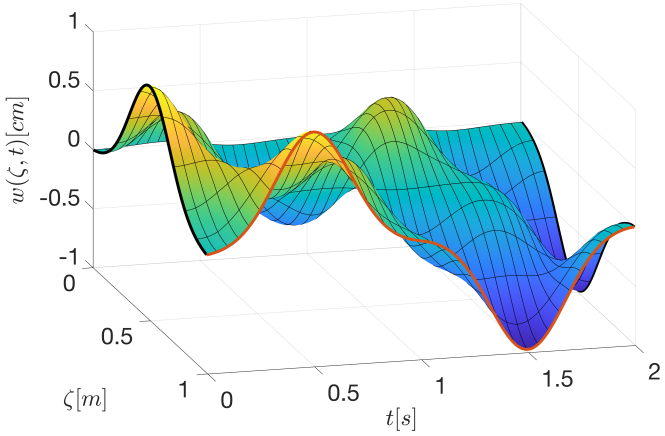

Figure IV.1 – String deformation

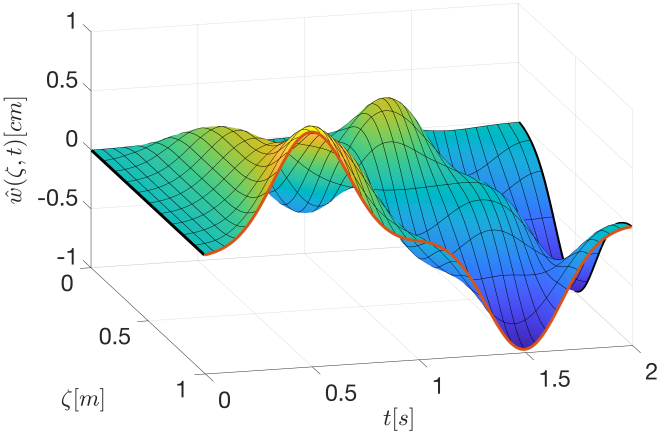

Figure IV.2 – Estimated deformation

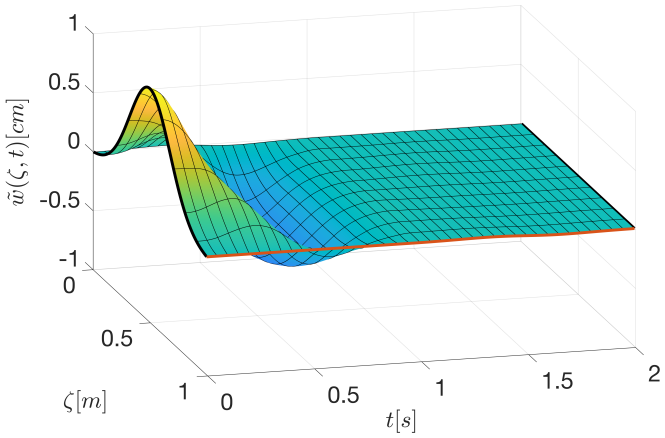

Figure IV.3 – Estimation error

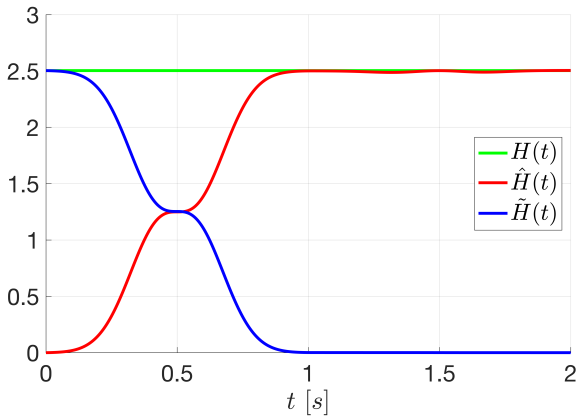

Figure IV.4 – Hamiltonian of the plant (green), observer (red) and error system (blue)

(*ii*) *Now, we consider that the conjugated output is partially measured with the following measured output:*

$$C_m = \begin{pmatrix} 1 & 0 \end{pmatrix} \quad \Rightarrow \quad y_m = C_m y(t) = -q(a,t).$$

Consider the following infinite-dimensional observer

$$\frac{\partial}{\partial t}\begin{pmatrix} \hat{q}(\zeta,t) \\ \hat{p}(\zeta,t) \end{pmatrix} = \begin{pmatrix} 0 & 1 \\ 1 & 0 \end{pmatrix} \frac{\partial}{\partial \zeta}\begin{pmatrix} \hat{q}(\zeta,t) \\ \hat{p}(\zeta,t) \end{pmatrix}, \quad \begin{pmatrix} \hat{q}(\zeta,0) \\ \hat{p}(\zeta,0) \end{pmatrix} = \begin{pmatrix} \hat{q}_0(\zeta) \\ \hat{p}_0(\zeta) \end{pmatrix},$$
$$\begin{pmatrix} \hat{p}(a,t) \\ \hat{q}(b,t) \end{pmatrix} = \begin{pmatrix} 1 \\ 0 \end{pmatrix} l_1 (y_m(t) - \hat{y}_m(t)),$$

with the scalar $l_1 > 0$. *The error system is*

$$\frac{\partial}{\partial t}\begin{pmatrix} \tilde{q}(\zeta,t) \\ \tilde{p}(\zeta,t) \end{pmatrix} = \begin{pmatrix} 0 & 1 \\ 1 & 0 \end{pmatrix} \frac{\partial}{\partial \zeta}\begin{pmatrix} \tilde{q}(\zeta,t) \\ \tilde{p}(\zeta,t) \end{pmatrix}, \quad \begin{pmatrix} \tilde{q}(\zeta,0) \\ \tilde{p}(\zeta,0) \end{pmatrix} = \begin{pmatrix} \tilde{q}_0(\zeta) \\ \tilde{p}_0(\zeta) \end{pmatrix},$$
$$\begin{pmatrix} \tilde{p}(a,t) \\ \tilde{q}(b,t) \end{pmatrix} = \begin{pmatrix} 1 \\ 0 \end{pmatrix} l_1 \begin{pmatrix} 1 & 0 \end{pmatrix} \begin{pmatrix} -\tilde{q}(a,t) \\ \tilde{p}(b,t) \end{pmatrix}$$

and its exponential convergence is shown using Proposition IV.3.2. To this end, we compute both sides of the second inequality of (IV.24) as follows:

$$\|\mathcal{H}(a)\tilde{x}(a,t)\|^2 = \tilde{q}(a,t)^2 + \tilde{p}(a,t)^2 = (l_1^2+1)\tilde{q}(a,t)^2,$$
$$\gamma\tilde{y}(t)^T C_m^T L C_m \tilde{y}(t) = \gamma l_1 \tilde{q}(a,t)^2,$$

where in the second line we have replaced the boundary condition of the error system $\tilde{p}(a,t) = l_1\tilde{q}(a,t)$. Finally, choosing $\gamma \geq (l_1^2+1)l_1^{-1}$, the condition $\|\mathcal{H}\tilde{x}(a,t)\|_{\mathbb{R}}^2 \leq \gamma\tilde{y}(t)^T C_m^T L C_m\tilde{y}(t)$ is satisfied and the infinite-dimensional observer converge to the BC-PHS. For simplicity, the observer is designed using $l_1 = 1$. Similarly as before, Figure IV.5, Figure IV.6, Figure IV.7, and Figure IV.8 show the string deformation, the observed, the error and the Hamiltonians. The observer converges to the real values approximately at $t = 2$. The main difference with respect to the full sensing scenario is that using only one sensor the convergence is slower than using two sensors.

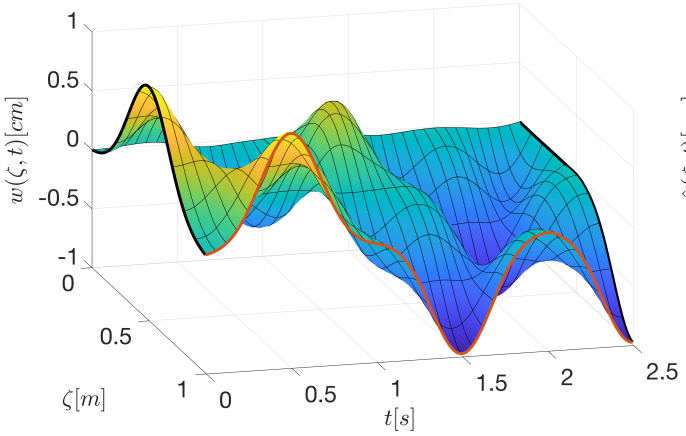

Figure IV.5 – String deformation

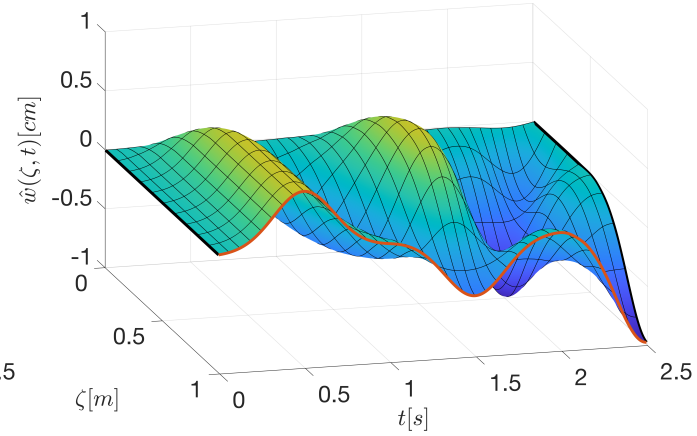

Figure IV.6 – Estimated deformation

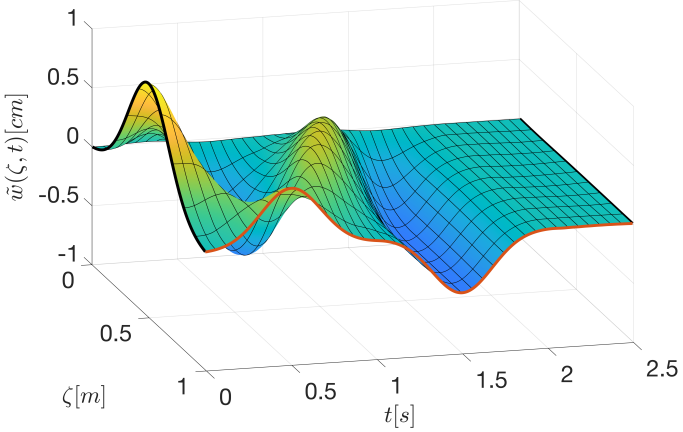

Figure IV.7 – Deformation error

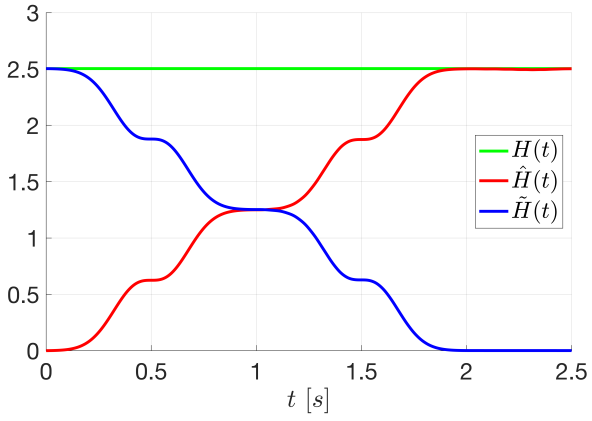

Figure IV.8 – Hamiltonian of the plant (green), observer (red) and error system (blue)

♣

The observers of Proposition IV.3.1 and Proposition IV.3.2 require the measurements of the conjugated output $y(t)$ of the BC-PHS (IV.1). This means that it is required to measure energy variables as for instance forces and velocities in mechanical systems. However, this is not always possible as for example when positions are measured instead of velocities. In these cases, the velocity has to be estimated for analysis and control. In the following section, these cases are presented for the considered class of BC-PHS and we propose the observer input $\hat{u}(t)$ of (IV.4) to achieve asymptotically convergent observers.

IV.3.2 The integral over time of the co-energy variables are measured

Co-energy variables are very useful to guarantee closed-loop stability. For example, in mechanical systems, velocities are usually required for a negative feedback on the force actuators. However, sometimes co-energy variables are difficult and even impossible to measure. In these cases, the velocity has to be estimated for control purposes. In this section, we extend the infinite-dimensional observer proposed in [Guo 09] (for the one-dimensional wave equation) to the class of impedance energy preserving BC-PHSs of interest in this thesis. We show that a more general result can be achieved using the interconnection properties of port-Hamiltonian systems. In the following proposition, the input of the observer (IV.4) is designed such that the state of the observer converges asymptotically to the state of the BC-PHS (IV.1).

Proposition IV.3.3. *Consider the BC-PHS (IV.1). Assume that the measurement is on the following form:*

$$y_m(t) = \int_0^t C_m y(\tau) d\tau + y_m(0), \quad \text{with} \quad C_m = \begin{pmatrix} 0_{p\times n-p} & I_p \end{pmatrix}. \tag{IV.30}$$

Assume that the BC-PHS is approximately observable [Curtain 12, Corollary 4.1.14] with respect to the output $C_m y(t)$. The state of the observer (IV.4) with

$$\begin{aligned} \hat{u}(t) &= u(t) + C_m^T L_1 (y_m(t) - \hat{y}_m(t) + \theta(t)), \\ \dot{\theta}(t) &= -L_2 (y_m(t) - \hat{y}_m(t) + \theta(t)), \quad \theta(0) = \theta_0. \end{aligned} \tag{IV.31}$$

converges asymptotically to the state of the BC-PHS (IV.1) if L_1, $L_2 \in \mathbb{R}^{p\times p}$ are both positive definite matrices. ◊

Proof. *Showing the asymptotic convergence of the observer is equivalent to show that the error system (IV.6) converges to zero asymptotically. Note that since the BC-PHS (IV.1) is approximately observable with respect to the output $C_m y(t)$, the error system is (IV.6) is approximately observable with respect to the output $C_m \tilde{y}(t)$. We use this property to show the asymptotic stability of the error system by using LaSalle's invariance principle.*

From (IV.31) and (IV.6) we obtain

$$\tilde{u}(t) = -C_m^T L_1 (y_m(t) - \hat{y}_m(t) + \theta(t)). \tag{IV.32}$$

We define the following auxiliary variable:

$$x_o(t) = \tilde{y}_m(t) + \theta(t) \tag{IV.33}$$

with

$$\tilde{y}_m(t) = y_m(t) - \hat{y}_m(t), \tag{IV.34}$$

and

$$\hat{y}_m(t) = \int_0^t C_m \hat{y}(\tau) d\tau + \hat{y}_m(0). \tag{IV.35}$$

The dynamic equation of $x_o(t)$ *in* (IV.33) *is obtained from* (IV.30) *and* (IV.31) *as follows:*

$$\begin{aligned} \dot{x}_o(t) &= \dot{\tilde{y}}_m(t) + \dot{\theta}(t), \\ &= C_m \tilde{y}(t) - L_2 x_o(t). \end{aligned} \tag{IV.36}$$

We define the following auxiliary finite-dimensional system:

$$P_o \begin{cases} \dot{x}_o(t) = A_o x_o(t) + B_o u_o(t), \\ y_o(t) = C_o x_o(t), \end{cases} \tag{IV.37}$$

with

$$A_o = -L_2, \quad B_o = C_m, \quad C_o = C_m^T L_1.$$

Then, the input of the error system (IV.32) *is equivalently obtained with the passive interconnection*

$$\begin{pmatrix} \tilde{u}(t) \\ u_o(t) \end{pmatrix} = \begin{pmatrix} 0 & -1 \\ 1 & 0 \end{pmatrix} \begin{pmatrix} \tilde{y}(t) \\ y_o(t) \end{pmatrix} \tag{IV.38}$$

between the error system (IV.6) *and the auxiliary system* (IV.37) *as shown in Figure IV.9.*

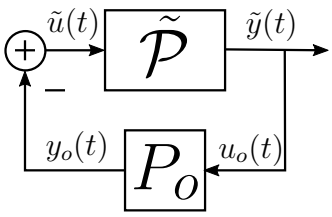

Figure IV.9 – Power preserving interconnection between the infinite-dimensional observer and the finite-dimensional auxiliary system.

Now, we use LaSalle's invariance principle to show that the system represented in Figure IV.9 converges asymptotically to zero. To this end, the reader is refer to [Villegas 07, Theorem 5.8] and [Villegas 07, Theorem 5.9] for the well-posedness and the compactness of the solutions of the system. We consider the following Lyapunov function:

$$V(t) = \frac{1}{2} \int_a^b \tilde{x}(\zeta, t)^T \mathcal{H}(\zeta) \tilde{x}(\zeta, t) d\zeta + \frac{1}{2} x_o(t)^T L_1 x_o(t).$$

It follows from LaSalle's invariance principle that all solutions of the system represented in Figure IV.9 tend to the maximal invariant set of

$$\vartheta_o = \{\tilde{x} \in L_2([a, b], \mathbb{R}^n),\ x_o \in \mathbb{R}^p \mid \dot{V}(t) = 0\}. \tag{IV.39}$$

We define the maximal invariant subset of ϑ_o as $\mathcal{I}$, and we show that $\mathcal{I}$ only contains the zero state, i.e. $\mathcal{I} = \{\tilde{x}(\zeta,t) = 0,\ x_o(t) = 0\}$. From (IV.6), and (IV.37), we obtain the following balance for the Lyapunov function:

$$\dot{V}(t) = -x_o(t)^T L_1 R_o L_1 x_o(t), \tag{IV.40}$$

with $R_o = L_2 L_1^{-1} > 0$ and $L_1 > 0$ by definition. Then, $\dot{V}(t) = 0$ implies $x_o(t) = 0$, which implies $\dot{x}_o(t) = 0$. Then, from (IV.37) and (IV.38) $B_o u_o(t) = C_m \tilde{y}(t) = 0$. Since $x_o(t) = 0$, from (IV.37) $y_o(t) = 0$. Since $y_o(t) = 0$, from the interconnection (IV.38) we can conclude $\tilde{u}(t) = 0$. Then, the maximal invariant set $\mathcal{I}$ contains $x_o = 0$ and the solution of the following BC-PHS

$$\begin{cases} \dfrac{\partial \tilde{x}}{\partial t}(\zeta,t) = P_1 \dfrac{\partial}{\partial \zeta}(\mathcal{H}(\zeta)\tilde{x}(\zeta,t)) + P_0 \mathcal{H}(\zeta)\tilde{x}(\zeta,t), \quad \tilde{x}(\zeta,0) = \tilde{x}_0(\zeta), \\ W_{\mathcal{B}} \begin{pmatrix} \tilde{f}_\partial(t) \\ \tilde{e}_\partial(t) \end{pmatrix} = 0, \\ C_m \tilde{y}(t) = C_m W_{\mathcal{C}} \begin{pmatrix} \tilde{f}_\partial(t) \\ \tilde{e}_\partial(t) \end{pmatrix} = 0. \end{cases}$$

The latter being approximately observable with respect to $C_m\tilde{y}(t)$ implies that if $C_m\tilde{y}(t) = 0$ for an interval of time, then the state is such that $\tilde{x}(\zeta,t) = 0$ (See [Curtain 12, Corollary 4.1.14]). Then, the maximal invariant set $\mathcal{I}$ only contains the states $\tilde{x}(\zeta,t) =$ and $x_o(t) = 0$. Thus, by LaSalle's invariance principle, the error system is asymptotically stable.

■

In the following example, we show that the state of the vibrating string can be asymptotically estimated using the observer (IV.4) with (IV.31) measuring the end-tip position only.

Example IV.3.2. *We consider the vibrating string of Example IV.3.1, and we assume that the end-tip deformation is measured at $\zeta = b$, i.e.*

$$y_m(t) = w(b,t).$$

Note that, the measured output (deformation at $\zeta = b$) is the integral over time of one of the conjugated outputs (velocity at $\zeta = b$). Using Proposition IV.3.3, the state of the following infinite-dimensional observer

$$\begin{aligned} \frac{\partial}{\partial t}\begin{pmatrix} \hat{q}(\zeta,t) \\ \hat{p}(\zeta,t) \end{pmatrix} &= \begin{pmatrix} 0 & 1 \\ 1 & 0 \end{pmatrix} \frac{\partial}{\partial \zeta}\begin{pmatrix} \hat{q}(\zeta,t) \\ \hat{p}(\zeta,t) \end{pmatrix}, \quad \begin{pmatrix} \hat{q}(\zeta,0) \\ \hat{p}(\zeta,0) \end{pmatrix} = \begin{pmatrix} \hat{q}_0(\zeta) \\ \hat{p}_0(\zeta) \end{pmatrix}, \\ \begin{pmatrix} \hat{p}(a,t) \\ \hat{q}(b,t) \end{pmatrix} &= \begin{pmatrix} 0 \\ l_1\left[y_m(t) - \hat{y}_m(t) + \theta(t)\right] \end{pmatrix}, \\ \dot{\theta}(t) &= -l_2\left[y_m(t) - \hat{y}_m(t) + \theta(t)\right], \quad \theta(0) = \theta_0, \end{aligned}$$

with $l_1,\ l_2 > 0$, $\theta \in \mathbb{R}$ and $\hat{y}_m(t) = \hat{w}(b,t)$, converges asymptotically to the state of the system. Since the measured output is on the form

$$y_m(t) = \int_0^t C_m y(\tau) d\tau + y_m(0), \qquad C_m = \begin{pmatrix} 0 & 1 \end{pmatrix},$$

one can show that the plant is approximately observable with respect to $C_m y(t) = p(b,t)$ (velocity at $\zeta = b$). Indeed, by using (IV.9), one can show that $\tilde{H}(\tau) \leq c(\tau) \int_0^\tau p(b,t)^2 dt$ satisfying the condition of exact observability (See [Curtain 12, Corollary 4.1.14 a.(iii)]), which is a stronger conditions than the approximate observability.

We can use Proposition IV.3.3 with $L_1 = l_1 > 0$ and $L_2 = l_2 > 0$, to prove the asymptotic stability of the error system. For simplicity, the observer is designed using $l_1 = l_2 = 1000$, and $\theta_0 = 0$. Similarly as in Example IV.3.1, Figure IV.10, Figure IV.11, and Figure IV.12 show the spatial and temporal responses of the string deformation, the estimated one, and the error one, respectively. The observer converge to the real values approximately at $t = 4$. Finally, in Figure IV.13, we show the Hamiltonians of the plant, the observer and the error system. We can see that due to the boundary conditions the Hamiltonian of the string ($H(t)$) is constant. The Hamiltonian of the error system converges to zero asymptotically ($\tilde{H}(t)$) and the Hamiltonian of the observer ($\hat{H}(t)$) reaches the Hamiltonian of the string. The main difference with respect to Example IV.3.1 is that in this case, since we can not measure the co-energy variables, we cannot guarantee the exponential convergence. ♣

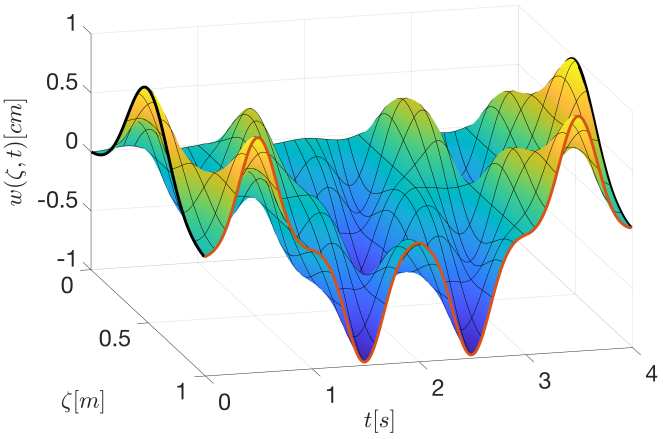

Figure IV.10 – String deformation

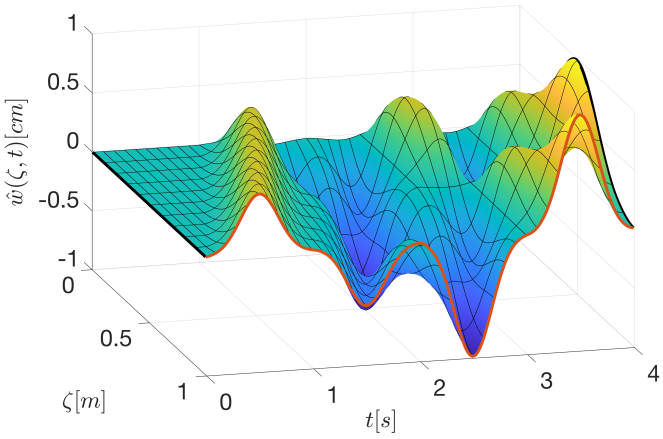

Figure IV.11 – Estimated deformation

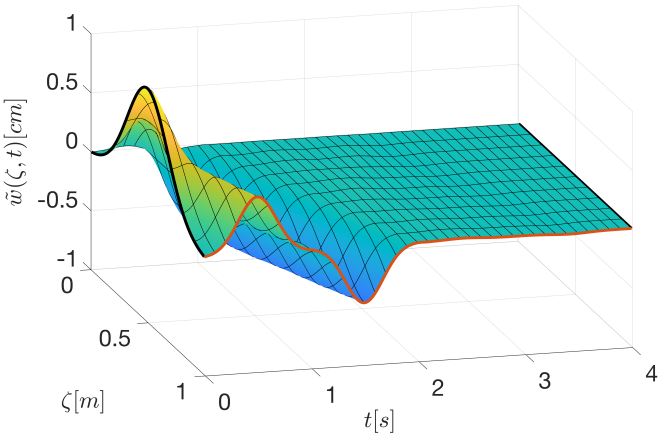

Figure IV.12 – Deformation error

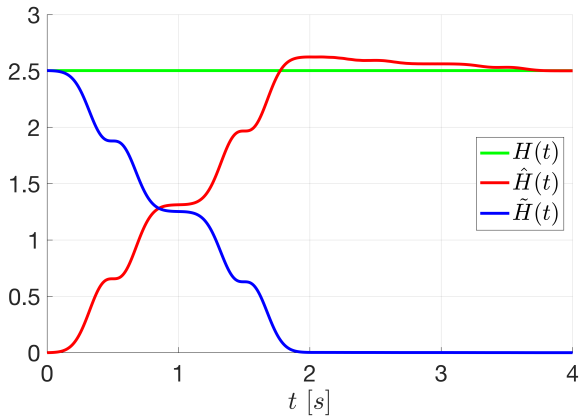

Figure IV.13 – Hamiltonian of the plant (green), observer (red) and error system (blue)

The observer presented in Example IV.3.2 was first introduced in [Guo 09]. In Proposition IV.3.3, we have generalized this idea to the class of impedance energy preserving BC-PHSs. In this way, we can use Proposition IV.3.3 to design an infinite-dimensional observer for the Timoshenko beam measuring the end-tip deformation and the end-tip rotation angle as it is shown in the following example.

Example IV.3.3. *Consider the one-dimensional Timoshenko beam of Example II.3.3 with unitary parameters and unitary length. The beam is clamped at the left side and free at the other side. The only measures are the transverse displacement and the rotation angle at the right side. We can write the system as a BC-PHS (IV.1) in the following form*

$$\mathcal{P}\begin{cases} \dfrac{\partial x}{\partial t}(\zeta,t) = P_1\dfrac{\partial}{\partial \zeta}(\mathcal{H}x(\zeta,t)) + P_0(\mathcal{H}x(\zeta,t)), \quad x(\zeta,0) = x_0(\zeta), \\ \begin{pmatrix} x_2(0,t) \\ x_4(0,t) \\ x_1(1,t) \\ x_3(1,t) \end{pmatrix} = 0, \quad y(t) = \begin{pmatrix} -x_1(0,t) \\ -x_3(0,t) \\ x_2(1,t) \\ x_4(1,t) \end{pmatrix} \\ y_m(t) = \begin{pmatrix} w(1,t) \\ \phi(1,t) \end{pmatrix}, \end{cases}$$

with $x(\zeta,t)$, P_1, P_0 defined in Example II.3.3, $\mathcal{H}(\zeta) = I_4$, $\zeta \in [0,1]$ and $t \geq 0$. Using Proposition IV.3.3, the following observer

$$\hat{\mathcal{P}}\begin{cases} \dfrac{\partial \hat{x}}{\partial t}(\zeta,t) = P_1\dfrac{\partial}{\partial \zeta}(\mathcal{H}\hat{x}(\zeta,t)) + P_0(\mathcal{H}\hat{x}(\zeta,t)), \quad \hat{x}(\zeta,0) = \hat{x}_0(\zeta), \\ \begin{pmatrix} \hat{x}_2(0,t) \\ \hat{x}_4(0,t) \\ \hat{x}_1(1,t) \\ \hat{x}_3(1,t) \end{pmatrix} = \begin{pmatrix} 0 \\ 0 \\ l_1(w(1,t) - \hat{w}(1,t) + \theta_1) \\ l_2(\phi(1,t) - \hat{\phi}(1,t) + \theta_2) \end{pmatrix}, \\ \dfrac{d}{dt}\begin{pmatrix} \theta_1(t) \\ \theta_2(t) \end{pmatrix} = \begin{pmatrix} -l_3(w(1,t) - \hat{w}(1,t) + \theta_1) \\ -l_4(\phi(1,t) - \hat{\phi}(1,t) + \theta_2) \end{pmatrix}, \quad \begin{pmatrix} \theta_1(0) \\ \theta_2(0) \end{pmatrix} = \theta_0, \end{cases}$$

with l_1, l_2, l_3, $l_4 > 0$ and θ_1, $\theta_2 \in \mathbb{R}$, converges asymptotically to the state of the system. Indeed, the measured output is on the form

$$y_m(t) = \int_0^t C_m y(\tau)d\tau + y_m(0), \quad C_m = \begin{pmatrix} 0 & 0 & 1 & 0 \\ 0 & 0 & 0 & 1 \end{pmatrix}.$$

We can choose $L_1 = \left[\begin{smallmatrix} l_1 & 0 \\ 0 & l_2 \end{smallmatrix}\right] > 0$ and $L_2 = \left[\begin{smallmatrix} l_3 & 0 \\ 0 & l_4 \end{smallmatrix}\right] > 0$. Then, using Proposition IV.3.3 we can conclude that the error system is asymptotically stable. For simplicity, the observer is designed with $l_1 = l_2 = 100$, $l_3 = l_4 = 150$. For the simulation, the plant and the observer are discretized using the same spatial and time discretization methods as in Example IV.3.1 (See [Trenchant 18] or Appendix A). We use 200 state variables to describe the beam and 200 state variables for the observer. The

step time is $\delta t = 0.1ms$ *and the initial initial conditions are*

$$x_0(\zeta) = \begin{bmatrix} 1 \\ 0 \\ 1-\zeta \\ 0 \end{bmatrix}, \quad \hat{x}_0(\zeta) = \begin{bmatrix} 0 \\ 0 \\ 0 \\ 0 \end{bmatrix}, \quad \begin{pmatrix} \theta_1(0) \\ \theta_2(0) \end{pmatrix} = \begin{pmatrix} \hat{w}(1,0) - w(1,0) \\ \hat{\phi}(1,0) - \phi(1,0) \end{pmatrix} = \begin{pmatrix} -1.3234 \\ -0.5000 \end{pmatrix},$$

that correspond to the beam in an equilibrium position where a force of $1\,N$ *and a torque of* $0\,Nm$ *are applied at* $\zeta = 1$*. Note that, the initial condition of* θ_1 *and* θ_2 *are chosen such that* $\dot{\theta}_1(0) = \dot{\theta}_2(0) = 0$*. The transverse displacement* $w(\zeta,t)$ *and the rotation angle* $\phi(\zeta,t)$ *are reconstructed from the state variables using the clamped condition at the left side* $(w(0,t) = \phi(0,t) = 0)$*. Similarly, for the observer we consider* $\hat{w}(0,t) = \hat{\phi}(0,t) = 0$*. The following formulas are implemented to reconstruct the deformation of the beam*

$$\begin{aligned}
\phi(\zeta,t) &= \phi(0,t) + \int_0^\zeta x_3(z,t)dz, \\
w(\zeta,t) &= w(0,t) + \int_0^\zeta [x_1(z,t) + \phi(z,t)]dz, \\
\hat{\phi}(\zeta,t) &= \hat{\phi}(0,t) + \int_0^\zeta \hat{x}_3(z,t)dz, \\
\hat{w}(\zeta,t) &= \hat{w}(0,t) + \int_0^\zeta [\hat{x}_1(z,t) + \hat{\phi}(z,t)]dz.
\end{aligned}$$

Figure IV.14 shows the beam deformation along time and space, Figure IV.15 shows the estimated one, and Figure IV.16 shows the deformation error. In each figure, the two black lines show the initial and final value of $w(\zeta,t)$*,* $\hat{w}(\zeta,t)$*, and* $\tilde{w}(\zeta,t)$*, and the orange line shows the end-tip deformations* $w(1,t)$*,* $\hat{w}(1,t)$*, and* $\tilde{w}(1,t)$*. The observer (Figure IV.15) starts from a zero initial condition and reaches the state of the BC-PHS approximately at* $t = 6$*. The error (Figure IV.16), starts from a non zero initial condition and reaches the zero approximately at* $t = 6$*. Finally, Figure IV.18 shows the conjugated outputs and their estimations.* ♣

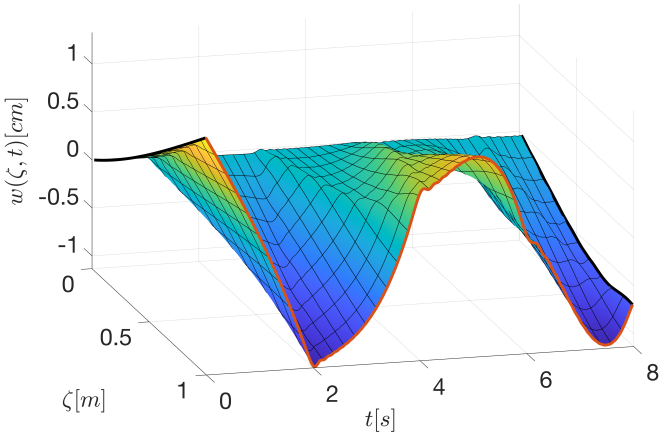

Figure IV.14 – Beam deformation

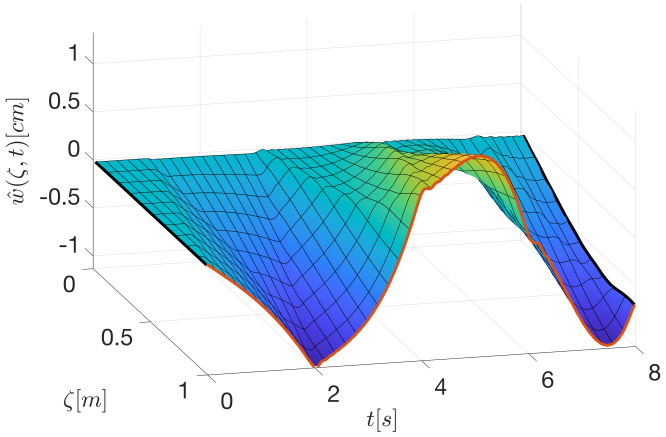

Figure IV.15 – Estimated deformation

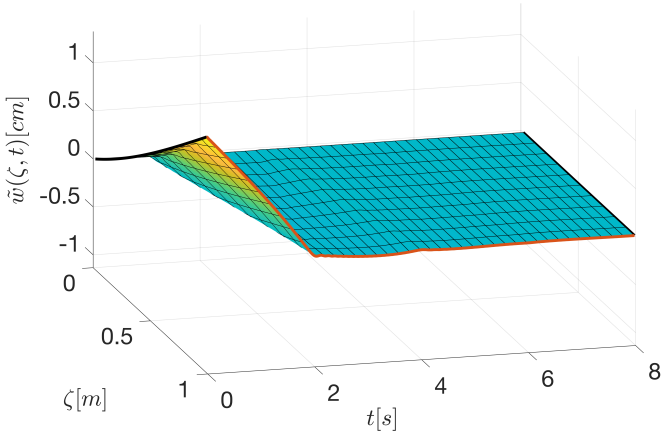

Figure IV.16 – Deformation error

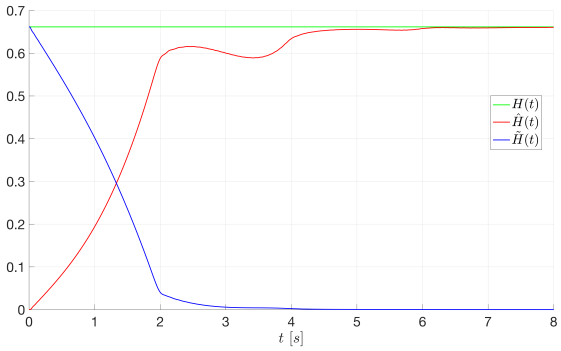

Figure IV.17 – Hamiltonian of the plant (green), observer (red) and error system (blue)

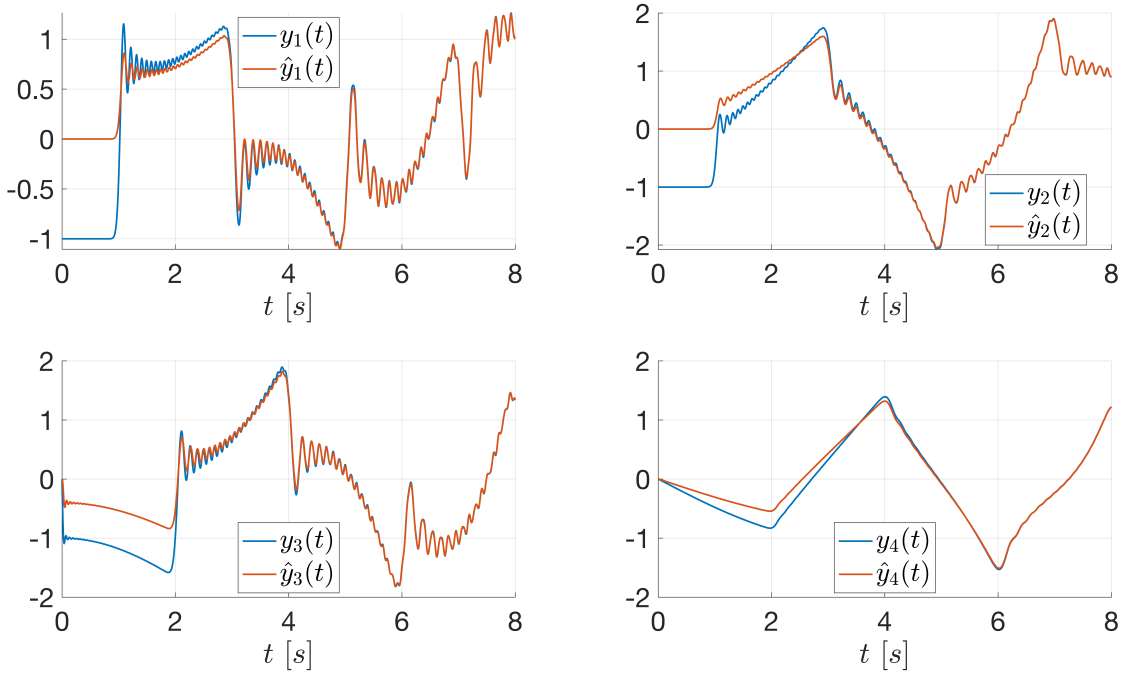

Figure IV.18 – Observer convergence of the conjugated output $\hat{y}(t)$ to $y(t)$. y_1 and y_2 are respectively, the negative force and negative torque at the left side of the beam. y_3 and y_4 are respectively, the transverse velocity and angular velocity at the right side of the beam.

The performances of the observer can be improved by adding more sensors. In particular, by adding sensors that measure the co-energy variables, the exponential convergence can be guaranteed. In the following section, we present the observer input and the conditions such that the observer (IV.4) achieves exponential convergence with a damping error injection plus an external dynamic injection.

IV.3.3 The co-energy variables and their integrals over time are both measured

In the previous sections, we have shown that when measuring co-energy variables, we can design infinite-dimensional observers with exponential convergence (Section IV.3.1) and when measuring the integral over time of co-energy variables, we can design infinite-dimensional observers with asymptotic convergence (Section IV.3.2). In this section, we show that when measuring a combination of both cases, we can also design infinite-dimensional observers with exponential convergence. In this case, we consider the following measurements:

$$y_{m1}(t) = C_m y(t), \quad y_{m2}(t) = \int_0^t y_{m1}(\tau)d\tau + y_{m2}(0), \tag{IV.41}$$

with

$$C_m = \begin{pmatrix} 0_{p\times(n-p)} & I_p \end{pmatrix}, \quad 0 < p \leq n.$$

Note that, $y_{m1}(t)$ contains p conjugated outputs and $y_{m2}(t)$ contains the integral over time of $y_{m1}(t)$. In mechanical systems, for example, this can be the case of measuring velocities ($y_{m1}(t)$) and displacements ($y_{m2}(t)$). Now, we aim to design $\hat{u}(t)$ from (IV.4) such that $\hat{x}(t)$ converges exponentially to $x(\zeta,t)$ from (IV.1). To this end, we define the error as $\tilde{x}(\zeta,t) = x(\zeta,t) - \hat{x}(\zeta,t)$. We define the observed outputs as follows:

$$\hat{y}_{m1}(t) = C_m \hat{y}(t), \quad \hat{y}_{m2}(t) = \int_0^t \hat{y}_{m1}(\tau)d\tau + \hat{y}_{m2}(0). \tag{IV.42}$$

Then, we define the error of the measured outputs as

$$\tilde{y}_{m1}(t) = y_{m1}(t) - \hat{y}_{m1}(t), \quad \tilde{y}_{m2}(t) = y_{m2}(t) - \hat{y}_{m2}(t) \tag{IV.43}$$

Finally, we define the conjugated inputs of $y_{m1}(t)$, $\hat{y}_{m1}(t)$ and $\tilde{y}_{m1}(t)$, respectively as:

$$u_{m1}(t) = C_m u(t), \quad \hat{u}_{m1}(t) = C_m \hat{u}(t), \quad \tilde{u}_{m1}(t) = u_{m1}(t) - \hat{u}_{m1}(t). \tag{IV.44}$$

The following proposition is the main result of this section. We emphasize that y_{m1} has to satisfy one of the two conditions in (IV.46). Then, $\hat{u}(t)$ from (IV.4) is designed to achieve the exponential convergence.

Proposition IV.3.4. *Consider the impedance energy preserving BC-PHS (IV.1) with measurements given by $y_{m1}(t)$ and $y_{m2}(t)$ in (IV.41). The state of the observer (IV.4) with*

$$\begin{aligned} \hat{u}(t) &= u(t) + C_m^T L_1(y_{m2}(t) - \hat{y}_{m2}(t) + \theta(t)) + C_m^T S_o(y_{m1}(t) - \hat{y}_{m1}(t)) \\ \dot{\theta}(t) &= -L_2(y_{m2}(t) - \hat{y}_{m2}(t) + \theta(t)), \quad \theta(0) = \theta_0 \in \mathbb{R}^p \end{aligned} \tag{IV.45}$$

converges exponentially to the state of the BC-PHS (IV.1) if L_1, L_2, $S_o \in \mathbb{R}^{p\times p}$ are all positive definite matrices and one of the following two inequalities

$$\begin{aligned} \epsilon\|\mathcal{H}(b)\tilde{x}(b,t)\|^2 &\leq \|\tilde{u}_{m1}(t)\|^2 + \|\tilde{y}_{m1}(t)\|^2, \quad \textit{or} \\ \epsilon\|\mathcal{H}(a)\tilde{x}(a,t)\|^2 &\leq \|\tilde{u}_{m1}(t)\|^2 + \|\tilde{y}_{m1}(t)\|^2 \end{aligned} \tag{IV.46}$$

is satisfied for some $\epsilon > 0$. ◊

Proof. *Showing the exponential convergence of the observer is equivalent to show that the error* $\tilde{x}(\zeta,t)$ *converges exponentially to zero. Using* (IV.45)*, the error dynamics is written as in* (IV.6) *with*

$$\begin{aligned}\tilde{u}(t) &= -C_m^T L_1(\tilde{y}_{m2}(t)+\theta(t)) - C_m^T S_o \tilde{y}_{m1}(t),\\ \dot{\theta}(t) &= -L_2(\tilde{y}_{m2}(t)+\theta(t)), \quad \theta(0)=\theta_0.\end{aligned} \tag{IV.47}$$

We define the following auxiliary variable:

$$x_o(t) = \theta(t) + \tilde{y}_{m2}(t). \tag{IV.48}$$

From (IV.47) *and* (IV.43) *we obtain:*

$$\begin{aligned}\dot{x}_o(t) &= \dot{\theta}(t) + \dot{\tilde{y}}_{m2}(t),\\ &= -L_2\left(\theta(t)+\tilde{y}_{m2}(t)\right) + \tilde{y}_{m1}(t),\\ &= -L_2 x_o(t) + C_m \tilde{y}(t).\end{aligned} \tag{IV.49}$$

We define the following finite-dimensional system:

$$P_o \begin{cases}\dot{x}_o(t) = A_o x_o(t) + B_o u_o(t)\\ y_o(t) = C_o x_o(t) + D_o u_o(t),\end{cases} \tag{IV.50}$$

with

$$A_o = -L_2, \quad B_o = C_m, \quad C_o = C_m^T L_1, \quad D_o = C_m^T S_o C_m.$$

Then, the error system (IV.6) *with input* (IV.47) *is equivalent to the interconnection*

$$\begin{bmatrix}\tilde{u}(t)\\ u_o(t)\end{bmatrix} = \begin{bmatrix}0 & -1\\ 1 & 0\end{bmatrix}\begin{bmatrix}\tilde{y}(t)\\ y_o(t)\end{bmatrix} \tag{IV.51}$$

between (IV.6) *and* (IV.50)*. In the following, we use the total energy (the energy of* (IV.6) *plus the energy of* (IV.50)*) as a Lyapunov function. We define the total energy as:*

$$V(t) = \frac{1}{2}\int_a^b \tilde{x}(\zeta,t)^T \mathcal{H}\tilde{x}(\zeta,t)d\zeta + \frac{1}{2}x_o(t)^T L_1 x_o(t). \tag{IV.52}$$

Now, we follow the same line of [Ramirez 14, Theorem IV.2] to show that the Lyapunov function satisfies $V(\tau) \leq \alpha V(0)$ *for some* $0 < \alpha < 1$ *and* $\tau > 0$*. To this end, we recall the following lemmas concerning the total energy* $V(t)$ *in* (IV.52) *and the energy of* (IV.50) *defined as* $H_o(t) = \frac{1}{2}x_o(t)^T L_1 x_o(t)$*.*

Lemma IV.3.1. *[Ramirez 14, Lemma IV.1] The total energy* $V(t)$ *satisfies for* τ *large enough*

$$\begin{aligned}V(\tau) &\leq c(\tau)\int_0^\tau \|\mathcal{H}(b)\tilde{x}(b,t)\|^2 dt + \frac{2c(\tau)}{c_1}\int_0^\tau H_o(t)dt,\\ V(\tau) &\leq c(\tau)\int_0^\tau \|\mathcal{H}(a)\tilde{x}(a,t)\|^2 dt + \frac{2c(\tau)}{c_1}\int_0^\tau H_o(t)dt\end{aligned} \tag{IV.53}$$

where $c(\tau)$ *is a positive constant that depends on* τ *and* c_1 *is a positive constant.* ◊

Lemma IV.3.2. *[Ramirez 14, Lemma III.4] For every $\delta_1 > 0$ there exists a $\delta_2 > 0$ such that for all $\tau > 0$, $H_o(t)$ satisfies the relation*

$$\int_0^\tau \left[\delta_1 H_o(t) + \|y_o(t)\|^2\right] dt \leq \delta_2 \int_0^\tau \left[H_o(t) + \|u_o(t)\|^2\right] dt. \tag{IV.54}$$

◊

Lemma IV.3.3. *[Ramirez 14, Lemma III.3] There exists positive constants ξ_1, ξ_1 and τ_0 such that for all $\tau > \tau_0$, $H_o(t)$ satisfies*

$$\int_0^\tau H_o(t)dt \leq \xi_1 \int_0^\tau x_o(t)^T L_1 L_2 x_o(t)dt + \xi_2 \int_0^\tau \|u_o(t)\|^2 dt. \tag{IV.55}$$

◊

The time derivative of the Lyapunov function (IV.52) is given by

$$\begin{aligned}
\dot{V}(t) &= \tilde{u}(t)^T \tilde{y}(t) + x_o(t)^T L_1 \dot{x}_o(t), \\
&= \tilde{u}(t)^T \tilde{y}(t) + x_o(t)^T L_1 \left(-L_2 x_o(t) + C_m u_o(t)\right) \\
&= \tilde{u}(t)^T \tilde{y}(t) - x_o(t)^T L_1 L_2 x_o(t) + x_o(t)^T L_1 C_m u_o(t) \\
&= \tilde{u}(t)^T \tilde{y}(t) - x_o(t)^T L_1 L_2 x_o(t) + x_o(t)^T C_o^T u_o(t) \\
&= \tilde{u}(t)^T \tilde{y}(t) - x_o(t)^T L_1 L_2 x_o(t) + \left(y_o(t)^T - u_o(t)^T D_o^T\right) u_o(t) \\
&= \tilde{u}(t)^T \tilde{y}(t) - x_o(t)^T L_1 L_2 x_o(t) + y_o(t)^T u_o(t) - u_o(t)^T D_o u_o(t) \\
&= -x_o(t)^T L_1 L_2 x_o(t) - u_o(t)^T D_o u_o(t) \\
&= -x_o(t)^T L_1 L_2 x_o(t) - u_o(t)^T C_m^T S_o C_m u_o(t) \\
&= -x_o(t)^T L_1 L_2 x_o(t) - \tilde{y}(t)^T C_m^T S_o C_m \tilde{y}(t) \\
&= -x_o(t)^T L_1 L_2 x_o(t) - \tilde{y}_{m1}(t)^T S_o \tilde{y}_{m1}(t).
\end{aligned} \tag{IV.56}$$

Since $S_o > 0$, $S_o \geq \sigma I_p$ with $\sigma > 0$, which it can be the smallest eigenvalue of S_o, for example. Then,

$$\begin{aligned}
\dot{V}(t) &\leq -x_o(t)^T L_1 L_2 x_o(t) - \sigma \tilde{y}_{m1}(t)^T \tilde{y}_{m1}(t), \\
&= -x_o(t)^T L_1 L_2 x_o(t) - \sigma \|\tilde{y}_{m1}(t)\|^2, \\
&= -x_o(t)^T L_1 L_2 x_o(t) - \epsilon_1 \sigma \|\tilde{y}_{m1}(t)\|^2 - \epsilon_2 \sigma \|\tilde{y}_{m1}(t)\|^2, \\
&= -x_o(t)^T L_1 L_2 x_o(t) - \epsilon_1 \sigma \|\tilde{y}_{m1}(t)\|^2 - \epsilon_2 \sigma \|\tilde{y}_{m1}(t)\|^2 \pm \epsilon_2 \sigma \|\tilde{u}_{m1}(t)\|^2, \\
&= -x_o(t)^T L_1 L_2 x_o(t) - \epsilon_1 \sigma \|\tilde{y}_{m1}(t)\|^2 + \epsilon_2 \sigma \|\tilde{u}_{m1}(t)\|^2 \\
&\quad - \epsilon_2 \sigma \left(\|\tilde{u}_{m1}(t)\|^2 + \|\tilde{y}_{m1}(t)\|^2\right),
\end{aligned}$$

where ϵ_1 and ϵ_2 are two positive constants such that $\epsilon_1 + \epsilon_2 = 1$. In this case we use the first inequality of (IV.46). However, using the second one, the proof follows the same line. Then, the Lyapunov function satisfies:

$$\dot{V}(t) \leq -x_o(t)^T L_1 L_2 x_o(t) - \epsilon_1 \sigma \|\tilde{y}_{m1}(t)\|^2 + \epsilon_2 \sigma \|\tilde{u}_{m1}(t)\|^2 - \epsilon_2 \sigma \epsilon \|\mathcal{H}(b)\tilde{x}(b,t)\|^2.$$

For simplicity, in the following, we omit the time dependency (t)*. We integrate the last inequality over time as follows:*

$$\begin{aligned} V(\tau) - V(0) &\leq \int_0^\tau \left[-x_o^T L_1 L_2 x_o - \epsilon_1 \sigma \|\tilde{y}_{m1}\|^2 + \epsilon_2 \sigma \|\tilde{u}_{m1}\|^2 - \epsilon_2 \sigma \epsilon \|\mathcal{H}(b)\tilde{x}(b)\|^2 \right] dt, \\ &\leq \int_0^\tau \left[-x_o^T L_1 L_2 x_o - \epsilon_1 \sigma \|\tilde{y}_{m1}\|^2 + \epsilon_2 \sigma \|\tilde{u}_{m1}\|^2 \right] dt \\ &\quad + \frac{\epsilon_2 \sigma \epsilon}{c(\tau)} \left[\frac{2c(\tau)}{c_1} \int_0^\tau H_o(t) dt - V(\tau) \right] \end{aligned}$$

where we have used $-c(\tau) \int_0^\tau \|\mathcal{H}(b)\tilde{x}(b,t)\|^2 dt \leq \frac{2c(\tau)}{c_1} \int_0^\tau H_o(t) dt - V(\tau)$ *from* (IV.53)*. The inequality can be written as:*

$$\begin{aligned} \left[1 + \frac{\sigma \epsilon_2 \epsilon}{c(\tau)} \right] V(\tau) - V(0) &\leq \int_0^\tau \left[-x_o^T L_1 L_2 x_o - \epsilon_1 \sigma \|\tilde{y}_{m1}\|^2 + \epsilon_2 \sigma \|\tilde{u}_{m1}\|^2 \right] dt \\ &\quad + \frac{2\epsilon_2 \sigma \epsilon}{c_1} \int_0^\tau H_o dt, \\ &= - \int_0^\tau x_o^T L_1 L_2 x_o dt - \epsilon_1 \sigma \int_0^\tau \|\tilde{y}_{m1}\|^2 dt \\ &\quad + \epsilon_2 \sigma \int_0^\tau \left[\|\tilde{u}_{m1}\|^2 + \frac{2\epsilon}{c_1} H_o \right] dt. \end{aligned}$$

Since $C_m = \begin{pmatrix} 0_{p\times(n-p)} & I_p \end{pmatrix}$*, from* (IV.47) *we obtain* $\|\tilde{u}\|^2 = \|\tilde{u}_{m_1}\|^2$*. Moreover, from the interconnection* (IV.51)*, we obtain* $\|\tilde{u}\|^2 = \|\tilde{u}_{m_1}\|^2 = \|y_o\|^2$*. Then, by using* (IV.54) *with* $\delta_1 = \frac{2\epsilon}{c_1}$*, the following inequality is satisfied*

$$\begin{aligned} \left[1 + \frac{\sigma \epsilon_2 \epsilon}{c(\tau)} \right] V(\tau) - V(0) &\leq - \int_0^\tau x_o^T L_1 L_2 x_o dt - \epsilon_1 \sigma \int_0^\tau \|\tilde{y}_{m1}\|^2 dt \\ &\quad + \epsilon_2 \sigma \int_0^\tau \left[\|y_o\|^2 + \frac{2\epsilon}{c_1} H_o \right] dt, \\ &\leq - \int_0^\tau x_o^T L_1 L_2 x_o dt - \epsilon_1 \sigma \int_0^\tau \|\tilde{y}_{m1}\|^2 dt \\ &\quad + \epsilon_2 \sigma \delta_2 \int_0^\tau \left[\|u_o\|^2 + H_o \right] dt, \end{aligned}$$

Grouping some terms and using the interconnection (IV.51)*, we obtain the following:*

$$\begin{aligned}\left[1+\frac{\sigma\epsilon_2\epsilon}{c(\tau)}\right]V(\tau)-V(0) &\leq -\int_0^\tau x_o^T L_1 L_2 x_o dt+\epsilon_2\sigma\delta_2\int_0^\tau H_o dt-\epsilon_1\sigma\int_0^\tau \|\tilde{y}_{m1}\|^2 dt\\ &\quad+\epsilon_2\sigma\delta_2\int_0^\tau \|u_o\|^2 dt,\\ &=-\int_0^\tau x_o^T L_1 L_2 x_o dt+\epsilon_2\sigma\delta_2\int_0^\tau H_o dt-\epsilon_1\sigma\int_0^\tau \|\tilde{y}_{m1}\|^2 dt\\ &\quad+\epsilon_2\sigma\delta_2\int_0^\tau \|\tilde{y}\|^2 dt,\\ &=-\int_0^\tau x_o^T L_1 L_2 x_o dt+\epsilon_2\sigma\delta_2\int_0^\tau H_o dt-\epsilon_1\sigma\int_0^\tau \|\tilde{y}_{m1}\|^2 dt\\ &\quad+\epsilon_2\sigma\delta_2\int_0^\tau \left[\|\tilde{y}_{m1}\|^2+\|\tilde{y}_{nm}\|^2\right] dt,\\ &\leq -\int_0^\tau x_o^T L_1 L_2 x_o dt+\epsilon_2\sigma\delta_2\int_0^\tau H_o dt-\epsilon_1\sigma\int_0^\tau \|\tilde{y}_{m1}\|^2 dt\\ &\quad+\epsilon_2\sigma\delta_2\int_0^\tau \|\tilde{y}_{m1}\|^2 dt,\\ &\leq -\int_0^\tau x_o^T L_1 L_2 x_o dt+\epsilon_2\sigma\delta_2\int_0^\tau H_o dt\\ &\quad+\sigma(\epsilon_2\delta_2-\epsilon_1)\int_0^\tau \|\tilde{y}_{m1}\|^2 dt\end{aligned}$$

where $\tilde{y}_{nm}(t)$ *is the non measured part of the conjugated output* $\tilde{y}(t)=\left[\begin{smallmatrix}\tilde{y}_{nm}(t)\\ \tilde{y}_{m1}(t)\end{smallmatrix}\right]$*. Finally, we use* (IV.55) *to bound the last inequality as follows:*

$$\begin{aligned}\left[1+\frac{\sigma\epsilon_2\epsilon}{c(\tau)}\right]V(\tau)-V(0) &\leq -\int_0^\tau x_o^T L_1 L_2 x_o dt+\sigma(\epsilon_2\delta_2-\epsilon_1)\int_0^\tau \|\tilde{y}_{m1}\|^2 dt\\ &\quad+\epsilon_2\sigma\delta_2\int_0^\tau H_o dt,\\ &\leq -\int_0^\tau x_o^T L_1 L_2 x_o dt+\sigma(\epsilon_2\delta_2-\epsilon_1)\int_0^\tau \|\tilde{y}_{m1}\|^2 dt\\ &\quad+\epsilon_2\sigma\delta_2\left[\xi_1\int_0^\tau x_o(t)^T L_1 L_2 x_o(t) dt+\xi_2\int_0^\tau \|u_o(t)\|^2 dt\right],\\ &\leq (\epsilon_2\sigma\delta_2\xi_1-1)\int_0^\tau x_o^T L_1 L_2 x_o dt\\ &\quad+\sigma(\epsilon_2\delta_2(1+\xi_2)-\epsilon_1)\int_0^\tau \|\tilde{y}_{m1}\|^2 dt\end{aligned}$$

Since $\epsilon_2>0$ *can be chosen arbitrarily such that* $\epsilon_1+\epsilon_2=1$ *and* $\sigma>0$*, we can chose* ϵ_2 *such that the following inequalities are satisfied*

$$\begin{aligned}\sigma\epsilon_2\delta_2\xi_2-1\leq 0\Rightarrow\epsilon_2\leq\frac{1}{\sigma\delta_2\xi_1},\\ \epsilon_2\delta_2(1+\xi_2)-\epsilon_1\Rightarrow\epsilon_2\leq\frac{1}{1+\delta_2(1+\xi)}.\end{aligned}\tag{IV.57}$$

If ϵ_2 *satisfies* (IV.57)*, then the Lyapunov function satisfies*

$$\left[1+\frac{\sigma\epsilon_2\epsilon}{c(\tau)}\right]V(\tau)-V(0)\leq 0\Rightarrow V(\tau)\leq\frac{c(\tau)}{c(\tau)+\sigma\epsilon_2\epsilon}V(0).\tag{IV.58}$$

This concludes the proof.

■

Example IV.3.4. *We consider the vibrating string of Example IV.3.1, and we assume that the end-tip deformation and the velocity are measured at $\zeta = b$*

$$y_m(t) = \begin{pmatrix} w(b,t) \\ p(b,t) \end{pmatrix}.$$

We can verify that the measurements are given by:

$$\begin{aligned} y_{m1}(t) &= C_m y(t) = p(b,t), \qquad & C_m &= \begin{bmatrix} 0 & 1 \end{bmatrix}, \\ y_{m2}(t) &= \int_0^t y_{m1}(\tau)d\tau + y_{m2}(0) = w(b,t). \end{aligned}$$

The conjugated input of $y_{m1}(t)$ is given by the force at $\zeta = b$ as follows:

$$u_{m1}(t) = q(b,t).$$

Then, one can verify

$$\epsilon\|\mathcal{H}(b)\tilde{x}(b,t)\|^2 \leq \|\tilde{u}_{m1}(t)\|^2 + \|\tilde{y}_{m1}(t)\|^2 \Leftrightarrow \epsilon(\tilde{q}(b,t)^2 + \tilde{p}(b,t^2)) \leq \tilde{q}(b,t)^2 + \tilde{p}(b,t)^2.$$

Using Proposition IV.3.4, the state of the following observer

$$\begin{aligned} \frac{\partial}{\partial t}\begin{bmatrix} \hat{q}(\zeta,t) \\ \hat{p}(\zeta,t) \end{bmatrix} &= \begin{bmatrix} 0 & 1 \\ 1 & 0 \end{bmatrix}\frac{\partial}{\partial \zeta}\begin{bmatrix} \hat{q}(\zeta,t) \\ \hat{p}(\zeta,t) \end{bmatrix}, \quad \begin{bmatrix} \hat{q}(\zeta,0) \\ \hat{p}(\zeta,0) \end{bmatrix} = \begin{bmatrix} \hat{q}_0(\zeta) \\ \hat{p}_0(\zeta) \end{bmatrix}, \\ \begin{bmatrix} \hat{p}(a,t) \\ \hat{q}(b,t) \end{bmatrix} &= \begin{bmatrix} 0 \\ l_1(w(b,t) - \hat{w}(b,t) + \theta(t)) + s_o(p(b,t) - \hat{p}(b,t)) \end{bmatrix}, \\ \dot{\theta}(t) &= -l_2(w(b,t) - \hat{w}(b,t) + \theta(t)), \quad \theta(0) = \theta_0, \end{aligned}$$

with l_1, l_2, $s_o > 0$ and $\theta \in \mathbb{R}$, converges exponentially to the state of the system ($L_1 = l_1$, $L_2 = l_2$, and $S_o = s_o$ from Proposition IV.3.4)

We choose $l_1 = l_2 = 1$, $s_o = 0.7$, and $\theta_0 = 0$. The main difference with respect to Example IV.3.2 is the damping term related to the parameter s_0. With this damping term we do not need high gains l_1 and l_2 to achieve a fast convergence. Moreover, in this case, we can guarantee the exponential convergence using the Lyapunov function $V(t)$ as shown in Figure IV.22.

Figure IV.19 shows the string deformation along time and space, Figure IV.20 shows the estimated one, and Figure IV.21 shows the error. In every figure, the two black lines show the initial and final value of $w(\zeta,t)$, $\hat{w}(\zeta,t)$, and $\tilde{w}(\zeta,t)$, and the orange line shows the end-tip deformations $w(1,t)$, $\hat{w}(1,t)$, and $\tilde{w}(1,t)$. The observer (Figure IV.20) starts from a zero initial condition and achieves the state of the BC-PHS approximately at $t = 4$. The error (Figure IV.21), starts from a non zero initial condition and achieves the zero approximately at $t = 4$. Finally, Figure IV.23 shows the conjugated outputs and its estimations.

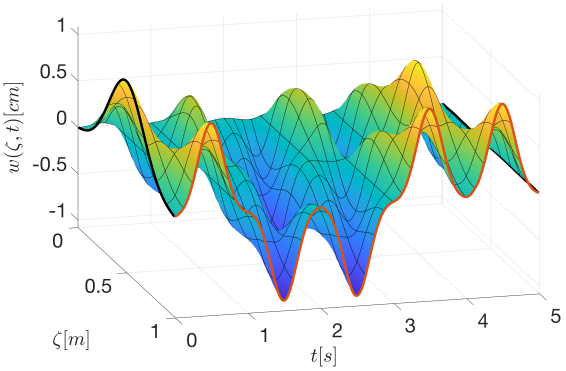

Figure IV.19 – String deformation

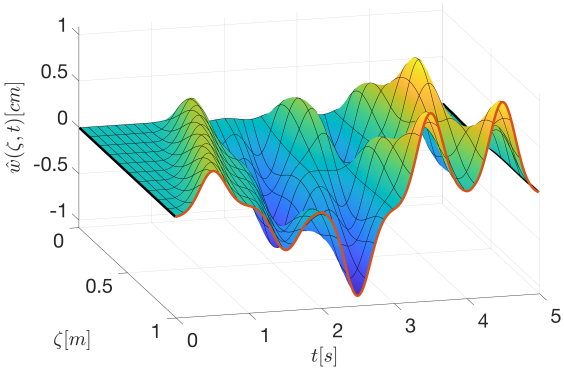

Figure IV.20 – Estimated deformation

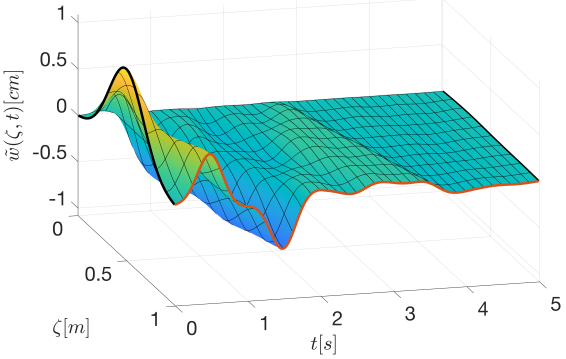

Figure IV.21 – Deformation error

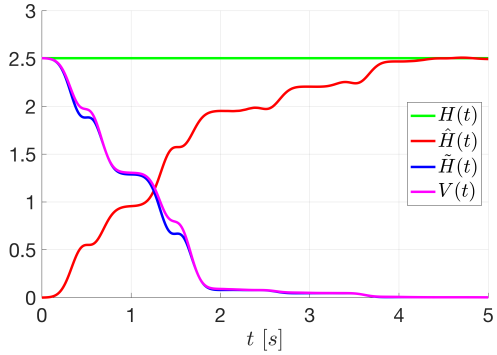

Figure IV.22 – Hamiltonian of the plant (green), observer (red) and error system (blue)

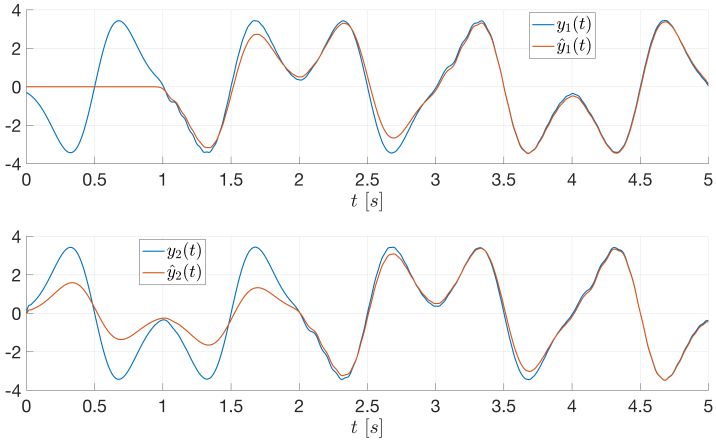

Figure IV.23 – Observer convergence of the conjugated output $\hat{y}(t)$ to $y(t)$. y_1 is the negative force at the left side of the string and y_2 is the velocity of the string at the right side.

IV.4 Observer-based damping injection: application to the vibrating string

In this section, we use the infinite-dimensional observers proposed in the previous section to apply an *observer-based damping injection* control strategy. With this control strategy, we aim to add damping at the non-measurable side of the vibrating string. We consider the vibrating string of Example II.3.2 in the fully actuated and partially sensed case, *i.e.* with actuators at both sides of the string and a sensor at one side of the string only. First, we consider the case where the force at the left side is measurable and second, the case where the displacement at the right side is measurable. The results presented in this section are some first steps towards *observer-based damping injection* using a *late-lumping* approach for BC-PHSs.

IV.4.1 Fully actuated string with a force sensor

In this part, we consider the vibrating string with actuators at both sides and with a force sensor at the left side of the string. We show that the extended system, composed by the BC-PHS and the infinite-dimensional observer, makes the closed-loop system exponentially stable using the observer-based damping injection strategy. We compare this strategy with the case where damping is applied at the measurable side only, and we verify by simulations that the settling time can be improved using the observer-based damping injection strategy.

We consider the vibrating string of Example IV.3.1 with a force sensor at the left side of the string. Note that, we have two inputs, two conjugated outputs and one measured output, *i.e.*

$$\begin{pmatrix} p(a,t) \\ q(b,t) \end{pmatrix} = u(t), \quad y(t) = \begin{pmatrix} -q(a,t) \\ p(b,t) \end{pmatrix}, \quad y_m(t) = -q(0,t).$$

We aim to apply a damping injection control law at both sides of the string. This is:

$$u(t) = -Ky(t) \quad \Leftrightarrow \quad \begin{pmatrix} p(a,t) \\ q(b,t) \end{pmatrix} = -\begin{pmatrix} k_1 & 0 \\ 0 & k_2 \end{pmatrix} \begin{pmatrix} -q(0,t) \\ p(1,t) \end{pmatrix}, \quad K = \begin{pmatrix} k_1 & 0 \\ 0 & k_2 \end{pmatrix},$$

where k_1 and k_2 are two positive scalars. However, since $p(1,t)$ is not measurable, it is not possible to implement it. In the previous section, we have shown that, in this example, when the conjugated output is partially measured, we can estimate the state $x(\zeta,t)$ with an infinite-dimensional observer (using Proposition IV.3.2 for example). In this case, we can use the following infinite-dimensional observer to estimate the state $x(\zeta,t)$ from the measurements of $y_m(t)$ and $u(t)$

$$\hat{\mathcal{P}} \begin{cases} \dfrac{\partial}{\partial t}\begin{pmatrix} \hat{q}(\zeta,t) \\ \hat{p}(\zeta,t) \end{pmatrix} = \begin{pmatrix} 0 & 1 \\ 1 & 0 \end{pmatrix} \dfrac{\partial}{\partial \zeta}\begin{pmatrix} \hat{q}(\zeta,t) \\ \hat{p}(\zeta,t) \end{pmatrix}, \quad \begin{pmatrix} \hat{q}(\zeta,0) \\ \hat{p}(\zeta,0) \end{pmatrix} = \begin{pmatrix} \hat{q}_0(\zeta) \\ \hat{p}_0(\zeta) \end{pmatrix}, \\ \begin{pmatrix} \hat{p}(0,t) \\ \hat{q}(1,t) \end{pmatrix} = u(t) + \begin{pmatrix} l_1 \\ 0 \end{pmatrix} (y_m(t) - \hat{y}_m(t)), \\ \hat{y}_m(t) = -\hat{q}(0,t). \end{cases} \tag{IV.59}$$

Finally, we implement the *observer-based damping injection* at the both sides of the string using the following control law:

$$u(t) = -\begin{pmatrix} k_1 & 0 \\ 0 & k_2 \end{pmatrix} \begin{pmatrix} -\hat{q}(0,t) \\ \hat{p}(1,t) \end{pmatrix} = \begin{pmatrix} k_1 \hat{q}(0,t) \\ -k_2 \hat{p}(1,t) \end{pmatrix}. \tag{IV.60}$$

In the following Proposition, we give the main result of this subsection concerning the existence of solutions and the stability of the closed-loop system composed by (IV.29), (IV.59), and (IV.60).

Proposition IV.4.1. *Consider the closed-loop system obtained between the BC-PHS* (IV.29) *and the observer-based control law* (IV.59)-(IV.60)*. The following holds:*

(i) The closed-loop system is well-posed if $k_1 > 0$, $k_2 > 0$, *and* $0 < l_1 \leq 4k_1$.

(ii) The closed-loop system is exponentially stable if there exists $\gamma > 0$ *such that*

$$\begin{pmatrix} 1+k_1^2 & -k_1 l_1 \\ -k_1 l_1 & 1+2l_1^2 \end{pmatrix} - \gamma \begin{pmatrix} k_1 & -\frac{l_1}{2} \\ -\frac{l_1}{2} & l_1 \end{pmatrix} \leq 0 \tag{IV.61}$$

$\Diamond$

Proof. *Defining the error variables as* $\tilde{q}(\zeta,t) = q(\zeta,t) - \hat{q}(\zeta,t)$ *and* $\tilde{p}(\zeta,t) = p(\zeta,t) - \hat{p}(\zeta,t)$*, the error system becomes*

$$\begin{aligned} \frac{\partial}{\partial t}\begin{pmatrix}\tilde{q}(\zeta,t)\\ \tilde{p}(\zeta,t)\end{pmatrix} &= \begin{pmatrix}0 & 1\\ 1 & 0\end{pmatrix}\frac{\partial}{\partial \zeta}\begin{pmatrix}\tilde{q}(\zeta,t)\\ \tilde{p}(\zeta,t)\end{pmatrix}, \quad \begin{pmatrix}\tilde{q}(\zeta,0)\\ \tilde{p}(\zeta,0)\end{pmatrix} = \begin{pmatrix}\tilde{q}_0(\zeta)\\ \tilde{p}_0(\zeta)\end{pmatrix}, \\ \begin{pmatrix}\tilde{p}(0,t)\\ \tilde{q}(1,t)\end{pmatrix} &= \begin{pmatrix}l_1\\ 0\end{pmatrix}\tilde{q}(0,t), \end{aligned}$$

and the extended closed-loop system can be written as

$$\begin{aligned} \frac{\partial}{\partial t}\begin{pmatrix}\hat{q}(\zeta,t)\\ \hat{p}(\zeta,t)\\ \tilde{q}(\zeta,t)\\ \tilde{p}(\zeta,t)\end{pmatrix} &= \begin{pmatrix}0 & 1 & 0 & 0\\ 1 & 0 & 0 & 0\\ 0 & 0 & 0 & 1\\ 0 & 0 & 1 & 0\end{pmatrix}\frac{\partial}{\partial \zeta}\begin{pmatrix}\hat{q}(\zeta,t)\\ \hat{p}(\zeta,t)\\ \tilde{q}(\zeta,t)\\ \tilde{p}(\zeta,t)\end{pmatrix}, \quad \begin{pmatrix}\hat{q}(\zeta,0)\\ \hat{p}(\zeta,0)\\ \tilde{q}(\zeta,0)\\ \tilde{p}(\zeta,0)\end{pmatrix} = \begin{pmatrix}\hat{q}_0(\zeta)\\ \hat{p}_0(\zeta)\\ \tilde{q}_0(\zeta)\\ \tilde{p}_0(\zeta)\end{pmatrix}, \\ \begin{pmatrix}\hat{p}(0,t)\\ \hat{q}(1,t)\\ \tilde{p}(0,t)\\ \tilde{q}(1,t)\end{pmatrix} &= \begin{pmatrix}k_1\hat{q}(0,t) - l_1\tilde{q}(0,t)\\ -k_2\hat{p}(1,t)\\ l_1\tilde{q}(0,t)\\ 0\end{pmatrix}. \end{aligned} \tag{IV.62}$$

In the following, we first show that the system (IV.62) *is well-posed and then that it is exponentially stable. For the well-posedness, we use Theorem II.2.2, and for the stability we use the port-Hamiltonian properties of Theorem IV.2.1. We define the following differential operator associated to the system* (IV.62)

$$\mathcal{A}z = P_z \frac{d}{d\zeta}(\mathcal{H}_z z) \tag{IV.63}$$

with

$$z(\zeta,t) = \begin{pmatrix}\hat{q}(\zeta,t)\\ \hat{p}(\zeta,t)\\ \tilde{q}(\zeta,t)\\ \tilde{p}(\zeta,t)\end{pmatrix}, \quad P_z = \begin{pmatrix}0 & 1 & 0 & 0\\ 1 & 0 & 0 & 0\\ 0 & 0 & 0 & 1\\ 0 & 0 & 1 & 0\end{pmatrix}, \quad \mathcal{H}_z = I_4. \tag{IV.64}$$

The boundary conditions of (IV.62) *are written with the following parametrization*

$$W_{\mathcal{B}}\begin{pmatrix}f_\partial(t)\\ e_\partial(t)\end{pmatrix} = 0 \tag{IV.65}$$

with

$$W_{\mathcal{B}} = \sqrt{2} V_{\mathcal{B}} \begin{pmatrix} P_z & -P_z \\ I_4 & I_4 \end{pmatrix}^{-1}, \quad V_{\mathcal{B}} = \begin{pmatrix} 0 & 0 & 0 & 0 & -k_1 & 1 & l_1 & 0 \\ 1 & k_2 & 0 & 0 & 0 & 0 & 0 & 0 \\ 0 & 0 & 0 & 0 & 0 & 0 & -l_1 & 1 \\ 0 & 0 & 1 & 0 & 0 & 0 & 0 & 0 \end{pmatrix}, \tag{IV.66}$$

and

$$\begin{pmatrix} f_\partial(t) \\ e_\partial(t) \end{pmatrix} = \frac{1}{\sqrt{2}} \begin{pmatrix} P_z & -P_z \\ I_4 & I_4 \end{pmatrix} \begin{pmatrix} \mathcal{H}_z(1) z(1,t) \\ \mathcal{H}_z(0) z(0,t) \end{pmatrix}. \tag{IV.67}$$

Note that, for simplicity we use the matrix $V_{\mathcal{B}}$, where the following is satisfied

$$W_{\mathcal{B}} \begin{pmatrix} f_\partial(t) \\ e_\partial(t) \end{pmatrix} = V_{\mathcal{B}} \begin{pmatrix} \mathcal{H}_z(1) z(1,t) \\ \mathcal{H}_z(0) z(0,t) \end{pmatrix} = 0. \tag{IV.68}$$

From Theorem II.2.2, $\mathcal{A}_z$ generates a contraction semigroup on $Z = L_2([0,1], \mathbb{R}^n)$ if and only if $W_{\mathcal{B}} \Sigma W_{\mathcal{B}}^T \geq 0$, with $\Sigma = \left(\begin{smallmatrix} 0_4 & I_4 \\ I_4 & 0_4 \end{smallmatrix}\right)$. To check this condition, we define the matrix $\Omega = W_{\mathcal{B}} \Sigma W_{\mathcal{B}}^T$ and its eigenvalues $\lambda(\Omega)$. We have

$$\Omega = \begin{pmatrix} 2k_1 & 0 & -l_1 & 0 \\ 0 & 2k_2 & 0 & 0 \\ -l_1 & 0 & 2l_1 & 0 \\ 0 & 0 & 0 & 0 \end{pmatrix}, \quad \lambda(\Omega) = \begin{pmatrix} 0 \\ 2k_2 \\ k_1 + l_1 + \sqrt{k_1^2 - 2k_1 l_1 + 2l_1^2} \\ k_1 + l_1 - \sqrt{k_1^2 - 2k_1 l_1 + 2l_1^2} \end{pmatrix}. \tag{IV.69}$$

Since k_1, k_2, and l_1 are positive values, $\Omega = W_{\mathcal{B}} \Sigma W_{\mathcal{B}}^T \geq 0$ if and only if $l_1 \leq 4k_1$. With the same conditions, $\mathcal{A}_z$ generates a contraction semigroup on $Z = L_2([0,1], \mathbb{R}^n)$ and (IV.62) is well-posed.

To show the exponential stability, we define the following Hamiltonian

$$\begin{aligned} H_T(t) &= \frac{1}{2} \|z(t)\|_{\mathcal{H}_z}^2 = \frac{1}{2} \int_0^1 z(\zeta,t)^T \mathcal{H}_z z(\zeta,t) d\zeta \\ &= \frac{1}{2} \int_0^1 [\hat{q}(\zeta,t)^2 + \hat{p}(\zeta,t)^2 + \tilde{q}(\zeta,t)^2 + \tilde{p}(\zeta,t)^2] d\zeta, \end{aligned} \tag{IV.70}$$

with time derivative given by

$$\dot{H}_T(t) = -\left[k_1 \hat{q}(0,t)^2 - l_1 \hat{q}(0,t)\tilde{q}(0,t) + l_1 \tilde{q}(0,t)^2\right] - k_2 \hat{p}(1,t)^2. \tag{IV.71}$$

where we have replaced the boundary conditions of (IV.62). Integrating over time we obtain

$$H_T(0) - H_T(\tau) - \int_0^\tau k_2 \hat{p}(1,t)^2 dt = \int_0^\tau \begin{pmatrix} \hat{q}(0,t) \\ \tilde{q}(0,t) \end{pmatrix}^T \begin{pmatrix} k_1 & -\frac{l_1}{2} \\ -\frac{l_1}{2} & l_1 \end{pmatrix} \begin{pmatrix} \hat{q}(0,t) \\ \tilde{q}(0,t) \end{pmatrix}. \tag{IV.72}$$

Note that, if we are able to show that the Hamiltonian $H_T(\tau)$ has an upper bound of the form

$$H_T(\tau) \leq \alpha \int_0^\tau \begin{pmatrix} \hat{q}(0,t) \\ \tilde{q}(0,t) \end{pmatrix}^T \begin{pmatrix} k_1 & -\frac{l_1}{2} \\ -\frac{l_1}{2} & l_1 \end{pmatrix} \begin{pmatrix} \hat{q}(0,t) \\ \tilde{q}(0,t) \end{pmatrix}, \tag{IV.73}$$

for some $\alpha > 0$, then, from (IV.72) and (IV.73), the following inequality is satisfied

$$H_T(\tau) \leq \frac{\alpha}{1+\alpha} \left(H_T(0) - \int_0^\tau k_2 \hat{p}(1,t)^2 dt \right) \tag{IV.74}$$

and the exponential stability is achieved, since $H_T(\tau) \leq \frac{\alpha}{1+\alpha} H_T(0)$. *To check that there exists* α *that satisfies* (IV.73), *we use the following bound on the Hamiltonian of a BC-PHS (See Theorem IV.2.1 or [Villegas 07, Theorem 5.17])*

$$\begin{aligned} H_T(\tau) &\leq c(\tau) \int_0^\tau \|\mathcal{H}_z(1) z(1,t)\|_{\mathbb{R}}^2 dt, \quad \text{and} \\ H_T(\tau) &\leq c(\tau) \int_0^\tau \|\mathcal{H}_z(0) z(0,t)\|_{\mathbb{R}}^2 dt. \end{aligned} \tag{IV.75}$$

for some constant $c(\tau)$ *that only depends on* τ. *Since the norm of the co-energy variables evaluated at* $\zeta = 0$ *is*

$$\begin{aligned} \|\mathcal{H}_z(0) z(0,t)\|_{\mathbb{R}}^2 &= \hat{q}(0,t)^2 + \hat{p}(0,t)^2 + \tilde{q}(0,t)^2 + \tilde{p}(0,t)^2 \\ &= \hat{q}(0,t)^2 + [k_1 \hat{q}(0,t) - l_1 \tilde{q}(0,t)]^2 + \tilde{q}(0,t)^2 + [l_1 \tilde{q}(0,t)]^2 \\ &= \begin{pmatrix} \hat{q}(0,t) \\ \tilde{q}(0,t) \end{pmatrix}^T \begin{pmatrix} 1+k_1^2 & -k_1 l_1 \\ -k_1 l_1 & 1+2l_1^2 \end{pmatrix} \begin{pmatrix} \hat{q}(0,t) \\ \tilde{q}(0,t) \end{pmatrix}, \end{aligned}$$

the second inequality of (IV.75) *is then equivalent to*

$$H_T(\tau) \leq c(\tau) \int_0^\tau \begin{pmatrix} \hat{q}(0,t) \\ \tilde{q}(0,t) \end{pmatrix}^T \Omega_1 \begin{pmatrix} \hat{q}(0,t) \\ \tilde{q}(0,t) \end{pmatrix} \leq c(\tau) \int_0^\tau \begin{pmatrix} \hat{q}(0,t) \\ \tilde{q}(0,t) \end{pmatrix}^T \gamma \Omega_2 \begin{pmatrix} \hat{q}(0,t) \\ \tilde{q}(0,t) \end{pmatrix},$$

with

$$\Omega_1 = \begin{pmatrix} 1+k_1^2 & -k_1 l_1 \\ -k_1 l_1 & 1+2l_1^2 \end{pmatrix}, \quad \Omega_2 = \begin{pmatrix} k_1 & -\frac{l_1}{2} \\ -\frac{l_1}{2} & l_1 \end{pmatrix} \tag{IV.76}$$

for some $\gamma > 0$ *if*

$$\Omega_1 \leq \gamma \Omega_2 \tag{IV.77}$$

Finally, since (IV.77) *is satisfied from assumption* (IV.61), *the Hamiltonian is bounded as*

$$H_T(\tau) \leq c(\tau) \int_0^\tau \begin{pmatrix} \hat{q}(0,t) \\ \tilde{q}(0,t) \end{pmatrix}^T \gamma \Omega_2 \begin{pmatrix} \hat{q}(0,t) \\ \tilde{q}(0,t) \end{pmatrix} = \alpha \int_0^\tau \begin{pmatrix} \hat{q}(0,t) \\ \tilde{q}(0,t) \end{pmatrix}^T \begin{pmatrix} k_1 & -\frac{l_1}{2} \\ -\frac{l_1}{2} & l_1 \end{pmatrix} \begin{pmatrix} \hat{q}(0,t) \\ \tilde{q}(0,t) \end{pmatrix},$$

with $\alpha = c(\tau)\gamma$. *Hence, inequality* (IV.73) *is satisfied and the exponential stability is corroborated.* ■

By using *observer-based damping injection*, we can add additional damping at the non-measurable side of the string. This is interesting when at the measurable side of the string the amount of damping is limited. This is the case, for instance, when the value of k_1 is restricted. In this case, we assume $k_1 = 0.3$ as shown in Table IV.4 (the greatest damping is obtained for $k_1 = 1$ [Krstic 08]). Then, we use the *observer-based damping injection* approach to add additional damping at the non-measurable side and reduce the settling time. Using the design parameter of Table IV.4, the conditions of Proposition IV.4.1 are satisfied since $k_1 > 0$, $k_2 > 0$, $0 < l_1 \leq 4k_1$, and (IV.61) is satisfied with $\gamma = 10$, for instance.

In Figure IV.24, we show the Hamiltonian of the string when three different control laws are applied. With the blue line we show the ideal case when all is measurable and the damping is applied at both sides without observer, with the red line we show the worst case when damping is applied at the measurable side only, and with the green line we show the new case when damping

Table IV.4 – Design parameters

Parameter	Value	
k_1	0.3	Damping coefficient at the measurable side
k_2	1	Damping coefficient at the non-measurable side
l_1	1	Observer gain

is applied at both sides using the observed values. The corresponding control laws are respectively given by

$$u(t) = -\begin{pmatrix} -k_1 q(0,t) \\ k_2 p(1,t) \end{pmatrix}, \quad u(t) = -\begin{pmatrix} -k_1 q(0,t) \\ 0 \end{pmatrix}, \quad u(t) = -\begin{pmatrix} -k_1 \hat{q}(0,t) \\ k_2 \hat{p}(1,t) \end{pmatrix},$$

and we can notice in Figure IV.24 that the *observer-based damping injection* approach improves the settling time with respect to the case where damping injection is applied at one side only.

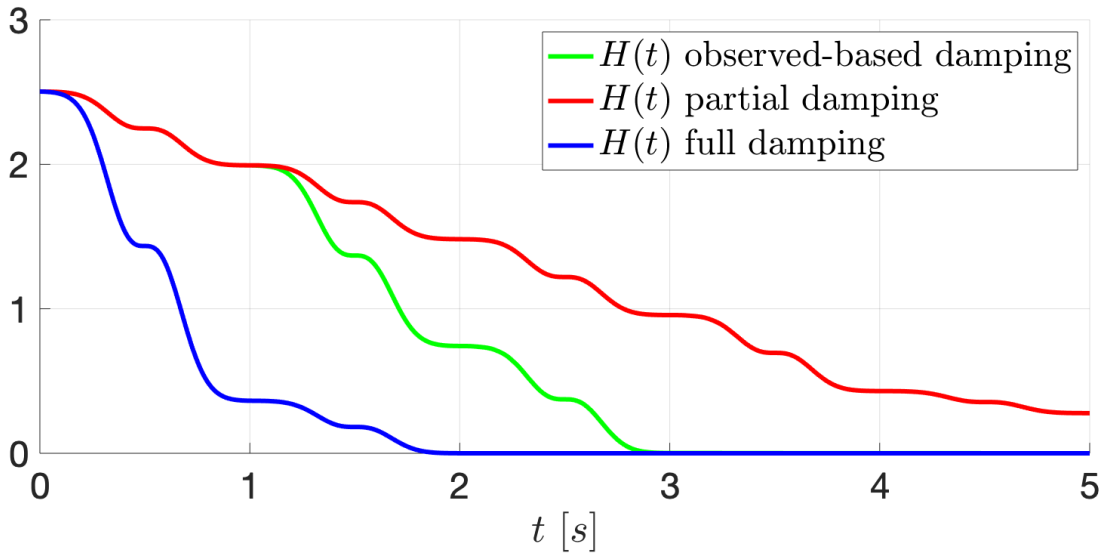

Figure IV.24 – Hamiltonian energy in the ideal case of full damping (blue), in a partial damping case due to the lake of sensors (red), and using the observer-based damping (green).

Figure IV.25 shows the string deformation along time and space, Figure IV.26 shows the estimated one, and Figure IV.27 shows the error. In each figure, the two black lines show the initial and final value of $w(\zeta,t)$, $\hat{w}(\zeta,t)$, and $\tilde{w}(\zeta,t)$, and the orange line shows the end-tip deformations $w(1,t)$, $\hat{w}(1,t)$, and $\tilde{w}(1,t)$. Since we applied damping at both side of the string using the observed values, the string deformation (Figure IV.25) converges to zero approximately at $t = 3$. The observed deformation (Figure IV.26) starts from a zero initial condition, reaches the string deformation approximately at $t = 2$ and follows the real system behavior (converging to zero approximately at $t = 3$). The error (Figure IV.27), starts from a non zero initial condition and reaches the zero approximately at $t = 2$. Finally, Figure IV.29 shows the conjugated outputs and its estimations.

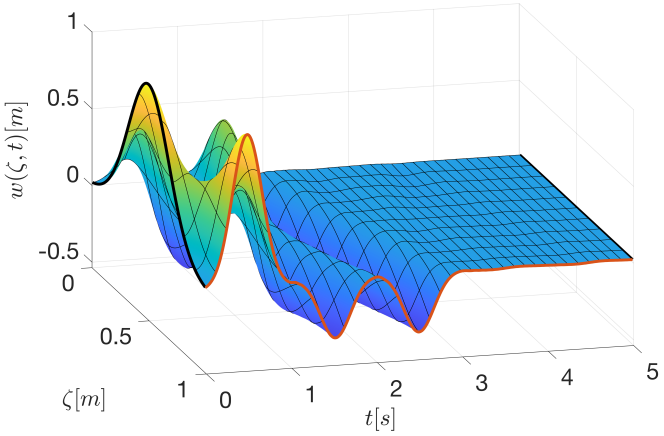

Figure IV.25 – String deformation

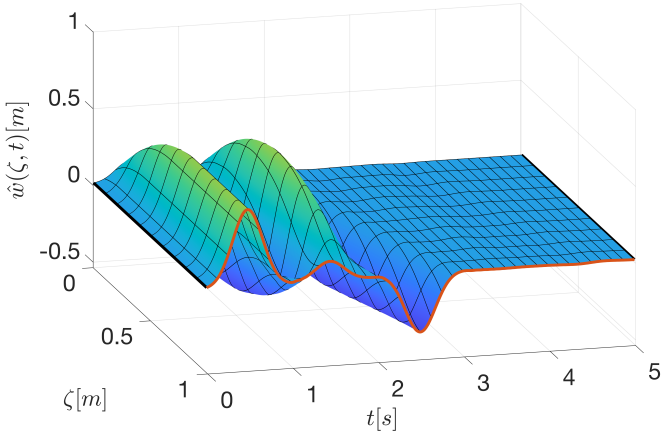

Figure IV.26 – Estimated deformation

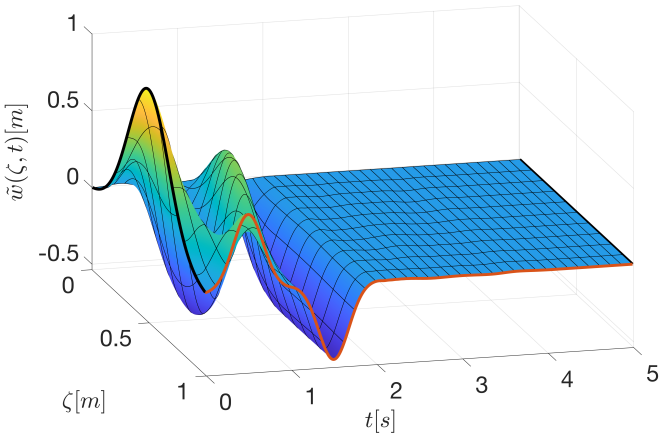

Figure IV.27 – Deformation error

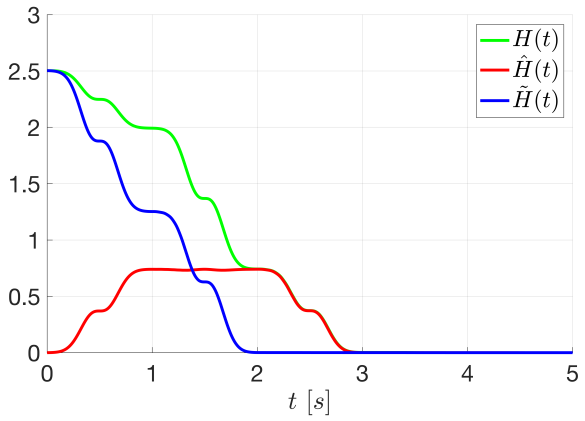

Figure IV.28 – Hamiltonian of the plant (green), observer (red) and error system (blue)

Remark IV.4.1. *For the simulation, the string deformation and its estimation are reconstructed numerically from the state variables. To this end, we integrate $q(\zeta,t)$ along the space and $p(\zeta,t)$ along the time as follows*

$$q(\zeta,t) = \frac{\partial w}{\partial \zeta}(\zeta,t) \Rightarrow w(\zeta,t) = w(0,t) + \int_0^\zeta q(s,t)ds, \tag{IV.78}$$

$$p(\zeta,t) = \frac{\partial w}{\partial t}(\zeta,t) \Rightarrow w(\zeta,t) = w(\zeta,0) + \int_0^t p(\zeta,\tau)d\tau. \tag{IV.79}$$

The velocity at the left side $p(0,t)$ is known from the input. The initial deformation at the left side $w(0,0)$ is considered known for the reconstruction of $w(\zeta,t)$. Then, we reconstruct $w(0,t)$ using (IV.79). Finally, we reconstruct $w(\zeta,t)$ using of (IV.78). Both integrals in (IV.78) and (IV.79) are solved numerically by mean of a rectangular approximation. For reconstructing the observed deformation, we consider $\hat{w}(0,t) = w(0,t)$, and we do exactly the same numerical integration as before. However, it is important to notice that this observer does not estimate $w(\zeta,t)$. Indeed, a displacement sensor is needed for reconstructing $w(\zeta,t)$ with an observer. ♣

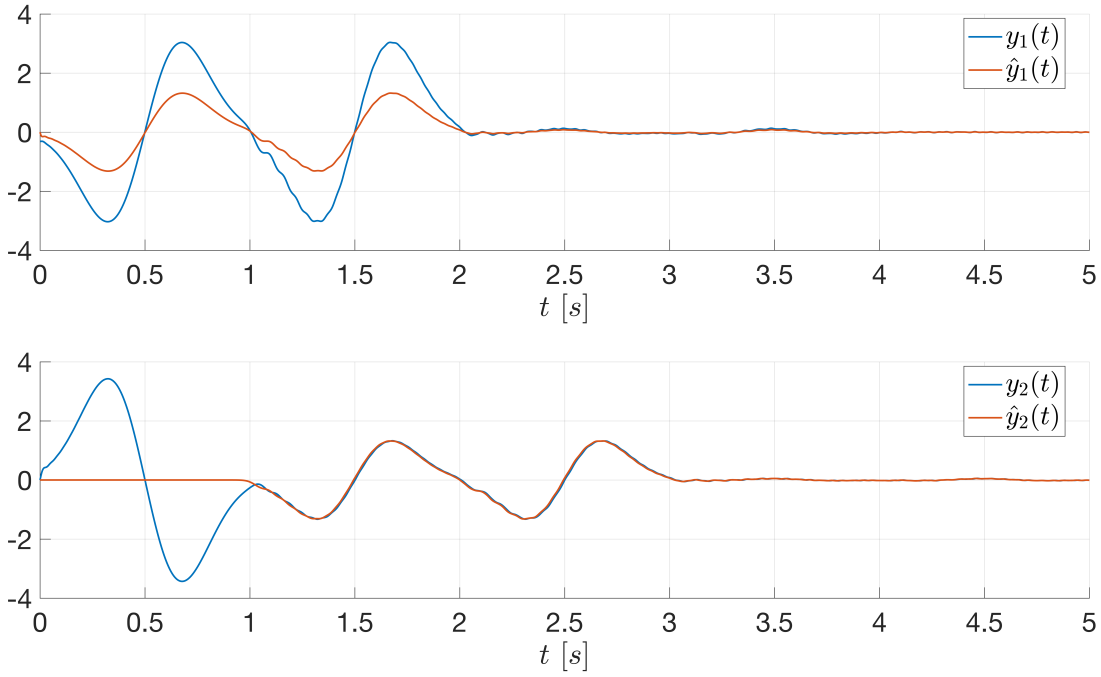

Figure IV.29 – Convergence of the observed output $\hat{y}(t)$ to the conjugated output $y(t)$.

IV.4.2 Fully actuated string with a displacement sensor

In this part, we consider the vibrating string with actuators at both sides and with a displacement sensor at the right side. We show that the extended system, composed of the BC-PHS, an infinite-dimensional observer, and an *observer-based damping injection* control strategy makes the closed-loop system asymptotically stable using damping injection on the observed states. The asymptotic stability of the closed-loop system is shown using LaSalle's invariance principle. To this end, we assume that the trajectories of the solution of the closed-loop system are precompact. Finally, we show with simulations that the observer-based damping injection improves the settling time compared to when damping is applied at one side only.

We consider the vibrating string of Example IV.3.1 with a displacement sensor

$$\begin{pmatrix} p(a,t) \\ q(b,t) \end{pmatrix} = u(t), \quad y(t) = \begin{pmatrix} -q(a,t) \\ p(b,t) \end{pmatrix}, \quad y_m(t) = w(1,t).$$

From Example IV.3.2, we know that the following observer estimates asymptotically the state of the system

$$\hat{\mathcal{P}} \begin{cases} \dfrac{\partial}{\partial t}\begin{pmatrix} \hat{q}(\zeta,t) \\ \hat{p}(\zeta,t) \end{pmatrix} = \begin{pmatrix} 0 & 1 \\ 1 & 0 \end{pmatrix} \dfrac{\partial}{\partial \zeta}\begin{pmatrix} \hat{q}(\zeta,t) \\ \hat{p}(\zeta,t) \end{pmatrix}, \quad \begin{pmatrix} \hat{q}(\zeta,0) \\ \hat{p}(\zeta,0) \end{pmatrix} = \begin{pmatrix} \hat{q}_0(\zeta) \\ \hat{p}_0(\zeta) \end{pmatrix}, \\ \begin{pmatrix} \hat{p}(0,t) \\ \hat{q}(1,t) \end{pmatrix} = u(t) + \begin{pmatrix} 0 \\ l_1(y_m(t) - \hat{y}_m(t) + \theta(t)) \end{pmatrix}, \\ \dot{\theta}(t) = -l_2(y_m(t) - \hat{y}_m(t) + \theta(t)), \quad \theta(0) = \theta_0, \end{cases} \tag{IV.80}$$

with l_1, $l_2 > 0$, and $\theta(t)$ an external dynamic with initial condition θ_0.

Remark IV.4.2. *As pointed out in [Guo 09], this is the best result in terms of convergence of the observer, and the exponential convergence is not possible to achieve.* ♣

We aim to apply the following control law to the BC-PHS (IV.29)

$$u(t) = -\begin{pmatrix} k_1 & 0 \\ 0 & k_2 \end{pmatrix}\begin{pmatrix} -\hat{q}(0,t) \\ \hat{p}(1,t) \end{pmatrix} = \begin{pmatrix} k_1\hat{q}(0,t) \\ -k_2\hat{p}(1,t) \end{pmatrix}. \tag{IV.81}$$

Note that, the control law is equivalent to a *damping injection* using the observed states at both sides of the string. In the following Proposition, we give the main result of this section concerning the existence of solutions and the stability of the closed-loop system composed by (IV.29), (IV.80), and (IV.81).

Proposition IV.4.2. *Consider the closed-loop system composed by the BC-PHS (IV.29) and the observer-based control law (IV.80)-(IV.81), with l_1, l_2, k_1, and k_2 positive scalars such that $0 < \frac{l_1}{4k_2l_2} < 1$. Assume that the solutions are precompact. The following holds*

(i) The closed-loop system is well-posed.

(ii) The closed-loop system is asymptotically stable.

◊

Proof. *Defining the error variables as*

$$\tilde{q}(\zeta,t) = q(\zeta,t) - \hat{q}(\zeta,t), \quad \tilde{p}(\zeta,t) = p(\zeta,t) - \hat{p}(\zeta,t),$$

the error system becomes

$$\begin{aligned} \frac{\partial}{\partial t}\begin{pmatrix} \tilde{q}(\zeta,t) \\ \tilde{p}(\zeta,t) \end{pmatrix} &= \begin{pmatrix} 0 & 1 \\ 1 & 0 \end{pmatrix}\frac{\partial}{\partial \zeta}\begin{pmatrix} \tilde{q}(\zeta,t) \\ \tilde{p}(\zeta,t) \end{pmatrix}, \quad \begin{pmatrix} \tilde{q}(\zeta,0) \\ \tilde{p}(\zeta,0) \end{pmatrix} = \begin{pmatrix} \tilde{q}_0(\zeta) \\ \tilde{p}_0(\zeta) \end{pmatrix}, \\ \begin{pmatrix} \tilde{p}(0,t) \\ \tilde{q}(1,t) \end{pmatrix} &= \begin{pmatrix} 0 \\ -l_1 \end{pmatrix} x_c(t), \\ \dot{x}_c(t) &= -l_2 x_c(t) + \tilde{p}(1,t), \qquad x_c(0) = c_{c0}, \end{aligned}$$

with $x_c(t) = y_m(t) - \hat{y}_m(t) + \theta(t) = \tilde{w}(1,t) + \theta(t)$. Then, the augmented open-loop system reads

$$\begin{aligned} \frac{\partial}{\partial t}\begin{pmatrix} \hat{q}(\zeta,t) \\ \hat{p}(\zeta,t) \\ \tilde{q}(\zeta,t) \\ \tilde{p}(\zeta,t) \end{pmatrix} &= \begin{pmatrix} 0 & 1 & 0 & 0 \\ 1 & 0 & 0 & 0 \\ 0 & 0 & 0 & 1 \\ 0 & 0 & 1 & 0 \end{pmatrix}\frac{\partial}{\partial \zeta}\begin{pmatrix} \hat{q}(\zeta,t) \\ \hat{p}(\zeta,t) \\ \tilde{q}(\zeta,t) \\ \tilde{p}(\zeta,t) \end{pmatrix}, \quad \begin{pmatrix} \hat{q}(\zeta,0) \\ \hat{p}(\zeta,0) \\ \tilde{q}(\zeta,0) \\ \tilde{p}(\zeta,0) \end{pmatrix} = \begin{pmatrix} \hat{q}_0(\zeta) \\ \hat{p}_0(\zeta) \\ \tilde{q}_0(\zeta) \\ \tilde{p}_0(\zeta) \end{pmatrix}, \\ \dot{x}_c(t) &= -l_2 x_c(t) + \tilde{p}(1,t), \qquad x_c(0) = c_{c0}. \\ \begin{pmatrix} \hat{p}(0,t) \\ \hat{q}(1,t) \\ \tilde{p}(0,t) \\ \tilde{q}(1,t) \end{pmatrix} &= \begin{pmatrix} 1 & 0 & 0 \\ 0 & 1 & l_1 \\ 0 & 0 & 0 \\ 0 & 0 & -l_2 \end{pmatrix}\begin{pmatrix} u(t) \\ x_c(t) \end{pmatrix}. \end{aligned} \tag{IV.82}$$

Using the control law (IV.81)*, the augmented closed-loop system becomes*

$$\frac{\partial}{\partial t}\begin{pmatrix}\hat{q}(\zeta,t)\\ \hat{p}(\zeta,t)\\ \tilde{q}(\zeta,t)\\ \tilde{p}(\zeta,t)\end{pmatrix} = \begin{pmatrix}0&1&0&0\\1&0&0&0\\0&0&0&1\\0&0&1&0\end{pmatrix}\frac{\partial}{\partial \zeta}\begin{pmatrix}\hat{q}(\zeta,t)\\ \hat{p}(\zeta,t)\\ \tilde{q}(\zeta,t)\\ \tilde{p}(\zeta,t)\end{pmatrix}, \quad \begin{pmatrix}\hat{q}(\zeta,0)\\ \hat{p}(\zeta,0)\\ \tilde{q}(\zeta,0)\\ \tilde{p}(\zeta,0)\end{pmatrix} = \begin{pmatrix}\hat{q}_0(\zeta)\\ \hat{p}_0(\zeta)\\ \tilde{q}_0(\zeta)\\ \tilde{p}_0(\zeta)\end{pmatrix},$$
$$\dot{x}_c(t) = -l_2 x_c(t) + \tilde{p}(1,t), \qquad x_c(0) = c_{c0}. \tag{IV.83}$$
$$\begin{pmatrix}\hat{p}(0,t)\\ \hat{q}(1,t)\\ \tilde{p}(0,t)\\ \tilde{q}(1,t)\end{pmatrix} = \begin{pmatrix}k_1\hat{q}(0,t)\\ -k_2\hat{p}(1,t)+l_1x_c(t)\\ 0\\ -l_1x_c(t)\end{pmatrix}.$$

We define the state of (IV.83) *as*

$$z(\zeta,t) = \begin{pmatrix}\hat{q}(\zeta,t)\\ \hat{p}(\zeta,t)\\ \tilde{q}(\zeta,t)\\ \tilde{p}(\zeta,t)\\ x_c(t)\end{pmatrix}, \tag{IV.84}$$

and the inner product

$$\langle z_1, z_2\rangle_Z = \frac{1}{2}\int_0^1 [\hat{q}_1\hat{q}_2 + \hat{p}_1\hat{p}_2]d\zeta + \frac{1}{2}\int_0^1 [\tilde{q}_1\tilde{q}_2 + \tilde{p}_1\tilde{p}_2]d\zeta + \frac{l_1}{2}x_{c1}x_{c2}, \tag{IV.85}$$

where $z_1 = (\hat{q}_1, \hat{p}_1, \tilde{q}_1, \tilde{p}_1, x_{c1})^T$ *and* $z_2 = (\hat{q}_2, \hat{p}_2, \tilde{q}_2, \tilde{p}_2, x_{c2})^T$*. Then, we write the system* (IV.83) *in the abstract state space representation. To this end, we define the state space as*

$$Z = L_2\left([0,1];\mathbb{R}^4\right)\times\mathbb{R} \tag{IV.86}$$

and the operator $\mathcal{A}$ *as*

$$\mathcal{A}z = \mathcal{A}\begin{pmatrix}\hat{q}\\ \hat{p}\\ \tilde{q}\\ \tilde{p}\\ x_c\end{pmatrix} = \begin{pmatrix}\hat{p}_\zeta\\ \hat{q}_\zeta\\ \tilde{p}_\zeta\\ \tilde{q}_\zeta\\ -l_2x_c + \tilde{p}(1)\end{pmatrix} \tag{IV.87}$$

with domain

$$D(\mathcal{A}) = \left\{(\hat{q},\hat{p},\tilde{q},\tilde{p})^T \in H^1([0,1],\mathbb{R}^4), x_c\in\mathbb{R} \;\middle|\; \begin{array}{l}\hat{p}(0)=k_1\hat{q}(0),\\ \hat{q}(1)=-k_2\hat{p}(1)+l_1x_c,\\ \tilde{p}(0)=0,\\ \tilde{q}(1)=-l_1x_c.\end{array}\right\}. \tag{IV.88}$$

Finally, the closed-loop system is represented in the abstract formulation as

$$\dot{z}(t) = \mathcal{A}z(t), \quad z(0) = z_0 \in Z. \tag{IV.89}$$

We use the Lümer-Phillips theorem to show that the operator $\mathcal{A}$ (IV.87) *with domain* $D(\mathcal{A})$ (IV.88) *generates a contraction semigroup, which is equivalent to show that the closed-loop system* (IV.29), (IV.80), (IV.81) *is well-posed. To this end, we follow the same steps than in [Augner 18,*

Theorem 3.3.6] (See also [Villegas 07, Theorem 5.8]). First, we show that the operator $\mathcal{A}$ is dissipative, and then we show that the range of the operator $I-\mathcal{A}$ is equivalent to the space defined for z in (IV.86).

For simplicity, we avoid the time and space dependency, and we use a dot for the time derivative, a subscript ζ for the spatial derivative and a subscript 0 or 1 when the variables are evaluated at $\zeta=0$ or $\zeta=1$, respectively. For example $\dot{\hat{q}}=\frac{\partial\hat{q}}{\partial t}(\zeta,t),\quad \hat{q}_\zeta=\frac{\partial\hat{q}}{\partial\zeta}(\zeta,t),\quad \hat{q}_1=\hat{q}(1,t)$.

To show that the operator $\mathcal{A}$ is dissipative, we have to show that the norm induced by (IV.85), defined as

$$E(t)=\langle z,z\rangle_Z=\frac{1}{2}\int_0^1\left[\hat{q}^2+\hat{p}^2+\tilde{q}^2+\tilde{p}^2\right]d\zeta+\frac{l_1}{2}x_c^2, \tag{IV.90}$$

is non increasing. To this end, we differentiate (IV.90) along time as follow:

$$\begin{aligned}
\dot{E}(t)&=\int_0^1\left[\hat{q}\dot{\hat{q}}+\hat{p}\dot{\hat{p}}+\tilde{q}\dot{\tilde{q}}+\tilde{p}\dot{\tilde{p}}\right]d\zeta+l_1x_c\dot{x}_c\\
&=\int_0^1\left[\tilde{q}\tilde{p}_\zeta+\tilde{p}\tilde{q}_\zeta+\hat{q}\hat{p}_\zeta+\hat{p}\hat{q}_\zeta\right]d\zeta+l_1x_c\left[-l_2x_c+\tilde{p}_1\right]\\
&=\hat{q}_1\hat{p}_1-\hat{q}_0\hat{p}_0+\tilde{q}_1\tilde{p}_1-\tilde{q}_0\tilde{p}_0+l_1\tilde{p}_1x_c-l_1l_2x_c^2\\
&=\left[-k_2\hat{p}_1+l_1x_c\right]\hat{p}_1-k_1\hat{q}_0^2-l_1\tilde{p}_1x_c-l_1l_2x_c^2+l_1\tilde{p}_1x_c\\
&=-k_2\hat{p}_1^2+l_1\hat{p}_1x_c-k_1\hat{q}_0^2-l_1l_2x_c^2\\
&=-k_2\hat{p}_1^2+l_1\hat{p}_1x_c-\epsilon_1l_1l_2x_c^2-k_1\hat{q}_0^2-\epsilon_2l_1l_2x_c^2\\
&=-\left[k_2\hat{p}_1^2-l_1\hat{p}_1x_c+\epsilon_1l_1l_2x_c^2\right]-k_1\hat{q}_0^2-\epsilon_2l_1l_2x_c^2\\
&=-\left[\sqrt{k_2}\hat{p}_1-\sqrt{\epsilon_1l_1l_2}x_c\right]^2-k_1\hat{q}_0^2-\epsilon_2l_1l_2x_c^2.
\end{aligned} \tag{IV.91}$$

where in the first line we have differentiated with respect to time, in the second line we have used (IV.89), in the third line we have used integration by part, in the fourth line we have replaced the boundary conditions given in (IV.88), in the fifth line we have grouped some terms, in the sixth line we have used $\epsilon_1+\epsilon_2=1$ with $0<\epsilon_1<1$ and $0<\epsilon_2<1$, and in the two last lines we have grouped some terms such that $\epsilon_1=\frac{l_1}{4k_2l_2}$. Since $\dot{E}(t)\leq 0$ for all $t\geq 0$, the energy norm is non increasing and hence the operator $\mathcal{A}$ is dissipative.

Now, we have to show that the range of the operator $I-\mathcal{A}$ is equal to Z in (IV.86). To do so, we solve the following ordinary differential equation

$$(I-\mathcal{A})z=f \tag{IV.92}$$

where $z\in D(\mathcal{A})$ is the unknown variable and $f\in Z$ is given. We define $f=(\hat{\sigma},\hat{\rho},\tilde{\sigma},\tilde{\rho},f_c)^T$, we replace it in (IV.92), and we use (IV.87) to obtain the following ODEs

$$\hat{q}-\hat{p}_\zeta=\hat{\sigma} \tag{IV.93a}$$
$$\hat{p}-\hat{q}_\zeta=\hat{\rho} \tag{IV.93b}$$
$$\tilde{q}-\tilde{p}_\zeta=\tilde{\sigma} \tag{IV.93c}$$
$$\tilde{p}-\tilde{q}_\zeta=\tilde{\rho} \tag{IV.93d}$$
$$x_c+l_2x_c-\tilde{p}(1)=f_c \tag{IV.93e}$$

Equations (IV.93a) – (IV.93d) *are written in compact form as*

$$x(\zeta) - P_1 \frac{d}{d\zeta} x(\zeta) = x_f(\zeta) \tag{IV.94}$$

with

$$x = \begin{pmatrix} \hat{q} \\ \hat{p} \\ \tilde{q} \\ \tilde{p} \end{pmatrix}, \; P_1 = \begin{pmatrix} 0 & 1 & 0 & 0 \\ 1 & 0 & 0 & 0 \\ 0 & 0 & 0 & 1 \\ 0 & 0 & 1 & 0 \end{pmatrix}, \; x_f = \begin{pmatrix} \hat{\sigma} \\ \hat{\rho} \\ \tilde{\sigma} \\ \tilde{\rho} \end{pmatrix}$$

Since P_1 *is invertible, we define* $A_f = P_1^{-1}$ *and* $B_f = -P_1^{-1}$*. Then, the ODE* (IV.94) *becomes*

$$\frac{d}{d\zeta} x(\zeta) = A_f x(\zeta) + B_f x_f(\zeta) \tag{IV.95}$$

which has a general solution

$$x(\zeta) = e^{\zeta A_f} x(0) + \int_0^\zeta e^{(\zeta - s)A_f} B_f x_f(s) ds \tag{IV.96}$$

where the term $x(0)$ *is partially known from the domain of* $\mathcal{A}$ *in* (IV.88)*. We aim to describe the full* $x(0)$ *in terms of the other known boundary conditions and also in terms of the external dynamics* (IV.93e)*. To do so, we write down the boundary conditions from the domain of* $\mathcal{A}$ *in* (IV.88) *and from* (IV.93e) *we obtain the following set of equations.*

$$\begin{aligned} \hat{p}(0) &= k_2 \hat{q}_0, \\ \hat{q}(1) &= -k_2 \hat{p}(1) + l_1 x_c, \\ \tilde{p}(0) &= 0, \\ \tilde{q}(1) &= -l_1 x_c, \\ (1 + l_2) x_c - \tilde{p}(1) &= f_c. \end{aligned} \tag{IV.97}$$

We reorganize the last equations as

$$\begin{aligned} \hat{p}(0) - k_2 \hat{q}_0 &= 0, \\ \hat{q}(1) + k_2 \hat{p}(1) - l_1 x_c &= 0, \\ \tilde{p}(0) &= 0, \\ \tilde{q}(1) + l_1 x_c &= 0, \\ (1 + l_2) x_c - \tilde{p}(1) &= f_c, \end{aligned} \tag{IV.98}$$

and we write them in matrix representation

$$\left(\begin{array}{cccc:cccc:c} 0 & 0 & 0 & 0 & -k_2 & 1 & 0 & 0 & 0 \\ 1 & k_2 & 0 & 0 & 0 & 0 & 0 & 0 & -l_1 \\ \hdashline 0 & 0 & 0 & 0 & 0 & 0 & 0 & 1 & 0 \\ 0 & 0 & 1 & 0 & 0 & 0 & 0 & 0 & l_1 \\ \hdashline 0 & 0 & 0 & -1 & 0 & 0 & 0 & 0 & 1 + l_2 \end{array}\right) \left(\begin{array}{c} \hat{q}(1) \\ \hat{p}(1) \\ \tilde{q}(1) \\ \tilde{p}(1) \\ \hdashline \hat{q}(0) \\ \hat{p}(0) \\ \tilde{q}(0) \\ \tilde{p}(0) \\ \hdashline x_c \end{array}\right) = \left(\begin{array}{c} 0 \\ 0 \\ 0 \\ 0 \\ \hdashline f_c \end{array}\right). \tag{IV.99}$$

We define

$$W_{\mathcal{B}}R_{ext} = \left(\begin{array}{cccc:cccc:c} 0 & 0 & 0 & 0 & -k_2 & 1 & 0 & 0 & 0 \\ 1 & k_2 & 0 & 0 & 0 & 0 & 0 & 0 & -l_1 \\ \hdashline 0 & 0 & 0 & 0 & 0 & 0 & 0 & 1 & 0 \\ 0 & 0 & 1 & 0 & 0 & 0 & 0 & 0 & l_1 \\ \hdashline 0 & 0 & 0 & -1 & 0 & 0 & 0 & 0 & 1+l_2 \end{array}\right), \tag{IV.100}$$

and

$$\begin{pmatrix} x(1) \\ x(0) \\ x_c \end{pmatrix} = \begin{pmatrix} \hat{q}(1) \\ \hat{p}(1) \\ \tilde{q}(1) \\ \tilde{p}(1) \\ \hat{q}(0) \\ \hat{p}(0) \\ \tilde{q}(0) \\ \tilde{p}(0) \\ x_c \end{pmatrix}, \quad \textit{and} \quad F_c = \begin{pmatrix} 0 \\ 0 \\ 0 \\ 0 \\ f_c \end{pmatrix}. \tag{IV.101}$$

Then, the set of equations (IV.99) *becomes*

$$W_{\mathcal{B}}R_{ext} \begin{pmatrix} x(1) \\ x(0) \\ x_c \end{pmatrix} = F_c. \tag{IV.102}$$

We obtain $x(1)$ *from the general solution* (IV.96) *evaluated at* $\zeta = 1$. *Then, the set of equation* (IV.102) *becomes*

$$\begin{aligned} W_{\mathcal{B}}R_{ext} \begin{pmatrix} e^{A_f}x(0) + \int_0^1 e^{(1-s)A_f}B_f x_f(s)ds \\ x(0) \\ x_c \end{pmatrix} &= F_c \\ W_{\mathcal{B}}R_{ext} \begin{pmatrix} e^{A_f}x(0) \\ x(0) \\ x_c \end{pmatrix} &= F_c - \begin{pmatrix} \int_0^1 e^{(1-s)A_f}B_f x_f(s)ds \\ 0 \\ 0 \end{pmatrix} \\ W_{\mathcal{B}}R_{ext} \begin{pmatrix} e^{A_f} & 0 \\ I & 0 \\ 0 & 1 \end{pmatrix} \begin{pmatrix} x(0) \\ x_c \end{pmatrix} &= F_c - \begin{pmatrix} \int_0^1 e^{(1-s)A_f}B_f x_f(s)ds \\ 0 \\ 0 \end{pmatrix} \\ \begin{pmatrix} x(0) \\ x_c \end{pmatrix} &= \Gamma^{-1} \left[F_c - \begin{pmatrix} \int_0^1 e^{(1-s)A_f}B_f x_f(s)ds \\ 0 \\ 0 \end{pmatrix} \right] \end{aligned} \tag{IV.103}$$

with

$$\Gamma = W_{\mathcal{B}}R_{ext} \begin{pmatrix} e^{A_f} & 0 \\ I & 0 \\ 0 & 1 \end{pmatrix} \tag{IV.104}$$

Now, $x(0)$ *and* x_c *are defined only in terms of* f *from* $(I - \mathcal{A})z = f$. *Replacing* $x(0)$ *in* (IV.96), *we can check that* $z = (x^T,\ x_c)^T \in D(\mathcal{A})$ *and is defined only in terms of* f. *So, the range of* $I - \mathcal{A}$ *is* Z, *which concludes that the operator* $\mathcal{A}$ (IV.87) *with domain* $D(\mathcal{A})$ (IV.88) *generates a contraction semigroup, or equivalently the closed-loop system* (IV.29), (IV.80), (IV.81) *is well-posed.*

We use LaSalle's invariance principle to show the second result of Proposition IV.4.1. Since the solutions of (IV.89) *are precompact and* $\dot{E} \leq 0$ (IV.91)*, the solutions converge asymptotically to the maximal invariant subset*

$$\mathcal{I} = \left\{ z \in Z \,\middle|\, \dot{E} = 0 \right\}. \tag{IV.105}$$

Hence, to show that the solutions of (IV.89) *converge asymptotically to zero, we have to show that the subset* $\mathcal{I}$ *in* (IV.105) *contains only the zero solution. To do so, we evaluate* $\dot{E} = 0$ *in* (IV.91)*, and we obtain* $\hat{p}_1 = \hat{q}_0 = x_c = 0$*. Since* $x_c = 0$ *implies* $\dot{x}_c = 0$*, from* (IV.83) *we can conclude* $\tilde{p}_1 = 0$*. Then, we can conclude that the only solution for* $\dot{\hat{x}} = P_1 \left(\begin{smallmatrix} 0 & 1 \\ 1 & 0 \end{smallmatrix}\right) \frac{\partial \hat{x}}{\partial \zeta}$*, with boundary conditions* $\hat{p}_0 = 0$*,* $\hat{q}_1 = 0$*,* $\hat{p}_1 = 0$*, and* $\hat{q}_0 = 0$*, is* $\hat{x} = 0$*. On the error side,* $x_c = 0$ *implies* $\tilde{q}_1 = 0$*. Then, the only solution for* $\dot{\tilde{x}} = P_1 \left(\begin{smallmatrix} 0 & 1 \\ 1 & 0 \end{smallmatrix}\right) \frac{\partial \tilde{x}}{\partial \zeta}$*, with boundary conditions* $\tilde{p}_0 = 0$*,* $\tilde{q}_1 = 0$*, and* $\tilde{p}_1 = 0$*, is* $\tilde{x} = 0$*. Since the only point contained in* $\mathcal{I}$ (IV.105) *is zero, then by using LaSalle's invariance principle, the state of the dynamic equation* (IV.89) *converges asymptotically to zero.*

■

Remark IV.4.3. *The result* (i) *from Proposition IV.4.1 is given for the particular example of the one-dimensional wave equation. However, it can be extended to the class of BC-PHSs if we assume that the matrix* Γ (IV.104) *is invertible.* ♣

Remark IV.4.4. *Using the LaSalle's invariance principle for the general case of BC-PHS is an open question.* ♣

Table IV.5 – Controller parameters

Parameter	Value
k_1	1
k_2	0.3

Table IV.6 – Observer parameters

Parameter	Value
l_1	1000
l_2	1000

Using the controller parameters of Table IV.5 and the observer parameters of Table IV.6, the conditions of Proposition IV.4.2 are satisfied since l_1, l_2, k_1, and k_2 are all positive scalars, and $0 < \frac{l_1}{4k_2 l_2} < 1$. Note that, we fix the damping coefficient smaller at the right side than at the left side to exemplify the case where the amount of damping at the right side is limited to not be the greatest damping ($k_2 = 1$), and at the left side we add the greatest damping for this example with $k_1 = 1$.

In Figure IV.30, we show the Hamiltonian of the string considering three different scenarios. With the blue line we show the ideal case when velocity and strain are measured at both sides of the spatial domain and *damping injection* is applied at both sides without observer, with the red line we show the worst case when damping is applied only at the measurable side using a velocity estimator at $\zeta = 1$, and with green line we show the new case when damping is applied at both side using the observed values. The corresponding control laws are respectively given by

$$u(t) = -\begin{pmatrix} -k_1 q(0,t) \\ k_2 p(1,t) \end{pmatrix}, \quad u(t) = -\begin{pmatrix} 0 \\ k_2 v_1(t) \end{pmatrix}, \quad u(t) = -\begin{pmatrix} -k_1 \hat{q}(0,t) \\ k_2 \hat{p}(1,t) \end{pmatrix}.$$

We can notice in Figure IV.30 that the *observer-based damping injection* approach improves the settling time with respect to the partial damping approach.

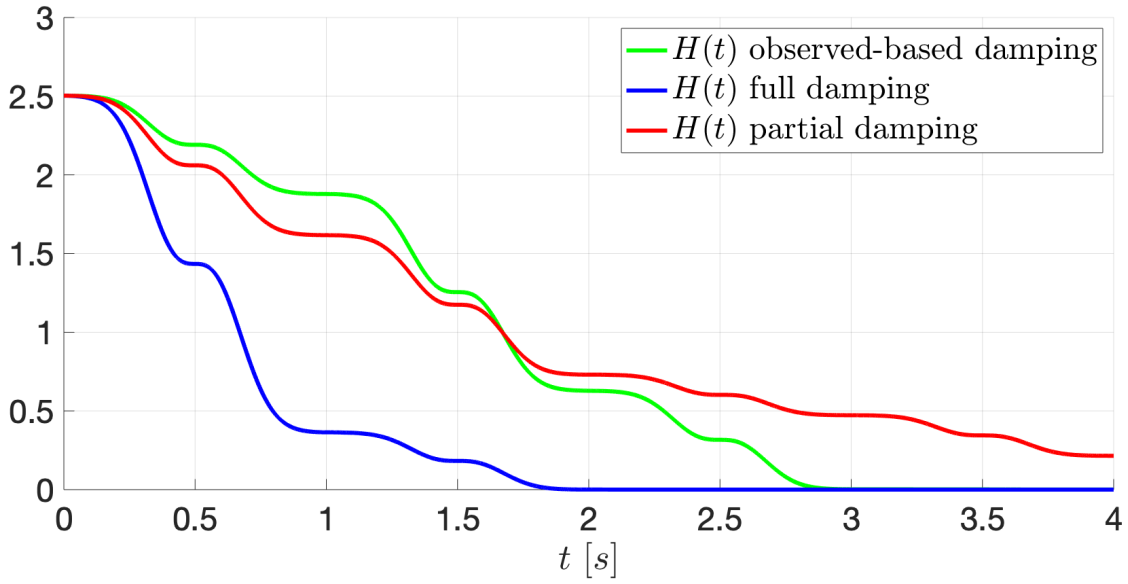

Figure IV.30 – Hamiltonian energy in the ideal case of full damping (blue), in a partial damping case due to the lake of sensors (red), and using the observer-based damping (green).

Figure IV.31 shows the string deformation, Figure IV.32 shows the estimated string deformation, and Figure IV.33 shows the deformation error between the BC-PHS and the observer. The three figures are shown along the time t and space ζ. In each figure, the two black lines show the initial and final values of $w(\zeta,t)$, $\hat{w}(\zeta,t)$, and $\tilde{w}(\zeta,t)$, and the orange line shows the end-tip deformations $w(1,t)$, $\hat{w}(1,t)$, and $\tilde{w}(1,t)$. Since we apply damping at both side of the string using the observed values, the string (Figure IV.31) converges to zero approximately in 3 seconds. The observer (Figure IV.32) starts from a zero initial condition and reaches the state of the BC-PHS approximately at $t = 2$ and as well as the string deformation, the estimated one converges to zero approximately at $t = 3$. The error (Figure IV.33), starts from a non zero initial condition and reaches the zero approximately at $t = 2$. Finally, Figure IV.35 shows the conjugated outputs and its estimations.

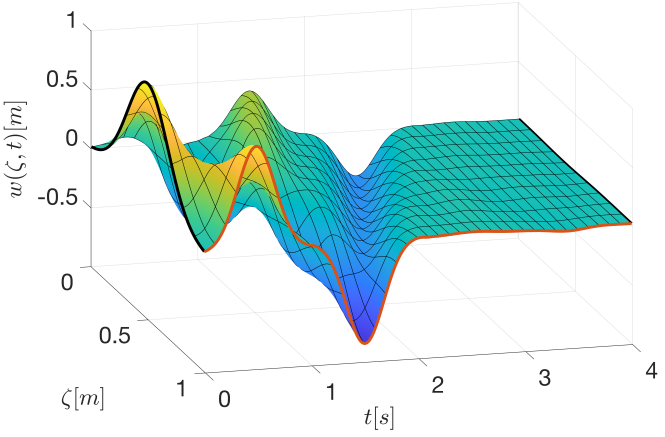

Figure IV.31 – String deformation

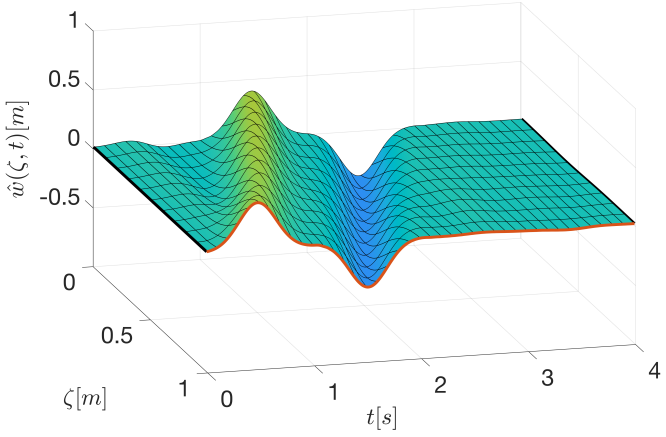

Figure IV.32 – Estimated deformation

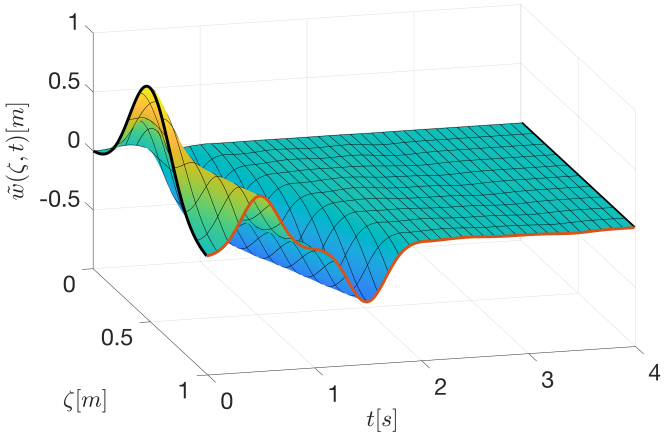

Figure IV.33 – Deformation error

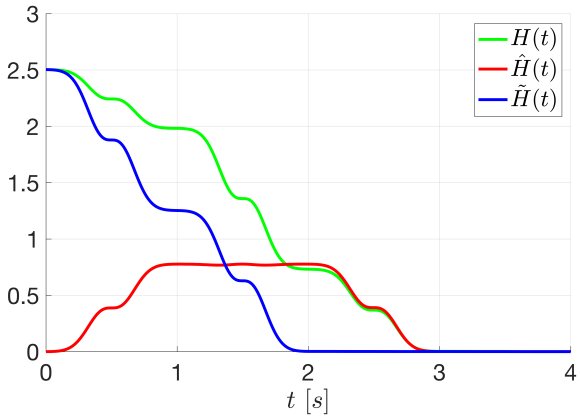

Figure IV.34 – Hamiltonian of the plant (green), observer (red) and error system (blue)

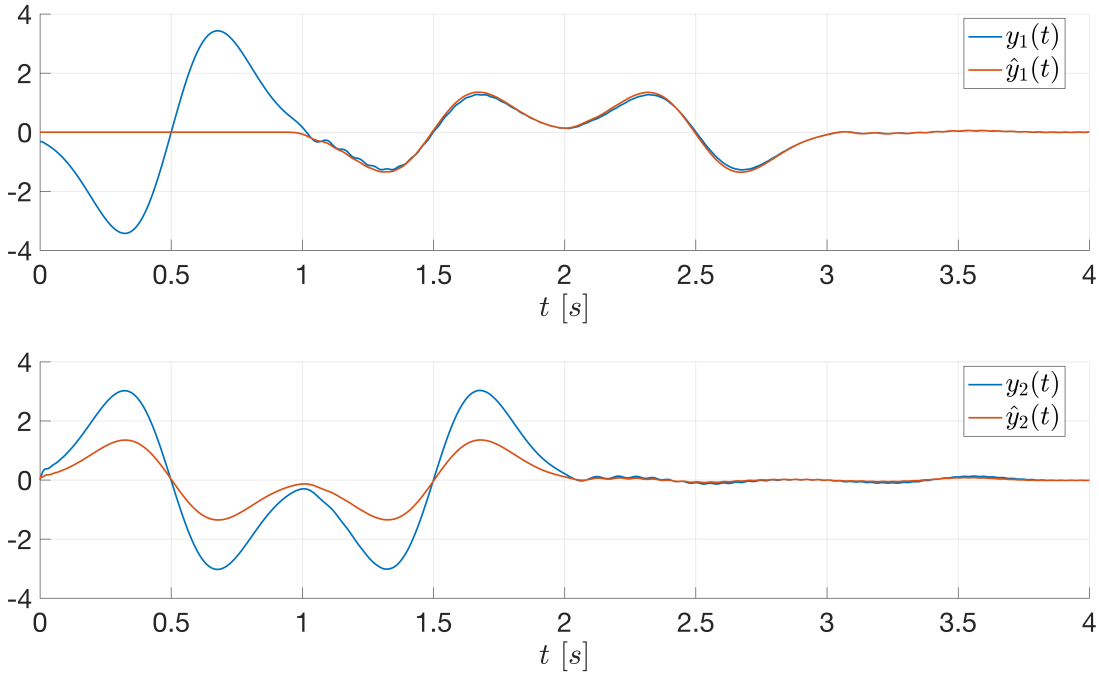

Figure IV.35 – Observer convergence of the conjugated output $\hat{y}(t)$ to $y(t)$.

IV.5 Observer-based damping injection and energy shaping: application to the vibrating string

In this section, we consider the vibrating string (Example II.3.2) attached at one side and with a force actuator and velocity sensor at the other side. The objective is to apply *energy shaping and damping injection*. Since the desired control law is a state feedback control law, we require the state variable knowledge to implement it. We use an infinite-dimensional observer to reconstruct the state of the system. Then, we implement the control law using the observed values from the infinite-dimensional observer.

The open loop BC-PHS is described by (See Example II.3.2)

$$\mathcal{P}\begin{cases}\dfrac{\partial}{\partial t}\begin{pmatrix}q(\zeta,t)\\p(\zeta,t)\end{pmatrix}=\begin{pmatrix}0&1\\1&0\end{pmatrix}\dfrac{\partial}{\partial\zeta}\begin{pmatrix}q(\zeta,t)\\p(\zeta,t)\end{pmatrix}, \quad \begin{pmatrix}q(\zeta,0)\\p(\zeta,0)\end{pmatrix}=\begin{pmatrix}q_0(\zeta)\\p_0(\zeta)\end{pmatrix},\\ p(0,t)=0,\\ q(1,t)=u(t),\\ y(t)=p(1,t),\end{cases} \tag{IV.106}$$

and the desired control law is given by

$$u(t)=-\int_0^1 q(\zeta,t)d\zeta-p(1,t). \tag{IV.107}$$

We have seen in the previous sections that the following infinite-dimensional observer

$$\hat{\mathcal{P}}\begin{cases}\dfrac{\partial}{\partial t}\begin{pmatrix}\hat{q}(\zeta,t)\\\hat{p}(\zeta,t)\end{pmatrix}=\begin{pmatrix}0&1\\1&0\end{pmatrix}\dfrac{\partial}{\partial\zeta}\begin{pmatrix}\hat{q}(\zeta,t)\\\hat{p}(\zeta,t)\end{pmatrix}, \quad \begin{pmatrix}\hat{q}(\zeta,0)\\\hat{p}(\zeta,0)\end{pmatrix}=\begin{pmatrix}\hat{q}_0(\zeta)\\\hat{p}_0(\zeta)\end{pmatrix},\\ \hat{p}(0,t)=0,\\ \hat{q}(1,t)=u(t)+y(t)-\hat{p}(1,t),\end{cases} \tag{IV.108}$$

estimates exponentially the state variables of (IV.106) for some $l_1>0$ (See Proposition IV.3.2). Then, we can apply the following control law

$$u(t)=-\int_0^1 \hat{q}(\zeta,t)d\zeta-\hat{p}(1,t) \tag{IV.109}$$

instead of the desired one (IV.107). As soon as the observer converge to the real state, the control law (IV.109) converges to the desired one (IV.107).

Remark IV.5.1. *Note that, the OBSF controller* (IV.108)-(IV.109) *is a particular case of a more general OBSF controller where* (IV.108) *is such that* $\hat{q}(1,t)=u(t)+l_1(y(t)-\hat{p}(1,t))$ *and* (IV.109) *is such that* $u(t)=-q_c\int_0^1\hat{q}(\zeta,t)d\zeta-d_c\hat{p}(1,t)$*, with* l_1*,* q_c *and* $d_c>0$ *some design parameters. For simplicity, we consider* $l_1=q_c=d_c=1$. ♣

We define the error states as $\tilde{q}(\zeta,t)=q(\zeta,t)-\hat{q}(\zeta,t)$ and $\tilde{p}(\zeta,t)=p(\zeta,t)-\hat{p}(\zeta,t)$, and we write the augmented closed-loop system composed by the observer and the error system

$$\begin{aligned}
\frac{\partial}{\partial t}\begin{pmatrix}\hat{q}(\zeta,t)\\ \hat{p}(\zeta,t)\\ \tilde{q}(\zeta,t)\\ \tilde{p}(\zeta,t)\end{pmatrix} &= \begin{pmatrix}0 & 1 & 0 & 0\\ 1 & 0 & 0 & 0\\ 0 & 0 & 0 & 1\\ 0 & 0 & 1 & 0\end{pmatrix}\frac{\partial}{\partial \zeta}\begin{pmatrix}\hat{q}(\zeta,t)\\ \hat{p}(\zeta,t)\\ \tilde{q}(\zeta,t)\\ \tilde{p}(\zeta,t)\end{pmatrix}, \quad \begin{pmatrix}\hat{q}(\zeta,0)\\ \hat{p}(\zeta,0)\\ \tilde{q}(\zeta,0)\\ \tilde{p}(\zeta,0)\end{pmatrix} = \begin{pmatrix}\hat{q}_0(\zeta)\\ \hat{p}_0(\zeta)\\ \tilde{q}_0(\zeta)\\ \tilde{p}_0(\zeta)\end{pmatrix},\\
\begin{pmatrix}\hat{p}(0,t)\\ \hat{q}(1,t)\\ \tilde{p}(0,t)\\ \tilde{q}(1,t)\end{pmatrix} &= \begin{pmatrix}0\\ -\int_0^1 \hat{q}(\zeta,t)d\zeta - \hat{p}(1,t) + \tilde{p}(1,t)\\ 0\\ -\tilde{p}(1,t)\end{pmatrix}.
\end{aligned} \tag{IV.110}$$

We use a Lyapunov function to show the asymptotic stability of (IV.110). To this end, we use LaSalle's invariance principle, assuming that the system (IV.110) is well-posed, the trajectories are precompact, and the system is *approximately observable* with respect to the outputs $\hat{p}(1,t)$ and $\tilde{p}(1,t)$. The Lyapunov function is the following:

$$V(t) = \frac{1}{2}\int_0^1 \left[\hat{q}(\zeta,t)^2 + \hat{p}(\zeta,t)^2 + \tilde{q}(\zeta,t)^2 + \tilde{p}(\zeta,t)^2\right]d\zeta + \frac{1}{2}\hat{w}(1,t)^2. \tag{IV.111}$$

For simplicity, we use the following notation

$$\hat{q}_1 = \hat{q}(1,t),\ \ \hat{q}_0 = \hat{q}(0,t),\ \ \tilde{q}_1 = \tilde{q}(1,t),\ \ \tilde{q}_1 = \tilde{q}(0,t),\ \ \hat{w}_1 = \hat{w}(1,t),$$

$$\hat{p}_1 = \hat{p}(1,t),\ \ \hat{p}_0 = \hat{p}(0,t),\ \ \tilde{p}_1 = \tilde{p}(1,t),\ \ \tilde{p}_1 = \tilde{p}(0,t),\ \ \hat{w}_0 = \hat{w}(0,t).$$

The derivative with respect to time of the Lyapunov function (IV.111) reads

$$\begin{aligned}
\dot{V}(t) &= \hat{q}_1\hat{p}_1 - \hat{q}_0\hat{p}_0 + \tilde{q}_1\tilde{p}_1 - \tilde{q}_0\tilde{p}_0 + \hat{w}_1\dot{\hat{w}}_1,\\
&= \left[-\hat{w}_1 - \hat{p}_1 + \tilde{p}_1\right]\hat{p}_1 - \tilde{p}_1^2 + \hat{w}_1\hat{p}_1,\\
&= -\tfrac{1}{2}\left(\hat{p}_1 - \tilde{p}_1\right)^2 - \tfrac{1}{2}\hat{p}_1^2 - \tfrac{1}{2}\tilde{p}_1^2.
\end{aligned} \tag{IV.112}$$

Since the system (IV.110) is well-posed, and the trajectories are precompact, we can use LaSalle's invariance principle extended to infinite-dimensional systems to show the closed-loop asymptotic stability (See [Luo 12, Theorem 3.64]). It follows then, that all solutions of the closed-loop system tend to the maximal invariant set of $\vartheta_c = \{\hat{q}(\zeta,t), \hat{p}(\zeta,t), \tilde{q}(\zeta,t), \tilde{p}(\zeta,t) \in L_2([a,b]),\ |\ \dot{V}(t) = 0\}$. We define the maximal invariant subset of ϑ_c as $\mathcal{I}$, and we show that $\mathcal{I}$ only contains the zero state, *i.e.* $\mathcal{I} = \{\hat{q}(\zeta,t) = \hat{p}(\zeta,t) = \tilde{q}(\zeta,t) = \tilde{p}(\zeta,t) = 0\}$. $\dot{V} = 0$ implies $\hat{p}_1 = 0$ and $\tilde{p}_1 = 0$. The system being *approximately observable* with respect to the outputs $\hat{p}_1$ and $\tilde{p}_1$ implies that $\hat{q}(\zeta,t) = \hat{p}(\zeta,t) = \tilde{q}(\zeta,t) = \tilde{p}(\zeta,t) = 0$ is the only point in $\mathcal{I}$ (See [Curtain 12, Corollary 4.1.14]). Thus, by LaSalle's invariance principle, the asymptotic stability of the closed-loop system is guaranteed.

We simulate the closed-loop system (IV.110) using the same spatial and time discretization method as in the previous sections. We note that for real implementations, the OBSF controller (IV.108)-(IV.109) has to be discretized using appropriate methods in such a way that it guarantees stability when applied to the infinite-dimensional system. For simplicity, in the following, we consider the same discretization size for the plant (IV.106) and the observer (IV.108). We show the string

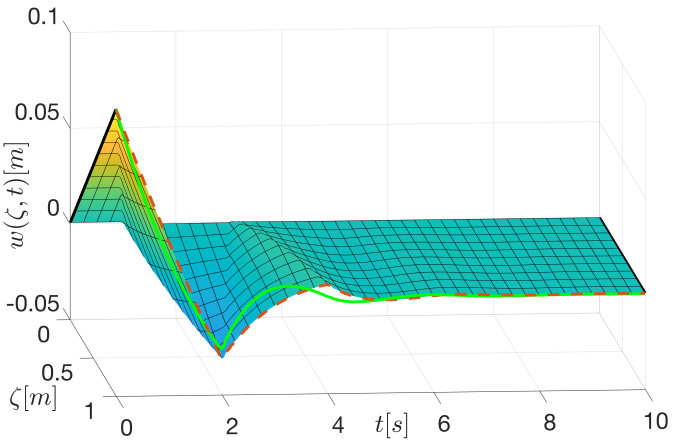

Figure IV.36 – String deformation

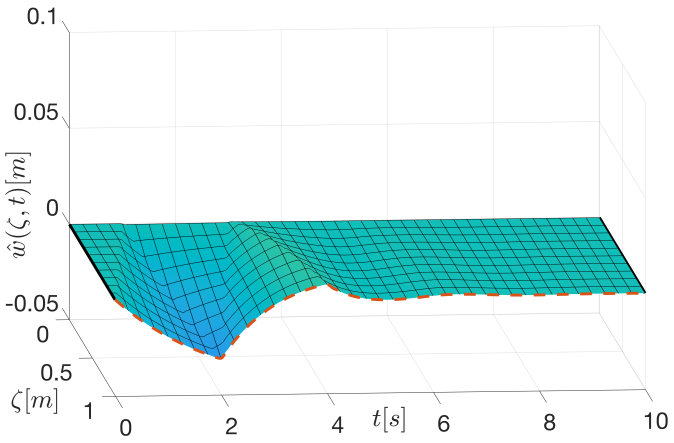

Figure IV.37 – Observed deformation

deformation along the time and the space in Figure IV.36. In Figure IV.37, we show the observed values. Both variables reach the zero equilibrium around $t = 6\,s$. In Figure IV.36, we show in a green line the desired end-tip behavior. This is, when (IV.107) is applied instead of (IV.109).

Finally, the control law (IV.109) is slightly modified in order to change the equilibrium point. Now, we consider the following control law

$$u(t) = 2w_1^* - \int_0^1 \hat{q}(\zeta,t)d\zeta - \hat{p}(1,t), \tag{IV.113}$$

where w_1^* represents the end-tip desired position. Now, we simulate the closed-loop system using the control law (IV.113) with zero initial condition for the system and nonzero initial condition for the observer. Note that, the initialization of the observer is chosen different to zero to show the influence of the observer dynamics on the spatial-temporal response. If the observer is initialized with the same initial condition than the one of the system, the temporal response is identical to the desired one. For the simulation we use $w_1^* = 0.1$. In Figure IV.38, we show the string deformation along the time and the space. The green line represents the desired end-tip deformation, when the control law uses the state of the system instead of the observed state. In Figure IV.39, we show the observed deformation along the time and the space. Similarly as in the previous simulation, both systems reach the equilibrium at $t = 6\,s$ approximately. The observed deformation converges to the real one at $t = 2\,s$ approximately. We can note that the reached equilibrium is independent of the initial condition of the observer.

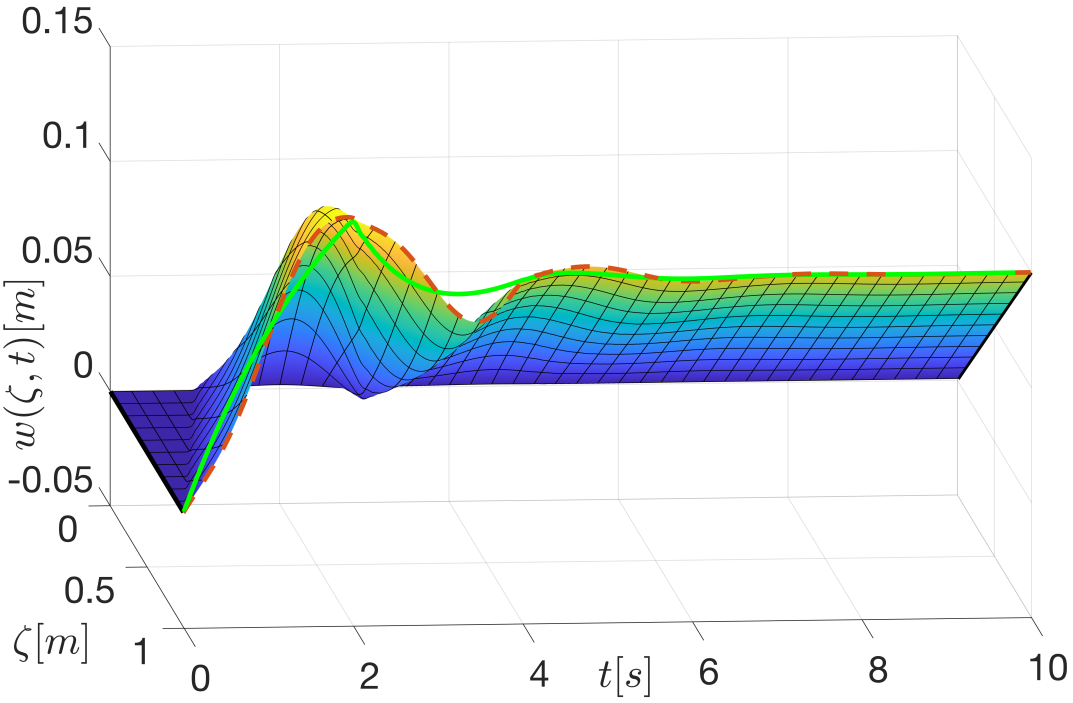

Figure IV.38 – String deformation

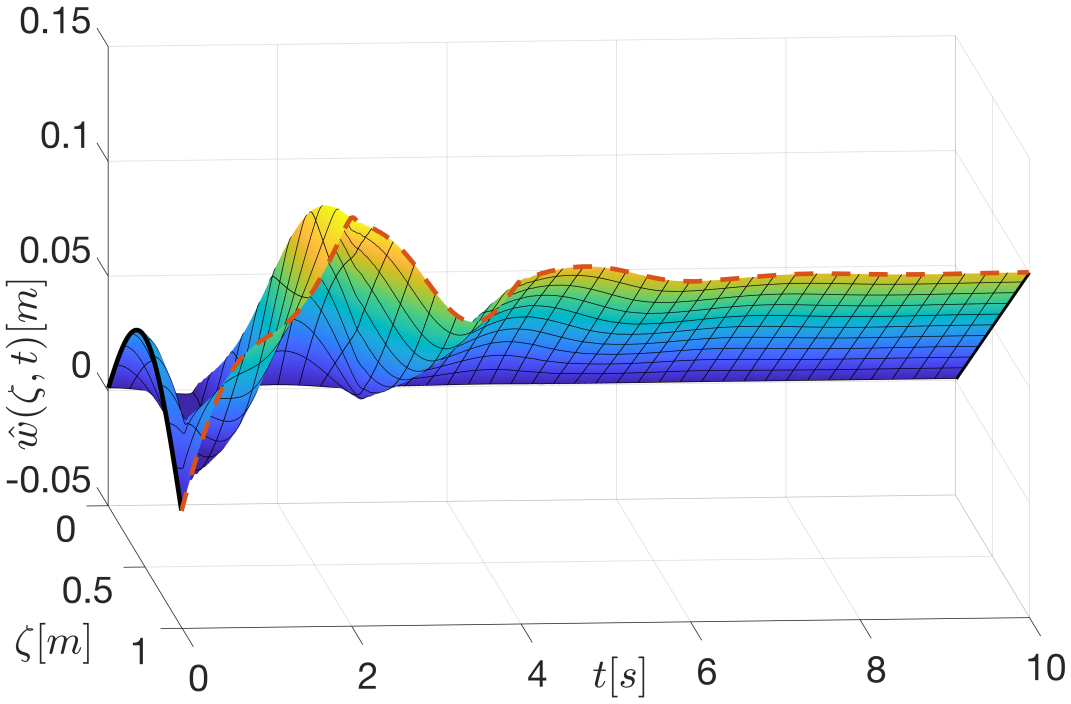

Figure IV.39 – Observed deformation

IV.6 Conclusion

We have presented a general setting for the design of infinite-dimensional observers for impedance energy preserving BC-PHSs. We have covered different scenarios depending on the available measurements. In the following, we enumerate the three cases covered in this chapter:

(i) The conjugated output is measured (fully or partially). We have shown that the state variable of the proposed infinite-dimensional observer converges exponentially to the system one.

(ii) The integral over time of the conjugated output is measured. We have shown that the state variable of the proposed infinite-dimensional observer converges asymptotically to the system one.

(iii) Scenarios (*i*) and (*ii*) together. We have shown that the state variable of the proposed infinite-dimensional observer converges exponentially to the system one.

We have used the infinite-dimensional observers proposed in this chapter to apply *energy shaping and damping injection* to the vibrating string example. The following cases have been covered in this chapter:

(i) We have considered that we measure the force at one side of the actuated string. We have proposed an infinite-dimensional observer to estimate the state variable of the system. Then, we have applied a *damping injection* strategy at both sides of the string using the observed values. We have shown the exponential stability of the closed-loop system.

(ii) We have considered that we measure the end-tip deformation of the string. We have proposed an infinite-dimensional observer to estimate the state variables of the system. Then, we have applied a *damping injection* strategy at both sides of the string using the observed values. We have shown the asymptotic stability of the closed-loop system.

(iii) Finally, we have considered the string attached at one side and with a force actuator and velocity sensor at the other side. We have proposed an infinite-dimensional observer to estimate the state variables of the system. Then, we have applied an *energy shaping and damping injection* strategy using the observed values. We have shown the asymptotic stability of the closed-loop system.

The results presented in this chapter are some first steps towards *observer-based energy shaping and damping injection* for impedance energy preserving BC-PHSs. The generalization to a larger class of BC-PHSs, including non impedance energy preserving systems and systems in 2D or 3D, can be investigated in the future. A model reduction of the OBSF controller is also proposed as future work. This is necessary for the real implementation, and the reduced OBSF controller has to guarantee the closed-loop stability when it is applied to the BC-PHS.

Chapter V
Conclusions and future works

V.1 Conclusions

In this thesis, we have considered the synthesis of *observer-based state feedback* (OBSF) control laws for linear impedance energy preserving *boundary controlled port-Hamiltonian systems* (BC-PHSs). To this end, we have used two different approaches, namely the *early-lumping* approach and the *late-lumping* approach.

Using an *early-lumping* approach, the synthesis of the OBSF controller follows the following steps:

1. The BC-PHS is discretized into a finite-dimensional model (discretized model).
2. The controller and observer gains are designed on the discretized model.
3. The OBSF controller is applied to the BC-PHS.

Using an illustrative example, we have shown that if we design the controller and observer gains independently of each other using classic control tools, the closed-loop stability is not always guaranteed when applying the OBSF controller to the BC-PHS. To handle this stability problem, we have imposed a passive structure on the OBSF controller. We have shown that if we use this structure, the OBSF controller stabilizes the BC-PHS. To achieve this structure, we have proposed two methodologies for the synthesis of the OBSF gains. These methodologies are summarized as follows:

1. The state feedback gain is designed independently using classic control tools like the *linear quadratic regulator* or the *pole placement*. Then, by solving an algebraic Riccati equation, the observer gain is designed such that the OBSF controller is passive.
2. The observer gain is designed independently using classic control tools like the *linear quadratic regulator* or the *pole placement*. Then, by solving a set of linear matrix inequalities, the state feedback gain is designed such that the OBSF is passive.

Using these approaches, one of the two gains of the OBSF controller is restricted to satisfy the passive structure. This design limitation allows to guarantee the closed-loop stability between the BC-PHS and the OBSF controller. We have proposed a design procedure for both methodologies, and they have been exemplified using the vibrating string and the Timoshenko beam models.

We have shown that the same procedures can be used to stabilize a class of *nonlinear time-invariant* (NTI) systems. Since the proposed OBSF controller is *output strictly passive* (OSP) and *zero state detectable* (ZSD), it stabilizes nonlinear systems that are OSP and ZSD too. In this case, the synthesis is based on a linearized model of the NTI system. We have shown that when applying the OBSF controller to the NTI system, closed-loop stability is guaranteed. We have used a microelectromechanical system to exemplify the synthesis method.

Using a *late-lumping* approach, the synthesis of the OBSF controller follows the following steps:

1. An infinite-dimensional observer is designed based on the infinite-dimensional BC-PHS.
2. The desired control law is applied using the state variable of the infinite-dimensional observer.
3. The OBSF controller has to be discretized for real implementation.

We have proposed a general setting for the synthesis of infinite-dimensional observers for impedance energy preserving BC-PHSs. We have studied the following cases:

1. The conjugated output is fully or partially measured. This is the case when forces and/or velocities in mechanical systems are measured.
2. The integral over time of the conjugated output is measured. This is the case when deformations or displacements in mechanical systems are measured.
3. Scenarios 1 and 2 together. This is the case when both velocities and displacements in mechanical systems are measured, for instance.

In the first case, we have shown that the error between the state of the BC-PHS and the state of the infinite-dimensional system converges to zero exponentially. In the second case, we have shown that the error converges asymptotically to zero and in the third one, we have shown that the error converges exponentially to zero. We have used the vibrating string and the Timoshenko beam with different types of measurements to exemplify the different scenarios.

Finally, we have used infinite-dimensional observers to apply *energy shaping and damping injection* to the vibrating string using the observed values. We have considered the following closed-loop scenarios

1. The force at one side of the vibrating string is measured. We have applied a *damping injection* strategy at both sides of the vibrating string using the observed state from an exponentially convergent observer. We have shown the exponential stability of the closed-loop system.
2. The end-tip deformation at one side of the vibrating string is measured. We have applied a *damping injection* strategy at both sides of the string using the observed state from an asymptotically convergent observer. We have shown the asymptotic stability of the closed-loop system.
3. The string attached at one side and with a force actuator and velocity sensor at the other side. We have applied an *energy shaping and damping injection* strategy using the observed values from an infinite-dimensional observer. We have shown the asymptotic stability of the closed-loop system.

V.2 Future works

Concerning the *early-lumping approach* presented in Chapter III, we propose the following future works

(i) The design methodologies for the OBSF gains proposed in Chapter III can be extended to 2D and 3D systems as soon as structure-preserving discretization methods are used [Brugnoli 19a, Brugnoli 19b, Serhani 19].

(ii) The closed-loop performances depend on the accuracy of the discretized model used for the design. The accuracy of the discretized model depends on the number of state variables of it. An optimal amount of elements could be proposed in such a way that the discretized model is small enough to avoid a huge amount of states in the controller and big enough to achieve the desired performances. This optimality could be characterized by defining some appropriate criteria.

(iii) The degrees of freedom concerning the synthesis of the OBSF gains could be reduced to optimize a cost function.

(iv) To reach some desired output, we can add an integrator to the error between the output and the desired one. Then, the OBSF design can be modified to obtain the integrator gains as well.

(v) The same methodologies for the synthesis of the OBSF controller could be formulated for the *in-domain* control problem.

(vi) A general setting of BC-PHSs with dissipation could be studied. In this case, the *strictly positive real* condition imposed on the OBSF controller could be relaxed for achieving the asymptotic or exponential stability in the closed-loop.

(vii) The OBSF formulation can be extended to the case when the plant is a couple of *partial differential equations* (PDEs) and *ordinary differential equations* (ODEs). This is the case, for instance, when the string is attached to a mass or a spring. The controller and observer gain could be designed similarly as in Chapter III including some extra conditions depending on the nature of the ODEs and the nature of the control inputs that can be in the PDEs or the ODEs.

(viii) Since the same methodologies can stabilize a class of nonlinear finite-dimensional system, it seems that the same methodologies could stabilize a class of nonlinear infinite-dimensional systems.

Concerning the *late-lumping approach* presented in Chapter IV, we propose the following future works

(i) The general setting of infinite-dimensional observers for BC-PHSs could be extended to the dissipative case and to a more general class of BC-PHSs where the Euler-Bernoulli beam is also included.

(ii) The general setting of *observer-based damping injection and energy shaping* could be studied for BC-PHSs.

(iii) The discretization of the controller using *observer-based damping injection and energy shaping* could be addressed in order to preserve the closed-loop stability.

(iv) Infinite-dimensional observers could be proposed for two-dimensional and three-dimensional BC-PHSs.

Appendix A
Appendix

A.1 Finite-differences spatial discretization

The reader is refereed to [Trenchant 18] for further details on this discretization method. The benefits of using this discretization method are the following

— The discretized model preserves the port-Hamiltonian structure.

— The boundary conditions can be modified easily.

— The code for simulation is easy to implement.

A.1.1 Vibrating string

We consider the vibrating string with spatial variable $\zeta \in [a, b]$, time variable $t \geq 0$ and with dynamical boundary conditions given by the velocity at $\zeta = a$ and the force $\zeta = b$. The system is written as follows

$$\mathcal{P}\begin{cases} \dfrac{\partial x}{\partial t}(\zeta,t) = P_1 \dfrac{\partial}{\partial \zeta}\left(\mathcal{H}(\zeta)x(\zeta,t)\right), \quad x(\zeta,0) = x_0(\zeta), \\ V_{\mathcal{B}}\begin{pmatrix}\mathcal{H}(b)x(b,t)\\ \mathcal{H}(a)x(a,t)\end{pmatrix} = u(t), \\ y(t) = V_{\mathcal{C}}\begin{pmatrix}\mathcal{H}(b)x(b,t)\\ \mathcal{H}(a)x(a,t)\end{pmatrix}, \end{cases} \tag{A.1}$$

with

$$x(\zeta,t) = \begin{pmatrix} q(\zeta,t)\\ p(\zeta,t)\end{pmatrix}, \quad x_0(\zeta) = \begin{pmatrix} q_0(\zeta)\\ p_0(\zeta)\end{pmatrix}, \quad P_1 = \begin{pmatrix} 0 & 1\\ 1 & 0\end{pmatrix}, \quad \mathcal{H} = \begin{pmatrix} T(\zeta) & 0\\ 0 & \frac{1}{\rho(\zeta)}\end{pmatrix},$$

$$V_{\mathcal{B}} = \begin{pmatrix} 0 & 0 & 0 & 1\\ 1 & 0 & 0 & 0\end{pmatrix}, \quad V_{\mathcal{C}} = \begin{pmatrix} 0 & 0 & -1 & 0\\ 0 & 1 & 0 & 0\end{pmatrix},$$

where $q(\zeta,t) := \frac{\partial w}{\partial \zeta}(\zeta,t)$ is the strain, $p(\zeta,t) := \rho(\zeta)\frac{\partial w}{\partial t}(\zeta,t)$ is the momentum, $w(\zeta,t)$ is the string deformation, $T(\zeta)$ is the Young's modulus, $\rho(\zeta)$ is the mass density of the string, and $x_0(\zeta)$ is the initial condition. $u(t)$ and $y(t)$ are the input and output, respectively.

The boundary conditions $V_{\mathcal{B}}\left(\begin{smallmatrix}\mathcal{H}(b)x(b,t)\\ \mathcal{H}(a)x(a,t)\end{smallmatrix}\right)$ define the staggered grid as we show in Figure A.1, where ζ_i^q is the spatial location for the strain variable and ζ_i^p for the momentum one with $i = \{1,2,3,4\}$. In this example, we take 4 states for describing the strain $q(\zeta,t)$ and 4 states for describing momentum $p(\zeta,t)$. Then, we define 4 finite-dimensional variables for each one as follows

$$\begin{aligned} q_1(t) &\approx q(\zeta_1^q,t), & p_1(t) &\approx p(\zeta_1^p,t),\\ q_2(t) &\approx q(\zeta_2^q,t), & p_2(t) &\approx p(\zeta_2^p,t),\\ q_3(t) &\approx q(\zeta_3^q,t), & p_3(t) &\approx p(\zeta_3^p,t),\\ q_4(t) &\approx q(\zeta_4^q,t), & p_4(t) &\approx p(\zeta_4^p,t), \end{aligned}$$

In this case, the length of the grid is given by $h = \frac{b-a}{n_d+1}$, with $n_d = 8$. We define $\rho_i = \rho(\zeta_i^p)$

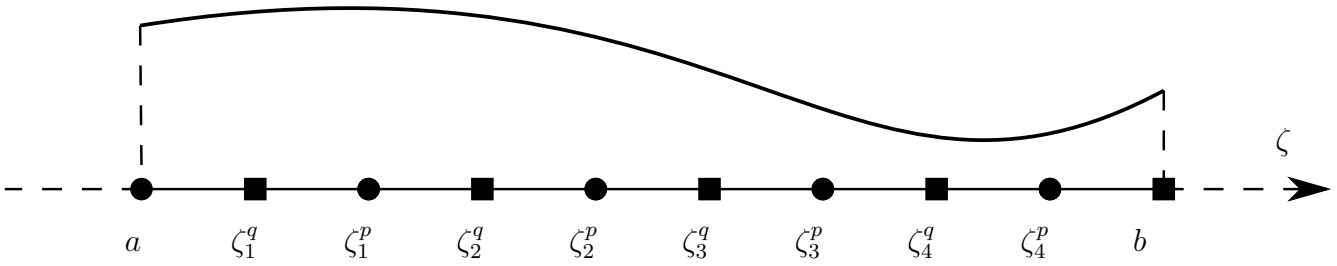

Figure A.1 – Discretization grid for the vibrating string.

and $T_i = T(\zeta_i^q)$ for $i = \{1, 2, 3, 4\}$. Then, using the finite-differences, the following discretization is obtained

$$\begin{aligned}
\dot{q}_1(t) &= \frac{1}{h}\left(\frac{1}{\rho_1}p_1(t) - v_a(t)\right), & \dot{p}_1(t) &= \frac{1}{h}\left(T_2 q_2(t) - T_1 q_1(t)\right), \\
\dot{q}_2(t) &= \frac{1}{h}\left(\frac{1}{\rho_2}p_2(t) - \frac{1}{\rho_1}p_1(t)\right), & \dot{p}_2(t) &= \frac{1}{h}\left(T_3 q_3(t) - T_2 q_2(t)\right), \\
\dot{q}_3(t) &= \frac{1}{h}\left(\frac{1}{\rho_3}p_3(t) - \frac{1}{\rho_2}p_2(t)\right), & \dot{p}_3(t) &= \frac{1}{h}\left(T_4 q_4(t) - T_3 q_3(t)\right), \\
\dot{q}_4(t) &= \frac{1}{h}\left(\frac{1}{\rho_4}p_4(t) - \frac{1}{\rho_3}p_3(t)\right), & \dot{p}_4(t) &= \frac{1}{h}\left(F_b(t) - T_4 q_4(t)\right),
\end{aligned}$$

where $v_a(t)$ is the velocity at $\zeta = a$ and $F_b(t)$ is the force $\zeta = b$. Then, we can write the equations in a matrix form

$$\frac{d}{dt}\begin{bmatrix} q_1 \\ q_2 \\ q_3 \\ q_4 \\ \hdashline p_1 \\ p_2 \\ p_3 \\ p_4 \end{bmatrix} = \frac{1}{h^2}\left[\begin{array}{cccc:cccc} 0 & 0 & 0 & 0 & 1 & 0 & 0 & 0 \\ 0 & 0 & 0 & 0 & -1 & 1 & 0 & 0 \\ 0 & 0 & 0 & 0 & 0 & -1 & 1 & 0 \\ 0 & 0 & 0 & 0 & 0 & 0 & -1 & 1 \\ \hdashline -1 & 1 & 0 & 0 & 0 & 0 & 0 & 0 \\ 0 & -1 & 1 & 0 & 0 & 0 & 0 & 0 \\ 0 & 0 & -1 & 1 & 0 & 0 & 0 & 0 \\ 0 & 0 & 0 & -1 & 0 & 0 & 0 & 0 \end{array}\right]\begin{bmatrix} hT_1 q_1 \\ hT_2 q_2 \\ hT_3 q_3 \\ hT_4 q_4 \\ \hdashline \frac{h}{\rho_1}p_1 \\ \frac{h}{\rho_2}p_2 \\ \frac{h}{\rho_3}p_3 \\ \frac{h}{\rho_4}p_4 \end{bmatrix} + \frac{1}{h}\left[\begin{array}{c:c} -1 & 0 \\ 0 & 0 \\ 0 & 0 \\ 0 & 0 \\ \hdashline 0 & 0 \\ 0 & 0 \\ 0 & 0 \\ 0 & 1 \end{array}\right]\begin{bmatrix} v_a \\ F_b \end{bmatrix}$$

where for simplicity, we have omitted the time dependency. We define the discretized strain as $q_d(t)$ and the discretized momentum as $p_d(t)$ as follows

$$q_d(t) = \begin{bmatrix} q_1(t) \\ \vdots \\ q_4(t) \end{bmatrix}, \qquad p_d(t) = \begin{bmatrix} p_1(t) \\ \vdots \\ p_4(t) \end{bmatrix}.$$

Then, we obtain the following finite-dimensional model

$$\frac{d}{dt}\left[\begin{array}{c} q_d(t) \\ \hdashline p_d(t) \end{array}\right] = \left[\begin{array}{c:c} 0 & D \\ \hdashline -D^T & 0 \end{array}\right]\left[\begin{array}{c} Q_T q_d \\ \hdashline Q_\rho p_d \end{array}\right] + \left[\begin{array}{c:c} b_a & 0 \\ \hdashline 0 & b_b \end{array}\right]\begin{bmatrix} v_a \\ F_b \end{bmatrix}$$

with

$$D = \frac{1}{h^2}\begin{bmatrix} 1 & 0 & 0 & 0 \\ -1 & 1 & 0 & 0 \\ 0 & -1 & 1 & 0 \\ 0 & 0 & -1 & 1 \end{bmatrix}, \quad b_a = \frac{1}{h}\begin{bmatrix} -1 \\ 0 \\ 0 \\ 0 \end{bmatrix}, \quad b_b = \frac{1}{h}\begin{bmatrix} 0 \\ 0 \\ 0 \\ 1 \end{bmatrix}$$

$$Q_T = h\begin{bmatrix} T_1 & 0 & 0 & 0 \\ 0 & T_2 & 0 & 0 \\ 0 & 0 & T_3 & 0 \\ 0 & 0 & 0 & T_4 \end{bmatrix}, \qquad Q_\rho = h\begin{bmatrix} \frac{1}{\rho_1} & 0 & 0 & 0 \\ 0 & \frac{1}{\rho_2} & 0 & 0 \\ 0 & 0 & \frac{1}{\rho_3} & 0 \\ 0 & 0 & 0 & \frac{1}{\rho_4} \end{bmatrix},$$

Finally, we can write the discretized model as a finite-dimensional port-Hamiltonian system

$$P\begin{cases} \dot{x}_d(t) &= (J-R)Qx_d(t) + Bu(t) \\ y(t) &= B^T Q x_d(t) \end{cases} \tag{A.2}$$

where

$$J = \begin{bmatrix} 0 & D \\ -D^T & 0 \end{bmatrix}, \quad R = \begin{bmatrix} 0 & 0 \\ 0 & 0 \end{bmatrix}, \quad Q = \begin{bmatrix} Q_T & 0 \\ 0 & Q_\rho \end{bmatrix}, \quad B = \begin{bmatrix} b_a & 0 \\ 0 & b_b \end{bmatrix}$$

$$x_d(t) = \begin{bmatrix} q_d(t) \\ p_d(t) \end{bmatrix}, \quad u(t) = \begin{bmatrix} v_a(t) \\ F_b(t) \end{bmatrix}, \quad y(t) = \begin{bmatrix} -T_1 q_1(t) \\ \frac{1}{\rho_4} p_4(t) \end{bmatrix}.$$

Note that, the discretized model A.2 has the same structure when n_d increase.

A.1.2 Timoshenko beam

In this section, we discretize the Timoshenko beam with dynamical boundary conditions given by the transversal velocity at the left side $v_a(t)$, the angular velocity at the left side $w_a(t)$, the force at the right side $F_b(t)$ and the torque at the right side $\Gamma_b(t)$. We use finite differences in staggered grids as in [Trenchant 18]. The model is given by

$$\mathcal{P}\begin{cases} \dfrac{\partial x}{\partial t}(\zeta,t) = P_1 \dfrac{\partial}{\partial \zeta}\left(\mathcal{H}(\zeta)x(\zeta,t)\right) + P_0\left(\mathcal{H}(\zeta)x(\zeta,t)\right), \quad x(\zeta,0) = x_0(\zeta), \\ V_{\mathcal{B}}\begin{pmatrix} \mathcal{H}(b)x(b,t) \\ \mathcal{H}(a)x(a,t) \end{pmatrix} = u(t), \\ y(t) = V_{\mathcal{C}}\begin{pmatrix} \mathcal{H}(b)x(b,t) \\ \mathcal{H}(a)x(a,t) \end{pmatrix}, \end{cases} \tag{A.3}$$

with

$$x(\zeta,t) = \begin{pmatrix} x_1(\zeta,t) \\ x_2(\zeta,t) \\ x_3(\zeta,t) \\ x_4(\zeta,t) \end{pmatrix}, \quad x_0(\zeta) = \begin{pmatrix} x_{10}(\zeta) \\ x_{20}(\zeta) \\ x_{30}(\zeta) \\ x_{40}(\zeta) \end{pmatrix},$$

$$P_1 = \begin{pmatrix} 0 & 1 & 0 & 0 \\ 1 & 0 & 0 & 0 \\ 0 & 0 & 0 & 1 \\ 0 & 0 & 1 & 0 \end{pmatrix}, \quad P_0 = \begin{pmatrix} 0 & 0 & 0 & -1 \\ 0 & 0 & 0 & 0 \\ 0 & 0 & 0 & 0 \\ 1 & 0 & 0 & 0 \end{pmatrix}, \quad \mathcal{H} = \begin{pmatrix} K(\zeta) & 0 & 0 & 0 \\ 0 & \frac{1}{\rho(\zeta)} & 0 & 0 \\ 0 & 0 & EI(\zeta) & 0 \\ 0 & 0 & 0 & \frac{1}{I_\rho(\zeta)} \end{pmatrix},$$

$$V_{\mathcal{B}} = \begin{pmatrix} 0 & 0 & 0 & 0 & 0 & 1 & 0 & 0 \\ 0 & 0 & 0 & 0 & 0 & 0 & 0 & 1 \\ 1 & 0 & 0 & 0 & 0 & 0 & 0 & 0 \\ 0 & 0 & 1 & 0 & 0 & 0 & 0 & 0 \end{pmatrix}, \quad V_{\mathcal{C}} = \begin{pmatrix} 0 & 0 & 0 & 0 & -1 & 0 & 0 & 0 \\ 0 & 0 & 0 & 0 & 0 & 0 & -1 & 0 \\ 0 & 1 & 0 & 0 & 0 & 0 & 0 & 0 \\ 0 & 0 & 0 & 1 & 0 & 0 & 0 & 0 \end{pmatrix},$$

where $x_1(\zeta,t) := \frac{\partial w}{\partial \zeta}(\zeta,t) - \phi(\zeta,t)$ is the shear displacement, $x_2(\zeta,t) := \rho(\zeta)\frac{\partial w}{\partial t}(\zeta,t)$ is the momentum, $x_3(\zeta,t) := \frac{\partial \phi}{\partial \zeta}(\zeta,t)$ is the angular displacement, $x_4(\zeta,t) := I_\rho(\zeta)\frac{\partial \phi}{\partial t}(\zeta,t)$ is the angular momentum, $w(\zeta,t)$ is the transverse displacement of the beam, and $\phi(\zeta,t)$ is the rotation angle of a filament of the beam. $K(\zeta)$, $\rho(\zeta)$, $EI(\zeta)$ and $I_\rho(\zeta)$ are respectively the shear modulus, the mass density, the Young's modulus of elasticity multiplied by the moment of inertia of a cross section and the rotary moment of inertia of a cross section.

The boundary conditions $V_{\mathcal{B}} \begin{pmatrix} \mathcal{H}(b)x(b,t) \\ \mathcal{H}(a)x(a,t) \end{pmatrix}$ define the staggered grid as we show in Figure A.2, where ζ_1^i is the spatial location for $x_1(\zeta,t)$ and $x_3(\zeta,t)$, and ζ_2^i is the spatial for $x_2(\zeta,t)$ and $x_4(\zeta,t)$ with $i = \{1,\ldots,m\}$, where m is the amount of finite-dimensional variables per infinite-dimensional variable. Then, the total state variables of the finite-dimensional system is $n_d = 4m$. We define the finite-dimensional variables as follows

$$\begin{array}{cccc} x_1^1(t) \approx x_1(\zeta_1^1,t), & x_2^1(t) \approx x_2(\zeta_2^1,t), & x_3^1(t) \approx x_3(\zeta_1^1,t), & x_4^1(t) \approx x_4(\zeta_2^1,t), \\ \vdots & \vdots & \vdots & \vdots \\ x_1^m(t) \approx x_1(\zeta_1^m,t), & x_2^m(t) \approx x_2(\zeta_2^m,t), & x_3^m(t) \approx x_3(\zeta_1^m,t), & x_4^m(t) \approx x_4(\zeta_2^m,t). \end{array}$$

The length of the grid is given by $h = \frac{b-a}{2m+1}$. We define $K_i = K(\zeta_1^i)$, $\rho_i = \rho(\zeta_2^i)$, $EI_i = EI(\zeta_1^i)$ and

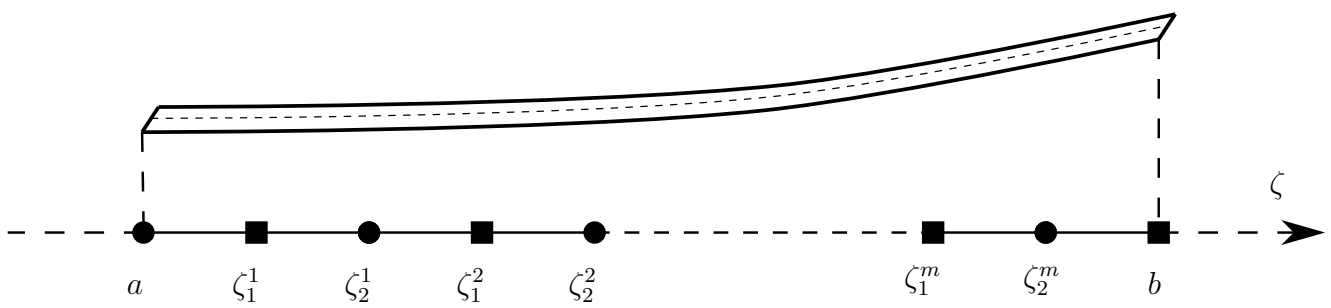

Figure A.2 – Discretization grid for the vibrating string.

$I_{\rho i} = I_\rho(\zeta_2^i)$ for $i = \{1, 2, \cdots, m\}$. Then, using the finite-differences, the following discretization is obtained

$$
\begin{aligned}
\dot{x}_1^1 &= \tfrac{1}{h}\left(\tfrac{1}{\rho_1}x_2^1 - v_a\right) - \tfrac{1}{2}\left(w_a + \tfrac{1}{I_{\rho 1}}x_4^1\right),\\
\dot{x}_1^2 &= \tfrac{1}{h}\left(\tfrac{1}{\rho_2}x_2^2 - \tfrac{1}{\rho_1}x_2^1\right) - \tfrac{1}{2}\left(\tfrac{1}{I_{\rho 1}}x_4^1 + \tfrac{1}{I_{\rho 2}}x_4^2\right),\\
&\vdots\\
\dot{x}_1^m &= \tfrac{1}{h}\left(\tfrac{1}{\rho_m}x_2^m - \tfrac{1}{\rho_{m-1}}x_2^{m-1}\right) - \tfrac{1}{2}\left(\tfrac{1}{I_{\rho(m-1)}}x_4^{m-1} + \tfrac{1}{I_{\rho m}}x_4^m\right),\\
\dot{x}_2^1 &= \tfrac{1}{h}\left(K_2x_1^2 - K_1x_1^1\right),\\
\dot{x}_2^2 &= \tfrac{1}{h}\left(K_3x_1^3 - K_2x_1^2\right),\\
&\vdots\\
\dot{x}_2^m &= \tfrac{1}{h}\left(F_b - K_mx_1^m\right),\\
\dot{x}_3^1 &= \tfrac{1}{h}\left(\tfrac{1}{I_{\rho 1}}x_4^1 - w_a\right)\\
\dot{x}_3^2 &= \tfrac{1}{h}\left(\tfrac{1}{I_{\rho 2}}x_4^2 - \tfrac{1}{I_{\rho 1}}x_4^1\right),\\
&\vdots\\
\dot{x}_3^m &= \tfrac{1}{h}\left(\tfrac{1}{I_{\rho m}}x_4^m - \tfrac{1}{I_{\rho(m-1)}}x_4^{m-1}\right),\\
\dot{x}_4^1 &= \tfrac{1}{h}\left(EI_2x_3^2 - EI_1x_3^1\right) + \tfrac{1}{2}\left(K_1x_1^1 + K_2x_1^2\right),\\
\dot{x}_4^2 &= \tfrac{1}{h}\left(EI_3x_3^3 - EI_2x_3^2\right) + \tfrac{1}{2}\left(K_2x_1^2 + K_3x_1^3\right),\\
&\vdots\\
\dot{x}_4^m &= \tfrac{1}{h}\left(\Gamma_b - EI_mx_3^m\right) + \tfrac{1}{2}\left(K_mx_1^m + F_b\right).
\end{aligned}
$$

We define the finite-dimensional variables related to the infinite-dimensional variables $x_1(\zeta,t)$, $x_2(\zeta,t)$, $x_3(\zeta,t)$, and $x_4(\zeta,t)$ respectively as

$$
x_1^d(t) = \begin{bmatrix} x_1^1(t) \\ \vdots \\ x_1^m(t) \end{bmatrix}, \quad x_2^d(t) = \begin{bmatrix} x_2^1(t) \\ \vdots \\ x_2^m(t) \end{bmatrix}, \quad x_3^d(t) = \begin{bmatrix} x_3^1(t) \\ \vdots \\ x_3^m(t) \end{bmatrix}, \quad x_4^d(t) = \begin{bmatrix} x_4^1(t) \\ \vdots \\ x_4^m(t) \end{bmatrix}.
$$

Then, we obtain the following matrix representation model

$$
\frac{d}{dt}\begin{bmatrix} x_1^d(t) \\ x_2^d(t) \\ x_3^d(t) \\ x_4^d(t) \end{bmatrix} = \begin{bmatrix} 0 & D & 0 & -F \\ -D^T & 0 & 0 & 0 \\ 0 & 0 & 0 & D \\ F^T & 0 & -D^T & 0 \end{bmatrix}\begin{bmatrix} Q_1x_1^d(t) \\ Q_2x_2^d(t) \\ Q_3x_3^d(t) \\ Q_4x_4^d(t) \end{bmatrix} + \begin{bmatrix} b_{11} & b_{12} & 0 & 0 \\ 0 & 0 & b_{23} & 0 \\ 0 & b_{32} & 0 & 0 \\ 0 & 0 & b_{43} & b_{44} \end{bmatrix}\begin{bmatrix} v_a \\ w_a \\ F_b \\ \Gamma_b \end{bmatrix}
$$

with

$$
D = \frac{1}{h^2}\begin{bmatrix} 1 & 0 & \cdots & 0 \\ -1 & 1 & \ddots & 0 \\ \vdots & \ddots & \ddots & \ddots \\ 0 & 0 & \cdots & 1 \end{bmatrix}, \; F = \frac{1}{2h}\begin{bmatrix} 1 & 0 & \cdots & 0 \\ 1 & 1 & \ddots & 0 \\ \vdots & \ddots & \ddots & \ddots \\ 0 & 0 & \cdots & 1 \end{bmatrix},
$$

$$Q_1 = h\begin{bmatrix} K_1 & \cdots & 0 \\ \vdots & \ddots & \vdots \\ 0 & \cdots & K_m \end{bmatrix}, \quad Q_2 = h\begin{bmatrix} \frac{1}{\rho_1} & \cdots & 0 \\ \vdots & \ddots & \vdots \\ 0 & \cdots & \frac{1}{\rho_m} \end{bmatrix},$$
$$Q_3 = h\begin{bmatrix} EI_1 & \cdots & 0 \\ \vdots & \ddots & \vdots \\ 0 & \cdots & EI_m \end{bmatrix}, \quad Q_4 = h\begin{bmatrix} \frac{1}{I_{\rho 1}} & \cdots & 0 \\ \vdots & \ddots & \vdots \\ 0 & \cdots & \frac{1}{I_{\rho m}} \end{bmatrix},$$

$$b_{11} = \frac{1}{h}\begin{bmatrix} -1 \\ 0 \\ \vdots \\ 0 \end{bmatrix}, \quad b_{12} = \frac{1}{2}\begin{bmatrix} -1 \\ 0 \\ \vdots \\ 0 \end{bmatrix}, \quad b_{23} = \frac{1}{h}\begin{bmatrix} 0 \\ 0 \\ \vdots \\ 1 \end{bmatrix}, \quad b_{43} = \frac{1}{2}\begin{bmatrix} 0 \\ 0 \\ \vdots \\ 1 \end{bmatrix}, \quad \begin{matrix} b_{32} = b_{11}, \\ b_{44} = b_{23}. \end{matrix}$$

Finally, we write the discretized model as a finite-dimensional port-Hamiltonian system

$$P\begin{cases} \dot{x}_d(t) & = (J-R)Qx_d(t) + Bu(t) \\ y(t) & = B^TQx_d(t) \end{cases} \tag{A.4}$$

where

$$J = \begin{bmatrix} 0 & D & 0 & -F \\ -D^T & 0 & 0 & 0 \\ 0 & 0 & 0 & D \\ F^T & 0 & -D^T & 0 \end{bmatrix}, \quad R = \begin{bmatrix} 0 & 0 & 0 & 0 \\ 0 & 0 & 0 & 0 \\ 0 & 0 & 0 & 0 \\ 0 & 0 & 0 & 0 \end{bmatrix},$$
$$Q = \begin{bmatrix} Q_1 & 0 & 0 & 0 \\ 0 & Q_2 & 0 & 0 \\ 0 & 0 & Q_3 & 0 \\ 0 & 0 & 0 & Q_4 \end{bmatrix}, \quad B = \begin{bmatrix} b_{11} & b_{12} & 0 & 0 \\ 0 & 0 & b_{23} & 0 \\ 0 & b_{32} & 0 & 0 \\ 0 & 0 & b_{43} & b_{44} \end{bmatrix} \tag{A.5}$$

$$x_d(t) = \begin{bmatrix} x_1^d(t) \\ x_2^d(t) \\ x_3^d(t) \\ x_4^d(t) \end{bmatrix}, \quad u(t) = \begin{bmatrix} v_a(t) \\ w_a(t) \\ F_b(t) \\ \Gamma_b(t) \end{bmatrix}, \quad y(t) = \begin{bmatrix} -K_1x_1^1(t) \\ -EI_1x_3^1(t) - \frac{1}{2m+1}K_1x_1^1(t) \\ \frac{1}{\rho_m}x_2^m(t) + \frac{1}{2m+1}\frac{1}{I_{\rho m}}x_4^m(t) \\ \frac{1}{I_{\rho m}}x_4^m(t) \end{bmatrix}.$$

A.2 Mid-point time discretization

Consider the following ordinary differential equation

$$\dot{x}(t) = Ax(t) + Bu(t) \tag{A.6}$$

with $x \in \mathbb{R}^n$, $u \in \mathbb{R}^m$, $A \in \mathbb{R}^{n\times n}$, $B \in \mathbb{R}^{n\times m}$, n, $m \in \mathbb{N}$ and $t \geq 0$. Given a step time $\delta_t > 0$ and $k \in \mathbb{N}$, x_k estimates $x(k\delta_t)$, *i.e.* $x_k \approx x(k\delta_t)$. Then, the following approximation is known as the midpoint time integration

$$\dot{x}(t) \approx \frac{x_{k+1} - x_k}{\delta_t} = A\left(\frac{x_{k+1} + x_k}{2}\right) + Bu_k \tag{A.7}$$

where after some algebra and assuming that $I_n - \frac{\delta_t}{2}A$ is invertible, with I_n the identity of size n, we can write the following discrete model

$$x_{k+1} = A_d x_k + B_d u_k \tag{A.8}$$

with

$$A_d = \left(I_n - \frac{\delta_t}{2}A\right)^{-1}\left(I_n + \frac{\delta_t}{2}A\right), \quad B_d = \left(I_n - \frac{\delta_t}{2}A\right)^{-1}\delta_t B.$$

A.3 An LMI approach to design K or L

In this appendix, we recall a proposition from [Prajna 02], that allows to solve the IDA-PBC problem for LTI systems. This approach can be seen as an alternative of *pole-placement*, *LQ-control*, or H_∞-*control*. We consider the following linear system subject to a state feedback controller:

$$\begin{aligned} \dot{x}(t) &= Ax(t) + Bu(t) \\ u(t) &= r(t) + Fx(t) \end{aligned} \tag{A.9}$$

with $x(t) \in \mathbb{R}^n$, $u(t) \in \mathbb{R}^m$ and $r(t) \in \mathbb{R}^m$ the state, the inputs, and the external input respectively. $A \in \mathbb{R}^{n\times n}$ and $B \in \mathbb{R}^{n\times m}$ known matrices, and $F \in \mathbb{R}^{m\times n}$ a matrix to design. For LTI system, the main idea of the IDA-PBC problem is to shape the closed-loop structure into a desired one of the form:

$$\dot{x}(t) = (J_d - R_d)Q_d x(t) + Br(t) \tag{A.10}$$

with $J_d = -J_d^\top$, $R_d = R_d^\top \geq 0$, $Q_d = Q_d > 0$ all real matrices of size $n \times n$. To this end, the objective is to fine the gain F such that

$$(J_d - R_d)Q_d = A + BF \tag{A.11}$$

In the following proposition, the existence of matrices J_d, R_d, Q_d and F such that (A.11) is verified by solving a set of LMIs.

Proposition A.3.1. *[Prajna 02] Denote by $B_\perp$ a full row rank $(n-m)\times n$ matrix that annihilates B, i.e. $B_\perp B = 0$. Let us also denote $E_\perp = B_\perp A$. There exist matrices $J_d = -J_d^\top$, $R_d = R_d^\top \geq 0$, $Q_d = Q_d > 0$ and F such that satisfies $(J_d - R_d)Q_d = A + BF$ if and only if we can find a solution $\mathbf{X} = \mathbf{X}^\top \in \mathbb{R}^{n\times n}$ of the following LMIs:*

$$\begin{aligned} \mathbf{X} &> 0, \\ -[E_\perp \mathbf{X} B_\perp^T + B_\perp \mathbf{X} E_\perp^T] &\geq 0. \end{aligned} \tag{A.12}$$

Given such an $\mathbf{X}$, compute S_d as follows:

$$S_d = \begin{pmatrix} B_\perp \\ B^T \end{pmatrix}^{-1} \begin{pmatrix} E_\perp \mathbf{X} \\ -B^T \mathbf{X} E_\perp^T (B_\perp B_\perp^T)^{-1} B_\perp \end{pmatrix}, \tag{A.13}$$

then the following matrices

$$\begin{aligned} J_d &= \tfrac{1}{2}(S_d - S_d^T), & R_d &= -\tfrac{1}{2}(S_d + S_d^T), \\ Q_d &= \mathbf{X}^{-1}, & F &= (B^T B)^{-1} B^T (S_d \mathbf{X}^{-1} - A) \end{aligned} \tag{A.14}$$

satisfy $J_d = -J_d^\top$, $R_d = R_d^\top \geq 0$, $Q_d = Q_d > 0$ and $(J_d - R_d)Q_d = A + BF$. ◊

Remark A.3.1. *Proposition A.3.1 is related to stabilizability. In fact, the LMI (A.12) has solution if and only if the pair (A, B) is stabilizable [Prajna 02, Proposition 9].* ♣

Remark A.3.2. *The dual problem consist in following Proposition A.3.1, but replacing A by A^T, B by C^T and F by $-L^T$. The reader can also refer to [Kotyczka 15, Proposition 1].* ♣

Remark A.3.3. *As well as in Remark A.3.1, the pair (A, C) is detectable if and only if the LMI (A.12) has solution with $E_\perp = B_\perp A^T$ and $B_\perp \in \mathbb{R}^{(n-m)\times n}$ a left annihilator of C^T, i.e. $B_\perp C^T = 0$.* ♣

The performances obtained using Proposition A.3.1 are in terms of a desired energy matrix Q_d and a dissipation energy matrix R_d. The LMI (A.12) can be slightly modified in order to keep the energy matrix in a desired interval and to regulate the damping.

Proposition A.3.2. *Under the same statements of Proposition A.3.1, if the following LMIs:*

$$\begin{aligned} \Lambda_2^{-1} - \mathbf{X} &< 0, \\ -\Lambda_1^{-1} + \mathbf{X} &< 0, \\ \Xi_1 + E_\perp \mathbf{X} B_\perp^T + B_\perp \mathbf{X} E_\perp^T + &\leq 0, \\ -\Xi_2 - E_\perp \mathbf{X} B_\perp^T - B_\perp \mathbf{X} E_\perp^T + &\leq 0, \end{aligned} \tag{A.15}$$

have solution $\mathbf{X} = \mathbf{X}^\top$ for some symmetric matrices Λ_1, $\Lambda_2 \in \mathbb{R}^{n\times n}$, Ξ_1, $\Xi_2 \in \mathbb{R}^{(n-m)\times(n-m)}$, such that $0 < \Lambda_1 < \Lambda_2$ and $0 \leq \Xi_1 < \Xi_2$, then $\Lambda_1 < Q_d < \Lambda_2$. Moreover, choosing

$$S_d = \begin{pmatrix} B_\perp \\ B^T \end{pmatrix}^{-1} \begin{pmatrix} E_\perp \mathbf{X} \\ -B^T \mathbf{X} E_\perp^T (B_\perp B_\perp^T)^{-1} B_\perp - \gamma B^T \end{pmatrix}, \tag{A.16}$$

with some scalar $\gamma > 0$, and the matrices J_d, R_d and F as in (A.14), then $A + BF = (J_d - R_d)Q_d$ with $R_d > 0$. ◊

Proof. *The proof of Proposition A.3.1 is a direct application of [Prajna 02, Proposition 7 and Remark 8]. See also [Kotyczka 15, Proposition 1].* ■

Remark A.3.4. *Matrices Λ_1 and Λ_2 fix the lowest and highest eigenvalue of Q_d respectively. Matrices Ξ_1 and Ξ_2 keep sufficient (Ξ_1) but not excessive (Ξ_2) damping, while the scalar $\gamma > 0$ implies $R_d > 0$ and then, the asymptotic behavior is ensured.* ♣

A.4 Abstract formulation of boundary control systems

Boundary control systems (BCSs) [Fattorini 68, Curtain 12] are a class of control systems where the dynamics are described by partial differential equations (PDEs), and the actuation and sensing are situated at the boundaries of the spatial domain. The following *abstract formulation* aims to represent a BCS in the standard state space representation:

$$\dot{x} = \mathcal{A}x(t), \quad x(0) = x_0 \tag{A.17a}$$

$$\mathcal{B}x(t) = u(t) \tag{A.17b}$$

where $\mathcal{A} : D(\mathcal{A}) \to X$ and $\mathcal{B} : D(\mathcal{B}) \to U$, X and U are separable Hilbert spaces, such that $D(\mathcal{A}) \subset D(\mathcal{B}) \subset X$.

Definition A.4.1. *[Curtain 12, Definition 3.3.2] The control system (A.17) is a boundary control system (BCS) if the following hold:*

1. *The operator $A : D(A) \to X$ with $D(A) = D(\mathcal{A}) \cap ker(\mathcal{B})$ and $Ax = \mathcal{A}x$ is the infinitesimal generator of a C_0-semigroup on X.*
2. *There exists an operator $B \in \mathcal{L}(U, X)$, such that for all $u \in U$, $Bu \in D(\mathcal{A})$, $\mathcal{A}B \in \mathcal{L}(U, X)$ and $\mathcal{B}Bu = u$.*

♣

From condition 1 of Definition A.4.1 we can conclude that if (A.17) is a BCS, then for $u(t) = 0$ the PDE has aunique solution, while condition 2 implies that any input in the space U can be applied to the system. The idea of representing the PDE with boundary conditions as a BCS is that for sufficiently smooth inputs $u(t)$ the system can be written in the standard state formulation $\dot{x}(t) = \mathcal{A}x(t) + \mathcal{B}u(t)$.

Example A.4.1. *[Jacob 12, Chapter 11] Consider the transport equation given by*

$$\frac{\partial w}{\partial t}(\zeta, t) = \frac{\partial w}{\partial \zeta}(\zeta, t), \qquad w(\zeta, 0) = w_0(\zeta), \tag{A.18a}$$

$$w(b, t) = u(t), \tag{A.18b}$$

where $\zeta \in [a, b]$ is the spatial variable, $t \geq 0$ is the time, $w(\zeta, t)$ is the transported variable, $w_0(\zeta)$ is the initial condition and $u(t)$ is the input variable. We can write this system as a BCS (A.17) with $\mathcal{A} = \frac{d}{d\zeta}$ and $\mathcal{B}$ a boundary operator which only takes the value of $w(\zeta, t)$ at $\zeta = b$. We can choose as state space $X = L^2([a, b], \mathbb{R})$, i.e. the space of all square-integrable functions, and $D(\mathcal{A}) = H^1([a, b], \mathbb{R})$, i.e. the space of all absolutely continuous function with square-integrable derivatives, and $D(\mathcal{B}) = D(\mathcal{A})$. The system (A.18) is a BCS, then we can conclude that for $u(t) = 0$ the PDE (A.18a) has a unique solution and that we can apply any input $u(t)$ on the space U. ♣

Definition A.4.2. *[Curtain 12, Definition 3.1.1] Consider the BCS (A.17) on the Hilbert space X. The function $x(t)$ is called classical solution of (A.17) on $[0, \tau]$ if $x(t) \in C^1([0, \tau]; X)$, $x(t) \in D(\mathcal{A})$ for all $t \in [0, \tau]$ and $x(t)$ satisfies (A.17) for all $t \in [0, \tau]$.* ♣

Definition A.4.3. *[Curtain 12, Definition 3.1.4] Consider that we are able to write the BCS (A.17) as* $\dot{x}(t) = \mathcal{A}x(t) + \mathcal{B}u(t)$ *and that* $\mathcal{A}$ *is the infinitesimal generator of a* C_0*-semigroup* $T(t)$*. The function* $x(t)$

$$x(t) = T(t)x_0 + \int_0^t T(t-s)\mathcal{B}u(s)ds \tag{A.19}$$

with $x_0 \in X$ *is called mild solution of (A.17) on* $[0, \tau]$*.* ♣

Definition A.4.4. *[Curtain 12, Definition 2.1.2] A strongly continuous semigroup (*C_0*-semigroup) is an operator-valued function* $T(t)$ *from* $\mathbb{R}^+$ *to* $\mathcal{L}(X)$ *that satisfies the following properties*

1. $T(t+s) = T(t)T(s)$*, for* $t, s \geq 0$*.,*
2. $T(0)$ I*,*
3. $\|T(t)x_0 - x_0\| \to 0$ *when* $t \to 0^+$ *for all* $x_0 \in X$*.*

♣

Bibliography

[Anderson 07] B. D. Anderson & J. B. Moore. Optimal control: linear quadratic methods. Courier Corporation, 2007.

[Andry 83] A. Andry, E. Shapiro & J. Chung. *Eigenstructure assignment for linear systems*. IEEE transactions on aerospace and electronic systems, no. 5, pages 711–729, 1983.

[Aoues 17] S. Aoues, F. L. Cardoso-Ribeiro, D. Matignon & D. Alazard. *Modeling and control of a rotating flexible spacecraft: a port-Hamiltonian approach*. IEEE Transactions on Control Systems Technology, vol. 27, no. 1, pages 355–362, 2017.

[Augner 14] B. Augner & B. Jacob. *Stability and stabilization of infinite-dimensional linear port-Hamiltonian systems*. Evolution Equations and Control Theory, vol. 3, no. 2, pages 207–229, 2014.

[Augner 18] B. Augner. *Stabilisation of infinite-dimensional port-Hamiltonian systems via dissipative boundary feedback*. PhD thesis, Universität Wuppertal, Fakultät für Mathematik und Naturwissenschaften . . . , 2018.

[Augner 19] B. Augner. *Well-posedness and stability of infinite-dimensional linear port-Hamiltonian systems with nonlinear boundary feedback*. SIAM Journal on Control and Optimization, vol. 57, no. 3, pages 1818–1844, 2019.

[Augner 20] B. Augner & H. Laasri. *Exponential stability for infinite-dimensional non-autonomous port-Hamiltonian Systems*. Systems & Control Letters, vol. 144, page 104757, 2020.

[Auriol 19] J. Auriol, K. A. Morris & F. Di Meglio. *Late-lumping backstepping control of partial differential equations*. Automatica, vol. 100, pages 247–259, 2019.

[Balas 78] M. J. Balas. *Active control of flexible systems*. Journal of Optimization theory and Applications, vol. 25, no. 3, pages 415–436, 1978.

[Bassi 07] L. Bassi, A. Macchelli & C. Melchiorri. *An algorithm to discretize one-dimensional distributed port Hamiltonian systems*. In Lagrangian and Hamiltonian methods for nonlinear control 2006, pages 61–73. Springer, 2007.

[Biedermann 18] B. Biedermann, P. Rosenzweig & T. Meurer. *Passivity-based observer design for state affine systems using interconnection and damping assignment*. In 2018 IEEE Conference on Decision and Control (CDC), pages 4662–4667. IEEE, 2018.

[Brasch 70] F. Brasch & J. Pearson. *Pole placement using dynamic compensators*. IEEE Transactions on Automatic Control, vol. 15, no. 1, pages 34–43, 1970.

[Brogliato 20] B. Brogliato, R. Lozano, B. Maschke & O. Egeland. *Passivity-based control*. In Dissipative Systems Analysis and Control, pages 491–573. Springer, 2020.

[Brugnoli 19a] A. Brugnoli, D. Alazard, V. Pommier-Budinger & D. Matignon. *Port-Hamiltonian formulation and symplectic discretization of plate models Part I: Mindlin model for thick plates*. Applied Mathematical Modelling, vol. 75, pages 940–960, 2019.

[Brugnoli 19b] A. Brugnoli, D. Alazard, V. Pommier-Budinger & D. Matignon. *Port-Hamiltonian formulation and symplectic discretization of plate models Part II: Kirchhoff model for thin plates*. Applied Mathematical Modelling, vol. 75, pages 961–981, 2019.

[Califano 18] F. Califano, M. Bin, A. Macchelli & C. Melchiorri. *Stability analysis of nonlinear repetitive control schemes*. IEEE control systems letters, vol. 2, no. 4, pages 773–778, 2018.

[Cardoso-Ribeiro 17] F. L. Cardoso-Ribeiro, D. Matignon & V. Pommier-Budinger. *A port-Hamiltonian model of liquid sloshing in moving containers and application to a fluid-structure system*. Journal of Fluids and Structures, vol. 69, pages 402–427, 2017.

[Cardoso-Ribeiro 21] F. L. Cardoso-Ribeiro, D. Matignon & L. Lefèvre. *A Partitioned Finite Element Method for power-preserving discretization of open systems of conservation laws*. IMA Journal of Mathematical Control and Information, vol. 38, no. 2, pages 493–533, 2021.

[Curtain 12] R. F. Curtain & H. Zwart. An introduction to infinite-dimensional linear systems theory, volume 21. Springer Science & Business Media, 2012.

[Dalsmo 98] M. Dalsmo & A. Van Der Schaft. *On representations and integrability of mathematical structures in energy-conserving physical systems*. SIAM Journal on Control and Optimization, vol. 37, no. 1, pages 54–91, 1998.

[Demetriou 04] M. A. Demetriou. *Natural second-order observers for second-order distributed parameter systems*. Systems & control letters, vol. 51, no. 3-4, pages 225–234, 2004.

[Duindam 09] V. Duindam, A. Macchelli, S. Stramigioli & H. Bruyninckx. Modeling and control of complex physical systems: the port-hamiltonian approach. Springer Science & Business Media, 2009.

[Ennsbrunner 05] H. Ennsbrunner & K. Schlacher. *On the geometrical representation and interconnection of infinite dimensional port controlled hamiltonian systems*. In Proceedings of the 44th IEEE Conference on Decision and Control, pages 5263–5268. IEEE, 2005.

[Fattorini 68] H. Fattorini. *Boundary Control Systems*. SIAM Journal on Control, vol. 6, no. 3, pages 349–385, 1968.

[Feng 16] H. Feng & B.-Z. Guo. *Observer design and exponential stabilization for wave equation in energy space by boundary displacement measurement only*. IEEE Transactions on Automatic Control, vol. 62, no. 3, pages 1438–1444, 2016.

[Golo 04] G. Golo, V. Talasila, A. Van Der Schaft & B. Maschke. *Hamiltonian discretization of boundary control systems*. Automatica, vol. 40, no. 5, pages 757–771, 2004.

[Gugat 05] M. Gugat, G. Leugering & G. Sklyar. *L^p-optimal boundary control for the wave equation*. SIAM Journal on Control and Optimization, vol. 44, no. 1, pages 49–74, 2005.

[Guo 07] B.-Z. Guo & C.-Z. Xu. *The stabilization of a one-dimensional wave equation by boundary feedback with noncollocated observation*. IEEE Transactions on Automatic Control, vol. 52, no. 2, pages 371–377, 2007.

[Guo 09] B.-Z. Guo & W. Guo. *The strong stabilization of a one-dimensional wave equation by non-collocated dynamic boundary feedback control*. Automatica, vol. 45, no. 3, pages 790–797, 2009.

[Hamroun 06] B. Hamroun, L. Lefèvre & E. Mendes. *Port-based modelling for open channel irrigation systems*. Transactions on Fluid Mechanics, vol. 1, no. 12, pages 995–1009, 2006.

[Hamroun 10] B. Hamroun, A. Dimofte, L. Lefèvre & E. Mendes. *Control by interconnection and energy-shaping methods of port Hamiltonian models. Application to the shallow water equations*. European Journal of Control, vol. 16, no. 5, pages 545–563, 2010.

[Hastir 19] A. Hastir, F. Califano & H. Zwart. *Well-posedness of infinite-dimensional linear systems with nonlinear feedback*. Systems & Control Letters, vol. 128, pages 19–25, 2019.

[Hidayat 11] Z. Hidayat, R. Babuska, B. De Schutter & A. Nunez. *Observers for linear distributed-parameter systems: A survey*. In 2011 IEEE international symposium on robotic and sensors environments (ROSE), pages 166–171. IEEE, 2011.

[Horn 12] R. A. Horn & C. R. Johnson. Matrix analysis. Cambridge university press, 2012.

[Jacob 12] B. Jacob & H. J. Zwart. Linear port-hamiltonian systems on infinite-dimensional spaces, volume 223. Springer Science & Business Media, 2012.

[Jacob 15] B. Jacob, K. Morris & H. Zwart. *C 0-semigroups for hyperbolic partial differential equations on a one-dimensional spatial domain*. Journal of evolution equations, vol. 15, no. 2, pages 493–502, 2015.

[Jacob 18] B. Jacob & H. Zwart. *An operator theoretic approach to infinite-dimensional control systems*. GAMM-Mitteilungen, vol. 41, no. 4, page e201800010, 2018.

[Jacob 19] B. Jacob & J. T. Kaiser. *On exact controllability of infinite-dimensional linear port-Hamiltonian systems*. IEEE Control Systems Letters, vol. 3, no. 3, pages 661–666, 2019.

[Jiang 94] J. Jiang. *Design of reconfigurable control systems using eigenstructure assignments*. International Journal of Control, vol. 59, no. 2, pages 395–410, 1994.

[John 49] F. John. *On linear partial differential equations with analytic coefficients unique continuation of data*. Communications on Pure and Applied Mathematics, vol. 2, no. 2-3, pages 209–253, 1949.

[Kalman 69] R. E. Kalman, P. L. Falb & M. A. Arbib. Topics in mathematical system theory, volume 1. McGraw-Hill New York, 1969.

[Kosmidou 07] O. I. Kosmidou. *Generalized Riccati equations associated with guaranteed cost control: An overview of solutions and features.* Applied Mathematics and Computation, vol. 191, no. 2, pages 511–520, 2007.

[Kotyczka 15] P. Kotyczka & M. Wang. *Dual observer-based compensator design for linear port-Hamiltonian systems.* In 2015 European Control Conference (ECC), pages 2908–2913. IEEE, 2015.

[Kotyczka 18] P. Kotyczka, B. Maschke & L. Lefèvre. *Weak form of Stokes–Dirac structures and geometric discretization of port-Hamiltonian systems.* Journal of Computational Physics, vol. 361, pages 442–476, 2018.

[Krstic 08] M. Krstic, B.-Z. Guo, A. Balogh & A. Smyshlyaev. *Output-feedback stabilization of an unstable wave equation.* Automatica, vol. 44, no. 1, pages 63–74, 2008.

[Lanzon 08] A. Lanzon, Y. Feng, B. D. Anderson & M. Rotkowitz. *Computing the positive stabilizing solution to algebraic Riccati equations with an indefinite quadratic term via a recursive method.* IEEE Transactions on Automatic Control, vol. 53, no. 10, pages 2280–2291, 2008.

[Le Gorrec 05] Y. Le Gorrec, H. Zwart & B. Maschke. *Dirac structures and boundary control systems associated with skew-symmetric differential operators.* SIAM journal on control and optimization, vol. 44, no. 5, pages 1864–1892, 2005.

[Le Gorrec 06] Y. Le Gorrec, B. Maschke, J. Villegas & H. Zwart. *Dissipative boundary control systems with application to distributed parameters reactors.* In 2006 IEEE Conference on Computer Aided Control System Design, 2006 IEEE International Conference on Control Applications, 2006 IEEE International Symposium on Intelligent Control, pages 668–673. IEEE, 2006.

[Liu 21] N. Liu, Y. Wu & Y. Le Gorrec. *Energy based modeling of ionic polymer metal composite actuators dedicated to the control of flexible structures.* IEEE/ASME Transactions on Mechatronics, pages 1–1, 2021.

[Luenberger 64] D. G. Luenberger. *Observing the state of a linear system.* IEEE transactions on military electronics, vol. 8, no. 2, pages 74–80, 1964.

[Luo 12] Z.-H. Luo, B.-Z. Guo & Ö. Morgül. Stability and stabilization of infinite dimensional systems with applications. Springer Science & Business Media, 2012.

[Macchelli 04a] A. Macchelli & C. Melchiorri. *Control by interconnection and energy shaping of the Timoshenko beam.* Mathematical and Computer Modelling of Dynamical Systems, vol. 10, no. 3-4, pages 231–251, 2004.

[Macchelli 04b] A. Macchelli & C. Melchiorri. *Modeling and control of the Timoshenko beam. The distributed port Hamiltonian approach.* SIAM Journal on Control and Optimization, vol. 43, no. 2, pages 743–767, 2004.

[Macchelli 05] A. Macchelli & C. Melchiorri. *Control by interconnection of mixed port Hamiltonian systems.* IEEE Transactions on Automatic Control, vol. 50, no. 11, pages 1839–1844, 2005.

[Macchelli 11] A. Macchelli. *Energy shaping of distributed parameter port-Hamiltonian systems based on finite element approximation.* Systems & Control Letters, vol. 60, no. 8, pages 579–589, 2011.

[Macchelli 13] A. Macchelli. *Boundary energy shaping of linear distributed port-Hamiltonian systems.* European Journal of Control, vol. 19, no. 6, pages 521–528, 2013.

[Macchelli 17] A. Macchelli, Y. Le Gorrec, H. Ramirez & H. Zwart. *On the Synthesis of Boundary Control Laws for Distributed Port-Hamiltonian Systems.* IEEE Transactions on Automatic Control, vol. 62, no. 4, pages 1700–1713, April 2017.

[Macchelli 18] A. Macchelli & F. Califano. *Dissipativity-based boundary control of linear distributed port-Hamiltonian systems.* Automatica, vol. 95, pages 54 – 62, 2018.

[Macchelli 20] A. Macchelli, Y. Le Gorrec & H. Ramírez. *Exponential Stabilization of Port-Hamiltonian Boundary Control Systems via Energy Shaping.* IEEE Transactions on Automatic Control, vol. 65, no. 10, pages 4440–4447, 2020.

[Malzer 19] T. Malzer, H. Rams & M. Schöberl. *Energy-Based In-Domain Control of a Piezo-Actuated Euler-Bernoulli Beam.* IFAC-PapersOnLine, vol. 52, no. 2, pages 144–149, 2019.

[Malzer 20a] T. Malzer, H. Rams, B. Kolar & M. Schöberl. *Stability Analysis of the Observer Error of an In-Domain Actuated Vibrating String.* IEEE Control Systems Letters, vol. 5, no. 4, pages 1237–1242, 2020.

[Malzer 20b] T. Malzer, J. Toledo, Y. L. Gorrec & M. Schöberl. *Energy-Based In-Domain Control and Observer Design for Infinite-Dimensional Port-Hamiltonian Systems.* arXiv preprint arXiv:2002.01717, 2020.

[Maschke 92] B. M. Maschke & A. J. van der Schaft. *Port-controlled Hamiltonian systems: modelling origins and systemtheoretic properties.* IFAC Proceedings Volumes, vol. 25, no. 13, pages 359–365, 1992.

[Maschke 98] B. M. Maschke, R. Ortega & A. J. van der Schaft. *Energy-based Lyapunov functions for forced Hamiltonian systems with dissipation.* In Proceedings of the 37th IEEE Conference on Decision and Control (Cat. No. 98CH36171), volume 4, pages 3599–3604. IEEE, 1998.

[Meurer 09] T. Meurer & A. Kugi. *Tracking control for boundary controlled parabolic PDEs with varying parameters: Combining backstepping and differential flatness.* Automatica, vol. 45, no. 5, pages 1182–1194, 2009.

[Meurer 11] T. Meurer & A. Kugi. *Tracking control design for a wave equation with dynamic boundary conditions modeling a piezoelectric stack actuator.* International Journal of Robust and Nonlinear Control, vol. 21, no. 5, pages 542–562, 2011.

[Meurer 12] T. Meurer. Control of higher–dimensional pdes: Flatness and backstepping designs. Springer Science & Business Media, 2012.

[Meurer 13] T. Meurer. *On the extended Luenberger-type observer for semilinear distributed-parameter systems.* IEEE T. Automat. Contr., vol. 58, no. 7, pages 1732–1743, 2013.

[Morgül 94] Ö. Morgül. *A dynamic control law for the wave equation.* Automatica, vol. 30, no. 11, pages 1785–1792, 1994.

[Morgul 98] O. Morgul. *Stabilization and disturbance rejection for the wave equation.* IEEE Transactions on Automatic Control, vol. 43, no. 1, pages 89–95, 1998.

[Morgül 02] Ö. Morgül. *An exponential stability result for the wave equation.* Automatica, vol. 38, no. 4, pages 731–735, 2002.

[Nishida 11] G. Nishida, K. Takagi, B. Maschke & T. Osada. *Multi-scale distributed parameter modeling of ionic polymer-metal composite soft actuator.* Control Engineering Practice, vol. 19, no. 4, pages 321–334, 2011.

[Ortega 02] R. Ortega, A. Van Der Schaft, B. Maschke & G. Escobar. *Interconnection and damping assignment passivity-based control of port-controlled Hamiltonian systems.* Automatica, vol. 38, no. 4, pages 585–596, 2002.

[Ortega 04] R. Ortega & E. Garcia-Canseco. *Interconnection and damping assignment passivity-based control: A survey.* European Journal of control, vol. 10, no. 5, pages 432–450, 2004.

[Ortega 08] R. Ortega, A. Van Der Schaft, F. Castanos & A. Astolfi. *Control by interconnection and standard passivity-based control of port-Hamiltonian systems.* IEEE Transactions on Automatic control, vol. 53, no. 11, pages 2527–2542, 2008.

[Pasumarthy 07] R. Pasumarthy & A. Van Der Schaft. *Achievable Casimirs and its implications on control of port-Hamiltonian systems.* International Journal of Control, vol. 80, no. 9, pages 1421–1438, 2007.

[Pasumarthy 12] R. Pasumarthy, V. Ambati & A. van der Schaft. *Port-Hamiltonian discretization for open channel flows.* Systems & control letters, vol. 61, no. 9, pages 950–958, 2012.

[Prajna 02] S. Prajna, A. van der Schaft & G. Meinsma. *An LMI approach to stabilization of linear port-controlled Hamiltonian systems.* Systems & control letters, vol. 45, no. 5, pages 371–385, 2002.

[Ramirez 14] H. Ramirez, Y. Le Gorrec, A. Macchelli & H. Zwart. *Exponential Stabilization of Boundary Controlled Port-Hamiltonian Systems With Dynamic Feedback.* IEEE Transactions on Automatic Control, vol. 59, no. 10, pages 2849–2855, Oct 2014.

[Ramirez 17a] H. Ramirez, H. Zwart & Y. Le Gorrec. *Stabilization of infinite dimensional port-Hamiltonian systems by nonlinear dynamic boundary control.* Automatica, vol. 85, pages 61 – 69, 2017.

[Ramirez 17b] H. Ramirez, H. Zwart, Y. Le Gorrec & A. Macchelli. *On backstepping boundary control for a class of linear port-Hamiltonian systems.* In 2017 IEEE 56th Annual Conference on Decision and Control (CDC), pages 658–663. IEEE, 2017.

[Rashad 20] R. Rashad, F. Califano, A. J. van der Schaft & S. Stramigioli. *Twenty years of distributed port-Hamiltonian systems: a literature review.* IMA Journal of Mathematical Control and Information, 2020.

[Schaum 18] A. Schaum, T. Meurer & J. A. Moreno. *Dissipative observers for coupled diffusion–convection–reaction systems*. Automatica, vol. 94, pages 307–314, 2018.

[Schöberl 08] M. Schöberl, H. Ennsbrunner & K. Schlacher. *Modelling of piezoelectric structures–a Hamiltonian approach*. Mathematical and Computer Modelling of Dynamical Systems, vol. 14, no. 3, pages 179–193, 2008.

[Schöberl 12] M. Schöberl & A. Siuka. *On Casimir functionals for infinite-dimensional port-Hamiltonian control systems*. IEEE Transactions on Automatic Control, vol. 58, no. 7, pages 1823–1828, 2012.

[Schöberl 14] M. Schöberl & A. Siuka. *Jet bundle formulation of infinite-dimensional port-Hamiltonian systems using differential operators*. Automatica, vol. 50, no. 2, pages 607–613, 2014.

[Serhani 19] A. Serhani, D. Matignon & G. Haine. *A partitioned finite element method for the structure-preserving discretization of damped infinite-dimensional port-Hamiltonian systems with boundary control*. In International Conference on Geometric Science of Information, pages 549–558. Springer, 2019.

[Seslija 12] M. Seslija, A. van der Schaft & J. M. Scherpen. *Discrete exterior geometry approach to structure-preserving discretization of distributed-parameter port-Hamiltonian systems*. Journal of Geometry and Physics, vol. 62, no. 6, pages 1509–1531, 2012.

[Smyshlyaev 05] A. Smyshlyaev & M. Krstic. *Backstepping observers for a class of parabolic PDEs*. Systems & Control Letters, vol. 54, no. 7, pages 613–625, 2005.

[Smyshlyaev 09] A. Smyshlyaev & M. Krstic. *Boundary control of an anti-stable wave equation with anti-damping on the uncontrolled boundary*. Systems & Control Letters, vol. 58, no. 8, pages 617–623, 2009.

[Staffans 05] O. Staffans. Well-posed linear systems, volume 103. Cambridge University Press, 2005.

[Stramigioli 01] S. Stramigioli. Modeling and ipc control of interactive mechanical systems—a coordinate-free approach. 2001.

[Toledo 20] J. Toledo, H. Ramirez, Y. Wu & Y. Le Gorrec. *Passive observers for distributed port-Hamiltonian systems*. In 21st IFAC World Congress, 2020, July 12-17, 2020, Berlin, Germany, 2020.

[Trenchant 18] V. Trenchant, H. Ramirez, P. Kotyczka & Y. Le Gorrec. *Finite differences on staggered grids preserving the port-Hamiltonian structure with application to an acoustic duct*. Journal of Computational Physics, vol. 373, pages 673–697, November 2018.

[Tucsnak 14] M. Tucsnak & G. Weiss. *Well-posed systems—The LTI case and beyond*. Automatica, vol. 50, no. 7, pages 1757–1779, 2014.

[van der Schaft 00] A. van der Schaft. L2-gain and passivity techniques in nonlinear control, volume 2. Springer, 2000.

[van der Schaft 02] A. van der Schaft & B. M. Maschke. *Hamiltonian formulation of distributed-parameter systems with boundary energy flow*. Journal of Geometry and Physics, vol. 42, no. 1-2, pages 166–194, 2002.

[Venkatraman 10a] A. Venkatraman & A. van der Schaft. *Full-order observer design for a class of port-Hamiltonian systems*. Automatica, vol. 46, no. 3, pages 555–561, 2010.

[Venkatraman 10b] A. Venkatraman & A. van der Schaft. *Energy shaping of port-Hamiltonian systems by using alternate passive input-output pairs*. European Journal of Control, vol. 16, no. 6, pages 665–677, 2010.

[Villegas 05] J. Villegas, H. Zwart, Y. Le Gorrec, B. Maschke & A. Van Der Schaft. *Stability and stabilization of a class of boundary control systems*. In Proceedings of the 44th IEEE Conference on Decision and Control, pages 3850–3855. IEEE, 2005.

[Villegas 07] J. Villegas. *A Port-Hamiltonian Approach to Distributed Parameter Systems*. PhD thesis, University of Twente, Netherlands, 2007.

[Villegas 09] J. A. Villegas, H. Zwart, Y. Le Gorrec & B. Maschke. *Exponential stability of a class of boundary control systems*. IEEE Transactions on Automatic Control, vol. 54, no. 1, pages 142–147, 2009.

[Vincent 16] B. Vincent, N. Hudon, L. Lefèvre & D. Dochain. *Port-Hamiltonian observer design for plasma profile estimation in tokamaks*. IFAC-PapersOnLine, vol. 49, no. 24, pages 93–98, 2016.

[Voß 14] T. Voß & J. M. Scherpen. *Port-hamiltonian modeling of a nonlinear timoshenko beam with piezo actuation*. SIAM Journal on Control and Optimization, vol. 52, no. 1, pages 493–519, 2014.

[Vu 17] N. M. T. Vu, L. Lefevre & R. Nouailletas. *Distributed and backstepping boundary controls for port-Hamiltonian systems with symmetries*. Mathematical and Computer Modelling of Dynamical Systems, vol. 23, no. 1, pages 55–76, 2017.

[Wu 18] Y. Wu, B. Hamroun, Y. Le Gorrec & B. Maschke. *Reduced order LQG control design for port Hamiltonian systems*. Automatica, vol. 95, pages 86–92, 2018.

[Yaghmaei 18] A. Yaghmaei & M. J. Yazdanpanah. *Structure preserving observer design for port-Hamiltonian systems*. IEEE Transactions on Automatic Control, vol. 64, no. 3, pages 1214–1220, 2018.

[Yang 05] K.-J. Yang, K.-S. Hong & F. Matsuno. *Robust boundary control of an axially moving string by using a PR transfer function*. IEEE Transactions on Automatic Control, vol. 50, no. 12, pages 2053–2058, 2005.

[Zhou 17] W. Zhou, B. Hamroun, F. Couenne & Y. Le Gorrec. *Distributed port-Hamiltonian modelling for irreversible processes*. Mathematical and Computer Modelling of Dynamical Systems, vol. 23, no. 1, pages 3–22, 2017.

[Zuazua 93] E. Zuazua. *Exact controllability for semilinear wave equations in one space dimension*. In Annales de l'Institut Henri Poincare (C) Non Linear Analysis, volume 10, pages 109–129. Elsevier, 1993.

[Zwart 10] H. Zwart, Y. Le Gorrec, B. Maschke & J. Villegas. *Well-posedness and regularity of hyperbolic boundary control systems on a one-dimensional spatial domain*. ESAIM: control, optimisation and calculus of variations, vol. 16, no. 4, pages 1077–1093, 2010.

List of Figures

List of Tables

Titre : Synthèse de lois de commande à base d'observateurs pour les systèmes à paramètres distribués: une approche Hamiltonienne à ports.

Mots clefs: Systèmes à dimension infinie, systèmes Hamiltonien à port, observateurs, commande.

Résumé : L'approche Hamiltonienne à ports s'est avérée être particulièrement bien adaptée à la modélisation et la commande des *systèmes à paramètres distribués* (SPD). A titre d'exemples de systèmes entrant dans cette classe de systèmes nous pouvons citer les ondes, les poutres vibrantes, les canaux ouverts, la dynamique des fluides, les structures piézoélectriques et les réacteurs chimiques. Dans cette thèse, nous proposons de nouveaux outils pour la synthèse de lois de *commandes basées observateurs d'état* (CBOE) pour une classe de SPD. Plus précisément la classe de SPD étudiée dans cette thèse est la classe des *systèmes Hamiltoniens à ports linéaires contrôlés à la frontière* (SHP-CF). Ce sont des systèmes décrits par des *équations différentielles partielles* dont les actionneurs et les capteurs sont situés à la frontière de leur domaine spatial. Pour la synthèse, nous utilisons deux approches : early-lumping et late-lumping. Pour la première approche, le système est dans un premier temps discrétisé et la commande basée observateurs est ensuite synthétisé en dimension finie. Pour cela nous proposons deux méthodes, l'une privilégiant la commande, l'autre l'observation. Dans les deux cas, nous combinons des outils de contrôle classiques comme le régulateur quadratique linéaire ou le placement de pôles avec l'approche Hamiltonienne pour garantir la stabilité du système en boucle fermée lorsque le correcteur CBOE d'ordre réduit est appliqué au SHP-CF. Pour la deuxième approche, nous proposons différents observateurs de dimension infinie pour les SHP-CF en fonction des mesures disponibles. Selon le cas considéré, la convergence asymptotique ou exponentielle de l'observateur est prouvée. Enfin, nous proposons quelques résultats préliminaires sur la commande par injection de dissipation ou modelage d'énergie en utilisant les observateurs précédemment étudiés et la corde vibrante comme exemple illustratif.

Title : Observer-based boundary control of distributed parameter systems: a port-Hamiltonian approach.

Keywords : Infinite-dimensional systems, port-Hamiltonian systems, observer-based state feedback.

Abstract : The port-Hamiltonian approach has shown to be well suited for the modelling and control of *distributed parameter systems* (DPSs). Some examples of this class of systems are the waves, beams, open channels, fluid motion, piezoelectric structures, and chemical reactors. In this thesis, we have provided some tools for the design of *observer-based state feedback* (OBSF) controllers for a class of DPSs. The class of DPSs studied in this thesis is the class of *boundary controlled port-Hamiltonian systems* (BC-PHSs). These are systems described by *partial differential equations* with actuators and sensors located at the spatial boundaries. For the synthesis, we have used two approaches : the early-lumping and the late-lumping approach. For the early lumping approach, we have proposed two methods to design the OBSF gains. In both, we combine classical control tools as the linear quadratic regulator or pole placement with the port-Hamiltonian approach to guarantee the closed-loop stability when applying the OBSF controller to the BC-PHS. For the late-lumping approach, we have proposed infinite-dimensional observers for BC-PHSs subject to different types of measurements. Depending on the case, the observer convergence is guaranteed to be asymptotic or exponential. Finally, some first steps toward the observer-based damping injection and energy shaping have been studied using the vibrating string as an example.

Université Bourgogne Franche-Comté
32, avenue de l'Observatoire
25000 Besançon